Identification of a gene defect associated with abnormal signal transmission in retinal ribbon-type synapses

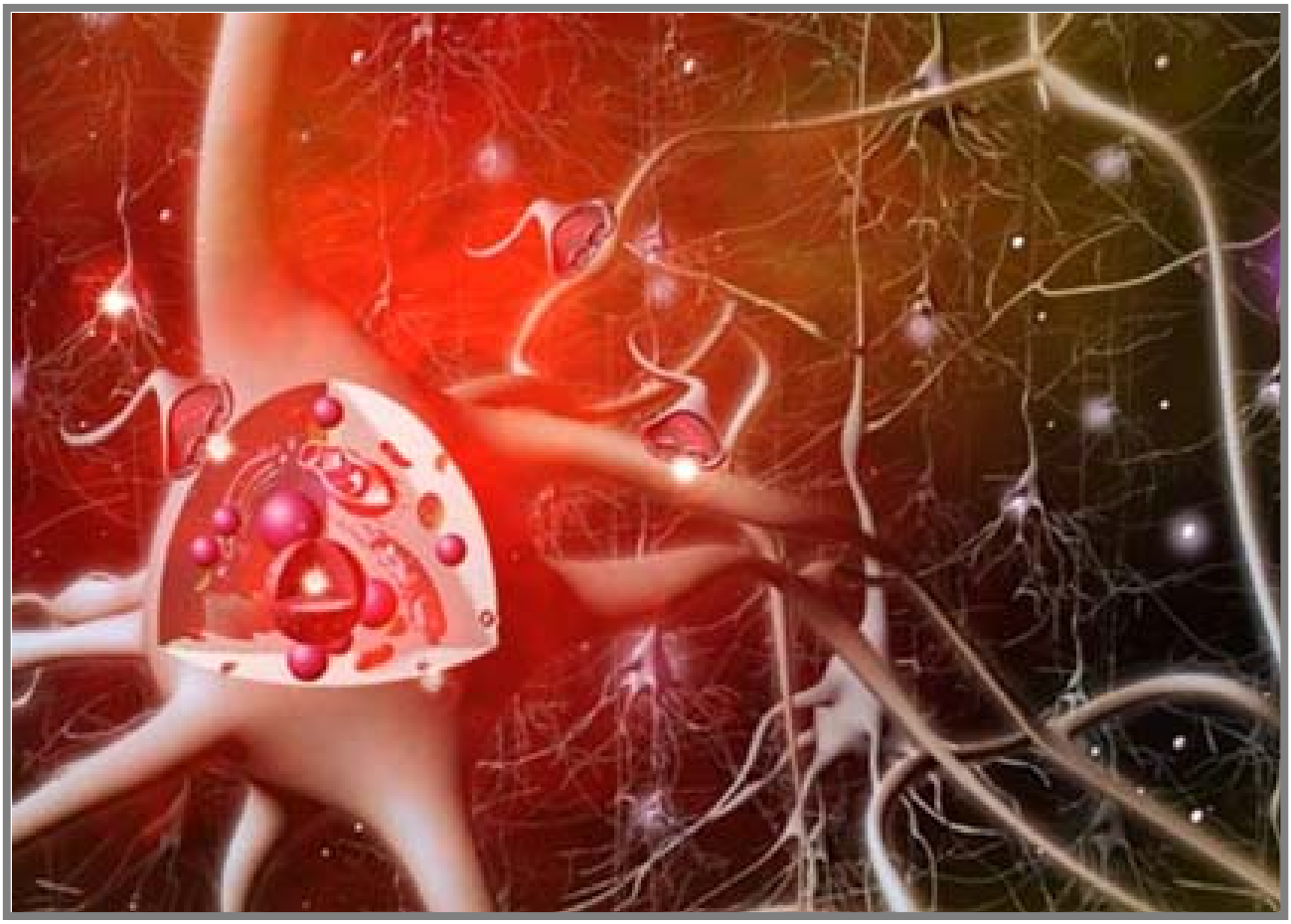

Katharina Agnes Wycisk

Identification of a Gene Defect Associated with Abnormal Signal Transmission in Retinal Ribbon-Type Synapses

Dissertation
zur
Erlangung der naturwissenschaftlichen Doktorwürde
(Dr. sc. nat.)
vorgelegt der
Mathematisch-naturwissenschaftlichen Fakultät
der
Universität Zürich

von

Katharina Agnes Wycisk

aus

Deutschland

Promotionskomitee

Prof. Dr. med. **Eric Berger (**Vorsitz**)**

Prof. Dr. rer. nat. **Wolfgang Berger (**Leitung der Dissertation**)**

Prof. Dr. rer. nat. **Stephan Neuhaus**

Zürich, 2006

Title of the dissertation:

Identification of a Gene Defect Associated with Abnormal Signal Transmission in Retinal Ribbon-Type Synapses

Title of document 1 (chapter 3.1, page 30):

Structural and Functional Abnormalities of Retinal Ribbon Synapses due to Cacna2d4 Mutation

http://www.iovs.org/cgi/content/abstract/47/8/3523

Title of document 2 (chapter 3.2, page 43):

Mutation in the Auxiliary Calcium Channel Subunit CACNA2D4 Cause Autosomal Recessive Cone Dystrophy

http://www.journals.uchicago.edu/cgi-bin/resolve?id=doi:10.1086/508944

Declaration

I declare that the present thesis was composed by myself and the enclosed experimental work was performed by my own. Exceptions are explicitly stated in the text.
This dissertation has not been submitted for any other degree or professional qualification except as specified.

Katharina Agnes Wycisk

Winterthur, 2006

dedicated to the creatures

Acknowledgement

The present study bears signs of encouragement, conceptual comments, excellent technical assistance and exemplary engagement of a large number of persons, to them particular acknowledgement is dedicated. To all of you, thank you so much, indeed.

First of all, I would send special thanks to Ursula and Benno, to those two persons, who steadily encouraged me in good and less good times, always concentrating my ambitions and energy to the true aims of the last years and continuously instructing me in being seriously oblivious of the irony of fate. *Best Thanks to you both!!!*

Prof. Wolfgang Berger, I would like to address my particular thanks for providing me the opportunity of a challenging project for the doctoral thesis, the steady supervision and all scientific implications and ideas, guiding my work to success. *Warm Thanks, Wolfgang!!!*

I also especially acknowledge Prof. Eric Berger for discussions, useful comments and the supervision of my thesis as the external "doctoral father", giving me as well a chance to gain insight into the ophthalmological medicine trough work and exchange with students of the medical faculty. *Thank you very much indeed!!!*

Prof. Klaus Rüther, Prof. Gian Carlo Demontis, Dr. Hannie Kremers and her laboratory colleges, Prof. Eberhart Zrenner and colleges, Dr. Birgit Budde and Sergej Skosyrski, I wish to express my appreciations to the scientific engagement, collaborations and experimental help which contributed to the wonderful results of this thesis. *Many Thanks!!!*

Regarding excellent assistance, I would like to stress my acknowledgement to those who proved to be of exemplary and unique help in the laboratory proceedings. Silke Feil, Mariana Wittmer, Esther Glaus, John Neidhardt, Gabor Matyas and Christina Zeitz, *Kind Thanks* for participation and support in several units of my project!!!

During the years of dissertation, I met nice persons and friends who stood behind me within working hours and beyond, making the time of the thesis a pleasant experience at the professional as well as social "stage". Silke, Mariana, Francesca and the Ticino front, Gaby, Sandra, Nico, Istvan, Philippe, Niels, Stefanie G., Stefanie D., for your help and encouragement in the laboratory, opened ears for loud protests about frustrating outcomes and for the moments shared together, in Pizol, Glarus, at sea and on mountains and, not at least, at the *"Desperado hacienda"*, *Thanks* to you all. I could not ask for better company!!!…and, although I am happy to finish my PhD, there were times with you I will be missing…Finally, sweet thanks to those friends, outside the scientific horizon, with whom I enjoyed the moments of friendship. Ela, Ferid, Maria, Claudia, Antje, Peter, Emanuele, Sabine M., Mailina M., Sabine L., Christian and the Berliner troupe, thanks for beautiful times "in between".

Abbreviations

A	adenine
aa	amino acid
ABR	acoustic brain response
ADP	adenosine diphosphate
AMP	adenosine monophosphate
ASR	acoustic startle response
ATP	adenosine triphosphate
BLAST	bacterial local alignment search tool
bp	base pair
BSA	bovine serum albumin
C	cytosine
°C	Celsius degrees
Ca	calcium element
CACHE	calcium channel and chemotaxis receptor domain
cDNA	complementary DNA
cM	centi-Morgan
COD	cone dystrophy
CORD	cone-rod dystrophy
CSNB	congenital stationary night blindness
cCSNB	complete CSNB
iCSNB	incomplete CSNB
cRNA	complementary RNA
Cyl	cylindrical
DEPC	diethylene pyrocarbonate
DMSO	dimethyl sulfoxide
DNA	deoxyribonucleic acid
dNTP	deoxyribonucleotide triphosphate
EDTA	ethylenediamine tetra acetic acid
ER	endoplasmatic reticulum
ERG	electroretinography
EST	expressed sequence tag
Fig	figure
G	guanine

GAPDH	glyceraldehyde-3-phosphate dehydrogenase
GC	ganglion cells
GCL	ganglion cell layer
GCT	ganglion cell nuclei thickness
HF	high frequency
HSD	herring sperm DNA
IHC	inner hair cells
INL	inner nuclear layer
IPL	inner plexiform layer
IT	implicit time
kbp	kilo base pairs
KO-mouse	knockout-mouse
LE	left eye
M	molar
mbp	mega base pairs
mRNA	messenger RNA
mut	mutant
mV	millivolt
NCBI	National Centre for Biotechnology Information
NIX	Nucleic Acid Identification
NMD	nonsense mediated decay
OD	oculus dexter (right eye)
OHC	outer hair cells
OMIM	Online Mendelian Inheritance in Man
ONL	outer nuclear layer
OPL	outer plexiform layer
ORF	open reading frame
OS	oculus sinester (left eye)
OS	outer segment
P	postnatal
PCR	polymerase chain reaction
RetNet	Retinal Information Network
RHO	rhodopsin
RNA	ribonucleic acid

RNase	ribonuclease
RP	retinitis pigmentosa
RPE	retinal pigment epithelium
rpm	revolution per minute
RT-PCR	reverse transcriptase polymerase chain reaction
S	photoreceptor segments
SER	smooth endoplasmic reticulum
SF	standard flash
Sph	spherical
T	thymine
Taq	*Thermus aquaticus* polymerase
u	unit
UTR	untranslated region
VA	visual acuity
VWFA	von Willebrand factor a domain
W	week
wt	wild type

Table of Content

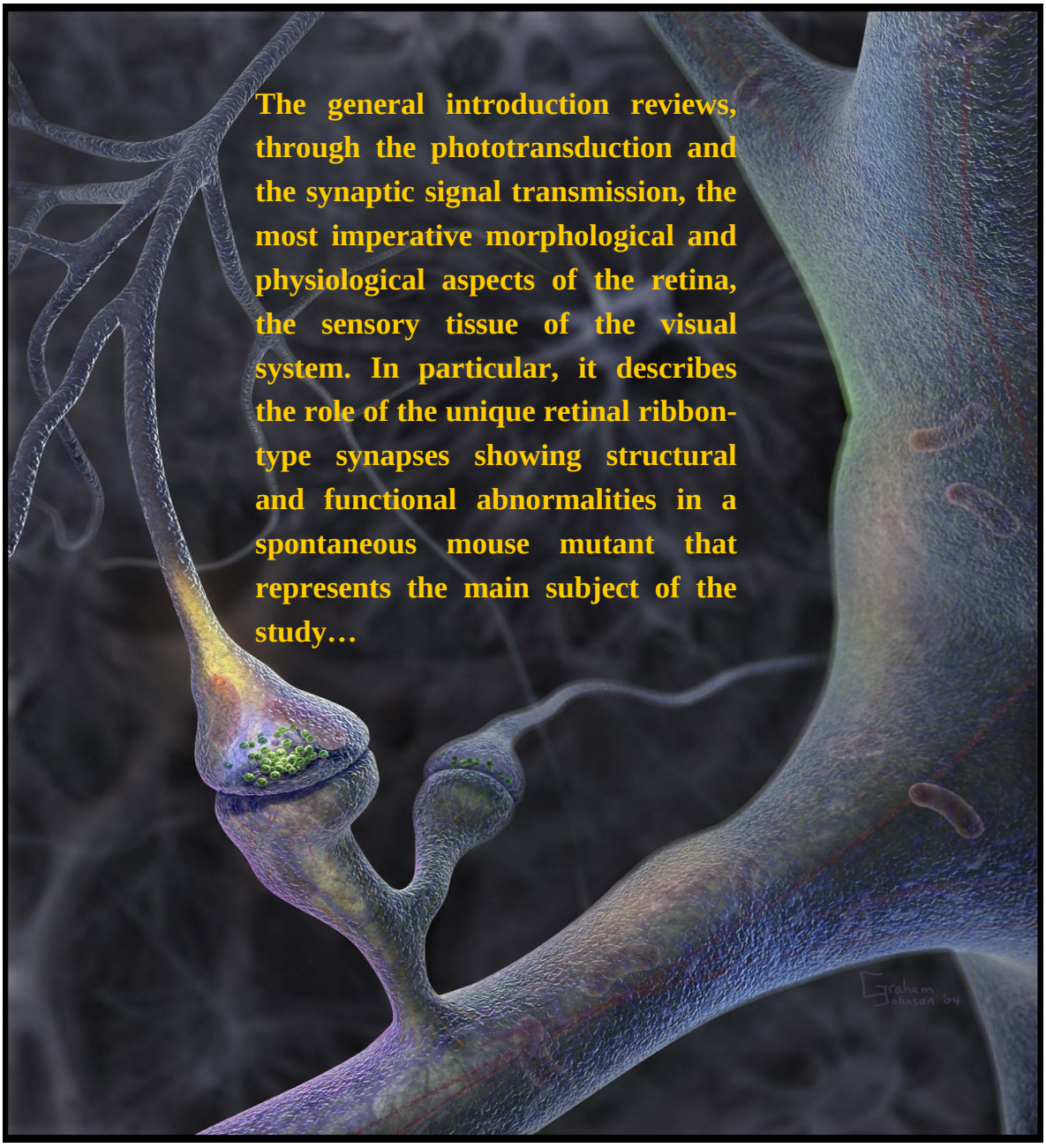

The general introduction reviews, through the phototransduction and the synaptic signal transmission, the most imperative morphological and physiological aspects of the retina, the sensory tissue of the visual system. In particular, it describes the role of the unique retinal ribbon-type synapses showing structural and functional abnormalities in a spontaneous mouse mutant that represents the main subject of the study…

General Introduction

1. General Introduction

1.1. Anatomy of the Mammalian Retina

The receptive key structure of the visual system constitutes a delicate innermost neuronal tunic surrounding the eye's interior surface (Fig. 1). Well-known as the sensory retina, it represents an extension of the brain and acts anatomically and physiologically as an outpost of the central nervous system. Involving a unique class of modified photosensitive neurons, the photoreceptors, it transduces light stimuli in a biochemical reaction cascade into electrical signals and relays them along the optic nerve to the visual cortex of the brain.

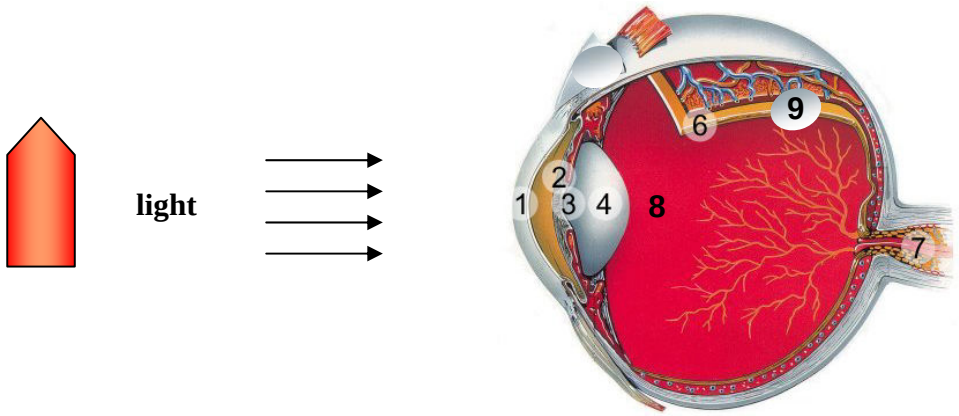

Figure 1. Representative scheme of the human eye. In a series of dioptric mechanisms, an accurate inverted image of an external object is thrown on the neural retina. Thereby, light reflected from the respective object passes through a refracting surface, termed **cornea** (**1**), providing 2/3 of the eye focusing power. The light further ingresses the **pupil** (**3**), a circular opening in the **iris** (**2**), and penetrates a crystalline **lens** (**4**), converging the entering light rays to a nodal point immediately behind the lens. Successively, the light disperses through the **vitreous humor** (**8**) and becomes projected onto the neural **retina** (**6**). A slight elevation in the central retina marks the area of entrance of the **optic nerve** (**7**). A **pigmented epithelial lamina** divides the neural retina from an outermost vascular network at the eye's backside (**9**) (www.fightforsight.org.uk/htm/research/anatomy_eye.html).

At the morphological level, a monolayer of retinal pigment epithelium separates the neural retina from an outer choroidal vascular system (Fig. 1). Interior, pigment epithelium cells extend tiny microvilli from their apical membrane, which surround the outer third of the photoreceptor ciliary outgrowths, the outer segments (Fig. 2). The retinal pigment epithelium sustains continuous photoreceptor renewal, an ongoing process in which the outer segments are shed, consumed and digested. Daily, 10% of the outer segments experience phagocytosis at their tips. The retinal pigment epithelium secretes growth and trophic factors required for photoreceptor survival and acts as a transporting tissue that moves nutrients, waste products, and oxygen between the choroidal blood vessels and the retina. In the visual cycle, it participates in the regeneration of the photoreceptor photosensitive pigments.

In the outermost retina, the photoreceptors constitute the first-order neurons and comprise two distinct receptor types, conical cones and cylindrical rods (Fig. 2). The conical cones may be of 50 µm length and 1.0 to 4.0 µm in diameter. Cylindrical rod photoreceptor bodies extend to approximately ~40 µm in length and ~1 µm in diameter. Both photoreceptor types subdivide morphologically in outer and inner segments. The outer segments establish compartments of the phototransduction cascade. They raise invaginations of their cell membranes creating 500-2000 interior stacks of highly ordered membranous disks which impart extended surface area for light absorption. Photosensitive pigments penetrate those disks as transmembrane proteins and participate in the initial steps of the phototransduction transforming external light into chemical energy[1-3]. The photoreceptor inner segments assemble to the outer segments by a thin ciliary axoneme, the connecting cilium, responsible for vectorial translocation of photosensitive pigments and metabolic exchange. The inner segments themselves constitute intracellular

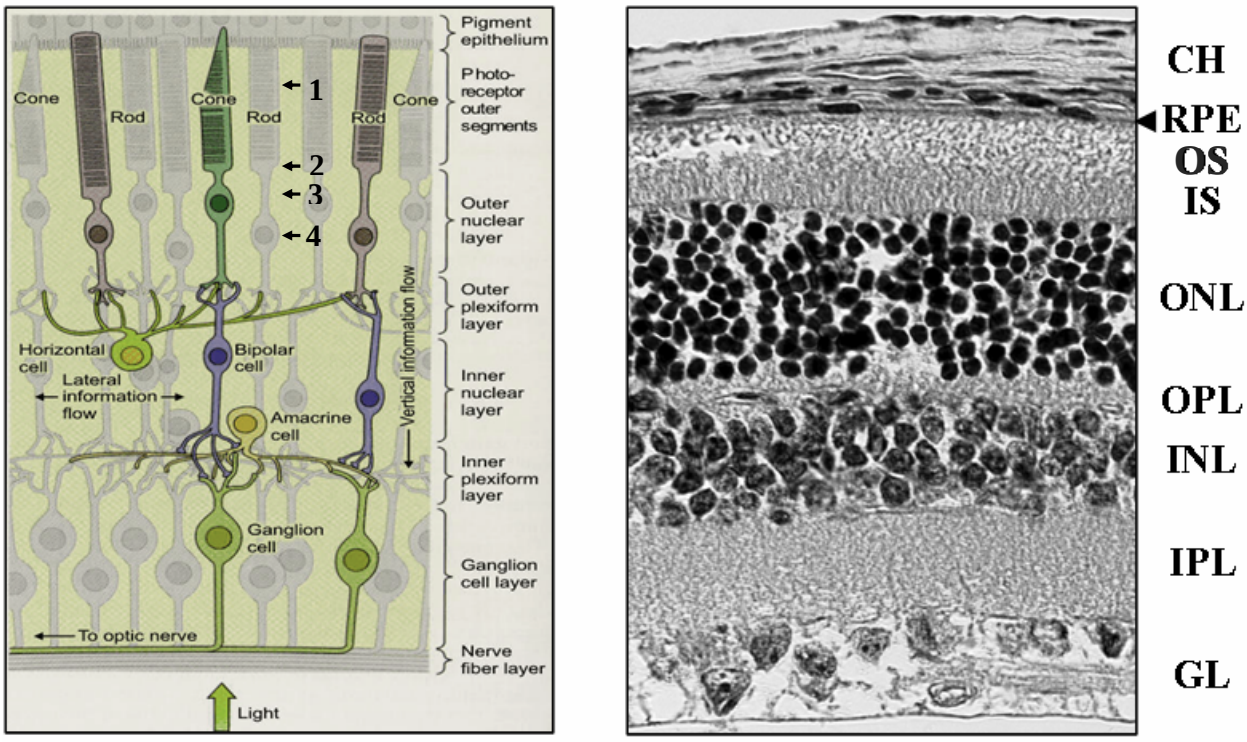

Figure 2. Cellular and structural organisation of the retina. Schematic representation (**left**). Photoreceptor outer segments (**1**), connecting cilium (**2**), photoreceptor inner segments (**3**), photoreceptor nucleus (**4**). Cross section through a representative mouse retina (**right**). At the exterior site, choroidal network (**CH**) surrounds the retina. The retinal pigment epithelium (**RPE**) faces the photoreceptor outer segments. The neural retina itself consists of seven major layers, the photoreceptor outer segments (**OS**), photoreceptor inner segments (**IS**), the photoreceptor outer nuclear layer (**ONL**), synaptic outer plexiform layer (**OPL**), inner nuclear layer (**INL**), synaptic inner plexiform layer (**IPL**) and the ganglion cell layer (**GL**) (www.fz-juelich.de/ibi/ibi-1/Photoreception).

sites of extensive biosynthetic activity. They comprise the photoreceptor nuclei, which, in turn, configure the first nuclear sublayer, the outer nuclear layer (Fig. 2). The density ratios of cones to rods range from 1:200, in the most nocturnal, to 20:1 in a few diurnal species[4]. In the nocturnal mouse, the average cone density accounts for 12.400 cells/mm^2 and ~180.000 in total. The rod density is estimated to 437.000 cells/mm^2 with totally ~6.4 millions of rods. The rod photoreceptors represent thus 95-98% of all photoreceptors in mice, whereas cones constitute 3-5%. Similar distribution is found in humans[5,6]. The retinal space unoccupied by photoreceptors is filled by neuronal processes of Muller cells (Fig. 3). These cells regularly arrange adherent junctional complexes with photoreceptor segments and contribute to metabolic support and structural integrity[7-9]. The axons arising from the photoreceptor cell bodies terminate in the outer synaptic layer, the outer plexiform layer (Fig. 2). Here, rod photoreceptors associate in ovoid spherules, whereas cone axons synapse through flat pedicles with the inner retinal cells[10].

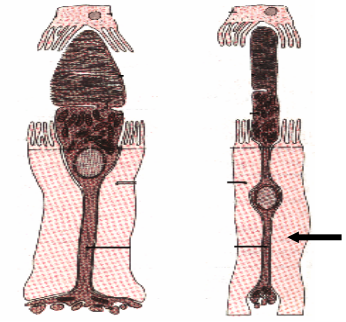

Figure 3. Schematic representation of photoreceptor synaptic terminals. Cones **(left)** form flat pedicles, whereas rods **(right)** develop ovoid spherules. Muller processes surround photoreceptors, extending from the inner segments to the synaptic axon terminals (*arrow*, www.studentenlabor.de).

The retinal second-order neurons situate in the inner nuclear layer and constitute a dense mosaic of bidirectional bipolar, amacrine, horizontal and Muller cells. The bipolar cells dominate thereby as the major morphological class and are primarily responsible for the signal transmission between the photoreceptors and the inner retina. The bipolar cells subdivide into one rod-specific and nine distinct cone-specific subtypes[11,12]. Horizontal and amacrine cells participate in the signal processing by establishing interactive circuitries networks between the photoreceptors and adjacent neurons. The axons of the second-order neurons pass through the synaptic inner plexiform layer and attach to dendrites of the third-order neurons, the ganglion cells, represented by 10 to 15 discrete morphological subclasses. The closely located ganglion cell nuclei compose the third nuclear lamina, the ganglion cell layer. Ganglion cell axons align superficially to the nuclei and form the optic nerve fibers. These extend toward the central retina and leave the eye as the optic nerve.

1.2. Retinal Processing and Signaling Pathways

In the transition from night to day, the illumination at the earth's surface varies over 11 orders of magnitude. The daily cycle of sensitivity adjustment is managed by diurnal switching between the respective photoreceptor types. Rod photoreceptors display remarkably high sensitivity to light and reliably reflect the absorption of a single photon mediating vision at low ambient illuminations. Cone photoreceptors require quantum rates for activation and operate at elevated

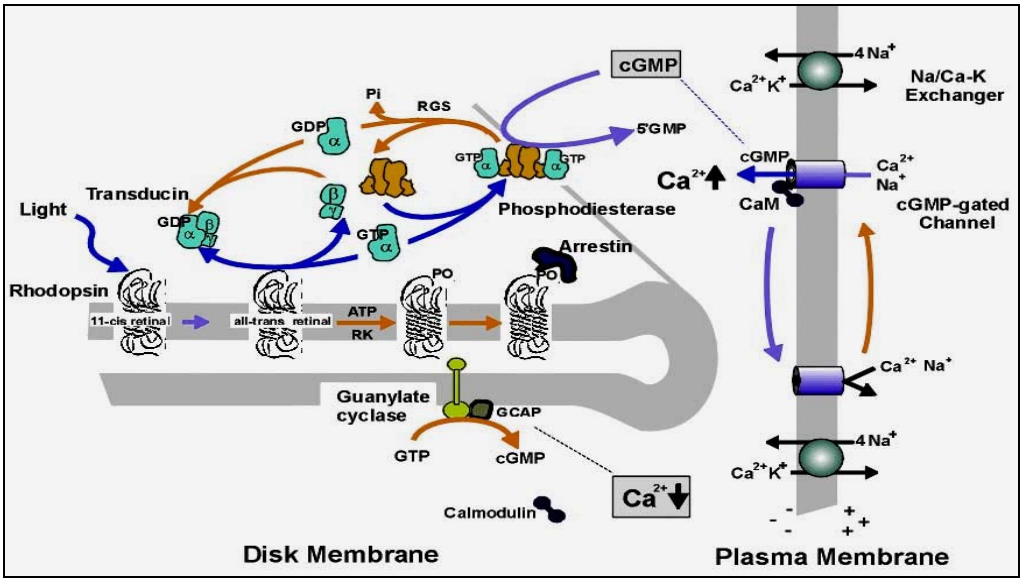

Figure 4. Phototransduction cascade in rod photoreceptors. In rods, light initiates phototransduction by the activation of **rhodopsin**, a seven pass domain membrane protein bound on the surface of the outer segment disks. Following absorption of a photon, the activated rhodopsin converts its **11-cis retinal chromophore** to an **all-trans isomer**. This reaction leads to a conformational change in rhodopsin and the activation of **transducin** (***GDPα, β, γ***), a heterotrimeric G protein composed of the α, β, and γ subunits. More than five hundred transducin molecules are activated by the photoexcitation of a single rhodopsin and contribute to the amplification of the signal generated by one photoisomerisation event. Indeed, the activated transducin dissociates into an α and β-γ transducin subunits, catalyzing GDP-GTP exchange on the α subunit and producing an active transducin α* isoform. Association of GTP with transducin triggers the release of active rhodopsin that continues transducin activation. These processes constitute the first amplification step in the phototransduction cascade. Two released α* transducin subunits contact and activate the **phosphodiesterase** enzyme stimulating the hydrolysis of the **cyclic GMP** (**cGMP**) to **5'-GMP**. An activated phosphodiesterase possess substantial catalytic power, as it hydrolyses ~4200 cGMP molecules in a second. Thus, this amplification attains reaction kinetics near those which are controlled by diffusion. Reduction of the cytoplasmic cGMP concentration leads to the closure of **cGMP-gated channels** and blockage of the inward flux of natrium and calcium ions, ensuing in a decline of cytoplasmic charges. Continuous release of calcium by pumps contributes further to the decrease of inner calcium concentrations inducing a hyperpolarisation of rod photoreceptor membranes[13] (www.biochem.ubc.ca/Faculty/Molday.html).

light intensities subserving daylight vision. The differences in sensitivity originate in the nature and amounts of the activated visual pigments and in discrete amplification factors of the phototransduction cascade. In this process, photons initiate complex chemical changes in these pigments resulting in hyperpolarisation of the photoreceptor membranes (Fig. 4). The resultant electrical impulse subsequently extends through the axonal surface toward photoreceptor synapses[14-17].

The spectral receptiveness of a photosensitive pigment is determined by the amino acid sequence of the respective opsin protein and the enclosed photon-activating chromophore. Whereas rod photoreceptors involve only one opsin, the rhodopsin, cones entail a family of homologous visual pigments, each of which resides within a discrete class of cones[18,19]. Those distinct cone opsins mediate color vision. Among eutherian mammals, primates posses trichromatic color vision. The most non-primate mammals, like mice, feature dichromatic color vision based on two spectral types of cones with two spectrally different visual pigments, the short-wave length (S) and long-wave length (L) opsins. The sensitivity maxima of the S-cones emerge in the blue to violet part of the spectrum, thus, these cones are sensitive to ultra violet light. L-cones show their absorption maxima in the range of the green light[20].

Main recipients of the photoreceptor output are the bipolar cells. They preserve a segregation of the respective signals of both photoreceptor types into two parallel vertical streams (Fig. 5). Therefore, the bipolar cells arrange functionally sign-inverting or sign-conserving synapses with the photoreceptors, termed the ON and OFF terminals, respectively[21-24]. Accordingly, dendrites of the bipolar cells either penetrate photoreceptor presynaptic membranes to form invaginating ON synapses or remain superficial establishing basal (flat) contacts, the OFF synaptic terminals. Alluding to the ON/OFF dichotomy, at least four morphological classes of correspondingly named OFF bipolar cells and six of the ON-type exist. Within the latest, one class represents a unique rod-specific type of ON bipolar neurons[21].

Functionally, ON bipolar cells depolarize in response to light. In the dark, the photoreceptors tonically release the neurotransmitter glutamate to their postsynaptic partners[25]. The postsynaptic membranes of the ON bipolar cell dendrites exploit the high-affinity metabotropic glutamate receptor, mGluR6[26,27]. Continuous binding of glutamate by this receptor initiates a transduction cascade which results in permanent closure of adjacent non-specific cation channels[27,28]. Blockade of those channels render bipolar cells hyperpolarized and “silent”. Light-evoked hyperpolarisation of photoreceptors suppresses glutamate fusion inducing postsynaptic channel

activation and thus depolarization of the ON bipolar cells[29,30]. In contrast, OFF bipolar neurons hyperpolarize in response to light stimuli. Their dendrites express ionotrophic AMPA- and kainate-type glutamate receptors inducing sign-conserving hyperpolarisation in response to light[31,32]. The following two distinct ON and OFF circuits are thought to improve transmission of finely graded signals which cover a wide temporal bandwidth[33-35]. Both functional types of bipolar cells attach to ganglion cell dendrites in the synaptic inner plexiform layer with matching response polarities[36]. The single morphological type of rod-specific bipolar cells exhibits ON centre physiology and rarely forms synaptic contact directly onto ganglion cells[36]. The occurrence of a ganglion cell dendrite in the respective synapse of the rod ON bipolar cell accounts for roughly 0.3%[37]. Rod-specific bipolars uniquely contact bistratified amacrine cells that function as true interneurons in the signal transmission (Fig. 5)[37]. These cells transfer rod signals to existing cone circuitries through association with synaptic terminals of the cone ON and OFF bipolar cells. In fact, the cone-mediated vision evolved primarily and pre-formed a framework upon which the rod circuitries likely superimposed[36]. This arrangement in the rod signaling pathway allowed one set of ganglion cells for the transmission of both scotopic and photopic signals to the brain.

The routes available for the propagation of rod signals are complemented by at least 2 further circuits. An alternative pathway relies on gap junction-mediated circuitries between rods and cones. Thereby, rod information is transmitted directly to cones via electrical synapses and employs the cone bipolar cells as a final conduit to the ganglion cells[38] (Fig. 5). The mammalian retina also provides a third rod signaling pathway. As an alternative, small fraction of rods (~20%) directly connects to a subgroup of cone OFF bipolar cells. Remaining rods may access to this pathway through rod-rod specific gap junctions[21,39].

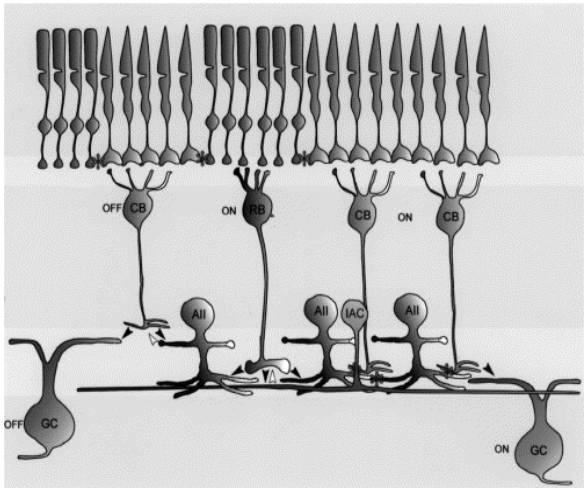

Figure 5. Main signaling pathways in the mammalian retina. The scheme emphasizes segregation of the visual information into ON and OFF streams. The respective ON bipolar cell axons terminate in the inner half and those of the OFF bipolars in the outer half of the inner plexiform layer. Both bipolar cell classes associate with ganglion cells preserving established polarity. The most straightforward rod pathway is rod to rod bipolar cells to amacrine cells to ON- or OFF-centre of cone bipolar cell axon terminals to ON- or OFF-centre ganglion cells. (∗) Gap junction between rod and cones[36].

1.3. Structural and Functional Properties of Retinal Ribbon Synapses

Chemical synapses and gap junctions are the two major classes of intercellular connections occurring at the interface between retinal neurons. Whereas gap junctions represent archaically structured electrical cell-cell contacts, chemical synapses constitute highly organized synaptic complexes which involve quantal neurotransmitter release for intercellular communication.

In conventional chemical synapses of the central nervous system, an action potential of fixed amplitude lasts few milliseconds and triggers a rapid and transient burst of vesicle fusion. Retinal neurons operate with finely graded alterations in membrane potentials to transmit sensory information over a broad dynamic range of light intensities. The continuous adjustment of the synaptic output to changes in the incoming signals is predominately sustained by a specialized subclass of chemical synapses, the ribbon-shaped synaptic terminals.

In the mammalian retina, ribbon-shaped synaptic complexes precisely translate variations in the amplitude of entering electrical signals into strict linear alterations in the rate of synaptic vesicle fusion. These synapses are arranged by both photoreceptor types, rods and cones, as well as by 80% of ON and 20% of OFF bipolar cell terminals[40-45]. In the outer plexiform layer, usually the

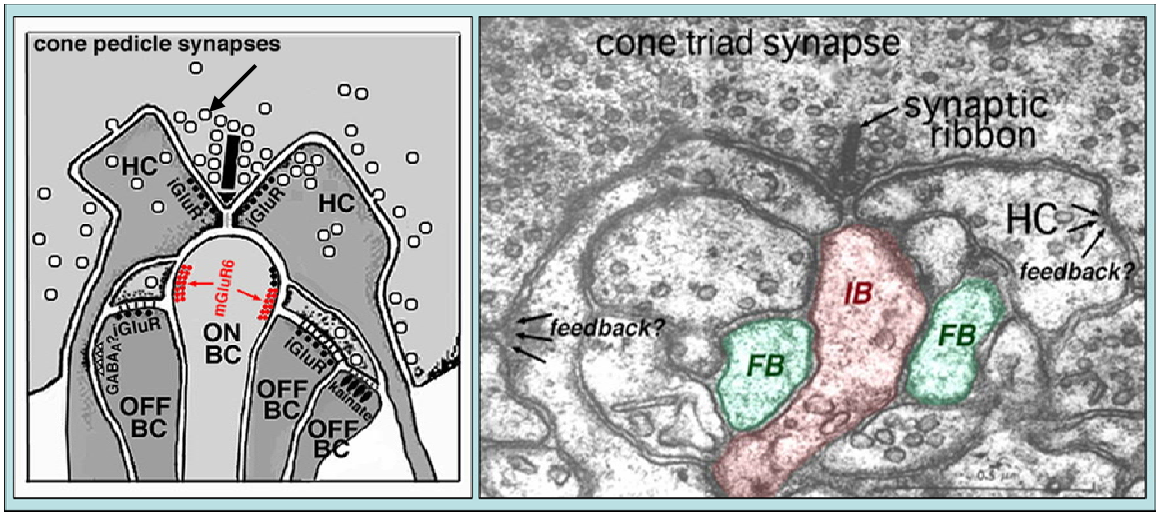

Figure 6. Anatomical organization of a cone ribbon synapse. Schematic representation (**left**). Dendritic tips of an ON bipolar (**ON BC**) and paired horizontal (**HC**) cells form invaginating contacts with the presynaptic membrane of a cone pedicle, called triad. At the ribbon synapse, the synaptic ribbon enveloped by a halo of synaptic vesicles is situated in the invagination ridge. The mGluR6 receptors of depolarizing ON bipolar cells are emphasized in red. OFF bipolar cells (**OFF BC**) adjust beneath to the ribbon synaptic complex through conventional basal contacts. Ionotrophic and kainate receptors of OFF bipolar cells are indicated in black. Electron micrograph of a cone ribbon synapse (**right**). Invaginating ON bipolar cell (**IB,** *red*), horizontal cell (**HC,** *gray*) and OFF bipolar cell (**FB,** *green*) are displayed (http://webvision.med.utah.edu).

presynaptic terminal of a rod photoreceptor associates postsynaptic dendrites of a rod-specific ON bipolar and two horizontal cells (Fig. 6). These postsynaptic processes are accommodated within an invagination of the presynaptic rod membrane and form the ribbon synapse-characteristic triad[45]. The extended cone presynaptic membrane allows the arrangement of up to 20 triads increasing the number of participating second-order neurons. In the synaptic inner plexiform layer, axon terminals of bipolar cells establish ribbon-type synaptic complexes, termed dyad, consisting of postsynaptic processes of two amacrine or an amacrine and a ganglion cells[37]. Besides retinal neurons, sensory hair cells of the cochlear and vestibular systems as well as the pinealocytes, electroreceptors, lateral line receptors of fishes, and several invertebrate neuromuscular junctions are found to synapse through ribbon-type complexes[46-50].

At the ultrastructural level, ribbon synapses are characterized by the presence of a unique presynaptic structure, the synaptic ribbon (Fig. 6, 7). These organelles rise from the presynaptic membrane as electron-dense bars in the vertical orientation over a hollow-like matrix, the arciform density, which defines the location of the synaptic active zone, the site of neurotransmitter release. Ribbon organelles assume varying profiles within cell types of the retinal tissue and in homologous retinal neurons across species. In the retina, they additionally experience diurnal alterations in shape and size in response to changes in ambient illuminations[50]. Cone photoreceptor synapses entail several ribbon structures, whereas rod photoreceptor terminals generally enclose one single synaptic body, in accordance to the number of arranged triads. In three dimensions, photoreceptor ribbons arise as flat plates of ~35 nm in thickness, up to ~1.0 µm in height and of ~1-2 µm in length. Ribbon bodies of the bipolar cells appear much smaller with a height of ~0.15-0.25 µm and a length of ~0.35 µm[51]. The ribbon surface is surrounded by numerous synaptic vesicles with diameters of ~40-45 nm, attached through ~1-5 thin filaments each. These tethers represent slender proteinaceous fibers up to ~50 nm long and ~8-10 nm in diameter[52]. At the molecular level, ribbon organelles lack delimiting membrane and are composed of largely unknown osmiophilic proteinaceous material (Fig. 7). Ribeye, a protein of 120 kDa, was identified to localize exclusively to synaptic ribbons and to constitute the major fraction of the ribbon central scaffold. Approximately 4000 Ribeye molecules participate in the composition of a single ribbon[53]. The synaptic body demarcates the arciform density complex positioned over a specialized depression in the presynaptic membrane, called the synaptic ridge[54]. Ultrastructurally, the arciform density is characterized as an electron-dense meshwork of cytoskeletal filaments intimately associated with the plasma membrane[55]. This cytoskeletal

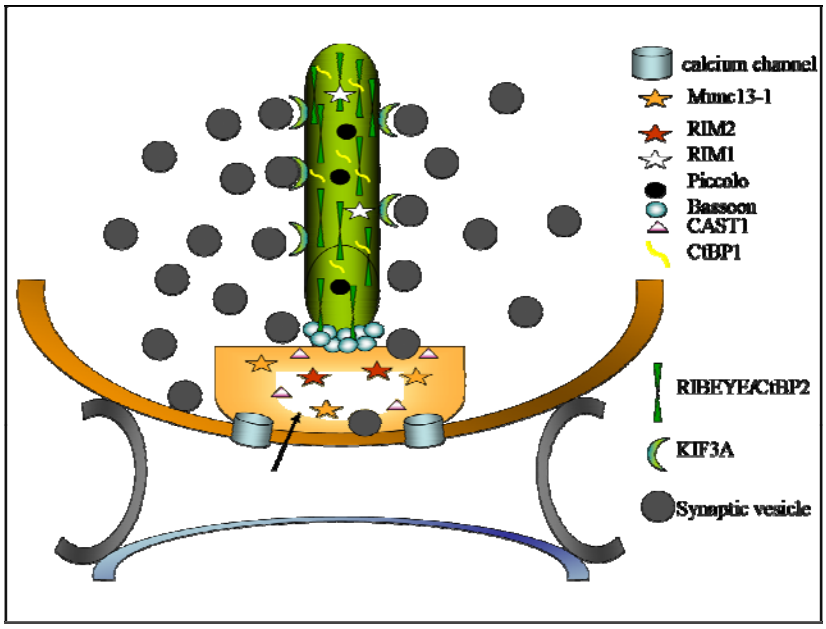

Figure 7. Structural organization of the ribbon organelle. Ribeye, Piccolo/Aczonin, CtBP1/Bars, Rim, kinesin II (Kif3A), Munc13-1, CAST1 and CtBP1 proteins (see legend) were detected to be involved in the composition of the presynaptic ribbon complex. RIBEYE/CtBP2 represents the matrix component of ribbon bodies (*green cylindrical* form). Bassoon locates at the base of the ribbon lamina and is crucial for their anchoring at the active zone (*brown*). A direct interaction between the Ribeye and Bassoon is responsible for the physical integrity of ribbons at synaptic active zones. Voltage gated L-type calcium channels are concentrated in the synaptic ridge underlying the arciform density (*orange* area indicated by an *arrow*). The electron dense synaptic ribbon is surrounded by a halo of synaptic vesicles. Postsynaptic membranes of invaginating processes (*blue* and *gray*) are involved in the schematic representation[10].

matrix regulates the mobilization of synaptic vesicles tethered at ribbons and plays a fundamental role in defining neurotransmitter release sites and maintaining them in register with the postsynaptic reception apparatus. Both structural proteins, Bassoon and Piccolo, are highly concentrated at the arciform density and probably serve as scaffolding components[10,56,57]. Bassoon, a several thousand amino acids long protein, appears to be crucial for maintaining the orientation of ribbon bodies in relation to other synaptic structures[57]. Piccolo likely binds calcium and play an important role in synaptic endocytosis, the process of synaptic vesicle recycling[58]. Kif3A, a member of the kinesin superfamily and component of the kinesin II motor protein holoenzyme, localizes with ribbons, however, its function in vesicle movement so far lacks evidence. Rim molecules, putative Rab3-interacting proteins, were detected in the arciform density complex and trigger vesicle movement[59-61]. In the membrane of the synaptic ridge, high voltage-gated L-type calcium channels are specifically concentrated in closed relation to ribbons[62,63].

The proximity of ribbon bodies to the active zone and the close association with vesicles indicate their instrumental role in the control of vesicle traffic. They potentially act as high capacity "anchor sites" for the synaptic vesicles. The most widely discussed function regards ribbons as conveyer-belts that translocate synaptic vesicles towards fusion zones[64]. In the conveyor-belt model, ribbons are assumed to be involved in recruitment of synaptic vesicles from the surrounding cytoplasmic space and to subsequent supply them to the exocytosis sites of an activated synapse. Once at the active zone, vesicles fuse with the plasma membrane to void their content into the synaptic cleft. After fusion, synaptic vesicles undergo quick retrieval back into the terminal and complete refilling with neurotransmitters. Reentering of empty vesicles must be prevented from engaging in exocytosis until they become refilled. Likely, vesicles filled with neurotransmitters can be selectively absorbed by the ribbon surface. Thus, ribbon bodies may further act as discriminatory vesicle capturers. Consequently, ribbons may substantially aid to high-efficiency neurotransmitter release for prolonged times[65]. Under physiological darkness conditions, photoreceptor ribbon synapses, indeed, tonically release transmitter into the second-order neurons at the highest rates[25,66]. Release from cone terminals of a turtle retina is estimated to 20-80 vesicles/ribbon/sec[67,68]. Mammalian rods continuously release at rates of 80-100 vesicles/ribbon/sec[54]. Cones involve the fusion of ~18 vesicles/ribbon/sec[25,69,70]. Light-induced hyperpolarisation suppresses the release of neurotransmitter at photoreceptors corresponding to illumination intensities and may completely subside release at saturating light conditions[36].

To remain operational, ribbon synapses are associated with a larger readily releasable pool of the vesicle population than conventional synapses. The giant bipolar terminal of the goldfish retina (up to ~10 µm) has as many as 1 million vesicles[51]. Cone terminals of a turtle retina with a diameter of ~6 µm comprise approximately ~250.000 synaptic vesicles[49,68,71]. A mammalian rod with a synapse of 2-3 µm in diameter numbers 8.000-27.000 synaptic vesicles within the terminal cytoplasm[72]. In the mammalian photoreceptors, ~700 vesicles from the total pool are constitutively attached to the ribbon surface and all constitute the releasable pool at each time point, regardless of their proximity to the active zone[73]. In contrast, in conventional synapses the total pool in the cytosol does not exceed 200 vesicles. A single action potential elicits the fusion of 1-3 vesicles and the synapse stops transmission after prolonged stimulation when the readily releasable pool of ~10 vesicles depletes[74].

Vesicle fusion at ribbon synapses follows calcium-dependent exocytosis and is specifically modulated by the activity of high voltage-gated L-type calcium channel complexes. At darkness, the membrane potential of the photoreceptor synapses stabilizes to approximately -40 mV and

allows the activation of these channels. The continuous dark calcium current stimulates steady glutamate release and the deactivation of the second-order neurons. The calcium ions entering through these channels increase thereby the ambient calcium concentration around the ribbons and induce release of vesicles from their tethers[75]. At sustained rise in the intraterminal calcium at darkness, vesicles at the highest position sense elevated calcium concentrations and fuse with their neighbor vesicles beneath to form vesicle chains, effectively participating in a wave of compound exocytosis[76]. The absorption of a single photon induces a re-hyperpolarisation of ~1 mV. The L-type calcium channels are able to faithfully track such small voltage change in membrane potentials and impart them to the synaptic vesicle release machinery. In this manner, they suppress inward calcium currents and elicit submicromolar alterations in calcium concentrations recognized by the fusion apparatus. At higher light intensities, photoreceptor hyperpolarisation induces an advanced closure of calcium channels. In consequence, photoreceptor synapses diminish the rate of neurotransmitter release to a variable degree as a function of the intensity of incident light stimuli.

Light moves the membrane potentials in the operating range of -40 to -70 mV. The L-type calcium channels smoothly regulate calcium entry in this voltage interval. Between the dark membrane potential and light-induced hyperpolarisation to more than - 55 mV, the calcium concentration in the presynaptic space may vary in the range of 0.3 to 2.0 µM. In bipolar cells, calcium levels must exceed 10 µM to evoke release[75].

The population of L-type calcium channels per an active zone and ribbon is estimated to amount ~500 complexes, with an average density of 460/µm^2. However, ~8 channels are constitutively activated at darkness to mediate the maximal tonical calcium influx into the synaptic terminal. The low number or effectively activated calcium channels results due to slow calcium- and voltage-dependent inactivation of the remaining calcium channels with a minimal inactivity time constant of 4.6 sec[51,77]. High number of the L-type calcium channels at ribbon synapses appears thus crucial to sustain tonic neurotransmitter release. Comparably, conventional synapses display considerably lower densities of 1 to 55 calcium channels per µm^2 [37,78].

The calcium-dependent exocytosis apparatus of ribbon synapses involves evolutionary conserved protein complexes, termed SNARE, NSF and SNAP, that are employed in all eukaryotic vesicle-based membrane traffics[79-81]. In the respective protein networks, only minor differences are found between conventional and ribbon synapses. This emphasizes the uniqueness of ribbon-shaped synapses relying on the occurrence of the ribbon body structures[82].

1.4. Structural Organisation of High Voltage-gated L-type Calcium Channels

At the molecular level, synaptic L-type calcium channels represent heteromeric protein complexes composed of the pore-forming α1 subunit found in association with the accessory subunits of the α2δ-, β- and γ-type (Fig. 8). The α1 subunit incorporates alone the voltage sensor and the gating apparatus, whereas the modulatory subunits influence the voltage-dependence, activation/inactivation kinetics and membrane trafficking of the α1 subunit. The mammalian L-type calcium channel complexes encompass four distinct α1 subunits, α1C, α1D, α1F and α1S.

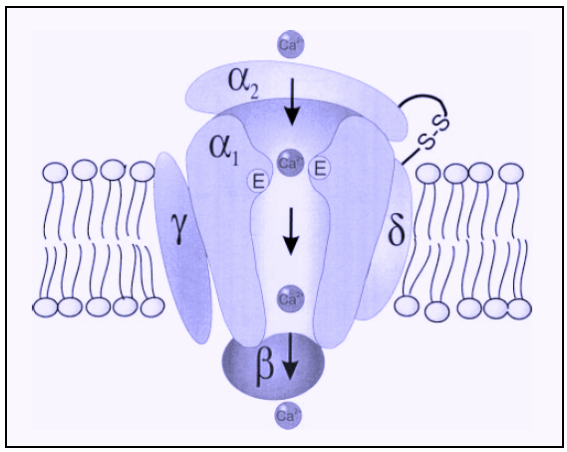

Figure 8. Structural organization of a calcium channel. The α1 subunit represents the pore-forming protein comprising 3 auxiliary subunits, the α2δ, β and γ subunits. Calcium ions within the pore are positioned by four glutamic acid residues (*E*), arranged in asymmetric configuration[83,84].

The α1C, α1D and α1F are expressed in the retina and participate in signal processing[85,86]. Thereby, the α1F constitutes a retina-specific subunit predominately found in rod ribbon synapses[87]. Each of the α1 encoding genes produces several protein products by alternative splicing. Four different genes were found to encode the β subunit, termed β1, β2, β3 and β4. Through alternative splicing, at least eight different β proteins have been detected. Thereby, the β2 subunit was identified to be crucial in photoreceptor synaptic transmission[88]. The α2δ subunit is represented by at least four homologues. It is encoded by a single gene posttranslationally cleaved into the α2 and δ peptides, subsequently linked via disulfide bridges (Fig. 8). The α2 subunit is entirely extracellular, whilst the δ subunit penetrates the plasma membrane and anchors via a transmembrane segment. The γ subunit coded by at least 10 distinct genes may be absent from a calcium channel complex[89]. Structurally, it comprises a transmembrane protein. The function of the α2δ and γ auxiliary subunits in the retinal signaling remains so far unknown.

1.5. Structural and Functional Alterations of Retinal Ribbon Synapses due to Genetic Defects

Structural and functional alterations of the ribbon-shaped synapses may severely affect processing of the visual information and lead to photoreceptor dystrophies. **Ribeye** deficiency in zebrafish was shown to profoundly alter retinal ribbon structure and to result in loss of retinal activities. Thereby, physiological examinations implied severe reduction in photoreceptor ribbon number and size[90]. Morphological characterisation of the ***Bassoon*** knockout mouse revealed lacking association of the retinal ribbon organelles with the presynaptic membranes. These structural changes underlined defective photoreceptor signal transmission in the *Bassoon* mutants[57]. ***Synaptojanin1****,* a ubiquitously expressed protein of the exocytosis machinery, was shown to be involved in regulation of the vesicle cycle and also in anchoring of ribbons in zebrafish[91,92]. A mutation in *synaptojanin1* was demonstrated to correlate morphologically with a detachment of ribbons from the active zones and to affect vision to the extent of complete blindness in the zebrafish mutants.

In the retina of ***Cacn2b***-knockout mice, the L-type calcium channel subunit β2 was eliminated from the retinal tissue[88]. The phenotype displayed complete lack of functional calcium channels and severely affected morphology of photoreceptor ribbon-shaped synapses.

Molecular defects of the human α1F subunit, ***CACNA1F***, are associated with the incomplete form of congenital stationary night blindness (iCSNB) and cone-rod dystrophies[93,94]. In the mouse model for human *CACNA1F*-mediated iCSNB, profound failure of ribbon synapse development was observed. Loss of α1F calcium channel complexes in those mutants was associated with complete blindness due to dysfunction in the cone-rod-specific processing pathway[95].

The ***CaBP4*** gene, a photoreceptor-specific member of the subfamily of neuronal calmodulin-like calcium-binding proteins (CaBPs), is essential for the development and maintenance of the mouse photoreceptor synapses[96]. The CaBP4 protein modulates the activity of synaptic L-type calcium channel complexes, predominately of those including retina-specific α1F main subunits. In *CaBP4*-deficient mice, electrophysiological recordings revealed attenuated responses of the secondary neurons indicating functional changes of the synaptic apparatus. Anatomically, the photoreceptor axon terminals in *CaBP4*-mutant mice were considerably disrupted and reduced in number. In addition, structural abnormalities of synaptic ribbons were observed[96].

Myosin Va constitutes an actin-based motor protein that belongs to the family of unconventional myosins[97]. The mouse model harbouring a mutation in this gene shows severe defects in retinal synaptic transmission[98]. Ultrastructurally, abnormal morphological profiles of ribbon organelles in rod photoreceptors are evident, suggesting the role of *Myosin Va* in the regulation of the ribbon body structure.

The cytoplasmic ***RIM1*** protein clusters around the ribbon organelles and is supposed to suppress vesicle fusion at ribbon synapses[99]. Mutations in human *RIM1* were implicated in cone-rod dystrophies[99,100]. Another gene underlying a cone-rod dystrophy in humans is caused by genetic defects in the synaptoplasm protein, **HRG4**, that was shown to predominately associate with synaptic vesicles[101]. The function of this gene remains elusive, however, it is highly enriched at photoreceptor synapses and probably involved in regulation of pro-apoptotic protein expression[102]. The mouse model for human *HRG4*-mediated cone-rod dystrophy exhibits severe degeneration of the photoreceptor axon terminals, which is accompanied by profound alterations in composition of mitochondrial membrane proteins and upregulation of apoptosis factors in photoreceptor synapses[102].

Mutations in postsynaptic proteins are mainly associated with functional rather than structural defects of ribbon-type synapses. One of the corresponding mouse models carries a spontaneous mutation in the ***Nyx*** gene that encodes a leucine-rich extracellular synaptic matrix protein, potentially localizing to the postsynaptic dendrite membranes of ON bipolar cells[103]. Several mutations in the orthologous human gene, ***NYX***, lead to the complete form of congenital stationary night blindness (cCSNB)[93,104]. In the *Nyx* mutant mice as well as in CSNB patients, electrophysiological photoreceptor-specific responses retain normal amplitudes, indicating sustained phototransduction activities. However, profound loss of rod bipolar cell activity suggests lack of responsiveness to glutamate. Similar phenotype manifests a naturally occurring mouse mutant comprising a mutation in the ***mGluR6*** gene, encoding a postsynaptic glutamate receptor. In the human orthologue, ***GRM6***, mutations were recently reported to underlie cCSNB[105]. Yet, despite apparent functional failures, absence of both Nyx and mGluR6 proteins is not accompanied by abnormal synaptic morphology[106,107].

1.6. Abnormalities of Retinal Ribbon Synapses in C57BL/10 Mice

An astonishing phenotype of retinal ribbon-shaped synapses was identified in a substrain of C57BL/10 mice[108]. Thereby, affected animals were randomly discovered by conventional electrophysiological examinations based on electroretinographic recordings (ERG) (Fig. 9A).

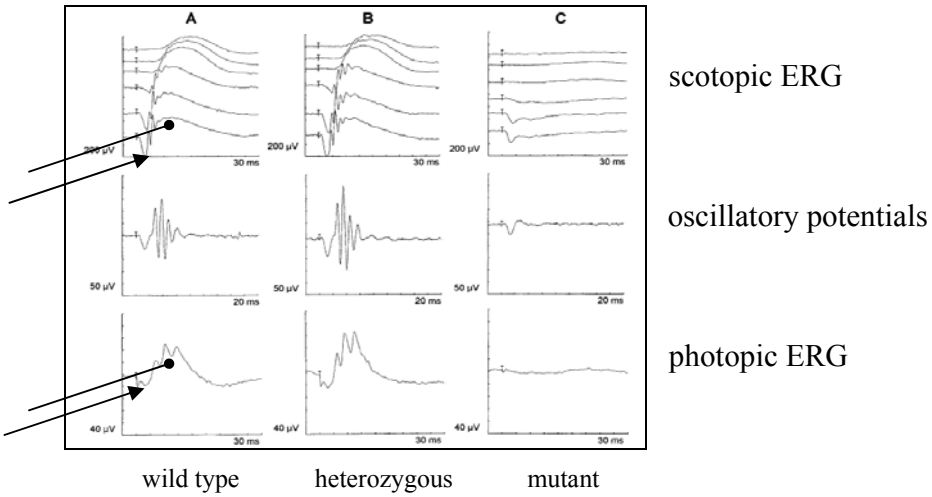

Figure 9. Electroretinographic examinations of affected C57BL/10 mice. ERG of a wild-type (**A**), heterozygous (**B**) and an affected animal (**C**). Graphic representations at the top represent scotopic electroretinography. Middle panel indicates oscillatory potential recordings. At the bottom, photopic electroretinographic responses are shown. The respective negative a-wave is marked with a head *arrow*, the positive b-wave with *point-head line*[108].

The scotopic electroretinography, performed upon dark adaptation, reflects retinal responsiveness of the rod-specific signaling pathway. Thereby, the negative scotopic a-wave indicates specific activities of the rod photoreceptors due to light stimuli. The following scotopic b-wave specifies responses of postphotoreceptoral neurons communicating with the respective activated rods. In the scotopic electroretinography of affected C57BL/10 mice, a considerable reduction of the a-wave amplitudes and complete loss of the b-wave were observed (Fig. 9C). The predominant absence of the scotopic b-wave strongly indicated defective signal transmission between rods and the second-order neurons. In addition, oscillatory potentials representing the activities in the synaptic inner plexiform layer were severely altered. This again suggested perturbed signal transfer into the inner retina[108]. In the light-adapted photopic electroretinography, the corresponding negative a-wave represents the activities of cone photoreceptors upon light-induced saturation of the rod system. The subsequent positive photopic b-wave features the responses of the cone system specific second-order neurons. In the photopic electroretinography of affected animals, no activities were detected. This strongly implicated a cone-rod-specific dysfunction[108].

Morphological examinations revealed lack of the specific triad arrangements, formed by photoreceptor ribbon synapses and the respective invaginating postphotoreceptoral processes (Fig. 10). In the inner plexiform layer, ribbon synapses of bipolar cells display severely perturbed morphology and loss of the characteristic dyad structures. The highly ordered arrangement of cone pedicles and rod spherules was disturbed in affected retinas. The location of cone pedicles in the outer plexiform layer showed abnormal variations. In rod synapses, complete loss of ribbon bodies was observed. In cone synaptic terminals, ribbon organelles exhibited pronounced morphological alteration. They appeared in clusters lacking the appropriate vertical orientation and anchoring to the presynaptic membrane. In contrast, conventional retinal synapses did not reveal any abnormalities in mutant mice. In addition, no changes in the ultrastructure of the photoreceptor outer segments were detected. However, the number of photoreceptor nuclei was reduced by one third and might correspond to the reduced amplitude of rod photoreceptor a-wave in the rod- dominated mouse retina.

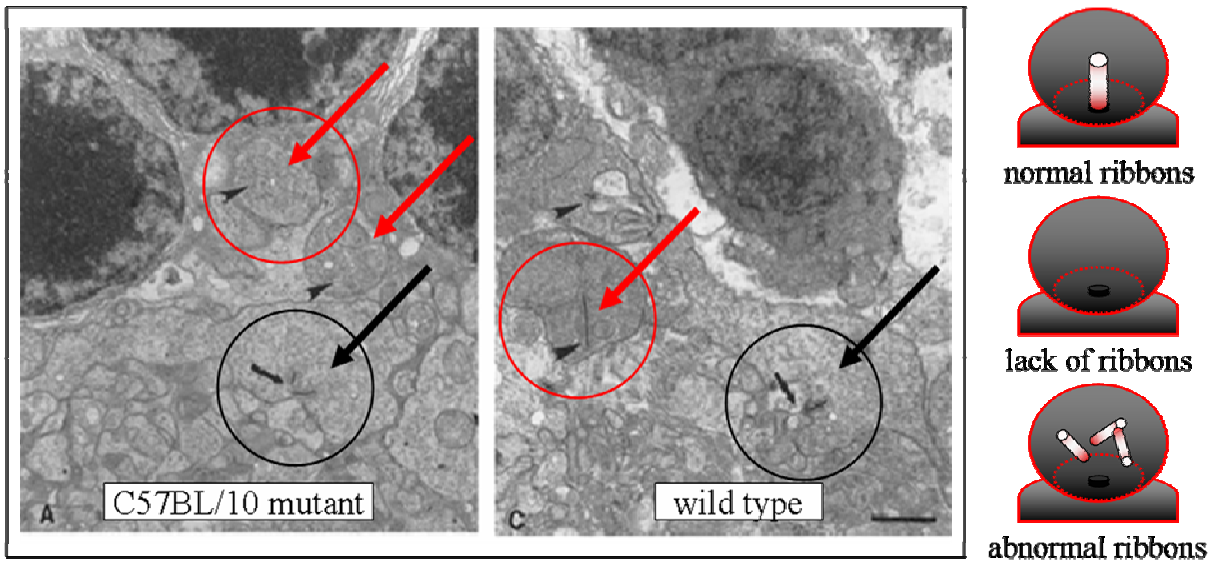

Figure 10. Abnormalities of photoreceptor ribbon synapses in C57BL/10 mutant mice. Electron microscopy (**left**). In 3-month-old affected animals, rod ribbon synapses lack their ribbons (*red circles*). In a cone pedicle, freely floating ribbons are visible (*black circles*). In comparison, normal morphology of ribbon synapses can be observed in an unaffected retina. In rod and cone synaptic terminals of a wild-type animal, single ribbons appear correctly anchored in a vertical orientation to the presynaptic membrane[108]. Schematic drawing of a ribbon body in a ribbon synapse (**right**). Normal morphology (*top*), lack of ribbons (*middle*), anomalous ribbons (*bottom*).

The view from light microscopy exhibited thinning of all retinal layers, particularly the synaptic outer plexiform layer was most severely affected (Fig. 11). The alterations observed in electroretinography were thus associated with severe morphological changes of retinal ribbon-type synapses. The overall thinning of the retinal layers as well as the reduction of photoreceptor number remained unexplained.

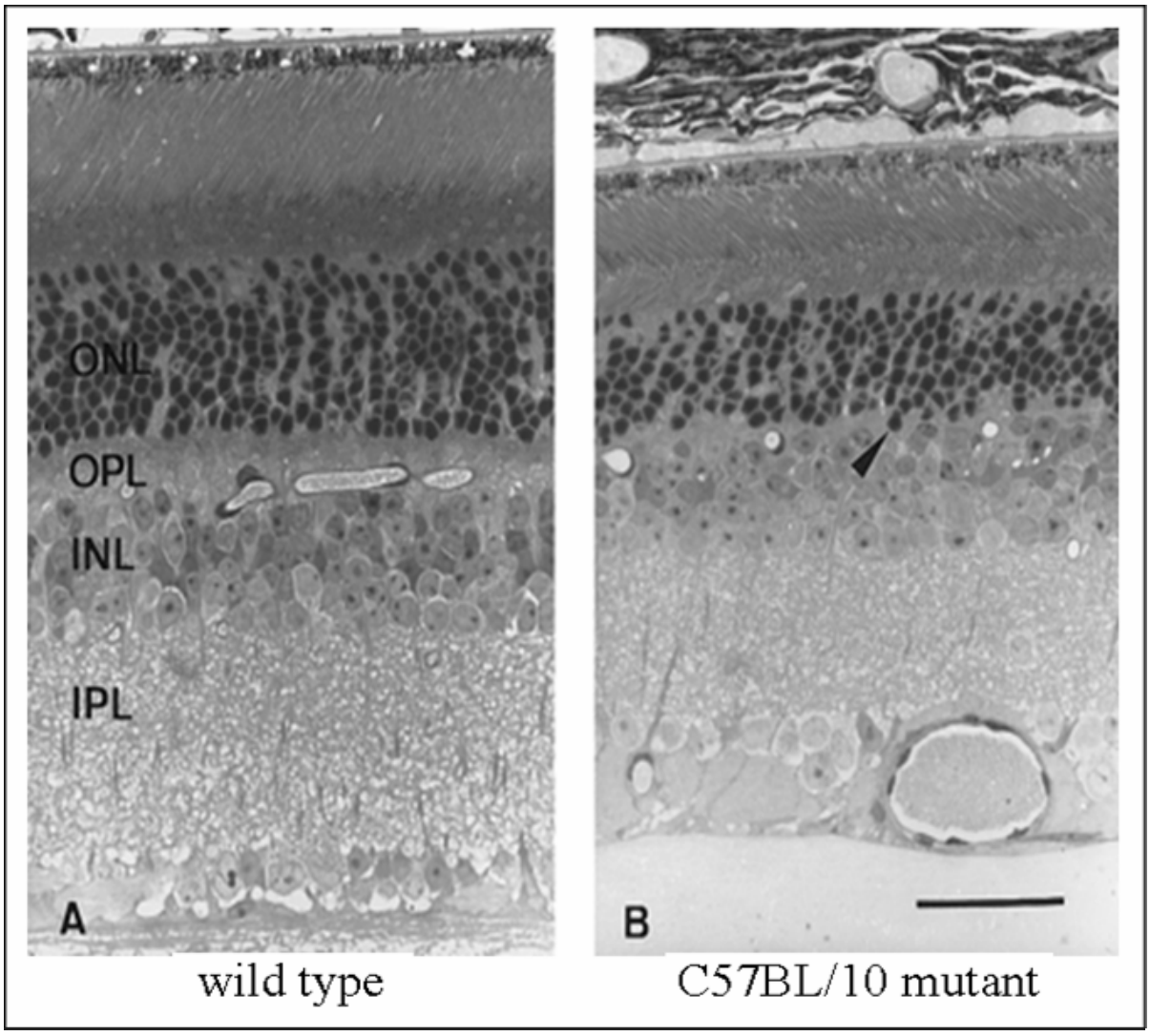

Figure 11. Light microscopic section of affected C57BL/10 retinas. Wild type (**A, left**), mutant (**B, right**). Photoreceptor outer nuclear layer (**ONL**), synaptic outer plexiform layer (**OPL**), inner nuclear layer (**INL**), synaptic inner plexiform layer (**IPL**) and the ganglion cell layer (**GL**). The photoreceptor synaptic outer plexiform layer emerges particularly reduced. Some photoreceptor nuclei dislocate into the synaptic layer (*arrow head*)[108].

Preliminary classical genetics indicated a monogenic, autosomal recessive mode of inheritance of the underlying mutation (Fig. 12). In the preceding linkage analysis, the mutation was localized to mouse chromosome 6 in a genetic region of 15.6 Mb. Thereby, affected female mice were

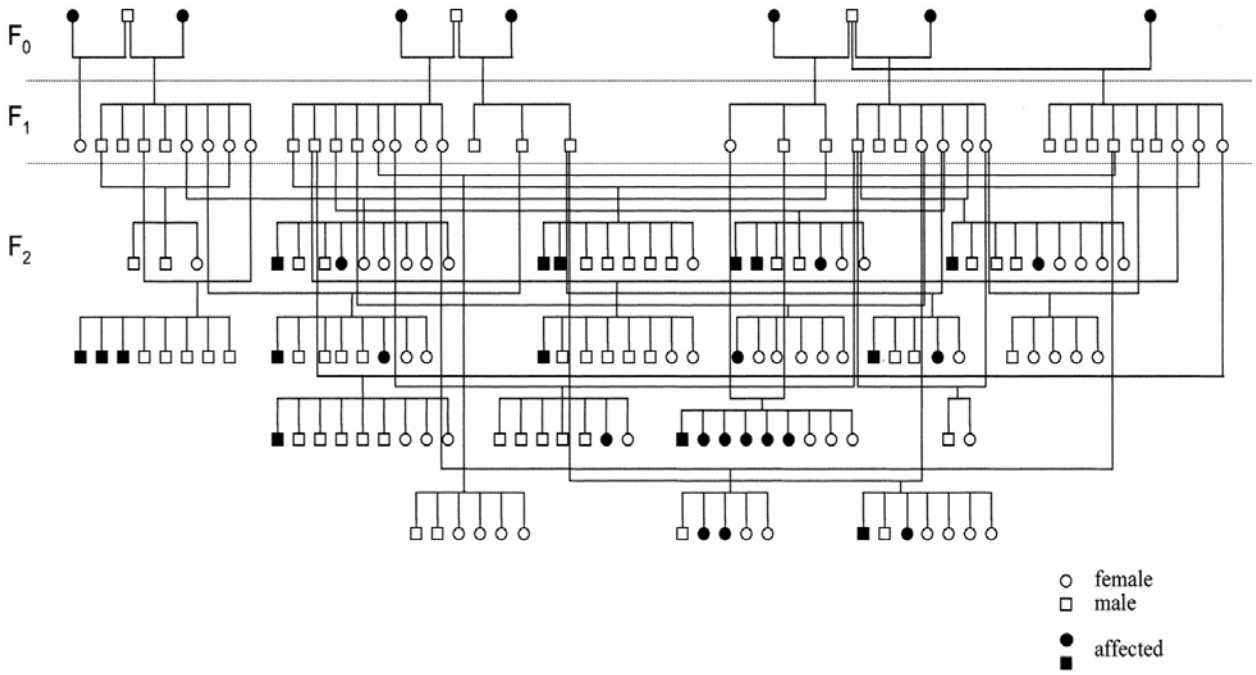

Figure 12. Pedigree of a C57BL/10 mouse population. The respective animals are indicated with circle (*female*), squares (*male*), filled (*affected*) and open (*unaffected*) symbols.

crossbred on the genetic background of a phylogenetically distinct AJ mouse strain to produce heterozygosity in polymorphic markers (Fig. 13). The F1 generation revealed uniformly heterozygous unaffected animals. The subsequently intercrossed F1 generation segregated in the following generation into affected and unaffected animals in the ratio of 25:75%, corresponding to the recessive mode of mutation transmission. Further progress in elucidation of this mutation was subject of the current study.

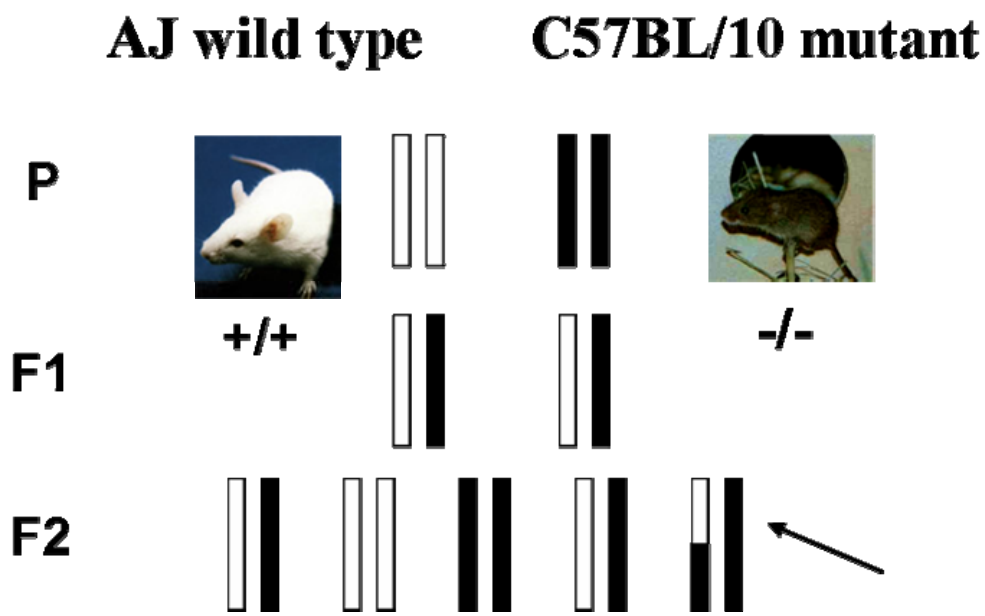

Figure 13. Schematic presentation of the animal breeding procedure for linkage analyses. Black bars demonstrate the mutation-carrying chromosome of C57BL/10 mutant mice (-/-). White bars represent the respective wild-type chromosome of the unaffected AJ strain (+/+). The homozygous parental generation (P) produces uniformly heterozygous F1 generation of unaffected animals. The subsequently crossbred F1 animals segregate phenotypically into affected and unaffected animals (F2). Among affected animals, recombinant mice appeared of particular importance for future fine mapping (indicated with an *arrow*).

1.7. References of the General Introduction

1. Applebury ML (1978) Proton Translocation - Primary Photo-Chemical Event in Vision. Bulletin of the American Physical Society 23:378-397
2. Applebury ML (1984) Dynamic Processes of Visual Transduction. Vision Research 24:1445-1454
3. Applebury ML, Hargrave PA (1986) Molecular-Biology of the Visual Pigments. Vision Research 26:1881-1896
4. Ahnelt PK, Kolb H (2000) The mammalian photoreceptor mosaic-adaptive design. Progress in Retinal and Eye Research 19:711-777
5. Peichl L, Pohl B (2000) Cone types and cone/rod ratios in the crab-eating raccoon and coati (Procyonidae). Investigative Ophthalmology & Visual Science 41:494-502
6. Peichl L, Rakotondraparany F, Kappeler P (2001) Photoreceptor types and distributions in nocturnal and diurnal Malagasy primates. Investigative Ophthalmology & Visual Science 42:48-56
7. Faude F, Biedermann B, Pannicke T, Francke M, Wiedemann P, Reichenbach A, Reichelt W (1995) Gaba and Glutamate Uptake Currents in Human Muller Cells. Investigative Ophthalmology & Visual Science 36:926-933
8. Reichenbach A, Grimm D, Mozhaiskaja N, Distler C (1995) Visualization of Muller (Retinal Glial) Cells by Bulk Filling with Procion-Yellow. Journal of Brain Research-Journal fur Hirnforschung 36:305-311
9. Reichenbach A, Siegel A, Rickmann M, Wolff JR, Noone D, Robinson SR (1995) Distribution of Bergmann Glial Somata and Processes - Implications for Function. Journal of Brain Research-Journal fur Hirnforschung 36:509-517
10. Dieck ST, Altrock WD, Kessels MM, Qualmann B, Regus H, Brauner D, Fejtova A, Bracko O, Gundelfinger ED, Brandstatter JH (2005) Molecular dissection of the photoreceptor ribbon synapse: physical interaction of Bassoon and RIBEYE is essential for the assembly of the ribbon complex. Journal of Cell Biology 168:825-836
11. Ghosh KK, Bujan S, Haverkamp S, Feigenspan A, Wassle H (2004) Types of bipolar cells in the mouse retina. Journal of Comparative Neurology 476:202-203
12. Ghosh S, Feany MB (2004) Comparison of pathways controlling toxicity in the eye and brain in Drosophila models of human neurodegenerative diseases. Human Molecular Genetics 13:2011-2018
13. Stojanovic A, Hwa J (2002) Rhodopsin and retinitis pigmentosa: Shedding light on structure and function. Receptors & Channels 8:33-50
14. Pugh EN, Lamb TD (1993) Amplification and Kinetics of the Activation Steps in Phototransduction. Biochimica et Biophysica Acta 1141:111-149
15. Sokolov M, Lyubarsky AL, Strissel KJ, Savchenko AB, Govardovskii VI, Pugh EN, Arshavsky VY (2002) Massive light-driven translocation of transducin between the two major compartments of rod cells: A novel mechanism of light adaptation. Neuron 34:95-106

16. Detwiler PB, Ramanathan S, Sengupta A, Shraiman BI (2000) Engineering aspects of enzymatic signal transduction: Photoreceptors in the retina. Biophysical Journal 79:2801-2817
17. Maeda T, Imanishi Y, Palczewski K (2003) Rhodopsin phosphorylation: 30 years later. Progress in Retinal and Eye Research 22:417-434
18. Jacobs GH, Williams GA, Fenwick JA (2004) Influence of cone pigment coexpression on spectral sensitivity and color vision in the mouse. Vision Research 44:1615-1622
19. Rowe MP, Jacobs GH (2004) Cone pigment polymorphism in New World monkeys: Are all pigments created equal?. Visual Neuroscience 21:217-222
20. Cowing JA, Poopalasundaram S, Wilkie SE, Robinson PR, Bowmaker JK, Hunt DM (2002) The molecular mechanism for the spectral shifts between vertebrate ultraviolet- and violet-sensitive cone visual pigments. Biochemical Journal 367:129-135
21. Boycott BB, Hopkins JM (1991) Cone Bipolar Cells and Cone Synapses in the Primate Retina. Visual Neuroscience 7:49-60
22. Boycott BB, Hopkins JM (1993) Cone Synapses of A Flat Diffuse Cone Bipolar Cell in the Primate Retina. Journal of Neurocytology 22:765-778
23. Hopkins JM, Boycott BB (1995) Synapses Between Cones and Diffuse Bipolar Cells of A Primate Retina. Journal of Neurocytology 24:680-694
24. Wassle H, Peichl L, Boycott BB (1978) Receptor Contacts of Horizontal Cells in Retina of Domestic Cat. Proceedings of the Royal Society of London Series B-Biological Sciences 203:247-263
25. Berntson A, Taylor WR, Morgans CW (2003) Molecular identity, synaptic localization, and physiology of calcium channels in retinal bipolar cells. Journal of Neuroscience Research 71:146-151
26. Nakajima Y, Iwakabe H, Akazawa C, Nawa H, Shigemoto R, Mizuno N, Nakanishi S (1993) Molecular characterization of a novel retinal metabotropic glutamate receptor mGluR6 with a high agonist selectivity for L-2-amino-4-phosphonobutyrate. Journal of Biological Chemistry 268:11868-11873
27. Vardi N, Duvoisin R, Wu G, Sterling P (2000) Localization of mGluR6 to dendrites of ON bipolar cells in primate retina. Journal of Comparative Neurology 423:402-412
28. Vardi N, Zhang LL, Payne JA, Sterling P (2000) Evidence that different cation chloride cotransporters in retinal neurons allow opposite responses to GABA. Journal of Neuroscience 20:7657-7663
29. Nawy S, Jahr CE (1991) Cgmp-Gated Conductance in Retinal Bipolar Cells Is Suppressed by the Photoreceptor Transmitter. Neuron 7:677-683
30. Nawy S, Jahr CE (1991) Effects of Cgmp on Light Responses of Depolarizing Bipolar Cells in Retinal Slices of the Tiger Salamander. Investigative Ophthalmology & Visual Science 32:1188
31. Rieke F, Schwartz EA (1994) A Cgmp-Gated Current Can Control Exocytosis at Cone Synapses. Neuron 13:863-873
32. DeVries SH, Schwartz EA (1999) Kainate receptors mediate synaptic transmission between cones and "off" bipolar cells in a mammalian retina. Nature 397:157-160

33. DeVries SH, Qi XF, Smith R, Makous W, Sterling P (2002) Electrical coupling between mammalian cones. Current Biology 12:1900-1907
34. DeVries SH (2005) Parallel processing at the mammalian cone photoreceptor synapse. Investigative Ophthalmology & Visual Science 46:587-593
35. DeVries SH, Li W, Saszik S (2006) Parallel processing in two transmitter microenvironments at the cone photoreceptor synapse. Neuron 50:735-748
36. Bloomfield SA, Dacheux RF (2001) Rod vision: pathways and processing in the mammalian retina. Progress in Retinal and Eye Research 20:351-384
37. Strettoi E, Dacheux RF, Raviola E (1990) Synaptic Connections of Rod Bipolar Cells in the Inner Plexiform Layer of the Rabbit Retina. Journal of Comparative Neurology 295:449-466
38. Tsukamoto Y, Morigiwa K, Ueda M, Sterling P (2001) Microcircuits for night vision in mouse retina. Journal of Neuroscience 21:8616-8623
39. Boycott BB, Wassle H (1991) Morphological Classification of Bipolar Cells of the Primate Retina. European Journal of Neuroscience 3:1069-1088
40. Lasansky A (1973) Organization of Outer Synaptic Layer in Retina of Larval Tiger Salamander. Philosophical Transactions of the Royal Society of London Series B-Biological Sciences 265:471-492
41. Derobertis E, Lasansky A (1960) Ultrastructure of Photoreceptors. Anatomical Record 136:181
42. Lasansky A (1972) Cell Junctions at Outer Synaptic Layer of Retina. Investigative Ophthalmology 11:265-273
43. Lasansky A (1971) Synaptic Organization of Cone Cells in Turtle Retina. Philosophical Transactions of the Royal Society of London Series B-Biological Sciences 262:365-372
44. Mariani AP, Lasansky A (1984) Chemical Synapses Between Turtle Photoreceptors. Brain Research 310:351-354
45. Lasansky A (1974) Synaptic Actions on Retinal Photoreceptors - Structural Aspects. Federation Proceedings 33:1069-1073
46. Spiwoks-Becker I, Lasarzik I, Vollrath L (2000) Transient synaptic ribbons in the mammalian retina at unusual sites. Journal of Neurocytology 29:81-89
47. Spiwoks-Becker I, Glas M, Lasarzik I, Vollrath L (2004) Mouse photoreceptor synaptic ribbons lose and regain material in response to illumination changes. European Journal of Neuroscience 19:1559-1571
48. Vollrath L, SpiwoksBecker I (1996) Plasticity of retinal ribbon synapses. Microscopy Research and Technique 35:472-487
49. Hsu A, Tsukamoto Y, Smith RG, Sterling P (1998) Functional architecture of primate cone and rod axons. Vision Research 38:2539-2549
50. Adly MA, Spiwoks-Becker I, Vollrath L (1999) Ultrastructural changes of photoreceptor synaptic ribbons in relation to time of day and illumination. Investigative Ophthalmology & Visual Science 40:2165-2172
51. von Gersdorff H, Vardi E, Matthews G, Sterling P (1996) Evidence that vesicles on the synaptic ribbon of retinal bipolar neurons can be rapidly released. Neuron 16:1221-1227

52. Usukura J, Yamada E (1987) Ultrastructure of the Synaptic Ribbons in Photoreceptor Cells of Rana-Catesbeiana Revealed by Freeze-Etching and Freeze-Substitution. Cell and Tissue Research 247:483-488
53. Schmitz F, Konigstorfer A, Sudhof TC (2000) RIBEYE, a component of synaptic ribbons: A protein's journey through evolution provides insight into synaptic ribbon function. Neuron 28:857-872
54. Rao-Mirotznik R, Buchsbaum G, Sterling P (1998) Transmitter concentration at a three-dimensional synapse. Journal of Neurophysiology 80:3163-3172
55. Zhai RG, Vardinon-Friedman H, Cases-Langhoff C, Becker B, Gundelfinger ED, Ziv NE, Garner CC (2001) Assembling the presynaptic active zone: a characterization of an active one precursor vesicle. Neuron 29:131-143
56. Dick O, Hack I, Altrock WD, Garner CC, Gundelfinger ED, Brandstatter JH (2001) Localization of the presynaptic cytomatrix protein piccolo at ribbon and conventional synapses in the rat retina: Comparison with bassoon. Journal of Comparative Neurology 439:224-234
57. Dick O, Dieck ST, Altrock WD, Ammermuller J, Weiler R, Garner CC, Gundelfinger ED, Brandstatter JH (2003) The presynaptic active zone protein bassoon is essential for photoreceptor ribbon synapse formation in the retina. Neuron 37:775-786
58. Fenster SD, Kessels MM, Qualmann B, Chung WJ, Nash J, Gundelfinger ED, Garner CC (2003) Interactions between Piccolo and the actin/dynamin-binding protein Abp1 link vesicle endocytosis to presynaptic active zones. Journal of Biological Chemistry 278:20268-20277
59. Bansal A, Singer JH, Hwang BJ, Xu W, Beaudet A, Feller MB (2000) Mice lacking specific nicotinic acetylcholine receptor subunits exhibit dramatically altered spontaneous activity patterns and reveal a limited role for retinal waves in forming ON and OFF circuits in the inner retina. Journal of Neuroscience 20:7672-7681
60. Wang MM, Janz R, Belizaire R, Frishman LJ, Sherry DM (2003) Differential distribution and developmental expression of synaptic vesicle protein 2 isoforms in the mouse retina. Journal of Comparative Neurology 460:106-122
61. Muresan V, Lyass A, Schnapp BJ (1999) The kinesin motor KIF3A is a component of the presynaptic ribbon in vertebrate photoreceptors. Journal of Neuroscience 19:1027-1037
62. Heidelberger R, Thoreson WB, Witkovsky P (2005) Synaptic transmission at retinal ribbon synapses. Progress in Retinal and Eye Research 24:682-720
63. Thoreson WB, Witkovsky P (1999) Glutamate receptors and circuits in the vertebrate retina. Progress in Retinal and Eye Research 18:765-810
64. Dowling JE (1987) Functional and Pharmacological Organization of the Retina. Archives of Neurology 44:1208-1213
65. Lenzi D, von Gersdorff H (2001) Structure suggests function: the case for synaptic ribbons as exocytotic nanomachines. Bioessays 23:831-840
66. Berntson A, Smith RG, Taylor WR (2004) Transmission of single photon signals through a binary synapse in the mammalian retina. Visual Neuroscience 21:693-702

67. Ashmore JF, Copenhagen DR (1983) An Analysis of Transmission from Cones to Hyperpolarizing Bipolar Cells in the Retina of the Turtle. Journal of Physiology-London 340:569-597
68. Copenhagen DR, Ashmore JF, Schnapf JK (1983) Kinetics of Synaptic Transmission from Photoreceptors to Horizontal and Bipolar Cells in Turtle Retina. Vision Research 23:363-369
69. Berntson A, Taylor WR (2003) The unitary event amplitude of mouse retinal on-cone bipolar cells. Visual Neuroscience 20:621-626
70. Berntson AK, Morgans CW (2003) Distribution of the presynaptic calcium sensors, synaptotagmin I/II and synaptotagmin III, in the goldfish and rodent retinas. Journal of Vision 3:274-280
71. Goede P, Kolb H (1994) Identification of the Synaptic Pedicles Belonging to the Different Spectral Types of Photoreceptor in the Turtle Retina. Vision Research 34:2801-2811
72. Thoreson WB, Rabl K, Townes-Anderson E, Heidelberger R (2004) A highly Ca2+-sensitive pool of vesicles contributes to linearity at the rod photoreceptor ribbon synapse. Neuron 42:595-605
73. Heidelberger R, Sterling P, Matthews G (2002) Roles of ATP in depletion and replenishment of the releasable pool of synaptic vesicles. Journal of Neurophysiology 88:98-106
74. Auger C, Marty A (1997) Heterogeneity of functional synaptic parameters among single release sites. Neuron 19:139-150
75. Beutner D, Voets T, Neher E, Moser T (2001) Calcium dependence of exocytosis and endocytosis at the cochlear inner hair cell afferent synapse. Neuron 29:681-690
76. Singer JH, Lassova L, Vardi N, Diamond JS (2004) Coordinated multivesicular release at a mammalian ribbon synapse. Nature Neuroscience 7:826-833
77. Thoreson WB, Tranchina D, Witkovsky P (2003) Kinetics of synaptic transfer from rods and cones to horizontal cells in the salamander retina. Neuroscience 122:785-798
78. Raviola E, Gilula NB (1975) Intramembrane Organization of Specialized Contacts in Outer Plexiform Layer of Retina - Freeze-Fracture Study in Monkeys and Rabbits. Journal of Cell Biology 65:192-222
79. Grabs D, Bergmann M, Urban M, Post A, Gratzl M (1996) Rab3 proteins and SNAP-25, essential components of the exocytosis machinery in conventional synapses, are absent from ribbon synapses of the mouse retina. European Journal of Neuroscience 8:162-168
80. von Kriegstein K, Schmitz F, Link E, Sudhof TC (1999) Distribution of synaptic vesicle proteins in the mammalian retina identifies obligatory and facultative components of ribbon synapses. European Journal of Neuroscience 11:1335-1348
81. Yang HD, Standifer KM, Sherry DM (2002) Synaptic protein expression by regenerating adult photoreceptors. Journal of Comparative Neurology 443:275-288
82. Chen F, Witkovsky P (1978) Formation of Photoreceptor Synapses in Retina of Larval Xenopus. Journal of Neurocytology 7:721-740
83. Klugbauer N, Lacinova L, Marais E, Hobom M, Hofmann F (1999) Molecular diversity of the calcium channel alpha2delta subunit. Journal of Neuroscience 19:684-691

84. Klugbauer N, Marais E, Hofmann F (2003) Calcium channel alpha2delta subunits: differential expression, function, and drug binding. Journal of Bioenergics and Biomembranes 35:639-647
85. Morgans CW, El Far O, Berntson A, Wassle H, Taylor WR (1998) Calcium extrusion from mammalian photoreceptor terminals. Journal of Neuroscience 18:2467-2474
86. Xu HP, Zhao JW, Yang XL (2002) Expression of voltage-dependent calcium channel subunits in the rat retina. Neuroscience Letters 329:297-300
87. Morgans CW, Bayley PR, Oesch NW, Ren G, Akileswaran L, Taylor WR (2005) Photoreceptor calcium channels: insight from night blindness. Visual Neuroscience 22:561-568
88. Ball SL, Powers PA, Shin HS, Morgans CW, Peachey NS, Gregg RG (2002) Role of the beta(2) subunit of voltage-dependent calcium channels in the retinal outer plexiform layer. Investigative Ophthalmology & Visual Science 43:1595-1603
89. Chu PJ, Robertson HM, Best PM (2001) Calcium channel gamma subunits provide insights into the evolution of this gene family. Gene 280:37-48
90. Wan L, Almers W, Chen WB (2005) Two ribeye genes in teleosts: The role of ribeye in ribbon formation and bipolar cell development. Journal of Neuroscience 25:941-949
91. Allwardt BA, Lall AB, Brockerhoff SE, Dowling JE (2001) Synapse formation is arrested in retinal photoreceptors of the zebrafish nrc mutant. Journal of Neuroscience 21:2330-2342
92. Van Epps HA, Hayashi M, Lucast L, Stearns GW, Hurley JB, De Camilli P, Brockerhoff SE (2004) The zebrafish nrc mutant reveals a role for the polyphosphoinositide phosphatase synaptojanin 1 in cone photoreceptor ribbon anchoring. Journal of Neuroscience 24:8641-8650
93. Bech-Hansen NT, Naylor MJ, Maybaum TA, Pearce WG, Koop B, Fishman GA, Mets M, Musarella MA, Boycott KM (1998) Loss-of-function mutations in a calcium-channel alpha1-subunit gene in Xp11.23 cause incomplete X-linked congenital stationary night blindness. Nature Genetics 19:264-267
94. Jalkanen R, Mantyjarvi M, Tobias R, Isosomppi J, Sankila EM, Alitalo T, Bech-Hansen NT (2006) X-linked cone-rod dystrophy, CORDX3, is caused by a mutation in the CACNA1F gene. Journal of Medical Genetics 43:699-704
95. Mansergh F, Orton NC, Vessey JP, Lalonde MR, Stell WK, Tremblay F, Barnes S, Rancourt DE, Bech-Hansen NT (2005) Mutation of the calcium channel gene Cacna1f disrupts calcium signaling, synaptic transmission and cellular organization in mouse retina. Human Molecular Genetics 14:3035-3046
96. Haeseleer F, Imanishi Y, Maeda T, Possin DE, Maeda A, Lee A, Rieke F, Palczewski K (2004) Essential role of Ca2+-binding protein 4, a Cav1.4 channel regulator, in photoreceptor synaptic function. Nature Neuroscience 7:1079-1087
97. Schlamp CL, Williams DS (1996) Myosin V in the retina: Localization in the rod photoreceptor synapse. Experimental Eye Research 63:613-619
98. Libby RT, Lillo C, Kitamoto J, Williams DS, Steel KP (2004) Myosin Va is required for normal photoreceptor synaptic activity. Journal of Cell Science 117:4509-4515

99. Michaelides M, Holder GE, Hunt DM, Fitzke FW, Bird AC, Moore AT (2005) A detailed study of the phenotype of an autosomal dominant cone-rod dystrophy (CORD7) associated with mutation in the gene for RIM1. British Journal of Ophthalmology 89:198-206
100. Johnson S, Halford S, Morris AG, Patel RJ, Wilkie SE, Hardcastle AJ, Moore AT, Zhang K, Hunt DM (2003) Genomic organisation and alternative splicing of human RIM1, a gene implicated in autosomal dominant cone-rod dystrophy (CORD7). Genomics 81:304-314
101. Kobayashi A, Kubota S, Mori N, McLaren MJ, Inana G (2003) Photoreceptor synaptic protein HRG4 (UNC119) interacts with ARL2 via a putative conserved domain. Febs Letters 534:26-32
102. Mori N, Ishiba Y, Kubota S, Kobayashi A, Higashide T, McLaren MJ, Inana G (2006) Truncation mutation in HRG4 (UNC119) leads to mitochondrial ANT-1-mediated photoreceptor synaptic and retinal degeneration by apoptosis. Investigative Ophthalmology & Visual Science 47:1281-1292
103. Morgans CW, Ren GY, Akileswaran L (2006) Localization of nyctalopin in the mammalian retina. European Journal of Neuroscience 23:1163-1171
104. Pusch CM, Zeitz C, Brandau O, Pesch K, Achatz H, Feil S, Scharfe C, Maurer J, Jacobi FK, Pinckers A, Andreasson S, Hardcastle A, Wissinger B, Berger W, Meindl A (2000) The complete form of X-linked congenital stationary night blindness is caused by mutations in a gene encoding a leucine-rich repeat protein. Nature Genetics 26:324-327
105. Dryja TP, Mcgee TL, Berson EL, Fishman GA, Sandberg MA, Alexander KR, Derlacki DJ, Rajagopalan AS (2005) Night blindness and abnormal cone electroretinogram ON responses in patients with mutations in the GRM6 gene encoding mGluR6. Proceedings of the National Academy of Sciences of the United States of America 102:4884-4889
106. Gregg RG, Mukhopadhyay S, Candille SI, Ball SL, Pardue MT, Mccall MA, Peachey NS (2003) Identification of the gene and the mutation responsible for the mouse nob phenotype. Investigative Ophthalmology & Visual Science 44:378-384
107. Masu M, Iwakabe H, Tagawa Y, Miyoshi T, Yamashita M, Fukuda Y, Sasaki H, Hiroi K, Nakamura Y, Shigemoto R, Takada M, Nakamura K, Nakao K, Katsuki M, Nakanishi S (1995) Specific Deficit of the on Response in Visual Transmission by Targeted Disruption of the Mglur6 Gene. Cell 80:757-765
108. Ruether K, Grosse J, Matthiessen E, Hoffmann K, Hartmann C (2000) Abnormalities of the photoreceptor-bipolar cell synapse in a substrain of C57BL/10 mice. Investigative Ophthalmology & Visual Science 41:4039-4047

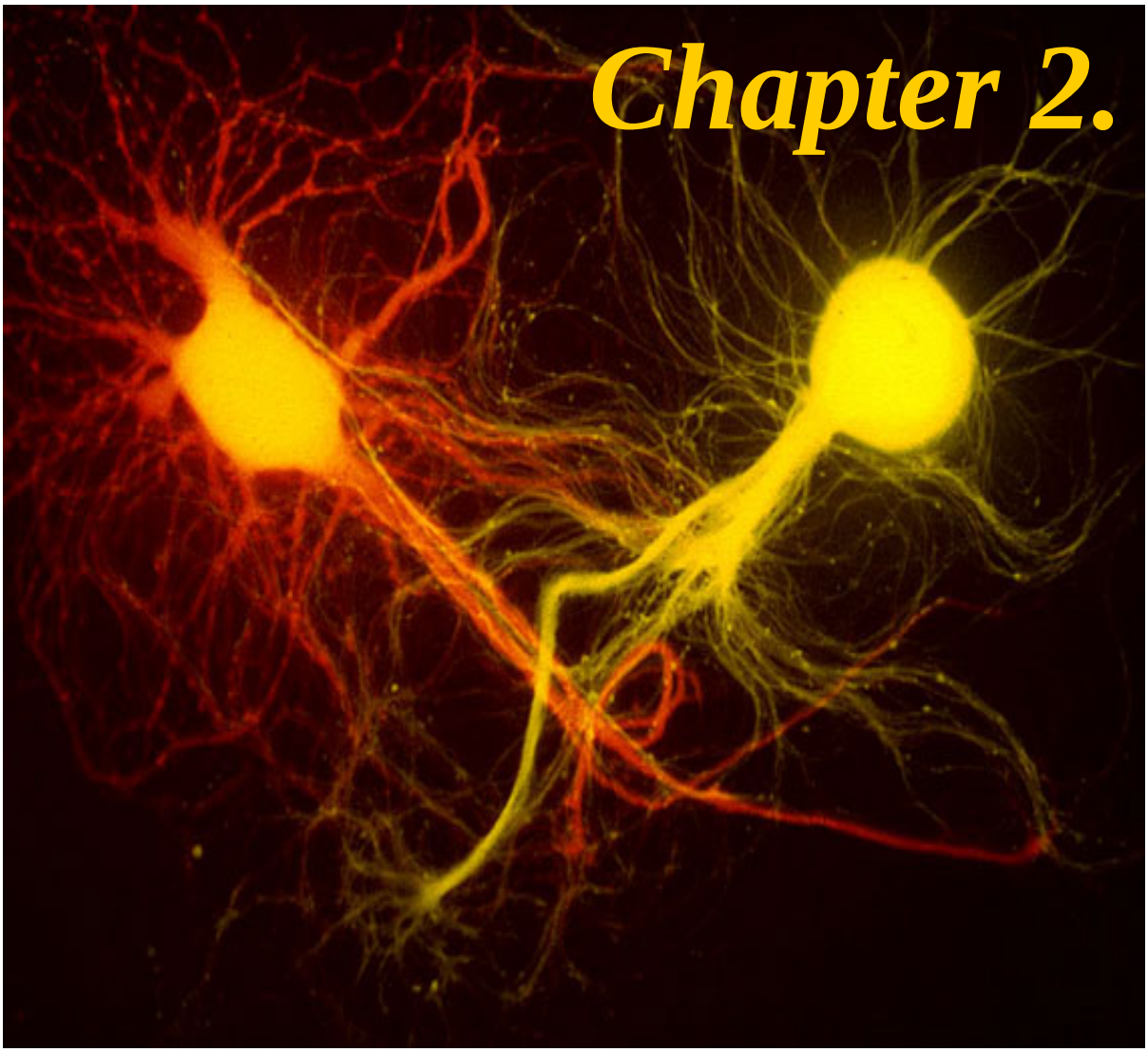

Chapter 2.

Aims of the Study

2. Aims of the Study

Tens of millions of people worldwide are affected by hereditary retinal diseases which range from moderate night blindnesses to severe forms of retinal degenerations and blindness. The elucidation of the underlying genetic defects is particularly important to gain more insights into the pathological mechanisms and future therapeutic interventions. Similarly, the identification of the mutation in C57BL/10 mice might help to better understand the processes of retinal signal transmission and the implicated pathology of ribbon-shaped synapses. Further, it might provide a new candidate gene for corresponding human retinal diseases.

The genome wide linkage approach localized the mutation on mouse chromosome 6 in an initial interval of 15.6 Mb. This preliminary mapping result underlined the basis for further genetic investigation.

The 15.6-Mb genomic distance comprised more than 400 potential candidate genes for a possible mutational screening. By means of positional cloning and candidate gene approach, it was the major aim of the study to identify the defective gene. For this, the experimental attempts should include a restriction of the respective linkage interval and fine-mapping of the causative mutation. Mutational analysis of candidate genes from the resulting interval should be implemented in parallel experiments. In further intention, the elucidation of the pathogenic mechanisms ongoing in the mouse mutant retina was considered. Following gene identification, the subsequent challenge of this project was to uncover the respective orthologous gene in human and to imply mutational analysis in patients with distinct forms of retinal diseases. The following three parts of the thesis presents the results of those experiments which were undertaken to accomplish these major objectives.

Chapter 3.

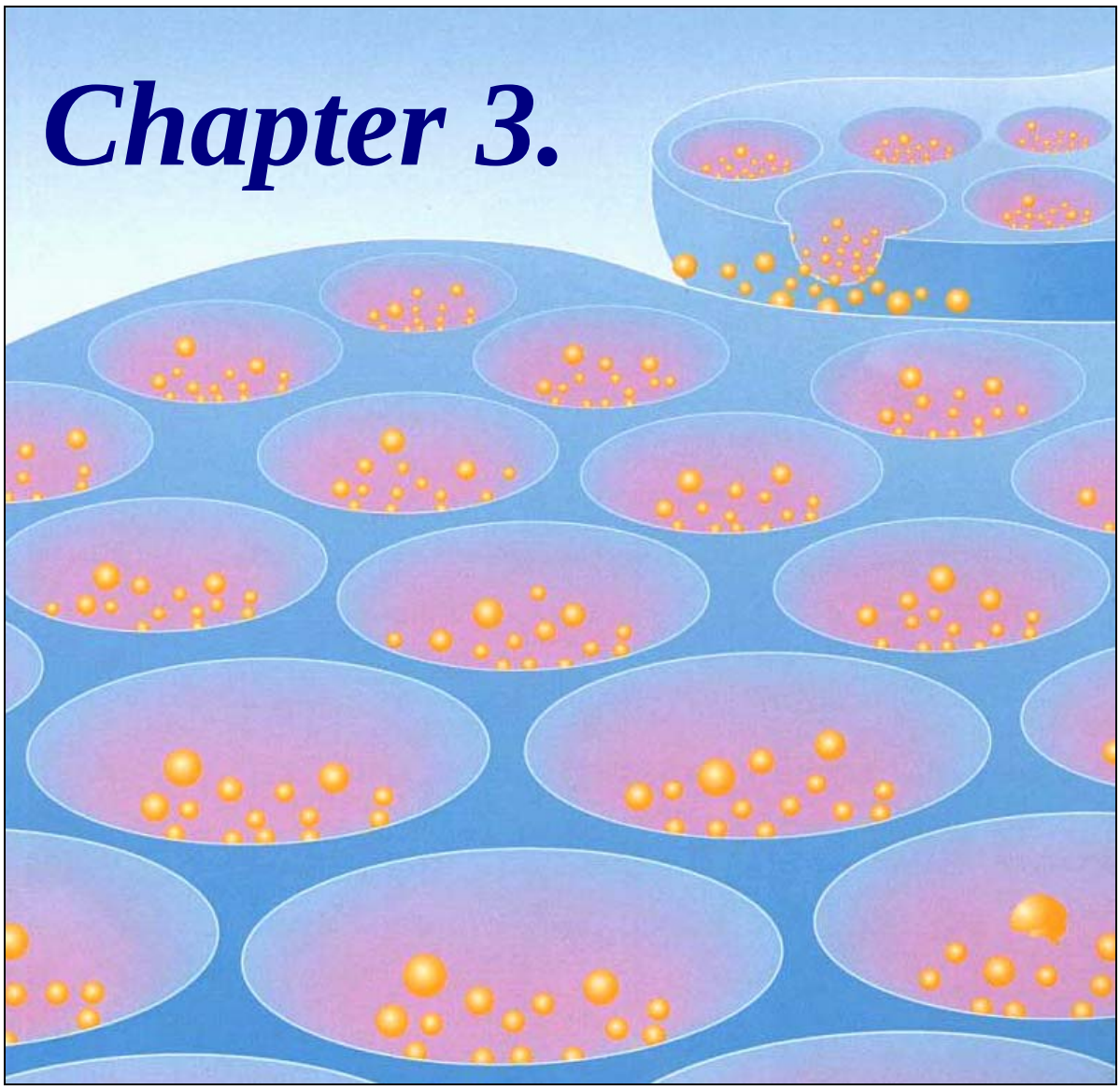

Results

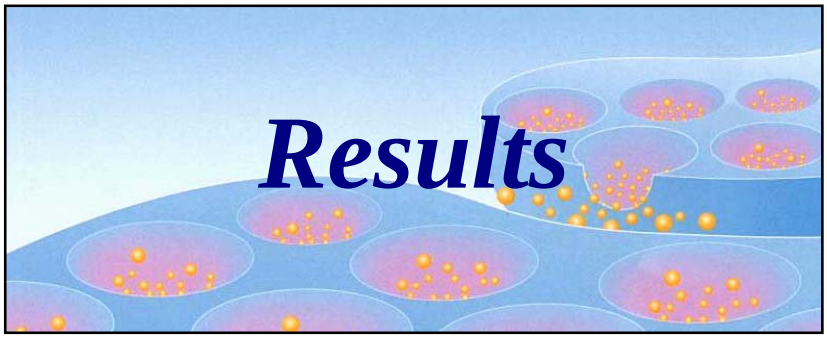

3. Results

3.1. Structural and Functional Abnormalities of Retinal Ribbon Synapses due to Cacna2d4 Mutation

K.A. Wycisk[1], B. Budde[2*], S. Feil[1*], S. Skosyrski[3], F. Buzzi[1], J. Neidhardt[1], E. Glaus[1], P. Nürnberg[2], K. Ruether[3], W. Berger[1]

[*]These authors contributed equally to this study and therefore should be considered equivalent authors.

Published in Investigative Ophthalmology and Visual Science, August 2006, Vol. 47, No. 8

[1]Division of Medical Molecular Genetics and Gene Diagnostics, Institute of Medical Genetics, University of Zurich, Schorentrsasse 16, 8603 Schwerzenbach, Switzerland; [2]Cologne Centre for Genomics and Institute for Genetics, University of Cologne, Zülpicher Strasse 47, 50674 Köln, Germany, [3]Charite-Virchow-Augenklinik, Ziegelstrasse 5-9, 10117 Berlin, Germany

Grant: Supported by the Foundation Fighting Blindness (USA), the Swiss National Science Foundation (Grant#3100-067786 to WB), the Deutsche Forschungsgemeinschaft (DFG Ru 457/1-1) and the German Federal Ministry of Science and Education through the National Genome Research Network (Grant#01GR0416 to PN).

Acknowledgements : The authors thank S. Derzsi, U. Luhmann, G. Matyas, G. Tanner, M. Wittmer and C. Zeitz for discussions and experimental assistance.

Structural and Functional Abnormalities of Retinal Ribbon Synapses due to *Cacna2d4* Mutation

Katharina A. Wycisk,[1] *Birgit Budde,*[2,3] *Silke Feil,*[1,3] *Sergej Skosyrski,*[4] *Francesca Buzzi,*[1] *John Neidhardt,*[1] *Esther Glaus,*[1] *Peter Nürnberg,*[2] *Klaus Ruether,*[4] *and Wolfgang Berger*[1]

Purpose. In a spontaneous mutant substrain of C57BL/10 mice, severely affected retinal ribbon-type synapses have been described. The retinopathy was accompanied by a substantial loss in the activities of the second-order neurons. Rod photoreceptor responses were maintained with reduced amplitude, whereas cone activities were absent. This study was conducted to identify the genetic defect underlying this hitherto unknown autosomal recessive cone–rod dysfunction.

Methods. Genome-wide linkage analysis and screening of positional candidate genes were used to identify the causative mutation. Tissue-specific transcriptional activity of the defective gene was determined by Northern blot analysis and RT-PCR approaches. The number of cone photoreceptors was estimated by immunohistochemistry.

Results. The mutation was localized to a 275-kb region of chromosome 6. Within this candidate interval, a homozygous frameshift mutation (c.2367insC) was identified in the *Cacna2d4* gene of affected animals. This gene codes for an L-type calcium channel auxiliary subunit of the $\alpha 2\delta$ type. The mutation introduces a premature stop codon that truncates one third of the predicted Cacna2d4 protein. A severe reduction in *Cacna2d4* transcript levels observed in mutant retinas probably results in the lack of Cacna2d4 protein. The mutation leads to significant loss of rods, whereas the number of cone cells remains unaffected until 6 weeks of age.

Conclusions. The *Cacna2d4* mutation underlies a novel channelopathy leading to cone–rod dysfunction in the visual system of mice and provides a new candidate gene for human retinal disorders including night blindness, retinitis pigmentosa, and cone–rod dystrophies. (*Invest Ophthalmol Vis Sci.* 2006;47: 3523–3530) DOI:10.1167/iovs.06-0271

From the [1]Division of Medical Molecular Genetics and Gene Diagnostics, Institute of Medical Genetics, University of Zurich, Schwerzenbach, Switzerland; the [2]Cologne Centre for Genomics and Institute for Genetics, University of Cologne, Cologne, Germany; and the [4]Charite-Virchow-Augenklinik, Berlin, Germany.

[3]Contributed equally to the work and therefore should be considered equivalent authors.

Supported by the Foundation Fighting Blindness, Swiss National Science Foundation Grant 3100-067786 (WB), Grant DFG Ru 457/1-1 from Deutsche Forschungsgemeinschaft, and Grant 01GR0416 from the German Federal Ministry of Science and Education through the National Genome Research Network (PN).

Submitted for publication March 14, 2006; revised April 19, 2006; accepted June 21, 2006.

Disclosure: **K.A. Wycisk**, None; **B. Budde**, None; **S. Feil**, None; **S. Skosyrski**, None; **F. Buzzi**, None; **J. Neidhardt**, None; **E. Glaus**, None; **P. Nürnberg**, None; **K. Ruether**, None; **W. Berger**, None

The publication costs of this article were defrayed in part by page charge payment. This article must therefore be marked "*advertisement*" in accordance with 18 U.S.C. §1734 solely to indicate this fact.

Corresponding author: Wolfgang Berger, Division of Medical Molecular Genetics and Gene Diagnostics, Institute of Medical Genetics, University of Zurich, Schorenstrasse 16, 8603 Schwerzenbach, Switzerland; berger@medgen.unizh.ch.

Clinical symptoms of hereditary retinal diseases range from moderate night blindness to severe visual impairment and complete blindness in various forms of retinal degenerations. The elucidation of the underlying genetic defects helps to understand retinal function and pathogenic mechanisms. In a previous study, an autosomal recessive cone–rod dysfunction was discovered in a substrain of C57BL/10 mice.[1] The phenotype is characterized by a disturbed signal transmission of photoreceptor cells to adjacent neurons. On dark- and light-adapted electroretinography, a profound loss of the b-wave, which requires synaptic transduction, has been detected in affected animals. The scotopic a-wave, which mainly reflects membrane potentials of rods, has a consistently reduced amplitude. Under photopic conditions however, cone-specific activity is absent. The substantial loss of postphotoreceptoral activities is associated with a severely compromised morphology of retinal ribbon-type synapses. The causative mutation of this disorder remains unknown.

Ribbon-shaped synapses are known to involve the high-voltage-gated L-type calcium channels preferentially in their signaling pathways.[2] These calcium channels are clustered at presynaptic membranes beneath ribbon organelles that guide synaptic vesicles to active zones for calcium-mediated fusion.[3] L-type calcium channels are heteromultimers composed of four independently encoded proteins, the pore-forming $\alpha 1$ subunit, which triggers calcium flow across the membrane, and the auxiliary subunits $\alpha 2\delta$, β, and γ.[4] Mutations affecting the functionality in two of these calcium channel subunits lead to failure of retinal processing. Allelic variants of the retina-specific $\alpha 1$F subunit (*CACNA1F*) were found to be responsible for X-linked incomplete congenital stationary night blindness type 2 (CSNB2).[5] Mutations either result in complete loss of function or modify *CACNA1F* kinetics.[6] Certain variants of *CACNA1F* were associated with clinical symptoms of cone–rod dystrophies.[7,8] An abnormal morphology of the photoreceptor ribbon synapses and seriously diminished signal transmission from photoreceptor terminals to the second-order neurons were detected in mice lacking the $\beta 2$ auxiliary subunit.[9] The recently reported mouse model for human *CACNA1F*-mediated CSNB2 revealed a cone–rod dysfunction due to a targeted deletion of the *Cacna1f* gene.[10] Of note, striking similarities were found between the phenotypic features of ribbon synapses in *Cacna1f*-mutant and affected C57BL/10 mice.

We applied genetic mapping and screening of positional candidate genes to elucidate the causative mutation in affected C57BL/10 mice. By genome-wide linkage analysis, we localized the causal mutation on chromosome 6 and identified the defect in the gene encoding the fourth L-type calcium channel $\alpha 2\delta$ auxiliary subunit, Cacna2d4. This gene may be responsible for proper assembly and auxiliary modulation of biophysical properties of L-type calcium channels, similar to the previously described human CACNA2D4 orthologue.[11] The mutation found in *Cacna2d4* underlies a novel channelopathy leading to cone–rod disease in the visual system of mice. Our results provide insights into a new pathophysiology of retinal ribbon-type synapses and a new candidate gene for human retinal

Investigative Ophthalmology & Visual Science, August 2006, Vol. 47, No. 8

disorders including night blindness, retinitis pigmentosa, and cone–rod dystrophies.

Materials and Methods

Animal Breeding

Mouse strains were obtained from regular providers of laboratory animals. The research was performed in accordance with the ARVO Statement for the Use of Animals in Ophthalmic and Vision Research.

To perform linkage, C57BL/10 mutant animals were crossed with animals of the AJ inbred mouse strain to generate heterozygosity in polymorphic markers. The heterozygous hybrids (F1) were subsequently mated for the second generation (F2). To refine linkage analysis, successive breeding strategy was repeated with new parental animals. Affected F2 mice were selected for mapping.

Phenotypic Characterization

In an earlier study, extended electrophysiological examinations of the phenotype were performed in animals up to the age of 14 months.[1] For screening purposes, the animals were characterized by scotopic ERG at the age of 3 to 6 weeks. Briefly, dark-adapted, anesthetized mice were placed in a Ganzfeld bowl exposing white-light flashes to the dilated eye of the mouse (flash energies ranging from 10^{-4} to 0.5 log cds/m^2). A monopolar contact lens electrode served as the recording electrode. Light-induced retinal activities were visualized in ERG recordings. Representative negative scotopic ERG recordings of affected animals exhibited reduction of the a-wave amplitude and a distinct attenuation of the b-wave. Cone ERGs were nonrecordable in affected animals at any age.

Retinal Morphology

To exclude modifying effects of the AJ genetic background, we looked for alterations in the retina of affected B10AF2 hybrids by light microscopy. Paraffin sections of 10 mutant and 10 wild-type eyes were stained with hematoxylin-eosin dye complex and evaluated with a microscopy station (Axioplan 2; Carl Zeiss Meditec, Inc., Feldbach, Switzerland). For this, eyes were enucleated from mice anesthetized and subsequently killed with CO_2 and fixed in Serra's (60% ethanol, 30% formalin, 10% acetic acid) over night. After dehydration in an isopropanol series (70%, 80%, 90%, 100%, 100%), eyes were embedded in paraffin blocks and sectioned into 5-μm slides.

Genotyping and Linkage Analysis

DNA was extracted from tail biopsy samples by standard methods. A whole-genome screen was performed with 75 informative microsatellite markers. Products of PCR assays with fluorescently labeled primers were analyzed by automated capillary genotyping (MegaBACE 1000, scored with genetic profiler analysis software; GE Healthcare). To identify linkage, homozygosity for C57BL/10 alleles was sought on chromosomes of 64 affected animals from the first B10A population. Significant linkage was confirmed by statistics computed by comparing the number of homozygous versus heterozygous mice and calculating χ^2 values. Genetic maps were constructed with the program Mapmaker.[12] To narrow the linkage interval, we screened the critical region for new polymorphic markers by alignment of the locus spanning C57BL/6J genomic contigs NM_000264 and NM_000265 to corresponding AJ genomic sequences obtained from the Celera database (http://www. celera.com/ Celera Genomics, Rockville, MD). In addition, the Mouse Single Nucleotide Polymorphism (http://mousesnp.roche.com, Roche Molecular Biochemicals, Indianapolis, IN) and Entrez SNP Database (http://www.ncbi.nlm.nih.gov/ provided in the public domain National Center for Biotechnology Information, Bethesda, MD) were scanned for further markers. Identified polymorphisms (6 annotated microsatellite markers, 3 known and 22 new SNPs) were verified by allele-specific PCR, denaturing polyacrylamide gels, or direct sequencing and used to genotype affected F2 animals from both B10A populations (Supplementary Table S1, available online at http://www.iovs.org/cgi/content/full/47/8/3523/DC1). Primers were purchased from Microsynth (Balgach, Switzerland). (Genomic sequences including identified SNPs and primers are available on request.) Unaffected B10AF2 animals were genotyped for flanking markers of the final interval.

Mutational Analysis

Candidate genes were selected on functional relevance and analyzed by direct sequencing of the open reading frame (ORF) or whole mRNA. Mainly, RT-PCR was directed from whole-eye cDNA of two mutants and two wild types to prescreen exon splicing and deletion or insertion defects, applying primers designed to amplify ORF/mRNA-spanning fragments of ~550 bp. As no mutation was found in all investigated candidate genes, we proceeded with sequence analysis of the entire interval, defined by fine mapping. We performed primer design through the region to amplify overlapping fragments of 500 to 650 bp corresponding to the genomic reference sequence of C57BL/6J mice (http://genome.ucsc.edu/ Human Genome Browser, provided in the public domain by UCSC Genome Bioinformatics, University of California at Santa Cruz, Santa Cruz, CA). Purified fragments (ExoSap-IT Kit; USB, Cleveland, OH) were bidirectionally sequenced for two mutants and two wild types (Prism 3100 Genetic Analyzer in accordance with the Prism Big Dye Chemistry ver. 1.1 protocol; Applied Biosystems [ABI], Rotkreuz; Switzerland). Sequences were then aligned (PRISM SeqScape; ABI) and examined for nucleotide exchanges. Putative mutations were verified in all affected animals and wild types.

RNA Isolation and cDNA Synthesis

After tissue homogenization with a glass pestle, total RNA extraction was performed (RNeasy Mini Kit; Qiagen, Basel, Switzerland). Through reverse transcription, 1.5 μg total RNA was transcribed into cDNA by random hexanucleotide priming (hexamer primers pd(N)$_6$, GE Healthcare, Otelfingen, Switzerland; and Superscript III; Invitrogen, Basel, Switzerland). cDNA synthesis efficiency and DNA contamination were examined by standardized *Gapdh* PCR including negative control experiments for each sample with no reverse transcriptase used during synthesis. Absent *Gapdh* product in the negative control experiments excluded DNA contamination.

RT-PCR and Real-Time PCR

Gene transcription and the exonic composition of *Cacna2d4* were verified by RT-PCR on total eye–retina RNA. For this, overlapping fragments spanning the entire mRNA were amplified in wild types and mutants and subsequently sequenced: (1) forward (for): 5′-ttgatcacctggggtggacc, reverse (rev): 5′-acaggatgattggcgtcttc; (2) for: 5′-ttgatcacctggggtggacc, rev: 5′-gtgttgtacagattcctgcc; (3) for: 5-ttgatcacctggggtggacc; rev: 5′-agcatggtctccatgtcctc; (4) for: 5′-ttgatcacctggggtggacc; rev: 5′-ccagccacggtttctgcagtc; (5) for: 5′-gcgtgtatatgtccgaagcc; rev: 5′-ccatgtaagcctctgtccag; (6) for: 5′-ggagtcatcgccttcgactgc; rev: 5′-agaaggcatagccatgcacc; (7) for: 5′-gtggccatgcctgtcttcag; rev: 5′-gtctctctgagatcaggacg; (8) for: 5′-cactgatctcgactgcttcg; rev: 5′-ttcttgtgcttgtgggagtg; and (9) for: 5′-tgttagagtggagtgcctgg; rev: 5′-gagacatcccacagcagtga. *Cacna2d4* mRNA amounts in eyes were examined with real-time PCR using cDNAs from five wild-type, five heterozygous, and five mutant animals from the B10A strain at the age of 6 weeks. The experiment was repeated four times. For each animal, two independent cDNA syntheses were performed and pooled after quality control. Subsequently, two independent dilutions were prepared from each cDNA pool. Quantitative RT-PCR for retinal tissue was performed by pooling six retinas for RNA extraction from three homozygous wild-type, three heterozygous, and three mutant animals each. Three dilutions of two independent cDNA syntheses were examined for *Cacna2d4* transcripts. The amplification (for: 5′-ctgccatgccttccatccag, rev: 5′-gagacatcccacagcagtga) was performed at 50°C for 2 minutes and 95°C for 10 minutes and then continued with 45 cycles of 15 seconds at 90°C and 1 minute at 60°C for detection of a 221-bp *Cacna2d4*-specific fragment (with SYBR Green nucleic acid stain; ABI) (exon 37–38)

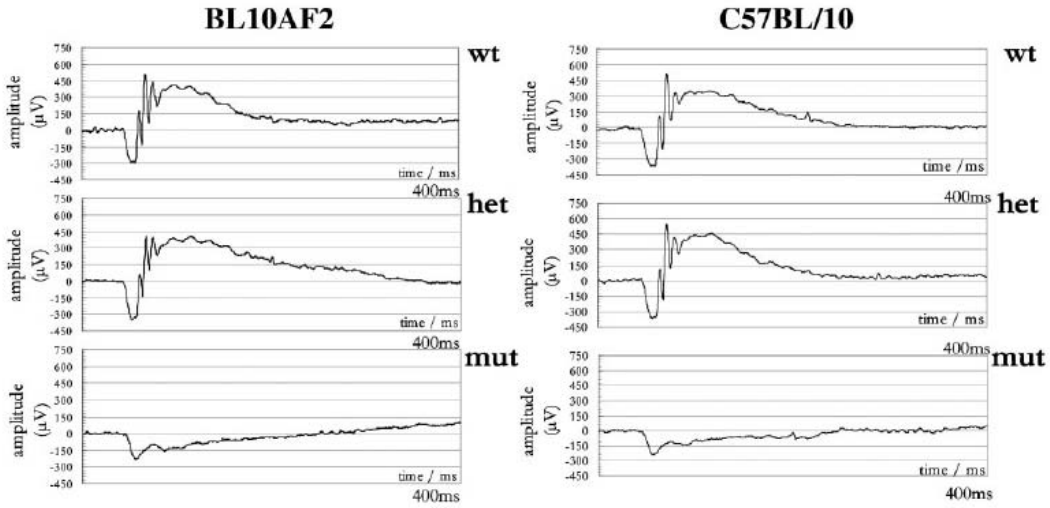

FIGURE 1. Phenotyping of B10A mice. Scotopic ERG response to a 0.5 log cd-s/m² white flash recorded from 6-week-old B10AF2 or C57BL/10 wild-type (wt), heterozygous (het) and affected mice (mut). In the mutant B10AF2 mouse, electronegative configuration of scotopic responses (absent b-wave) is observed, similar to that in affected animals of the original C57BL/10 strain.

on a detection system (7900HT Prism; ABI). A melting curve was analyzed to verify single-product amplification. In addition, the specificity of the amplicons was confirmed by sequencing. Transcript levels were normalized to 18S rRNA (*Taq*Man Ribosomal RNA Control Reagent; ABI) and quantified to the mean level in homozygous wild types according to the ΔC_t-method.

Northern Blot Analysis

For hybridization, a 550-bp cDNA fragment encoding the *Cacna2d4*-specific 3′end (exons 33–38; for: 5′-tgttagagtggagtgcctgg, rev: 5′-gagacatcccacagcagtga) was used as a probe. Labeling with [α-^{32}P]dCTP* (10 μCi/μL; Hartmann Analytic, Braunschweig, Germany) was performed according to the manufacturer's instructions (Prime-It II Random Primer Labeling Kit; Stratagene, Amsterdam, The Netherlands). Denatured DNA probe was transferred to a hybridization tube (ULTRAhyb hybridization buffer; Ambion, Cambridgeshire, UK), Mouse Cot-DNA and a Northern blot preincubated for 50 minutes at 42°C. We hybridized a Poly A$^+$ RNA commercial murine northern blot (Multi Choice; OriGene, Rockville, MD). After incubation for 15 hours at 42°C, the blot was washed twice with 2× SSC and 0.1% SDS for 5 minutes at 42°C and twice with 0.1× SSC and 0.1% SDS for 15 minutes at 65°C. Finally, the blot was exposed to film (BioMax; Eastman Kodak, Rochester, NY) at −80°C overnight. As the loading control, mouse β-actin probe (OriGene) hybridization was included.

Cell Quantification in the Retina

Immunohistochemistry was preformed on 8-μm whole-eye cryosections of six affected and six wild-type littermates, as described elsewhere.[13] Gα cone transducin primary antibody (Santa Cruz Biotechnology, Santa Cruz, CA) was used to detect the cones.[14] As a secondary antibody, Cy3 labeled anti-rabbit IgG was applied (Dianova, Hamburg, Germany). Subsequently, tissue sections were embedded in mounting medium that contained DAPI (Vectashield; Vector Laboratories, Burlingame, CA), to visualize cell nuclei. Images were generated at 63× magnification by the fluorescence microscopy station (Axioplan2; Carl Zeiss Meditech) from three sections per animal, representing retinas including the optic nerve. Cone marker-positive cells were quantified in two 200 × 50-μm² subfields of the peripheral and two of the central outer nuclear layer per each image. In addition, the number of cells in the central outer and inner nuclear layers was counted in a 163 × 18-μm² subfield (n = 4) in DAPI-stained retinal cryosections for each animal.

Statistics

Statistical relevance for ERG measurements, real-time PCR and cell number quantification was analyzed with the Mann-Whitney test (SPSS ver. 13 for Windows; SPSS Inc., Chicago, IL) and accepted if $P < 0.05$. Graphic data interpretations included the calculation of the SE visualized in confidence intervals.

RESULTS

Genome-Wide Linkage Analysis

To identify the mutation, we crossed the C57BL/10 mutant genome to the genetic background of the phylogenetically distant AJ mouse strain generating substantial heterozygosity in the alleles of genetic markers. Heterozygous (C57BL/10 x AJ)F1 mice revealed no phenotypic alterations. Subsequently, (C57BL/10 x AJ)F1 mice were intercrossed. In total, two independent C57BL/10 x AJ breedings were performed.

In the B10AF2 generation, segregation into affected and unaffected phenotypes in a ratio of 25:75% was found in accordance with the originally suggested autosomal recessive transmission of the mutation. Among a total number of 580 F2 mice, 142 animals (24.48%) showed the characteristic negative ERG in scotopic conditions (Fig. 1).

Structural and functional alterations in affected B10AF2 animals were similar to the symptoms of the inbred line C57BL/10 (Fig. 2).[1] Affected B10AF2 offspring displayed significant reduction of the scotopic a-wave and profound loss of the b-wave. In affected B10AF2 mice, the a-wave amplitude was attenuated to 80.3% (Fig. 2A). The severe reduction of the b-wave amplitude was reflected by the a/b-waves, calculated as the difference between the a- and b-wave maxima. The a/b-wave revealed a decrease to 25% in affected B10AF2 animals

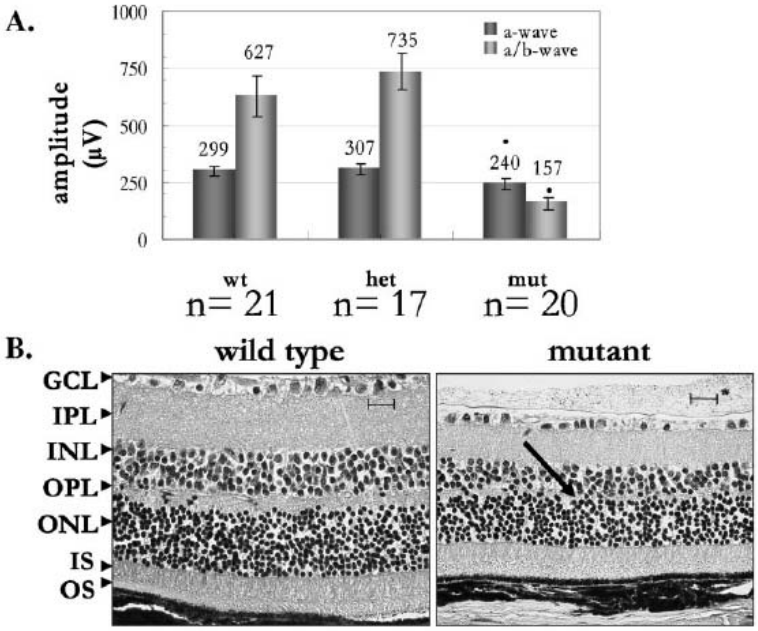

FIGURE 2. Phenotype verification in the B10A strain. (A) Significant reduction of the a- and a/b-wave amplitudes in 6-week-old B10AF2 mutants (mut) in comparison to wild-type (wt) mice ($P < 0.05$). (B) Confirmation of synaptic disorganization in retina of a B10AF2 mutant. Morphology was obtained by light microscopy of a retinal section stained with hematoxylin-eosin. B10AF2 mutants at 6 weeks of age display reduction of the photoreceptor synaptic layer (*arrow*). Outer segments (OS), inner segments (IS), outer nuclear layer (ONL), outer plexiform layer (OPL), inner nuclear layer (INL), inner plexiform layer (IPL), ganglion cell layer (GCL). Magnification ×63; scale bar, 20 µm.

(Fig. 2A). Corresponding to the defective signal transmission, the loss of the b-wave was associated with a significantly attenuated photoreceptor synaptic layer (outer plexiform layer, OPL; Fig. 2B). Homozygous and heterozygous B10AF2 unaffected mice revealed no differences on scotopic electroretinography and morphology. Accordingly, the genetic background of the AJ strain did not apparently modify the retinal phenotype.

For genetic localization of the mutation, 64 affected mice from the first B10AF2 breeding were included in a genome-wide linkage analysis with an initial marker-spacing of 20 cM. A homozygosity region was detected on chromosome 6 between the markers *D6Mit389* and *D6Mit218*, comprising an interval of 15.6 Mb (Figs. 3A, 3B). Linkage to chromosome 6 was evident through a distance of >30 cM, as revealed by allelic frequencies resulting in significant χ^2 values (Supple-

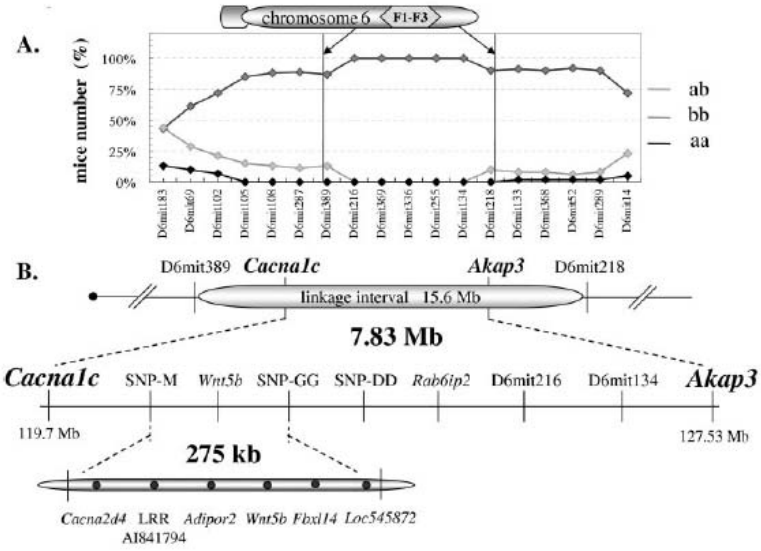

FIGURE 3. Linkage analysis. (A) Allele distribution on chromosome 6. *Line* aa: homozygous AJ; *line* bb: homozygous C57BL/10; *line* ab: heterozygous B10AT2 allele combinations. The number of mice homozygous for C57BL/10 alleles (bb) significantly increases between the markers *D6Mit102* and *D6Mit14*. *Shaded area*: initial linkage interval of 15.6 Mb occurring between the cytogenetic bands F1–F3 on chromosome 6. (B) Physical map of the critical region on chromosome 6. The linkage interval is represented on *top*. The refined critical region is indicated in the *bottom* line. Selected DNA markers are included. The finally identified locus comprises 275 kb of genomic DNA and six genes.

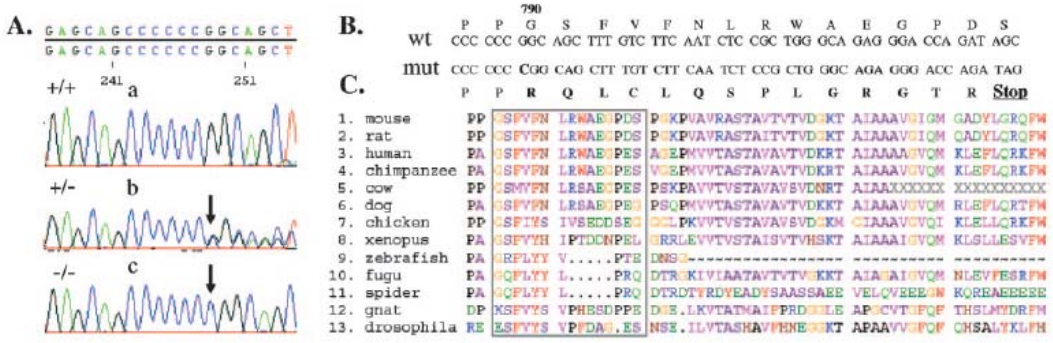

FIGURE 4. Mutation analysis. (A) Sequence examination of *Cacna2d4* exon 25. The electropherograms indicate a cytosine monorepeat sequence of a wild-type (a), heterozygous (b), and mutant (c) animal. Genotypes are indicated by +/+ (wild-type), +/− (heterozygous), and −/− (mutant). (B) The mutant sequence (mut) shows an insertion of a single nucleotide (in *bold*) resulting in a frameshift and the substitution of 14 amino acids (indicated in *bold*, bottom panel). The 15th subsequent codon encodes a premature stop codon in mutant mice. (C) Partial sequence alignment of mouse Cacna2d4 and orthologous proteins from 12 species. *Boxed area*: The conserved region substituted in mutant animals. (GenBank accession no.: rat ENSRNOG00000008031; human ENSG00000151062; chimpanzee ENSPTRG00000004521, cow ENSBTAG00000021994; dog ENSCAFG00000015970; chicken ENSGALG00000013007; xenopus ENSXETG00000000900; zebrafish ENSDARG00000026855; fugu SINFRUG00000149170; spider GSTENG00014501001; and gnat ENSANGG00000018436; drosophila CG12295.

mentary Table S2, http://www.iovs.org/cgi/content/full/47/8/3523/DC1). We detected no further linkage elsewhere in the genome of the B10A hybrid strain (Supplementary Fig. S1, http://www.iovs.org/cgi/content/full/47/8/3523/DC1). The linkage interval was refined by genotyping of additional SNPs and microsatellite markers to an interval of 7.83 Mb flanked by SNPs in *Cacna1c* and *Akap3* genes. For further fine mapping, we proceeded by generating and genotyping a second B10AF2 hybrid population (total $n = 319$, affected $n = 78$) and reduced the interval to 275 kb (Fig. 3B).

Identification of Sequence Variants in *Cacna2d4*

In parallel experiments, we excluded sequence variations in 33 candidate genes from the initially identified 15.6-Mb region (Supplementary Table S3, http://www.iovs.org/cgi/content/full/47/8/3523/DC1). In the final 275-kb interval, six potential candidate genes remained (Fig. 3B). In their annotated mRNA sequences, no mutations were detected. Thus, considering the occurrence of a defect in an additional exonic or noncoding region, we sequenced the entire 275-kb locus. We identified two DNA sequence variations segregating with the phenotype. The first was found in a compound tetranucleotide repeat in intron 6 of *Cacna2d4* and showed an insertion of an additional GAAA unit in a 12-unit GAAA replicon. However, RT-PCR examinations for a potential splicing defect revealed no exon skipping in affected mice (data not shown). In addition, sequencing of the orthologous repeat in the AJ mouse strain identified the variant of 14 GAAAs, strongly suggesting a polymorphic nature of the tetranucleotide repeat.

The second sequence alteration was detected in a recently annotated 3953-bp long variant of *Cacna2d4* mRNA (BK005394). This transcript consists of 38 exons and comprises 114.032 kb of genomic DNA. The 3350-bp ORF begins in exon 1 (ATG = 181 bp) and extends to exon 38 (TGA = 3531 bp), coding for a protein of 1116 amino acids.

In a short $C_{(n = 6)}$ monorepeat, affected animals displayed an insertion of a cytosine nucleotide ($C_{(n = 7)}$) in exon 25 of the *Cacna2d4* gene (Fig. 4A). The mutation was confirmed in all affected animals ($n = 142$, B10AF2 and $n = 30$, C57BL/10). In unaffected mice, exclusively homozygous ($C_{(n = 6)}$) or heterozygous ($C_{(n = 6/7)}$) allelic combinations were detected ($n > 500$).

The identified insertion (c.2367insC) induces a frameshift that substitutes 14 amino acids and subsequently results in a premature stop in the corresponding protein sequence (Fig. 4B). The mutation removes 327 amino acid residues from the carboxyl terminus of the Cacna2d4 subunit representing 29.3% of the protein.

Qualitative and Quantitative Analysis of *Cacna2d4* mRNA

We confirmed the predicted exonic structure and analyzed the expression of *Cacna2d4* in wild-type and mutant retinas by RT-PCR (Fig. 5A). RT-PCR of fragment 7 (exons 14–29) revealed a single product that included exon 25 (Fig. 5B). The mutation was verified in mutant animals by direct sequencing of RT-PCR products. No additional fragments were detected in amplicon 7, which may correspond to alternatively spliced *Cacna2d4* transcripts lacking exon 25 (Fig. 5B).

Real-time PCR experiments revealed a significant reduction of *Cacna2d4* mRNA levels in eyes and retinas of affected and heterozygous animals (Figs. 6A, 6B). The relative amount of *Cacna2d4* transcripts in eyes of homozygous mutant mice was diminished to 45% in comparison to wild-type animals. In the retina, a decline to 31% was observed. In the retina of heterozygous animals, a significant decrease to 73% was detected (Figs. 6A, 6B). In eyes of heterozygous mice, statistical analysis indicated significant reduction to 82% in comparison to wild-type control animals.

We also examined *Cacna2d4* expression in 13 additional mouse tissues. On a Poly A^+ Northern blot including 12 tissues, we detected bands in the size range of 1.5 to 5 kb, most likely corresponding to alternative splice variants of *Cacna2d4* as suggested from EST databases (GenBank accession no.: XM_132795 with 2.2 kb, AK030723 with 2.6 kb, AK044427 with 3.23 kb, XM_132794 with 4.8 kb, and AK137847 with 3.1 kb; Fig. 6C). Strongest signals occurred at the size of ~4.6 and ~2.0 kb in most tissues. In brain, muscle and spleen, remarkably weaker signals were detected compared with other organs. Nevertheless, transcription of *Cacna2d4* was evident in all tissues analyzed, indicating a ubiquitous expression pattern. Broad *Cacna2d4* expression was confirmed by RT-PCR of fragment 9 (exons 33–38) in 12 tissues (Fig. 6D). Additional

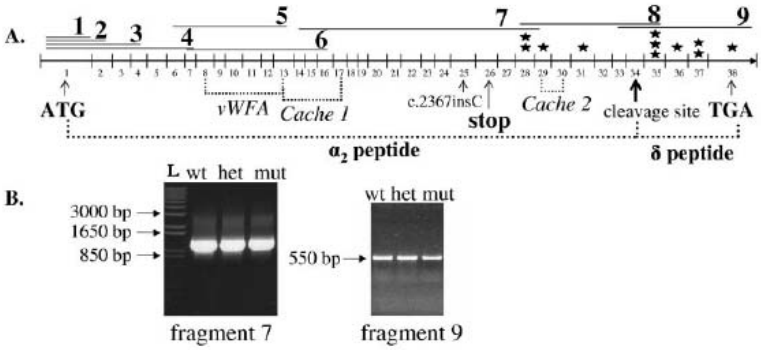

FIGURE 5. Schematic drawing of *Cacna2d4* transcript and RT-PCR analyses. (A) Exons are labeled by numbers (length of exons is not to scale). Overlapping RT-PCR fragments are represented by *lines* 1 to 9. These fragments were amplified and sequenced to confirm the exonic structure of the *Cacna2d4* transcript. (⋆) Conserved cysteine residues in the truncated part of the protein. (B) RT-PCR of fragment 7 (exons 14–29) and 9 (exons 33–38) in retina of wild-type (wt), heterozygous (het), and mutant (mut) animals. L, the DNA ladder.

bands detected in amplicon 9 occurred in the range of 300 to 400 bp in kidney, muscle, spleen, and stomach and may indicate alternative splicing at the 3′ end of *Cacna2d4*.

Examination of Cone Numbers in Affected Mice

In previous studies, attenuated scotopic photoreceptor responses in mutants (scotopic a-wave) have been interpreted to reflect reduced rod photoreceptor number.[1] The complete absence of cone-specific activities remained unexplained. To elucidate whether a preferential loss of cone photoreceptors occurs in mutant animals, immunohistochemical staining of cones was performed. No obvious alterations in the pattern of cones were detected. The cone density in the central and peripheral retina of 6-week-old mutant animals did not significantly differ from that of wild-type mice (Fig. 7A). However, a ~15% reduction in the number of cells in the outer nuclear layer was detected, indicating an early degeneration of rod photoreceptors (Fig. 7B).

DISCUSSION

In the present study, we report genetic mapping of the respective trait and the identification of the disease-causing mutation in the voltage-gated L-type calcium channel auxiliary subunit Cacna2d4. This gene is ubiquitously expressed and shows significantly reduced transcript amounts in the retina of affected and heterozygous animals. The disease is caused by a homozygous single nucleotide insertion in exon 25 of *Cacna2d4* which results in a frameshift that truncates one third of the predicted amino acid sequence. This defect represents a novel channelopathy that disturbs synaptic signal processing in the retina and leads to functional failure of cones and early onset degeneration of rods.

The causative nature of the identified mutation is supported by several lines of evidence. Linkage analysis revealed a single locus limited to only 275 kb on chromosome 6. No further candidate regions were detected in the mouse genome on linkage analysis. The mutation perfectly segregates with the disease phenotype. Homozygosity for this mutation was detected only in affected animals ($n = 172$). In unaffected mice ($n > 500$), homozygosity for wild-type alleles or heterozygosity were observed. No sequence variations were found in any other gene from the linkage interval. Moreover, the expression of the respective *Cacna2d4* mRNA was confirmed by RT-PCR analyses in the mouse retina and the mutation was verified in affected animals by direct sequencing of the relevant RT-PCR

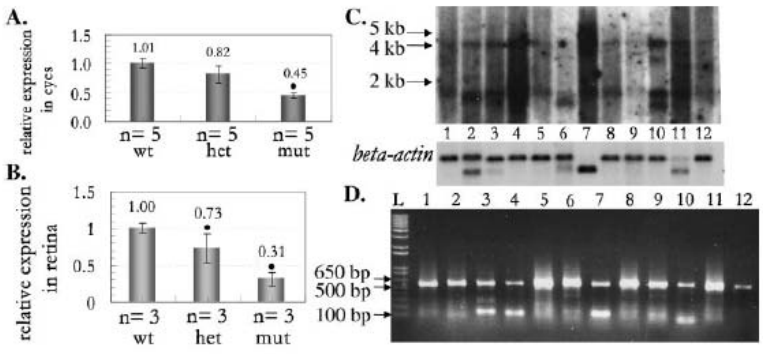

FIGURE 6. *Cacna2d4* transcript analysis. (A) Eye-specific expression of *Cacna2d4* by real-time PCR. Confidence intervals (error bars) represent biological variability of five animals for each genotype. The *Cacna2d4* transcript amount of each animal was normalized to the median value of the wild-type controls. The diagram displays a significant reduction of *Cacna2d4* transcript abundance in eyes of affected animals compared with wild types ($P < 0.05$). In heterozygous animals, the confidence interval overlaps with wild type; however, statistical analyses indicate a significant tendency toward reduced transcript levels in those animals. (B) Retina-specific expression of *Cacna2d4* by real-time PCR. Confidence intervals indicate experimental and biological variability of the quantitative RT-PCR performed with three cDNA dilutions from pooled retinas of three mice per genotype. Homozygous mutant and heterozygous animals show significantly reduced transcript levels in comparison to wild-type mice ($P < 0.05$) (C) Expression of *Cacna2d4* in nonocular mouse tissues. Multitissue Poly A^+ Northern blot analysis detects *Cacna2d4* transcripts in 12 tissues: *lane 1*: brain; *lane 2*: heart; *lane 3*: kidney; *lane 4*: liver; *lane 5*: lung; *lane 6*: muscle; *lane 7*: skin; *lane 8*: small intestine; *lane 9*: spleen; *lane 10*: stomach; *lane 11*: testis; *lane 12*: thymus. Tissue-specific alternative splice variants were observed. (D) RT-PCR of fragment 9 comprising exon 33 to 38 in 12 mouse tissues: *lane L*: DNA ladder, *lane 1*: brain; *lane 2*: heart; *lane 3*: kidney; *lane 4*: liver; *lane 5*: lung; *lane 6*: muscle; *lane 7*: skin; *lane 8*: spleen; *lane 9*: stomach; *lane 10*: testis; *lane 11*: olfactory bulb; *lane 12*: eye. Bands occurring at the size of ~100 to 200 bp are PCR primer dimers. Bands of 300 to 400 bp in kidney, muscle, spleen, and stomach may indicate alternatively spliced isoforms of *Cacna2d4*.

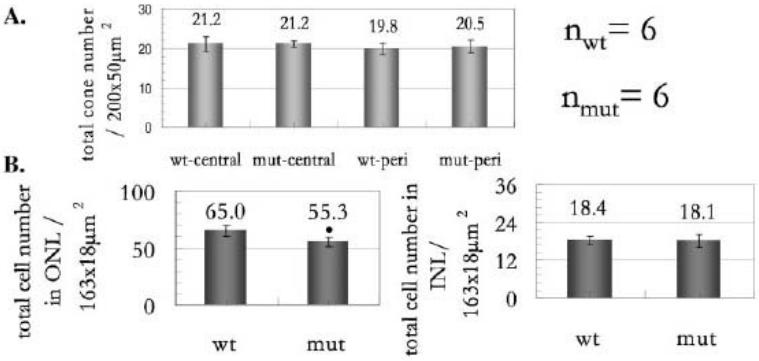

FIGURE 7. Comparison of cell numbers in homozygous mutant and wild-type retinas. (**A**) The average density of cone Gα transducin-immunopositive photoreceptors examined at central (central) and peripheral (peri) retina in 163 × 18-μm^2 subfields of six wild-type (wt) and six mutant (mut) mice. (**B**) Number of cells in a 163 × 18-μm^2 subfield of the ONL (outer nuclear layer) and INL (inner nuclear layer) examined at central retina. In the ONL, significant reduction of photoreceptor cell number occurs ($P < 0.05$). Error bars, confidence intervals.

fragments. The premature termination signal may lead to selective mRNA degradation by nonsense mediated decay (NMD), to prevent translation of truncated proteins.[15] Indeed, we found significantly reduced mRNA levels in homozygous mutant mice by quantitative RT-PCR. The mutation introduces a premature stop codon 77 nucleotides upstream of the boundary of exons 26/27, a position that is efficiently recognized by the NMD machinery. It is noteworthy that we did not obtain evidence by RT-PCR for alternative splice variants of *Cacna2d4* lacking exons 25 and 26. This observation suggests that these two exons are constitutively expressed in the retina.

Nevertheless, residual mutant *Cacna2d4* transcripts may undergo translation. However, this probably results in a nonfunctional product as it lacks almost one third of the protein at the C terminus. The deduced mouse sequence of Cacna2d4 shows a high degree of sequence identity and conserved domain structure in many species, as demonstrated by comparative protein alignments (part of data shown in Fig. 4C). The human CACNA2D4 protein shares 79% identical amino acid residues with its mouse orthologue. The truncated part of Cacna2d4 displays 93% similarity in both species on the amino acid level and contains functionally important domains. Each α2δ subunit identified so far consists of a single-gene product cleaved posttranslationally into α2 and δ peptides linked by disulfide bridges.[4,16] The δ peptides possess a conserved single transmembrane segment at the carboxyl terminus for cell surface attachment.[17] In human CACNA2D4, a homologous highly hydrophobic region encoded by the last two exons (37 and 38) potentially acts as the transmembrane domain.[11] This motif is removed in mutant mice by the premature stop codon (Fig. 5A). Furthermore, the proteolytical cleavage site between the α2 and δ peptides is encoded by a conserved alanine residue at position 971 in exon 34. The premature translational stop occurs at amino acid position 802 (exon 26) and thus eliminates the entire δ subunit. Hence, membrane integration of Cacna2d4 is probably abolished as a major consequence.[18] An additional 170 amino acid residues (802-971) are truncated from the C terminus of the α2 peptide (exons 26–34). This deletion comprises one of the two Cache domains formed by amino acid residues 869-879. These domains, highly conserved in all α_2 subunits, are supposed to be involved in interaction with calcium channel complexes.[19] Finally, at least 11 cysteine residues, conserved in all murine and human α2δ subunits, are removed by the truncation.[20]

Loss of Cacna2d4 function may have severe effects on the retinal physiology in C57BL/10 mutant animals. The α2δ subunits are determinants of auxiliary stimulation of calcium channel complexes.[17,21] Beyond this, they aid in augmentation of α1 subunits on the plasma membrane increasing the density of functional channels on the cell surface and thus accelerating calcium current amplitudes.[22,23] In cell lines, human CACNA2D4 enhances the α1C/β3-mediated calcium influx threefold.[11] The precisely modulated calcium signaling and the overall integrity of α1 subunits into the presynaptic membranes may be severely affected in C57BL/10 mutant mice and therefore result in compromised neurotransmission of the retinal ribbon synapses. Loss of function of the retina-specific α1F subunit in the recently described *Cacna1f* mouse mutant revealed absence of synaptic signaling and was associated with substantial degeneration of photoreceptor ribbon terminals.[10] Transgenic mice deficient for the β2 auxiliary subunit demonstrate loss of synaptic processing due to lack of trafficking and proper assembly of α1F complexes in photoreceptor synaptic membranes.[9] Similar to our mutants, loss of ribbon-type synapses was detected.

Two additional L-type α1 subunits, Cacna1c and Cacna1d, are involved in neurotransmission and synaptic plasticity of retinal ribbon synapses.[24–28] Strong expression of N- and P/Q-type calcium channels at plasma membranes of retinal neurons was also observed.[29,30] Because α2δ subunits have been identified as components of all voltage-gated calcium channel complexes, these channels may be subject to Cacna2d4 modulation. Likewise, other retinal channels may underlie Cacna2d4-mediated stimulation.[31] Preliminary results in immunofluorescence microscopy of retinal sections stained with antibodies detecting α1 subunits of voltage-gated calcium channels (anti-pan Cavα1 antibody (Alomine Laboratories, Munich, Germany), anti-α1C and anti-α1F (Santa Cruz Biotechnology, Santa Cruz, CA; data not shown) indicated reduced signals in the OPL of mutant animals. This may be a consequence of the reduced thickness of the OPL or may imply a decreased density of α1 subunits at the synaptic terminals.

The phenotype in mutant mice is restricted to retina, as no further apparent abnormalities are detectable, although the expression is ubiquitous. Affected animals display normal behavior and body weight and regular breeding. In correlation to the cone–rod dysfunction of the *Cacna1f*-mutant, these mice are probably congenitally blind.[10] Yet, the elimination of ~15% of photoreceptor cells in mutant animals may indicate additional degenerative processes. As minor alterations in calcium concentration modulate a diversity of molecular processes, the dysregulation of the calcium homeostasis may activate further pathogenic mechanisms responsible for the rod photoreceptor cell death.[32] The identification of the *Cacna2d4* defect may have implications for corresponding retinal diseases in human patients. The deficiency of Cacna2d4 may be associated with rare human autosomal recessive incomplete CSNB. However, because a mutation in *CACNA1F* was also found in a family

with a cone–rod dystrophy,[7] the CACNA2D4-mediated channelopathy may involve both night blindness and cone–rod dystrophy. Finally, the early degeneration of rod photoreceptors in mutant mice may indicate a causative role of mutations in this gene, also in patients with retinitis pigmentosa.

Acknowledgments

The authors thank Stefanie Derzsi, Ulrich Luhmann, Gabor Matyas, Gaby Tanner, Mariana Wittmer, and Christina Zeitz for discussions and experimental assistance.

References

1. Ruether K, Grosse J, Matthiessen E, Hoffmann K, Hartmann C. Abnormalities of the photoreceptor-bipolar cell synapse in a substrain of C57BL/10 mice. *Invest Ophthalmol Vis Sci.* 2000;41:4039–4047.
2. Heidelberger R, Thoreson WB, Witkovsky P. Synaptic transmission at retinal ribbon synapses. *Prog Retin Eye Res.* 2005;24:682–720.
3. Beaumont V, Llobet A, Lagnado L. Expansion of calcium microdomains regulates fast exocytosis at a ribbon synapse. *Proc Natl Acad Sci USA.* 2005;102:10700–10705.
4. Catterall WA. Structure and regulation of voltage-gated Ca2+ channels. *Annu Rev Cell Dev Biol.* 2000;16:521–555.
5. Bech-Hansen NT, Naylor MJ, Maybaum TA, et al. Loss-of-function mutations in a calcium-channel alpha1-subunit gene in Xp11.23 cause incomplete X-linked congenital stationary night blindness. *Nat Genet.* 1998;19:264–267.
6. Hoda JC, Zaghetto F, Koschak A, Striessnig J. Congenital stationary night blindness type 2 mutations S229P, G369D, L1068P, and W1440X alter channel gating or functional expression of Ca(v)1.4 L-type Ca2+ channels. *J Neurosci.* 2005;25:252–259.
7. Nakamura M, Ito S, Piao CH, Terasaki H, Miyake Y. Retinal and optic disc atrophy associated with a CACNA1F mutation in a Japanese family. *Arch Ophthalmol.* 2003;121:1028–1033.
8. Jalkanen R, Demirci FY, Tyynismaa H et al. A new genetic locus for X linked progressive cone-rod dystrophy. *J Med Genet.* 2003;40:418–423.
9. Ball SL, Powers PA, Shin HS, Morgans CW, Peachey NS, Gregg RG. Role of the beta(2) subunit of voltage-dependent calcium channels in the retinal outer plexiform layer. *Invest Ophthalmol Vis Sci.* 2002;43:1595–1603.
10. Mansergh F, Orton NC, Vessey JP et al. Mutation of the calcium channel gene Cacna1f disrupts calcium signaling, synaptic transmission and cellular organization in mouse retina. *Hum Mol Genet.* 2005;14:3035–3046.
11. Qin N, Yagel S, Momplaisir ML, Codd EE, D'Andrea MR. Molecular cloning and characterization of the human voltage-gated calcium channel alpha(2)delta-4 subunit. *Mol Pharmacol.* 2002;62:485–496.
12. Lander ES, Green P, Abrahamson J et al. MAPMAKER: an interactive computer package for constructing primary genetic linkage maps of experimental and natural populations. *Genomics.* 1987;1:174–181.
13. Akimoto M, Filippova E, Gage PJ, Zhu X, Craft CM, Swaroop A. Transgenic mice expressing Cre-recombinase specifically in M- or S-cone photoreceptors. *Invest Ophthalmol Vis Sci.* 2004;45:42–47.
14. Blanks JC and Johnson LV. Specific binding of peanut lectin to a class of retinal photoreceptor cells: a species comparison. *Invest Ophthalmol Vis Sci.* 1984;25:546–557.
15. Conti E, Izaurralde E. Nonsense-mediated mRNA decay: molecular insights and mechanistic variations across species. *Curr Opin Cell Biol.* 2005;17:316–325.
16. De Jongh KS, Warner C, Catterall WA. Subunits of purified calcium channels: alpha 2 and delta are encoded by the same gene. *J Biol Chem.* 1990;265:14738–14741.
17. Sipos I, Pika-Hartlaub U, Hofmann F, Flucher BE, Melzer W. Effects of the dihydropyridine receptor subunits gamma and alpha2delta on the kinetics of heterologously expressed L-type Ca2+ channels. *Pflugers Arch.* 2000;439:691–699.
18. Brodbeck J, Davies A, Courtney JM, et al. The ducky mutation in Cacna2d2 results in altered Purkinje cell morphology and is associated with the expression of a truncated alpha 2 delta-2 protein with abnormal function. *J Biol Chem.* 2002;277:7684–7693.
19. Anantharaman V, Aravind L. Cache-a signaling domain common to animal Ca(2+)-channel subunits and a class of prokaryotic chemotaxis receptors. *Trends Biochem Sci.* 2000;25:535–537.
20. Gurnett CA, De Waard M, Campbell KP. Dual function of the voltage-dependent Ca2+ channel alpha 2 delta subunit in current stimulation and subunit interaction. *Neuron.* 1996;16:431–440.
21. Gurnett CA, Felix R, Campbell KP. Extracellular interaction of the voltage-dependent Ca2+ channel alpha2delta and alpha1 subunits. *J Biol Chem.* 1997;272:18508–18512.
22. Hobom M, Dai S, Marais E, Lacinova L, Hofmann F, Klugbauer N. Neuronal distribution and functional characterization of the calcium channel alpha2delta-2 subunit. *Eur J Neurosci.* 2000;12:1217–1226.
23. Lacinova L, Klugbauer N. Modulation of gating currents of the Ca(v) 3.1 calcium channel by alpha 2 delta 2 and gamma 5 subunits. *Arch Biochem Biophys.* 2004;425:207–213.
24. Xu HP, Zhao JW, Yang XL. Expression of voltage-dependent calcium channel subunits in the rat retina. *Neurosci Lett.* 2002;329:297–300.
25. Mize RR, Graham SK, Cork RJ. Expression of the L-type calcium channel in the developing mouse visual system by use of immunocytochemistry. *Brain Res Dev Brain Res.* 2002;136:185–195.
26. Wilkinson MF, Barnes S. The dihydropyridine-sensitive calcium channel subtype in cone photoreceptors. *J Gen Physiol.* 1996;107:621–630.
27. Nachman-Clewner M, St Jules R, Townes-Anderson E. L-type calcium channels in the photoreceptor ribbon synapse: localization and role in plasticity. *J Comp Neurol.* 1999;415:1–16.
28. Puro DG, Hwang JJ, Kwon OJ, Chin H. Characterization of an L-type calcium channel expressed by human retinal Muller (glial) cells. *Brain Res Mol Brain Res.* 1996;37:41–48.
29. Breustedt J, Vogt KE, Miller RJ, Nicoll RA, Schmitz D. Alpha1E-containing Ca2+ channels are involved in synaptic plasticity
30. Witcher DR, De Waard M, Sakamoto J, et al. Subunit identification and reconstitution of the N-type Ca2+ channel complex purified from brain. *Science.* 1993;261:486–489.
31. Vallazza-Deschamps G, Cia D, Gong J, et al. Excessive activation of cyclic nucleotide-gated channels contributes to neuronal degeneration of photoreceptors. *Eur J Neurosci.* 2005;22:1013–1022.
32. Leo S, Bianchi K, Brini M, Rizzuto R. Mitochondrial calcium signalling in cell death. *FEBS Lett.* 2005;272:4013–4022.

3.1.1. Supplementary Material

Supplementary Table S1. Summary of relative allelic distribution for genetic markers. Locus determining markers are shaded in grey. Significance of linkage is visualized by X^2 values. Markers homozygous for C57BL/10 allele (bb), homozygous for AJ (aa) and heterozygous (ab).

marker	cM	Mb	bb	ab	aa	X^2
D6mit183	**26.5**	**53.4**	0.4	**0.4**	**0.1**	**12.2**
D6mit69	**31.5**	**84.0**	0.6	**0.3**	**0.1**	**43.9**
D6mit102	**38.5**	**93.9**	0.7	**0.2**	**0.1**	**72.5**
D6mit105	**45.5**	**108.3**	0.9	**0.2**	**0.0**	**121.8**
D6mit108	**48.1**	**111.9**	0.9	**0.1**	**0.0**	**134.0**
D6mit287	**49.0**	**112.6**	0.9	**0.1**	**0.0**	**140.6**
D6mit389	48.2	112.7	0.9	0.1	0.0	265.1
D6mit369	58.8	121.1	1.0	0.0	0.0	354.5
D6mit216	58.6	121.6	1.0	0.0	0.0	343.8
D6mit336	60.7	125.2	1.0	0.0	0.0	192.0
D6mit255	60.3	125.7	1.0	0.0	0.0	342.2
D6mit134	57.5	126.0	1.0	0.0	0.0	337.7
D6mit218	61.2	127.7	0.9	0.1	0.0	266.6
D6mit133	**58.5**	**128.0**	0.9	**0.1**	**0.0**	**147.1**
D6mit368	**55.0**	**128.3**	0.9	**0.1**	**0.0**	**141.2**
D6mit52	**61.0**	**128.5**	0.9	**0.1**	**0.0**	**151.2**
D6mit289	**62.3**	**129.5**	0.9	**0.1**	**0.0**	**144.1**
D6mit14	**71.2**	**146.6**	0.7	**0.2**	**0.1**	**75.8**

Supplementary Table S2. List of analyzed candidate genes.

Table 2. List of analyzed candidate genes.

gene symbol	gene name	GI number	sequence analysis	putative function
Akap3	A kinase (PRKA) anchor protein 3	6753025	ORF	signaling
Tmem16b	transmembrane protein 16B	23956389	whole mRNA	unknown
Atp6v1e1	ATPase, H+ transporting, V1 subunit E isoform 1	45504358	ORF	hydrogen ion transporter
Adipor2	Adiponectin receptor 2	39841015	whole mRNA	fatty acid metabolism
Bcap37	B-cell receptor-associated protein 37	6671621	ORF	signaling
Cacna1c	calcium channel, voltage-dependent, L type, alpha 1C	6753227	ORF	signal transduction
LOC245882	similar to voltage-gated calcium channel alpha(2)delta-4	28544679	whole mRNA	signal transduction
5730412N02Rik	similar to voltage-gated calcium channel alpha(2)delta-4	28544677	whole mRNA	signal transduction
Cacna2d4	similar to voltage-gated calcium channel alpha(2)delta-4	55832799	whole gene	signal transduction
AB114826	beta 1,4-N-acetylgalactosaminyltransferase-transferase-III	38566699	whole mRNA	adhesion
Clecs8	carbohydrate recognition domain lectin, superfamily member 8	4159800	ORF	adhesion
Clecsf9	carbohydrate recognition domain lectin, superfamily member 9	13096843	ORF	adhesion
Cops7a	COP9 constitutive photomorphogenic	7242141	ORF	adhesion
Cs3	Calsynthenin -3	32822766	ORF	adhesion
Edr1	early development regulator1	6681270	ORF	transcription factor
Eno2	Enolase2	55494	ORF	transcription factor
Fhx	Mus musculus fork head transcription factor	11118639	ORF	transcription factor
Fbxl14	F-box and leucine-rich repeat protein 14	19527157	whole mRNA	ubiquitin cycle
Gabt2	solute carrier family 6 / neurotransmitter transporter	19526805	ORF	signal transduction
Gat3	solute carrier family 6 / neurotransmitter transporter	21362294	ORF	signal transduction
Gpr92	G protein-coupled receptor	51712654	whole mRNA	signal transduction
Gnb2	guanine nucleotide binding protein, beta 3	17390552	ORF	signal transduction
LOC333154	similar to karyopherin (importin) alpha 2	28544764	whole mRNA	signal transduction
Kcna1	potasium channel	31560569	ORF	signal transduction
Kcna5	potasium channel	22122428	ORF	signal transduction
Kcna6	potasium channel	34328479	ORF	signal transduction
Lpr7b	leucine rich protein, B7 gene	7305240	ORF	adhesion
AI841794	expressed sequence AI841794	40254213	whole mRNA	unknown
Ninj2	Ninjurin 2	7710069	ORF	adhesion
Ntf3	Neurotrophin 3	52694681	ORF	transcription factor
Rab6ip1	Rab6 interacting protein 2	16716510	ORF	protein transport
Rho	Rhodopsin	26336445	ORF	signal transduction
Sec13r	SEC13-like 1 (S. cerevisiae)	31343633	ORF	adhesion
Syn2	Synapsin2	8567409	ORF	synaptic vesicle
Tulp3	tubby-like protein 3	3372490	ORF	synaptic vesicle
Vamp1	Synaptobrevin	31543936	ORF	synaptic vesicle
Wnt5b	wingless-related MMTV integration site 5B	12850441	whole mRNA	signaling
Zfp329	zinc finger protein 239	49087127	ORF	transcription factor

Supplementary Table S3. Markers identified and applied in fine mapping.

Table 3. Markers identified and applied in fine mapping.

SNP name	position / bp UCSC database mouse genome broser March 2005	AJ strain	C57Bl/10 strain	% bb	% aa	% ab
Cacna1c	119.540.822-119.540.222	C	G	98.47	0	1.53
SNP-A	119.611.249-119.611.671	G	A	98.47	0	1.53
SNP-G	119.647.932-119.648.261	G	A	98.47	0	1.53
SNP-P	119.623.976-119.624.265	C	A	98.47	0	1.53
SNP- M (A)	119.657.413-119.657.832	C	T	98.47	0	1.53
SNP-M (B)	119.657.413-119.657.832	A	G	98.47	0	1.53
SNP-Y	119.661.652-119.661.991	C	T	100	0	0
Wnt5b	119.694.099-119.694.538	C	T	100	0	0
SNP-WW	119.915.178-119.915.591	G	A	100	0	0
SNP-GG	119.918.638-119.919.228	T	C	99.24	0	0.76
SNP-FF	119.920.711-119.921.060	C	T	99.24	0	0.76
SNP-EE	119.923.572-119.924.011	C	T	99.24	0	0.76
SNP-DD	119.929.420-119.929.779	G	A	99.24	0	0.76
SNP-VV (A)	119.934.302-119.934.630	G	C	99.24	0	0.76
SNP-VV (B)	119.934.302-119.934.630	C	T	99.24	0	0.76
SNP-RR (A)	119.943.385-119.943.841	T	A	99.24	0	0.76
SNP-RR (B)	119.943.385-119.943.841	A	T	99.24	0	0.76
SNP-RR (C)	119.943.385-119.943.841	A	"-"	99.24	0	0.76
SNP-FE (A)	119.950.501-119.950.957	C	T	99.24	0	0.76
SNP-FE (B)	119.950.501-119.950.957	T	G	99.24	0	0.76
SNP-FE (C)	119.950.501-119.950.957	G	C	99.24	0	0.76
SNP-FE (D)	119.950.501-119.950.967	A	G	99.24	0	0.76
SNP-MM	119.955.297-119.955.794	G	A	99.24	0	0.76
SNP-OO (A)	119.961.848-119.962.237	C	T	99.24	0	0.76
SNP-OO (B)	119.961.848-119.962.237	G	A	99.24	0	0.76
SNP-PP	120.005.033-120.005.377	A	G	99.24	0	0.76
Rab6ip2 -1	120.175.970-120.185.609	G	A	98.47	0	1.53
Rab6ip2 -2	120.126.828-120.145.857	G	A	98.47	0	1.53
Gpr92	125.737.223-125.738.577	C	T	97.71	0	2.29
M6pr-1	122.976.417-122.976.817	G	T	97.71	0	2.29
M6pr -2	122.970.560-122.970.980	C	T	97.71	0	2.29
Vamp1	125.876.311-125.876.761	T	C	96.18	0	3.82
D6Mit217	125.975.504-125.975.688	CT	"-"	96.18	0	3.82
Tnfrsfla	125.889.991-125.893.708	GCGGGCG	"-"	96.18	0	3.82
Akap3(A)	127.533.163-127.533.701	T	C	94.66	0	5.34
Akap3(B)	127.533.163-127.533.701	G	A	94.66	0	5.34

* Shaded area shows SNPs of the final linkage interval.

Supplementary Figure S1. Mouse genome scan. The three possible allele combinations of a genetic marker in F2 affected animals are discriminated by colours. *Line bb*: derived from the C57BL/10 strain, represents a homozygous mutant, *line aa*: derived from the AJ strain a wild-type, and *line ab*: a heterozygous allele pair. The number of animals with the respective allelic combination is expressed in percent and visualized for each chromosome. Marker names at the X-axis are positioned corresponding to the chromosomal order from centromere to telomere. The chromosome numbers are indicated by the first digit of the marker name (for example *D1Mit136* correspond to chromosome number 1, *D8Mit31* to chromosome number 8). Absence of linkage between disease and marker is evident from the allele distribution following the ratio of 25% : 50% : 25% for *aa : ab* : *bb*. In contrast, linkage results in a significant increase in the number of animals homozygous for marker alleles of the C57BL/10 substrain and reduction of remaining allele combinations, as exclusively observed for chromosome 6.

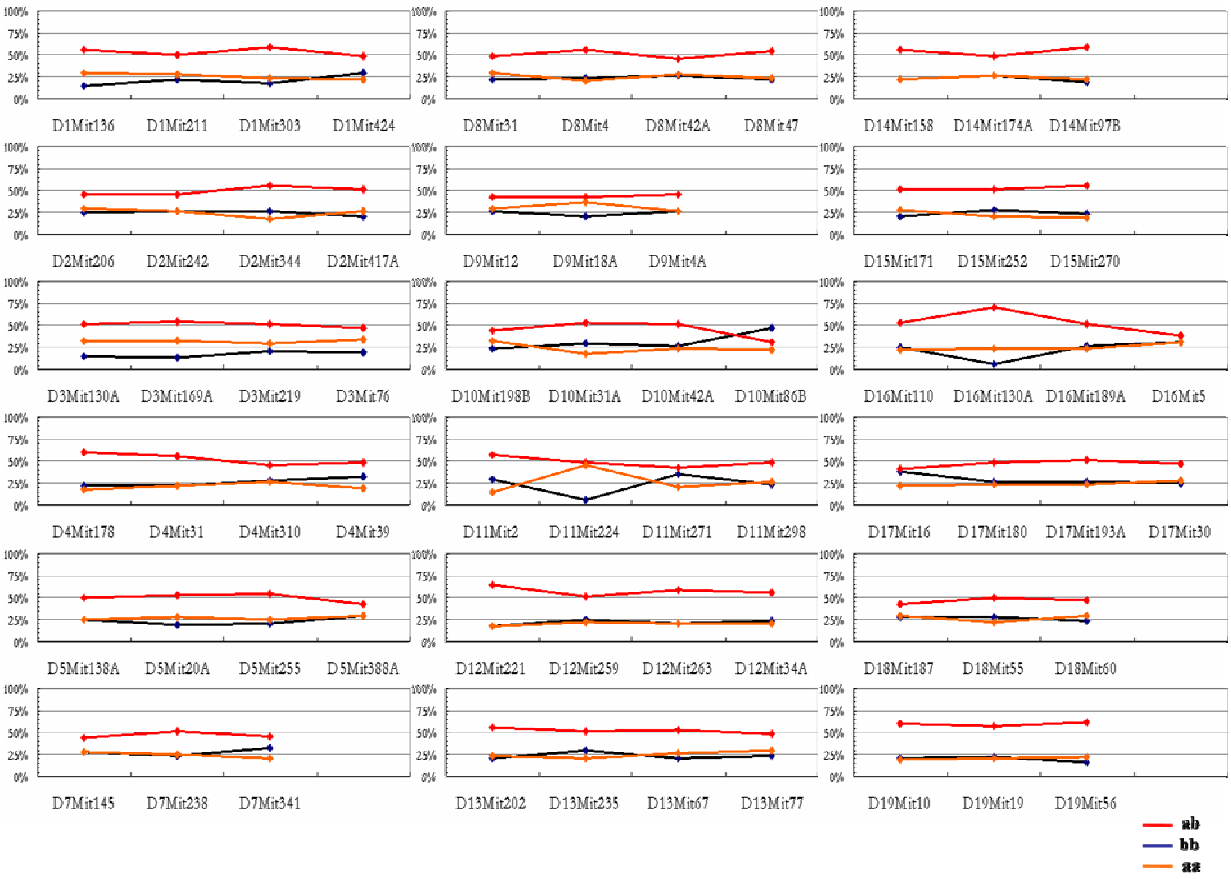

3.2. Mutation in the Auxiliary Calcium Channel Subunit CACNA2D4 Cause Autosomal Recessive Cone Dystrophy

Running title: Cone dystrophy due to *CACNA2D4* mutation

K. A. Wycisk[1*], C. Zeitz[1*], S. Feil[1], M. Wittmer[1], U. Forster[1], J. Neidhardt[1], B. Wissinger[2,3], E. Zrenner[3], R. Wilke[3], S. Kohl[2,3], W. Berger[1]

[*]These authors contributed equally to this study and therefore should be considered equivalent authors.

Epub ahead of print, September 7th, 2006, American Journal of Human Genetics

[1]Division of Medical Molecular Genetics and Gene Diagnostics, Institute of Medical Genetics, University of Zurich, Schorenstrasse 16, 8603 Schwerzenbach, Switzerland; [2]Molecular Genetics Laboratory, University Eye Hospital, Roentgenweg 11, 72076 Tuebingen, [3]University Eye Hospital, Eberhard-Karls University Tuebingen, Schleichstrasse 12-16, 72076 Tuebingen, Germany

Acknowledgements: The authors would like to thank patients and family members for participation in this study as well as Stefanie Derzsi, Barbara Kloeckener-Gruissem, Gábor Mátyás and Philippe Reuge for discussions and experimental assistance. This study was supported by the Foundation Fighting Blindness (USA), the Swiss National Science Foundation (Grant#3100-067786 to WB), Velux Foundation (Grant #162 to WB and CZ), Hartman Mueller Foundation Switzerland (Grant #1002 to CZ) and EUFP6 integrated project "EVI-GENORET" (Grant # LSHG-CT-2005–512036 to E.Z).

3.2.1. Abstract

Retinal signal transmission depends on the activity of high voltage-gated L-type calcium channels in photoreceptor ribbon synapses. We recently identified a truncating frameshift mutation in the *Cacna2d4* gene in a spontaneous mouse mutant with profound loss of retinal signaling and an abnormal morphology of ribbon synapses in rods and cones. The *Cacna2d4* gene encodes an L-type calcium channel auxiliary subunit of the α2δ type. Mutations in its human orthologue, *CACNA2D4,* were not yet associated with a disease. We performed mutation analyses in 34 patients initially diagnosed with night blindness and detected a homozygous nucleotide substitution (c.2406C>A) in *CACNA2D4* of two affected siblings. The mutation introduces a premature stop codon which truncates one third of the corresponding open reading frame. Both patients share symptoms of slowly progressing cone dystrophy. These findings represent the first report of a mutation in the human *CACNA2D4* gene and define a novel gene defect causing autosomal recessive cone dystrophy.

3.2.2. Introduction

Voltage-gated L-type calcium channels are known to contribute in the retinal signal transmission[1]. They predominantly cluster in presynaptic membranes of photoreceptors and ON-type bipolar cells, an excitatory class of second-order neurons, and mediate calcium-dependent neurotransmitter release[2,3]. At the molecular level, these calcium channels constitute heteromultimeric protein complexes composed of a pore-forming α1 subunit, which triggers calcium influx across the synaptic membrane, and the auxiliary subunits β, γ and α2δ[4]. The α1 subunit imparts most of the conductive properties of the channel, whereas the accessory subunits modulate resultant calcium currents and channel activation/inactivation kinetics[5-7]. The auxiliary subunits are also involved in proper assembly and membrane localization of the calcium channel complexes[6]. Channelopathies due to mutations in some L-type voltage-gated calcium channel subunits underlie perturbed retinal signal transmission and result in severe forms of visual impairments in human and animals[8,9]. Genetic defects in the retina-specific L-type α1F subunit, *CACNA1F*, were identified to cause incomplete X-linked congenital stationary night blindness, characterized by impaired night vision and varying symptoms of myopia, hyperopia, strabismus and nystagmus [OMIM number 300071, 300110][10-16]. Upon electrophysiological examinations, *CACNA1F* patients constitute profoundly reduced activities of the second-order neurons and absent oscillatory potentials under photopic conditions, whereas photoreceptor responses to light, although attenuated, are maintained. Thus, visual impairment arises primarily from a decrease in efficiency of photoreceptor-specific synaptic signal transmission[17,18]. Of note, mutations in the α1F subunit are also associated with clinical manifestation of retinal and optic disc atrophy as well as cone-rod dystrophy, a progressive photoreceptor degeneration resulting in particularly severe visual impairment[19,20]. By positional cloning, we recently identified a homozygous protein truncating frameshift mutation in exon 25 of the *Cacna2d4* gene of affected C57BL/10 mice, which encodes the fourth voltage-gated L-type calcium channel auxiliary subunit of the α2δ type[21]. So far, mutations in its human orthologue, *CACNA2D4*, were not associated with a disease. Alluding to the retinal phenotype of *Cacna2d4*-mutant animals, genetic defects in *CACNA2D4* seemed likely to cause human retinal disorders. We therefore performed *CACNA2D4* mutation studies in 34 patients initially diagnosed with night blindness. Here, we report for the first time an autosomal recessive cone dystrophy due to a mutation in the human *CACNA2D4* gene.

3.2.3. Subjects and Methods

Patients

The research was performed in accordance with the tenets of the Declaration of Helsinki and approved by the institutional review board of the University Hospital Tuebingen. Signed informed consent was obtained from all patients and family members before blood sampling.

For mutation analyses, DNA of 34 unrelated patients was included. On the basis of electroretinography (ERG), most of those patients were classified as suffering from stationary night blindness. The fact that under dark- and light-adapted conditions almost normal photoreceptor responses but reduced activities of adjacent secondary retinal neurons were recorded, indicated a clear transmission defect, typical for the incomplete form of congenital stationary night blindness (iCSNB).

In all patients of unspecified night blindness-like disorder, mutations in both *NYX* and *GRM6* genes, known to underlie the complete form of congenital stationary night blindness (CSNB), were excluded prior to mutational examinations in *CACNA2D4*, according to previous mutation studies[16,22-25]. In 10 patients with a diagnosis of the incomplete night blindness, absence of pathogenic sequence variants in the *CACNA1F* gene was proven by mutational pre-screening, in accordance to the methods described before[16].

Clinical Evaluation

Phenotype analysis consisted of complete clinical ophthalmologic examination, including visual acuity (VA), Goldmann perimetry, panel D15 colour vision testing, thresholds for light perception upon 30 min of dark adaptation, fundus photography, Ganzfeld electroretinography, and vitamin A and retinol-binding protein level estimations. Panel D15 colour vision was evaluated by calculation of the total error score (TES) in accordance to the methodology of Vingris et al.[26]. ERG responses were recorded with a UTAS 2000 system (LKC Technologies, Gaithersburg, USA) and DTL electrodes, accordingly to International Society for Clinical Electrophysiology of Vision (ISCEV) standards[27]. For this, rod responses were recorded after 20 min of dark adaptation, using a dim flash of strength 2.5 log units below the white standard flash (SF), defined by standard intensities of 2.4 cds/m^2. Recordings of the maximal combined responses (rod/cone) were performed upon the SF at dark adapted conditions. The respective oscillatory potentials (rod/cone) were recorded in the dark adapted state, using the SF and a bandpass filter of 100 – 300Hz. Single flash cone responses were recorded subsequently to 10

min of light adaptation, applying the SF and a rod suppressing background (25cd/m^2). 30-Hz flicker responses were obtained using the SF with the same rod suppressing background at a repetition rate of 30-Hz.

Mutation analyses

The *CACNA2D4* gene comprises 38 exons that span approximately 130 kb of the human chromosome 12 (12.p13.3). Three splice variants of *CACNA2D4* are suggested from EST databases. The longest transcript of 5335 bp includes all 38 exons (GenBank accession number: NM_172364.3) and codes for an open reading frame of 3414 bp (exons 1 to 38), translated into a protein of 1137 amino acid residues. The remaining two mRNA variants are assembled upon alternative exclusion of exons 28 or 30 (GenBank accession number: NM_001005766; NM_001005737, www.ncbi.nlm.nih.gov).

For *CACNA2D4* mutational analyses, genomic DNA was extracted from blood samples by standard methods. For each patient, the complete coding region of the longest *CACNA2D4* splice variant was analyzed by direct sequencing. Primers (Microsynth, Balgach, Switzerland) were designed to amplify exon- and splice site spanning fragments from genomic DNA. In addition, putative alternative *CACNA2D4* exons 1b and 37L were included in our mutation screening[28]. For all fragments, primer sequences, PCR amplification and cycle sequencing conditions have been summarized in Table 2. The respective amplicons were generated in 33 independent reactions, prepared in a total volume of 20 µl, including 1 unit of polymerase (HotFirePoly DNA polymerase, Solis, Biodyne, Tartu, Estonia), 2 µl buffer, 0.5 µl of 10 mM dNTPs, 1.0 µl of each primer (10 µM), and 5-100 ng of genomic DNA. The $MgCl_2$ and Q-solution amounts (Qiagen, Hombrechtikon, Switzerland) for each PCR are indicated in Table 2. The reactions followed 40 cycles of 1 min at 95°C, 1 min at annealing temperature and 1.5 min at 72°C, including an initial denaturation step of 15 min at 95°C and a final elongation step of 10 min at 72°C. After purification (ExoSap-IT Kit, USB, Cleveland, USA), PCR products were bidirectionally sequenced on an ABI PRISM®3100 Genetic Analyzer in accordance to ABI PRISM® Big Dye Chemistry v1.1 protocol (Applied Biosystems, Rotkreuz; Switzerland). Sequences were aligned by ABI PRISM® SeqScape (Applied Biosystems) software and subsequently examined for sequence variants in comparison to the reference sequence NM_172364.3. Mutations in patients were verified by two independent sequence reactions on two independent blood samples each, and excluded from 224 control alleles from unrelated person[29].

3.2.4. Results

Mutation analyses

Among 34 patients examined, we detected a homozygous c.2406C>A transversion in exon 25 of the *CACNA2D4* gene in the index patient II-1 (42 years of age), diagnosed with a slightly progressing cone dystrophy (Fig. 1). The family of this patient consists of an affected sister, eight unaffected siblings and the unaffected father. Sequence analysis of his affected sister and two unaffected sibling as well as his father revealed co-segregation of the respective mutant allele with the disease. The affected sister (II-2: 55 years of age) also showed homozygosity for this

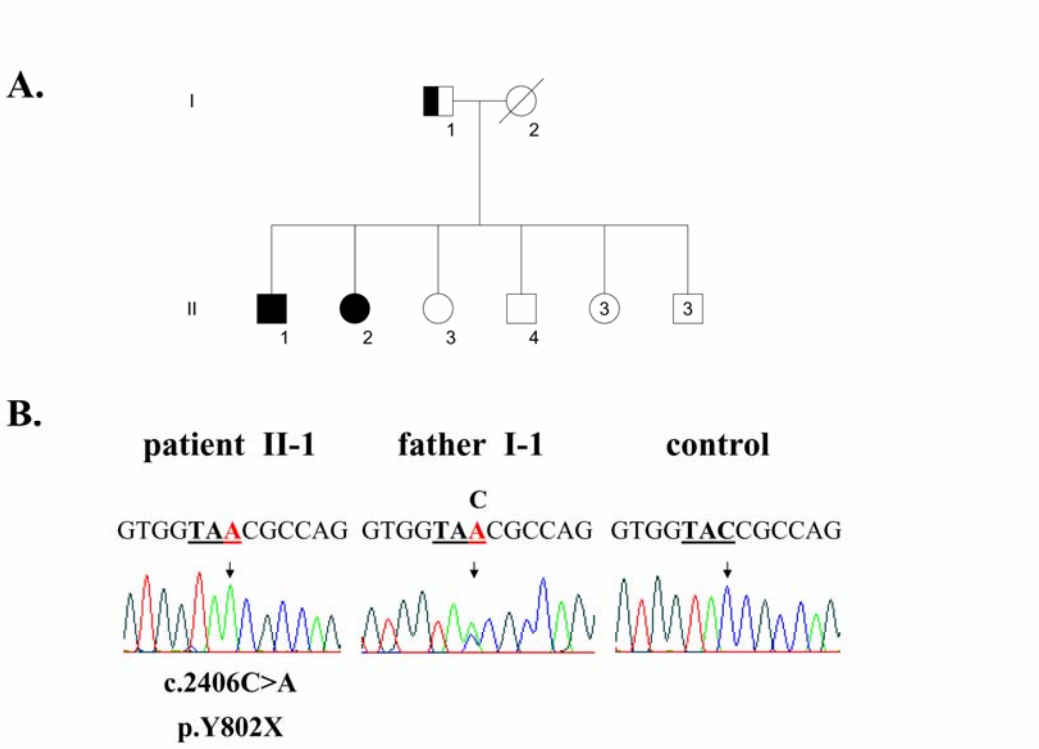

Figure 1. Mutation analysis in *CACNA2D4* of index patient II-1. (A) Pedigree of the family of patient II-1. Filled symbols indicate affected, semifilled mutation carrier, unfilled healthy, squares male, and circles female individuals. The family of the index patient II-1 consists of an affected sister (II-2), four unaffected sisters, four unaffected brothers and an unaffected father (I-1). Sequence analysis revealed a homozygous c.2406C>A mutation in the index patient as well as his affected sister (II-2) and the carrier status of the father (I-1). Mutation analyses of the two unaffected siblings (II-3, II-4) displayed homozygosity for the wild type allele. (B) Electropherograms show the respective DNA sequences of exon 25 of *CACNA2D4*. The homozygous c.2406C>A mutation in patient II-1 (left), the heterozygous mutation in the unaffected father I-1 (middle) and the wild type allele of a control DNA (right) are indicated. The position of the mutated nucleotide is highlighted by arrows.

DNA sequence variant, whereas the unaffected father (I-1) was heterozygous for the mutation (Fig. 1B). Two unaffected siblings (II-3: 51 years of age, II-4: 47 years of age) displayed homozygosity for the wild type allele. This mutation was excluded from 224 control chromosomes by direct sequencing.

The nucleotide substitution (c.2406C>A) introduces a premature termination codon at amino acid position 802 (p.Y802X) and presumably removes 335 amino acid residues (29.6%) from the C-terminus of CACNA2D4. At the protein level, this truncation likely eliminates the entire δ peptide of CACNA2D4, encoded by residues 992-1137 (Fig. 2). The δ peptide contains the transmembrane domain of CACNA2D4. In addition, 189 residues (19.2%) are presumably deleted from the C-terminus of the CACNA2D4 α2 peptide (802-991 residues). Thus, the aberrant *CACNA2D4* transcript codes for a truncated protein sequence of 801 amino acids, which lacks essential protein domains and the membrane anchoring peptide.

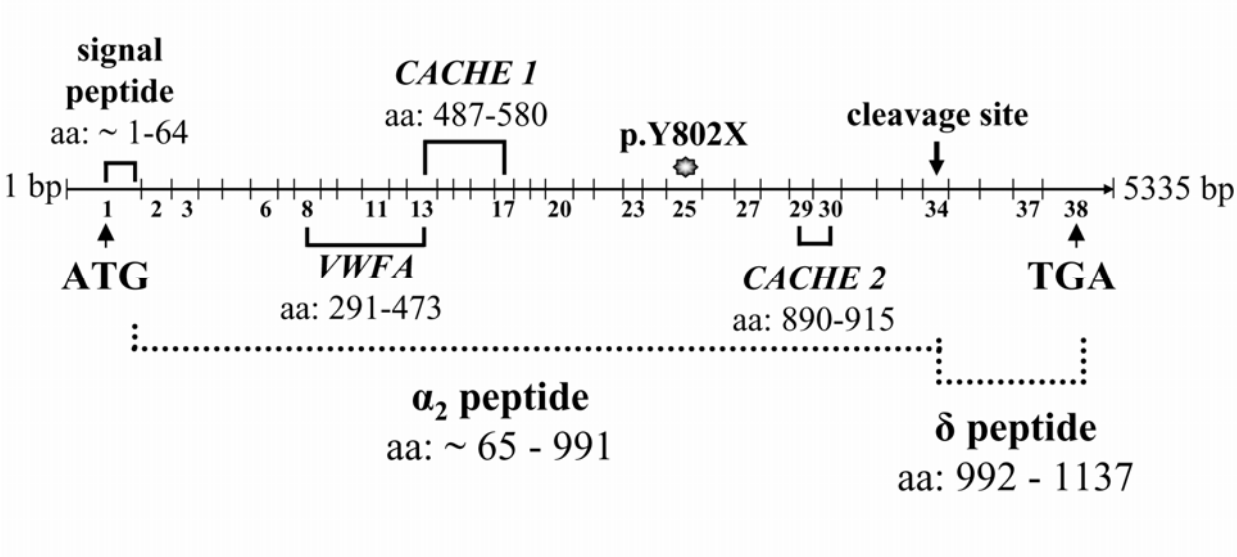

Figure 2. Schematic representation of *CACNA2D4* transcript. The schematic drawing shows the longest transcript variant of human *CACNA2D4* (GenBank accession number: NM_172364.3, figure not to scale). Its open reading frame codes for a protein of 1137 amino acid residues (aa), posttranslationally cleaved into the α2 (aa: 65-991, 232-3204 bp) and the δ (aa: 992-1137, 3205-3645 bp) peptides. The cleavage site between the α2 and δ peptides, encoded by an alanine residue at position 992 (exon 34) is indicated by an arrow. The locations of the conserved Von Willebrand Factor A (VWFA) domain and the Calcium Channel and Chemotaxis Receptor (CACHE) domains are illustrated in the transcript scheme. The CACHE domains probably constitute binding sites for small ligands, whereas the VWFA domain is responsible for protein-protein interactions of the α2δ protein with α1 subunits. At the N-terminus, CACNA2D4 protein also contains a putative signal peptide of 64 amino acid residues[41,42].

Clinical features of p.Y802X patients

The two patients, II-1 and II-2, reported a mild decrease in visual acuity (VA) noted only in the third decade of life (Table 1). They did not complain of night blindness or other visual problems except for moderate photophobia since early childhood.

The index patient II-1 was 33 years old at the time of examinations. His VA was determined to 0.7 in both eyes. Noteworthy, a decrease in VA was first noticed at the age of 23 years. In the Goldman kinetic perimetry, the visual field appeared almost normal except for very mild concentric constriction in the mid-periphery (isopter I/2e). The final threshold of the 30-minute-dark adaptation was slightly elevated by 0.3 to 0.5 log units. Colour vision discrimination, as tested by desaturated Panel D15 tests, showed four errors for each eye, corresponding to a total error score of 18.1 OD and 19.6 OS. A TES of 11.4 represents unaffected colour vision. Fundus examination exhibited physiological reflexes of the macula and slight pigment mottling in the foveal area, but otherwise normal findings (Fig. 3). Full-field electroretinography revealed well-preserved rod photoreceptor responses. The ISCEV rod response was just outside the lower percentile (5%) of unaffected controls (Fig. 4A).

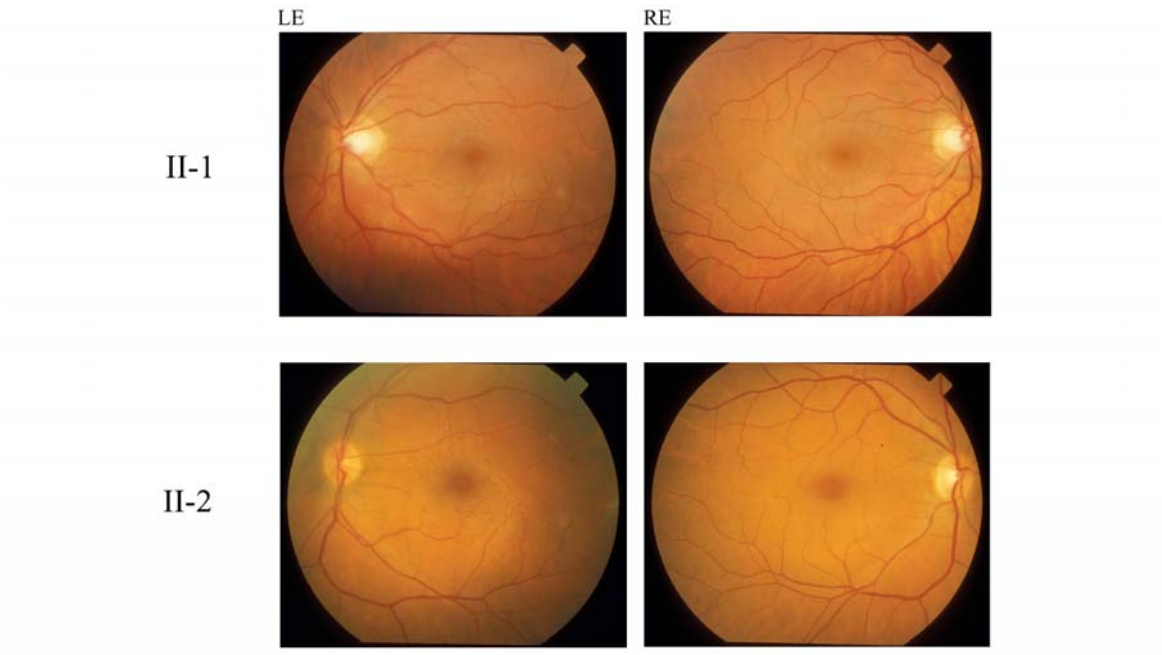

Figure 3. Fundus photographs of patients II-1 and II-2. Fundus of patient II-1 (upper panel) and patient II-2 (lower panel) of left eye (LE) and right eye (RE), respectively, showing nearly normal appearance.

Table 1. Clinical characterization of patients with p.Y802X mutation.

Patient number	First symptoms (age and course)	Age of examination	VA	Refractive error	Color vision (total error score)	Visual field	Dark adaptation	ERG	Anterior segment and fundus
II-1	glare sensitivity (early childhood), slight progressive reduction of VA from 20/20 at age 18, first subjective changes at age 23	33	OD:20/32 OS:20/32	OD:-0.75sph,-0.25cyl OS:-0.25sph,-0.50cyl	OD:18.1 OS:19.6	mild concentric constriction (I/2e)	final threshold slightly elevated (0.5logU)	Scotopic: ISCEV rod response just outside the lower percentile (5%) range of unaffected, mixed rod/cone response (SF) slightly reduced, IT normal, b/a ratio markedly reduced ("negative" ERG) Photopic: markedly reduced, prolonged IT	anterior segments normal, slight mottling of the pigment epithelium in the foveal region, otherwise inconspicuous
II-2	glare sensitivity (early childhood), slow progressive reduction of VA, first subjective changes at age 30	46	OD:20/32 OS:20/32	OD:-0.50sph,-0.50cyl OS:-0.25sph,-0.50cyl	OD:22.8 OS:23.3	very mild concentric constriction (I/2e)	final threshold normal	Scotopic: ISCEV rod response just outside the lower percentile (5%) range of unaffected, mixed rod/cone response (SF) slightly reduced, IT normal, b/a ratio markedly reduced ("negative" ERG) Photopic: markedly reduced, prolonged IT	anterior segments: posterior synechiae after iridocyclitis (33 years) LE, slight mottling of the pigment epithelium in the foveal region, epiretinal gliosis LE, otherwise inconspicuous

Visual acuity (VA), left eye (LE), implicit time (IT), standard flash (SF), spherical (sph), cylindric (cyl), units (U).

The total amplitude of the maximal combined rod/cone-responses was reduced to ~ 50% of the median and was dominated by an almost normal a-wave, but remarkably attenuated b-wave (Fig. 4B). The corresponding b/a-wave ratio accounted for 1.1 in both eyes and reflected a decline of the scotopic b-wave when compared with b/a-values of >1.4 for normal eyes. Implicit times of all scotopic recordings according to ISCEV standards were normal, except for a slight prolongation of oscillatory potentials of ~ 1 ms above the limit of the norm (Fig. 4C). In photopic electroretinography, the amplitude of the single-flash cone response was completely reduced (Fig. 4D). 30-Hz flicker amplitudes under light-adapted conditions were below the lower percentile (5%) of unaffected individuals with a phase shift of approximately 8 ms (Fig. 4E).

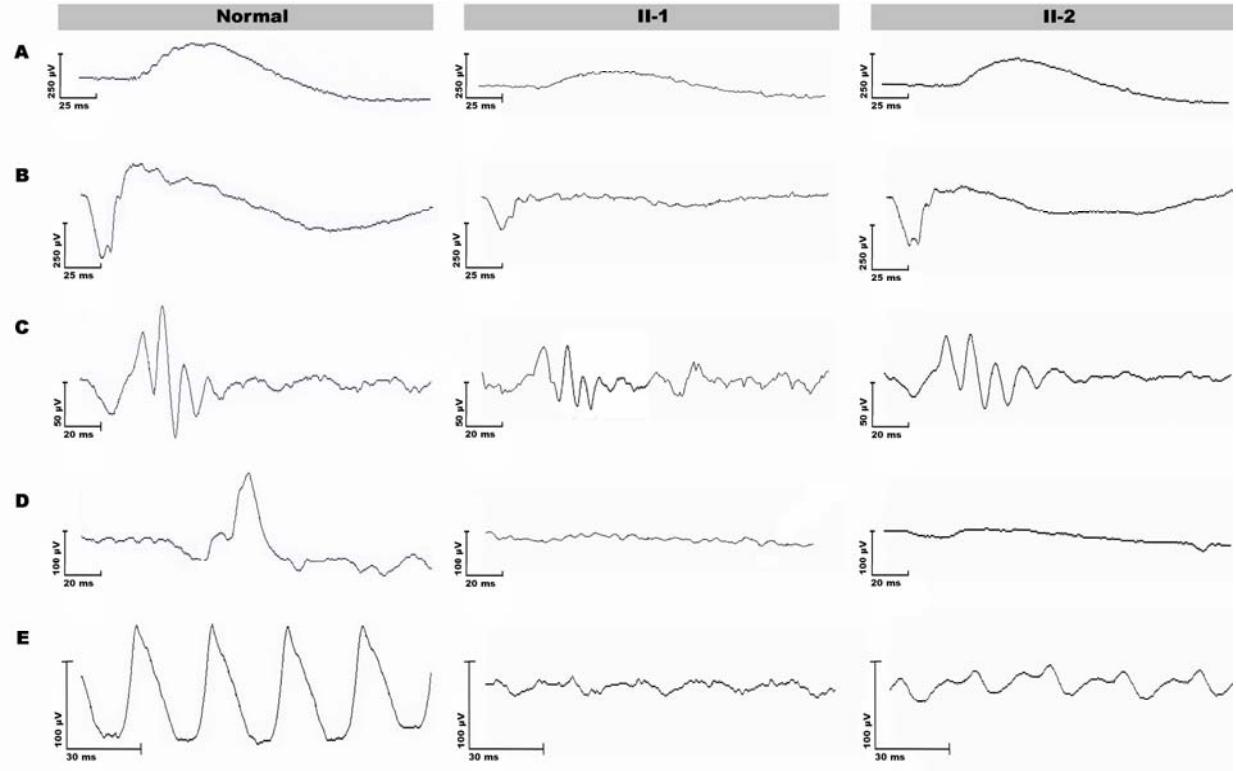

Figure 4. Electroretinography of patients carrying p.Y802X mutation. ERG recordings in the RE of patients II-1 and II-2. The left panel shows representative traces of a normal subject, middle panel the recordings of patient II-1, right panel traces of patient II-2. Rod responses (A), maximal combined responses (B), oscillatory potentials (C), single flash cone responses (D), 30-Hz flicker responses (E), each according to ISCEV standard[43]. The negative-oriented a-wave of an ERG response reflects the hyperpolarisation of photoreceptors due to a flash of light. The positive-oriented b-wave represents a summation of responses evoked by activities of secondary neurons during photoreceptor synaptic signal transmission. Both patients share a frequency doubling of the 30-Hz flicker ERG.

Vitamin A level in the serum was determined to 0.8 mg/litre (normal values 0.2 to 1.2 mg/litre)[30]. Retinol-binding protein contents were estimated to 4.7 mg/dl (normal values 3.0 to 6.0 mg/dl)[31].

The sister (II-2) of patient II-1 noticed a decline in visual acuity first at the age of 30 years. Her later corrected visual acuity was 0.6 in both eyes. Except for photophobia, she did not report any additional symptoms, particularly regarding night blindness, visual field loss or colour vision disturbances. Similar to the brother, her visual field was mildly constricted, specifically in the mid-periphery (isopter I/2e). Colour vision showed a slightly increased number of errors with a total error score of OD 22.8 and OS 23.3. Slit-lamp tests were unremarkable, except for posterior synechiae following iridocyclitis at age 33. Fundus examinations revealed regular physiological reflex of the macula and slight mottling of the pigment epithelium. In other respects, fundus findings were normal (Fig. 3). Light sensitivity measured upon 30 minutes of dark adaptation was within the normal range.

The full-field ERG was identical to that of her brother in almost every aspect (Fig. 4). Exclusively, the maximal combined rod/cone response showed decreased b/a ratio of 1.2 indicating slighter reduction of the respective a- and b-waves (Fig. 4B).

Her vitamin A and retinol-binding protein levels were of 0.6 mg/l and 3.4 mg/dl, respectively (normal values above).

To summarize our clinical findings, the two patients are not suffering from night blindness but rather from a mild form of cone dystrophy. Although the rod and cone ERG tends towards the direction of incomplete stationary night blindness, the disease in our patients is progressive and not stationary.

Table 2. Primer sequences and PCR conditions in *CACNA2D4* mutational analyses.

fragment	exon	forward primer (5´-3´)	reverse primer (5´-3´)	annealing temperature	$MgCl^2$ (25mM)	5XQ solution
1	1	aggctcgccaaggcacggaa	gtggtcagtcgcagccactg	58°C	1.6 µl	"-"
2	2	tgtctacgcgtgtgtttctg	ctcacagcaccggcatttgg	58°C	1.6 µl	"-"
3	3	ggagaggttggaggccatgc	tgacatcgggagggtcactc	58°C	1.6 µl	4.0 µl
4	4	tcacaggtgcatggcctctg	tcagtggatcgccaccctac	58°C	1.6 µl	"-"
5	5 and 6	tctccgcctg tcccggtgct; *nested 5: ccgtgggcctcacccgtcca *nested 6: accctcaccg ggcatgatca	ccagggtccatcttcagtgc; *nested 5: tgatcatgcccggtgagggt *nested 6: tttccagagaagaatcccag	62°C	1.2 µl	"-"
6	7	ctgttccctagctccaaagc	cggaagtggaggaggatgag	58°C	1.6 µl	"-"
7	8 and 9	aactgcagacccctttggtcagg	tctcattccaggtgccatgg	58°C	1.6 µl	"-"
8	10 and 11	ctgcatcatggagacacagg	catccttctagggtccctgc	58°C	1.2 µl	"-"
9	12	acccgaagactgagaggcac	gcaggatggagacagagctg	60°C	1.2 µl	4.0 µl
10	13	tcggctatgagccatctgcagctg	aatgttccctaaggaggtgc	58°C	1.6 µl	"-"
11	14	cgagtgcggcaaaccagtgg	gccaagtcaagaatcactgg	58°C	1.6 µl	"-"
12	15	gcttcctcttccaggctctg	cctggagagaggctcccatc	58°C	1.6 µl	"-"
13	16	cggtttggaaaggactcctc	ccactcatcagtcatttcac	58°C	1.2 µl	"-"
14	17	gagctctgtatcaggtggaa	tcacagccacacagctgacc	58°C	1.6 µl	"-"
15	18	ggatcacctctaatctggtc	aggctaagtccaggtccctc	58°C	1.6 µl	"-"
16	19	gtacagtgacgatgaagacc	acctgcattctaggctacac	58°C	1.6 µl	4.0 µl
17	20	ccagggtcctgcttaggaag	gggagctgggaggctgtcac	58°C	1.2 µl	4.0 µl
18	21 and 22	cactgggtggctgtttctac	gtgctaatgggatagggctg	58°C	1.6 µl	4.0 µl
19	23	catagacacgttcaggaagc	tctcctgagccaccagccag	58°C	1.6 µl	"-"
20	24	gatctgccgaggcagagagg	tggcccaggaacacaccatg	60°C	1.2 µl	4.0 µl
21	25	ccagccaagttgaccttgtg	ggaaccctggtggtctggac	58°C	1.6 µl	"-"
22	26	ccaaggatgccttcgcctgc	gtgcagggccttctgctgtg	58°C	1.6 µl	"-"
23	27	ctcagtcctcccatccgctg	ctcaaggcagtggagcatcc	58°C	1.6 µl	4.0 µl
24	28 and 29	gtaccacacacacagcattc	gacctttcacctgaattggc	58°C	1.6 µl	"-"
25	30	ctggcaccaaaagcctcgac	caggaccacttagcgtcagc	58°C	1.6 µl	"-"
26	31	gatgctctgctagtaaagcc	gaagatggagatggtcaagg	58°C	1.6 µl	"-"
27	32 and 33	ctctctgagggtggtgctgg; *nested 32_33: caccctcacccttggaccta	tggtctcacgttagtggacc; *nested 32_33: gtggaccaaaatgccactgc	58°C	1.6 µl	"-"
28	34	atcttgggacaccgccactc	cctgggacaggtcatggagg	58°C	1.6 µl	"-"
29	35	acgcgtgtcctgagaactgc	ctctgcacttagacgcatcc	58°C	1.6 µl	"-"
30	36 and 37	tggtcgccacggagccatcc	gcacagacccaggcacagag	60°C	1.2 µl	4.0 µl
31	38	cccaaattagtggtggaagc; *nested 38: ttagtggtggaagcccctcc	gcgacccaactgcagttag; *nested 38: aactgcagttagctgcatcc	58°C	1.6 µl	"-"
32	1b	caggagaacctgccgaggac	gcgtagacatatgggttcac	58°C	1.6 µl	"-"
33	37L	cagagcaggttcttccagac	gcacctatcaccctaatcag	58°C	1.6 µl	"-"

3.2.5. Discussion

Signal transmission between photoreceptors and the second-order neurons depends on the activity of L-type calcium channels in synaptic layers, which mediate calcium entry into photoreceptor terminals and promote subsequent neurotransmitter release. The pathogenic relevance of sequence variations in the CACNA2D4 calcium channel subunit for human visual dysfunctions has been recently suggested by a mutation identified in the mouse *Cacna2d4* orthologue, which was associated with disturbed processing in photoreceptor synapses[21]. We performed mutation analyses in 34 patients and detected a homozygous nonsense transversion in two affected siblings with a mild cone dystrophy.

The identified nonsense mutation probably activates nonsense mediated decay (NMD), a regulatory pathway that promotes degradation of truncating mRNAs to limit synthesis of anomalous proteins[32]. The premature termination signal occurs 64 bp upstream of the boundary of exons 25/26, a position which is expected to be recognized by the NMD machinery[32]. In the *Cacna2d4*-affected mice, the truncating frameshift mutation, which also occurs in exon 25, showed a reduction of retinal *Cacna2d4* mRNA levels to ~30%[21]. At the protein level, the mutation is assumed to lead to a premature termination of the CACNA2D4 translation and results in a truncation of 335 amino acid residues. As the main consequence of the truncation, membrane anchoring of CACNA2D4 is presumably abolished due to the lack of the δ peptide. The δ peptides of all α2δ subunits possess a transmembrane segment at the C-terminus for the attachment to the cell surface[33]. In native CACNA2D4, a highly hydrophobic region, encoded by amino acid residues 1118-1135 (exons 37-38), acts potentially as a transmembrane domain[28].

In consequence, CACNA2D4 deficiency presumably involves lack of the auxiliary stimulation and thus a reduction of properly operating calcium channels in retinal synaptic terminals of our two patients. The modulation by native CACNA2D4 is suggested to consist of an acceleration of calcium channel activation/inactivation kinetics and a facilitation of calcium conduction during channel opening[28]. CACNA2D4 deficiency may also result in an attenuation of calcium channel densities at synaptic membranes. Besides auxiliary stimulation, α2δ subunits interact with immature α1 calcium channel proteins and facilitate their trafficking to the plasma membranes[34]. At membranes, α2δ subunits further reduce the rate of channel complex turn over. In cell line experiments, absence of CACNA2D4 has been demonstrated to diminish the augmentation of calcium channel complexes at the cell surface and to result in a decrease of the calcium currents up to 3-folds[28].

In addition, translation of aberrant CACNA2D4 proteins may contribute to patients` retinal disease. If not efficiently degraded, anomalous CACNA2D4 proteins may interact with the respective α1 subunits in cytosolic compartments and reduce their transport to the cell surfaces, leading to decreased channel densities. Similarly, the α2δ-2 subunit genetically mutated in the Von Willebrand Factor A domain was shown to interfere with membrane trafficking of the α1 subunits in cell lines, eliciting intracellular α1 retention and a ~ 5-fold attenuation of calcium currents[35]. Thus, the reduction of functional CACNA2D4 protein in synaptic terminals of patients II-1 and II-2 may lead to inefficient photoreceptor signal transmission and account for the electronegative ERG. The deficiency in calcium signaling at synaptic terminals may underly permanent excitability of the post-photoreceptoral cells at darkness and loss of proper visual information transfer during illumination. The synaptic dysfunction over years probably contributes to the slow progression of the disease. Nonetheless, both affected patients, although visually impaired, retain activities of the rod and cone signaling pathways and are not blind. Considering remaining visual capabilities, human photoreceptors may utilize additional α2δ subunits in ribbon synapses or involve an upregulated expression of homologous α2δ subunits for compensatory effects. Absence of CACNA2D4 activity in affected individuals during development may specifically lead to changes in retinal circuitries that partially compensate for the failure in signal transmission. For instance, upregulation of gap junctions between rods or rods and cones might occur. Rod signals can be transmitted through electrical gap junctions between both photoreceptor types and pass through the OFF-specific pathways of cones. These circuitries predominantly involve conventional (80%) rather than ribbon-type (20%) synapses, which are dependent on the activity of distinct calcium channels than those of the L-type[36].

From the clinical point of view, the mutation described in the CACNA2D4 protein causes a functional alteration in the retina which is not noticed by the patient in early life, but progresses with symptoms of increasing photophobia, mildly decreasing visual acuity as well as moderate attenuated rod and markedly diminished cone responses. In this sense, it is not a stationary but a progressive disease with symptoms of such mildness that it may go unnoticed over the first three decades of life. Thus, the patients clearly display a mild cone dystrophy that is typically marked by progressive decline of the visual acuity, increased photophobia, cone ERG loss and mild morphological signs in the pigment epithelium. However, the possibility cannot be excluded that the mild rod affectation may be stationary and overlaid by a progressive cone dysfunction.

In comparison to the human *CACNA2D4*-associated retinopathy, the corresponding mouse mutant shows profound loss of rod-specific signal transmission from birth, reflected by an almost complete loss of the b-wave and oscillatory potentials in the scotopic ERG[37]. The rod b-wave declines with time, indicating a progressive rather than stationary disease also in mice[37]. In addition, mouse rod photoreceptor cells probably degenerate (Wycisk et al., 2006). The more severe rod phenotype in mice may indicate a specific role of the *Cacna2d4* gene in both photoreceptor systems whereas in humans this gene is important for signal transmission between cones and second order neurons. Phenotypic differences between human and mouse were also reported for other gene defects in retinal diseases. Regarding the progression in patients with mutated *CACNA2D4*, recent studies also show that retinal channelopathies due to *CACNA1F* and *CABP4* mutations may underly stationary as well as progressive disorders[9,13,38-40]. These results may have implications for diagnostic testing and genetic counselling of patients and their families with mutations in these genes.

3.2.6. References

1. Baumann L, Gerstner A, Zong X, Biel M, Wahl-Schott C (2004) Functional characterization of the L-type Ca2+ channel Cav1.4alpha1 from mouse retina. Investigative Ophthalmology & Visual Science 45:708-713
2. Beaumont V, Llobet A, Lagnado L (2005) Expansion of calcium microdomains regulates fast exocytosis at a ribbon synapse. Proceedings of the National Academy of Sciences of the United States of America 102:10700-10705
3. Berntson A, Taylor WR, Morgans CW (2003) Molecular identity, synaptic localization, and physiology of calcium channels in retinal bipolar cells. Journal of Neuroscience Research 71:146-151
4. Catterall WA (2000) Structure and regulation of voltage-gated Ca2+ channels. Annual Review of Cell and Developmental Biology 16:521-555
5. Song H, Nie L, Rodriguez-Contreras A, Sheng ZH, Yamoah EN (2003) Functional interaction of auxiliary subunits and synaptic proteins with Ca(v)1.3 may impart hair cell Ca2+ current properties. Jounal of Neurophysiology 89:1143-1149
6. Arikkath J, Campbell KP (2003) Auxiliary subunits: essential components of the voltage-gated calcium channel complex. Current Opinion in Neurobiology 13:298-307
7. Gurnett CA, De Waard M, Campbell KP (1996) Dual function of the voltage-dependent Ca2+ channel alpha 2 delta subunit in current stimulation and subunit interaction. Neuron 16:431-440
8. Ball SL, Powers PA, Shin HS, Morgans CW, Peachey NS, Gregg RG (2002) Role of the beta(2) subunit of voltage-dependent calcium channels in the retinal outer plexiform layer. Investigative Ophthalmology & Visual Science 43:1595-1603
9. Mansergh F, Orton NC, Vessey JP, Lalonde MR, Stell WK, Tremblay F, Barnes S, Rancourt DE, Bech-Hansen NT (2005) Mutation of the calcium channel gene Cacna1f disrupts calcium signaling, synaptic transmission and cellular organization in mouse retina. Human Molecular Genetics 14:3035-3046
10. Zito I, Allen LE, Patel RJ, Meindl A, Bradshaw K, Yates JR, Bird AC, Erskine L, Cheetham ME, Webster AR, Poopalasundaram S, Moore AT, Trump D, Hardcastle AJ (2003) Mutations in the CACNA1F and NYX genes in British CSNBX families. Human Mutation 21:169-173
11. Allen LE, Zito I, Bradshaw K, Patel RJ, Bird AC, Fitzke F, Yates JR, Trump D, Hardcastle AJ, Moore AT (2003) Genotype-phenotype correlation in British families with X linked congenital stationary night blindness. British Journal of Ophthalmology 87:1413-1420
12. Strom TM, Nyakatura G, Apfelstedt-Sylla E, Hellebrand H, Lorenz B, Weber BH, Wutz K, Gutwillinger N, Ruther K, Drescher B, Sauer C, Zrenner E, Meitinger T, Rosenthal A, Meindl A (1998) An L-type calcium-channel gene mutated in incomplete X-linked congenital stationary night blindness. Nature Genetics 19:260-263
13. Bech-Hansen NT, Naylor MJ, Maybaum TA, Pearce WG, Koop B, Fishman GA, Mets M, Musarella MA, Boycott KM (1998) Loss-of-function mutations in a calcium-channel alpha1-subunit gene in Xp11.23 cause incomplete X-linked congenital stationary night blindness. Nature Genetics 19:264-267
14. Boycott KM, Maybaum TA, Naylor MJ, Weleber RG, Robitaille J, Miyake Y, Bergen AA, Pierpont ME, Pearce WG, Bech-Hansen NT (2001) A summary of 20 CACNA1F mutations identified in 36 families with incomplete X-linked congenital stationary night blindness, and characterization of splice variants. Human Genetics 108:91-97
15. Jacobi FK, Hamel CP, Arnaud B, Blin N, Broghammer M, Jacobi PC, Apfelstedt-Sylla E, Pusch CM (2003) A novel CACNA1F mutation in a french family with the incomplete type

of X-linked congenital stationary night blindness. American Journal of Ophthalmology 135:733-736

16. Zeitz C, Minotti R, Feil S, Matyas G, Cremers FPM, Hoyng CB, Berger W (2005) Novel mutations in CACNA1F and NYX in Dutch families with X-linked congenital stationary night blindness. Molecular Vision 11:179-183
17. Tremblay F, Laroche RG, De B, I (1995) The electroretinographic diagnosis of the incomplete form of congenital stationary night blindness. Vision Research 35:2383-2393
18. Miyake Y, Yagasaki K, Horiguchi M, Kawase Y (1987) On- and off-responses in photopic electroretinogram in complete and incomplete types of congenital stationary night blindness. Japanese Journal of Ophthalmology 31:81-87
19. Nakamura M, Ito S, Piao CH, Terasaki H, Miyake Y (2003) Retinal and optic disc atrophy associated with a CACNA1F mutation in a Japanese family. Archives of Ophthalmol 121:1028-1033
20. Jalkanen R, Mantyjarvi M, Tobias R, Isosomppi J, Sankila EM, Alitalo T, Bech-Hansen NT (2006) X-linked cone-rod dystrophy, CORDX3, is caused by a mutation in the CACNA1F gene. Journal of Medical Genetics 43:699-704
21. Wycisk K.A., Budde B., Feil S., Skosyrski S., Buzzi F., Neidhardt J., Glaus E., Nürnberg P., Ruether K., Berger W. (2006) Structural and functional abnormalities of retinal ribbon synapses due to Cacna2d4 mutation. Investigative Ophthalmology & Visual Science 47:3523-3530
22. Dryja TP, Mcgee TL, Berson EL, Fishman GA, Sandberg MA, Alexander KR, Derlacki DJ, Rajagopalan AS (2005) Night blindness and abnormal cone electroretinogram ON responses in patients with mutations in the GRM6 gene encoding mGluR6. Proceedings of the National Academy of Sciences of the United States of America 102:4884-4889
23. Pusch CM, Zeitz C, Brandau O, Pesch K, Achatz H, Feil S, Scharfe C, Maurer J, Jacobi FK, Pinckers A, Andreasson S, Hardcastle A, Wissinger B, Berger W, Meindl A (2000) The complete form of X-linked congenital stationary night blindness is caused by mutations in a gene encoding a leucine-rich repeat protein. Nature Genetics 26:324-327
24. Bech-Hansen NT, Naylor MJ, Maybaum TA, Sparkes RL, Koop B, Birch DG, Bergen AA, Prinsen CF, Polomeno RC, Gal A, Drack AV, Musarella MA, Jacobson SG, Young RS, Weleber RG (2000) Mutations in NYX, encoding the leucine-rich proteoglycan nyctalopin, cause X-linked complete congenital stationary night blindness. Nature Genetics 26:319-323
25. Zeitz C, Scherthan H, Freier S, Feil S, Suckow V, Schweiger S, Berger W (2003) NYX (nyctalopin on chromosome X), the gene mutated in congenital stationary night blindness, encodes a cell surface protein. Investigative Ophthalmology & Visual Science 44:4184-4191
26. Vingrys AJ, KingSmith PE (1988) A Quantitative Scoring Technique for Panel Tests of Color-Vision. Investigative Ophthalmology & Visual Science 29:50-63
27. Marmor MF, Zrenner E (1995) Standard for Clinical Electroretinography (1994 Update). Documenta Ophthalmologica 89:199-210
28. Qin N, Yagel S, Momplaisir ML, Codd EE, D'Andrea MR (2002) Molecular cloning and characterization of the human voltage-gated calcium channel alpha(2)delta-4 subunit. Molecular Pharmacology 62:485-496
29. Collins JS, Schwartz CE (2002) Detecting polymorphisms and mutations in candidate genes. American Journal of Human Genetics 71:1251-1252
30. Hildebrandt G., Gilch G., Gries G. (1984) Eine einfache Methode zur Routinemässigen Bestimmung von Vitamin A und E im Serum mit HPLC. Laboratoriumsmedizin, pp. 191-193.
31. McPherson R.A. (2006) Tietz`clinical Guide to Laboratory Tests. Saunders W.B. Company (*book*)

32. Holbrook JA, Neu-Yilik G, Hentze MW, Kulozik AE (2004) Nonsense-mediated decay approaches the clinic. Nature Genetics 36:801-808
33. Sipos I, Pika-Hartlaub U, Hofmann F, Flucher BE, Melzer W (2000) Effects of the dihydropyridine receptor subunits gamma and alpha2delta on the kinetics of heterologously expressed L-type Ca2+ channels. Pflugers Archives 439:691-699
34. Felix R, Gurnett CA, De Waard M, Campbell KP (1997) Dissection of functional domains of the voltage-dependent Ca2+ channel alpha2delta subunit. Journal of Neuroscience 17:6884-6891
35. Canti C, Nieto-Rostro M, Foucault I, Heblich F, Wratten J, Richards MW, Hendrich J, Douglas L, Page KM, Davies A, Dolphin AC (2005) The metal-ion-dependent adhesion site in the Von Willebrand factor-A domain of alpha2delta subunits is key to trafficking voltage-gated Ca2+ channels. Proceedings of the National Academy of Sciences of the United States of America 102:11230-11235
36. Sharpe LT, Fach CC, Stockman A (1993) The Spectral Properties of the 2 Rod Pathways. Vision Research 33:2705-2720
37. Ruether K, Grosse J, Matthiessen E, Hoffmann K, Hartmann C (2000) Abnormalities of the photoreceptor-bipolar cell synapse in a substrain of C57BL/10 mice. Investigative Ophthalmology & Visual Science 41:4039-4047
38. Miyake Y (2002) [Establishment of the concept of new clinical entities--complete and incomplete form of congenital stationary night blindness]. Nippon Ganka Gakkai Zasshi 106:737-755
39. Haeseleer F, Imanishi Y, Maeda T, Possin DE, Maeda A, Lee A, Rieke F, Palczewski K (2004) Essential role of Ca2+-binding protein 4, a Cav1.4 channel regulator, in photoreceptor synaptic function. Nature Neuroscience 7:1079-1087
40. Zeitz, C., Kloeckener-Gruissem B., Forster U., Kohl S., Magyar I., Bernd W., Mátyás G., Borruat F., Schorderet D.F., Zrenner E., Munier F.L., and Berger, W. (2006) Mutations in CABP4, encoding the Ca2+-binding protein 4, cause autosomal recessive night blindness. American Journal of Human Genetics (*in press*)
41. Brown JP, Gee NS (1998) Cloning and deletion mutagenesis of the alpha(2)delta calcium channel subunit from porcine cerebral cortex - Expression of a soluble form of the protein that retains [H-3]gabapentin binding activity. Journal of Biological Chemistry 273:25458-25465
42. Wang M, Offord J, Oxender DL, Su TZ (1999) Structural requirement of the calcium-channel subunit alpha2delta for gabapentin binding. Biochemistry Journal 342:313-320
43. Marmor MF, Zrenner E (1999) Standard for clinical electroretinography (1999 update). Documenta Ophthalmologica 97:143-156

3.3. Histological and Molecular Characterisation of Cacna2d4 Mice (Additive)

Katharina A. Wycisk[1], Francesca Buzzi[1]*, Silke Feil[1]*, Sergej Skosyrski[2], Hannie Kremers[3], Andy J. Beynon[3], Theo Peters[3], Klaus Ruether[2], Niels Hagenbuch[4], Gian Carlo Demontis[5#], Wolfgang Berger[1]

*These authors contributed equally to this study.

#This author will not contribute to the final version of this publication.

Manuscript in preparation (preliminary data)

[1]Division of Medical Molecular Genetics and Gene Diagnostics, Institute of Medical Genetics, University of Zurich, Schorenstrasse 16, 8603 Schwerzenbach, Switzerland; [2]Charite-Virchow-Augenklinik, Berlin, Germany, [3]Department of Otorhinolaryngology, Radboud University Medical Center Nijmegen, Nijmegen, The Netherlands, [4] Laboratory of Behavioural Neurobiology, Swiss Federal Institute of Technology Zurich, Schorenstrasse 16, 8603 Schwerzenbach, Switzerland, [5] Department of Psychiatry and Neurobiology, University of Pisa, Via Bonanno Pisano 6, 56126 Pisa, Italy

Acknowledgement

The authors thank Sandra Brunner, Stefanie Derzsi, Joram Feldon, Barbara Kloeckener, Ulrich Luhmann, Gabor Matyas, John Neidhardt, Nikolaus Schäfer, Mariana Wittmer, Benjamin K. Yee, for discussions and experimental assistance. This study was supported by the Foundation Fighting Blindness (USA), the Swiss National Science Foundation (Grant#3100-067786 to WB) and the Deutsche Forschungsgemeinschaft (DFG Ru 457/1-1).

3.3.1. Introduction

Voltage-gated L-type calcium channels mediate depolarization-induced calcium influx across plasma membranes and elicit neurotransmitter release in photoreceptor and cochlear ribbon-type synapses during sensory signal transmission[1-3]. At the ultrastructural level, L-type channels consist of the pore-forming α1 subunit and the auxiliary subunits α2δ, β and γ. Whereas the α1 subunit incorporates the voltage sensor and ion gating apparatus, the remaining stimulatory proteins are responsible for the α1 membrane trafficking and the biophysical modulation of calcium channel properties[4-8]. The importance of L-type calcium channels in retinal signal transduction is emphasized by mutations in the α1F (CACNA1F) and ß2 (Cacnb2) calcium channel subunits that result in night blindness or severe cone-rod dystrophies[9-13]. Consistent with retinal phenotypes of defective synaptic transmission, mutations in the cochlear α1D (Cacna1d) calcium channel subunit are associated with disturbed signaling in ribbon synapses of the organ of Corti and lead to hair cell degeneration and deafness[14].

We recently identified a homozygous truncating mutation (c.2367insC) in exon 25 of the mouse *Cacna2d4* gene that codes for the fourth voltage-gated calcium channel auxiliary subunit of the α2δ-type[15]. The genetic defect underlies a cone-rod-specific dysfunction in mice characterized by absent neurotransmission from photoreceptors to the second-order neurons[16]. At the morphological level, *Cacna2d4*-mutant animals display profound structural alterations in the photoreceptor ribbon synapses as well as reduced nuclei number in the outer retina[16]. In the human *CACNA2D4* orthologue, a deleterious mutation, currently found to cause a cone dystrophy, manifests upon severely affected signal transmission between photoreceptors and the secondary neurons[17].

To understand the functional consequences of *CACNA2D4*-associated channelopathies in human and mice, we focused on molecular and histological characterisation of the *Cacna2d4*-mutant animals. Upon patch-clamp experiments, we tended to establish the effects of the *Cacna2d4* mutation on in retinal calcium signaling. In addition, we applied histological examinations of the mutant retina to elucidate whether the photoreceptor reduction observed in mutant mice is stationary or a result of progressive retinal degeneration. Electrophysiological examinations of the cochlear system were also performed to characterize possible pathological effects of the *Cacna2d4* mutation on ribbon-shaped synapses in the organ of Corti. Since perturbed calcium signaling in mouse models of retinal channelopathies was shown to involve the retraction of the photoreceptor synaptic layer, loss of ribbon organelles, photoreceptor degeneration and, in some

instances, ectopic synaptogenesis, we incorporated an expression profile analysis to unravel genes activated or inactivated due to *Cacna2d4* deficiency[12,13,18]. So far, such analysis was not performed in a retinal channelopathy.

3.3.2. Material and Methods

Animal breeding and genotyping

B10A (fourth generation) and C57BL/10 mice were bred in accordance with the ´ARVO (American Association for Research in Vision and Ophthalmology) statement for the use of animals in ophthalmic and vision research´. Genotypes were examined by direct sequencing of a genomic DNA fragment comprising exon 25 of *Cacna2d4* (ABI PRISM® Big Dye Chemistry v1.1 protocol, ABI PRISM®3100 Genetic Analyzer, Applied Biosystems, Rotkreuz; Switzerland)[15]. Mutant animals were homozygous for the c.2367insC mutation[15]. Primers are available upon request.

For the c.753G>A mutation in the *Cadherin23* (*Cdh23*) gene, animals were genotyped by direct sequencing of a genomic DNA fragment representing the *Cdh23* exon 7 and its adjacent intronic slice sites (primers: forward 5`-agaggtcacataccacagcc, reverse: 5`-gcttaagtccacagccatcc; Microsynth, Balgach, Switzerland)[19]. The *Cdh23*-mutant animals displayed homozygosity for the c.753G>A substitution (at the last position of exon 7, 5`-splice site).

Histology

Retinal histopathology of *Cacna2d4*-mutant mice was analyzed by light microscopy at seven stages, the postnatal (P) days P10, P15, P21 and postnatal weeks (W) W6, W15, W27 and W53. For each time point, eyes from 6 wild type and 6 mutant animals were used, except for P10 with 5 wild type and 5 mutant mice.

Eyes were enucleated from CO_2 anesthetized and subsequently sacrificed mice and fixed in Serra`s (60% ethanol, 30% formalin, 10% acetic acid) over night. Upon dehydration in an isopropanol series of 70%, 80%, 90%, 2 x 100%, two hours each, eyes were embedded in paraffin blocks. Per each state, paraffin blocks were simultaneously prepared from eyes of all mice included and, regarding varying experimental conditions, sectioned into 4-8 µm slides (P15, P21 and W15 eyes into 4µm, P10 and W27 into 5 µm, W6 and W53 into 8 µm). Sections representing retinas in the region of the optic nerve head were stained with hematoxylin/eosin dye complex (H&E) and evaluated with Zeiss Axioplan 2 microscopy station. For each eye, four to six stained sections were selected for further analysis. Images of each section were taken at 63x magnification. Two images in the central (~250 µm from the optic nerve) and two in the

peripheral retina (~250 µm from the peripheral end) were generated and represented ~175-µm long regions of the retina, each (Fig. 1). Of note, the selected retinal regions were representative for a considered age of animals` eyes, but, due to developmental expansion of the retinal tissue with time, not overlapping with chosen regions of retinas within other stages.

Ten datasets were separately taken from the central and peripheral retina (Fig. 1). Cell counts in the outer nuclear layer (ONL, including photoreceptors) and inner nuclear layer (INL, representing bipolar, horizontal and amacrine cells) were performed in six to ten vertical rows in a distance of ~10 µm, each. Besides, thickness of the ONL, INL, the photoreceptor segments (S), outer plexiform layer (OPL), inner plexiform layer (IPL), and ganglion cell layer (GCL) were determined. Complementary, the diameter of the ganglion cell nuclei (GCT) was considered. Six to ten measurements were taken for each morphometric size in a 175 µm image. The number of cell nuclei in the ganglion cell layer (GC, involving ganglion cells and amacrine cells) was estimated along a constant length of 175 µm in an image.

Cochlear paraffin sections (5 µm) of two wild type and two mutant mice were prepared as described for eyes and qualitatively examined by light microscopy.

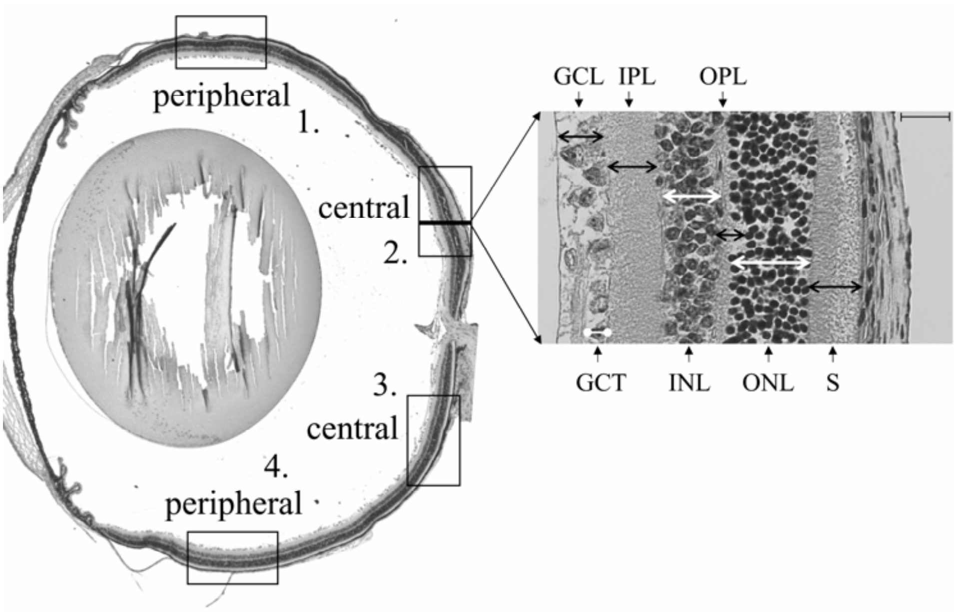

Figure 1. Histology assay. (**left**) In each retinal cross-section, two regions in the central (~250 µm from the optic nerve, ~175 µm long) and two in the peripheral retina (~250 µm from the peripheral end, ~175µm long) were selected for measurements (indicated by *boxes*). Magnification 5 x. (**right**) Ten datasets were taken from each selected region. Cell counts were performed in the outer nuclear layer (ONL), inner nuclear layer (INL), and ganglion cell layer (GCL). Thickness (*double head arrows*) was determined for the ONL, INL, photoreceptor segments (S), outer plexiform layer (OPL), inner plexiform layer (IPL) and ganglion cell layer (GCL). Complementary, the diameter of the ganglion cell nuclei (GCT) was measured. Magnification bar 50 µm.

Acoustic startle reactivity

Possible association of the *Cacna2d4* mutation with a hearing impairment in mutant mice was pre-examined upon acoustic startle reaction paradigm. Although not a hearing test in the strict sense, the acoustic startle reflex (ASR) represents a fast (24 h) and non-invasive test which can detect hearing deficits.

The acoustic startle reactivity test was performed with 26 animals of the B10A strain at six months of age. Fifteen wild type (8 females, 7 males) and eleven *Cacna2d4*-mutant mice (5 females, 6 males) were involved. For technical details see Yee et al. (2005)[20]. Briefly, the apparatus (SR-LAB, San Diego Instruments, San Diego, USA), placed in a sound-isolating chamber, consisted of a non-restrictive cylindrical Plexiglas enclosure attached horizontally to a mobile platform. A piezoelectric unit mounted underneath the platform converted the enclosure vibrations evoked by the whole-body startle response of an animal into an analogue signal, fed directly into a computer station. During the testing period, a continuous background noise of 65 dB[A] produced by a high-frequency loudspeaker was present. Each animal was acclimatized to the apparatus for 2 min. The startle reaction was initially stabilized by a total of 6 startle trials that were excluded from later analysis. Subsequently, the animals were exposed to 100 test trials. To evoke startle responses, a succession of white noise stimuli of 69, 73, 77, 81, 85, 90, 95, 100, 110, 120 dB[A], lasting for 20 and 40 ms, was presented in a pseudorandom order. The average startle response amplitude (in arbitrary units) of the two exposure times was used to determine the reactivity to each tone.

Auditory brain stem responses

Isogenic C57BL/10 *Cacna2d4*-mutant and wild type mice were examined for auditory brainstem responses (ABR). ABRs were recorded differentially by using needle electrodes (vertex for positive, bilateral mastoids for negative, and halfway tail for ground). Clicks (100 μs) and high frequent (HF) 8 kHz, 16 kHz and 32 kHz tone burst stimuli (1ms rise/fall, 3ms plateau time) were presented with a stimulation rate of 30 pps in a soundfield by a HF-tweeter (type Elac Jet III) 6 cm in front of each ear. A standard clinical recording EEG-system (5-channel Synergy, Oxford Instruments) with an internal stimulator was used to obtain the click-evoked ABR, for the higher tone burst frequencies, the same EEG-system was modified to obtain external trigger pulses from an external computer/stimulator that was developed to generate HF-stimuli using a DAQ-card 6062E (National Instruments). Loudness levels were calibrated according to IEC 61672-2 standards (2004) using a Bruel & Kjaer 2260 analyzer and corrected for the soundfield. Mice were i.p. anesthetized with ketamine (80 mg/kg) and xylazine (14 mg/kg). The analysis time window was set at a pre-stimulus time of 1.5 ms to assess the baseline, followed by a time

window of 13.5 ms from onset of stimulus. EEG-signals were recorded using a 100 Hz–3000 Hz bandpass filter settings, auto-reject mode set at 100 µV and 60 Hz notch-filter. All averaged signals were obtained at different stimulation levels according to standard audiometrical top-down procedures and ABR-peaks were identified according to the Jewett & Williston nomenclature[21]. The auditory hearing threshold was defined as the level in decibels at which no reproducible ABR peak morphology was recognized in the ipsilateral measured ear.

Microarray hybridization

Array hybridization was performed in strong accordance to the Affymetrix `Small Sample Labelling Protocol vII` (detailed procedure on www.affymetrix.com.) Briefly, total RNA was extracted with RNeasy Mini Kit (Qiagen, Basel, Switzerland) from eyes of three C57BL/10 mutant and three C57BL/10 wild type mice of six months of age. RNA concentration and quality were determined by Agilent 2100 Bioanalyzer (Agilent Technologies, Palo Alto, CA, USA).

250 ng of total RNA were used to generate adequate cRNA amounts from each RNA sample, according to the Affymetrix `Small Sample Labelling Protocol vII`. Fifteen micrograms of biotin-labeled (Enzo Life Science, Inc. Farmingdale, NY) and into 50- to 200-bp fragmented cRNA from each animal (n=6) were then individually processed on Mouse Genome 430 2.0 GeneChips (Affymetrix, Inc., Santa Clara, Canada) (n=6), representing >12,000 genes, each.

After hybridization, staining with R-phycoerythrin-streptavidin (Merck, Darmstadt, Germany) and washing steps were performed on the Automated Slide Processor (ASP, Affymetrix), according to the protocol. The arrays were scanned with the Affymetrix 428^{TM} Array Scanner, and the images were analysed using Microarray Suite 5.0 (Affymetrix). Candidate genes for quantitative PCR verification were selected, using a >1.5 and <0.5 ratio cut-off upon statistical analysis based on Welch t-test ($P<0.05$) (Microarray Suite 5.0, Affymetrix).

Quantitative RT-PCR

Transcript levels of candidate genes selected upon microarray analysis were verified by quantitative RT-PCR. For this, cDNA was prepared from total eye RNA of five wild type and five mutant animals of six months of age (B10A strain). For each animal, two independent cDNA syntheses were performed and pooled after quality control. Subsequently, 2 independent dilutions were prepared from each cDNA pool. Briefly, after eye homogenization in a glass pestle, total RNA extraction was performed in accordance to the RNeasy Mini Kit manual (Qiagen). 1.5 µg of total RNA was transcribed into cDNA by random hexanucleotide priming (Hexamer Primers $pd(N)_6$, Amersham Biosciences, Otelfingen, Switzerland), according to the protocol of Superscript^{TM}III (Invitrogen, Basel, Switzerland). cDNA synthesis efficiency and DNA contamination were examined by standardized *Gapdh* PCR, including negative controls for each

sample supplemented with no reverse transcriptase during synthesis. Absent *Gapdh* product in negative controls excluded DNA contamination.

Quantitative PCR was performed in a total volume of 25 µl containing 12.5 µl of SYBR Green Fluorescein Mix (Applied Biosystems, Rotkreuz, Switzerland), 0.1 µl of each primer (10 mM stock solution, Microsynth, Balgach, Switzerland) and 2 µl of a cDNA dilution. *Rho*, *Pde6b* and *Pdc* transcripts were analyses with transcript-specific TaqMan probes (Applied Biosystems), according to Applied Biosystems protocols. Amplification was running upon initial denaturation of 2 min at 50°C and 10 min at 95°C and then continued with 45 cycles of 15 s at 90°C and 1 min at 60°C for a SYBR® Green or Vic/Tamra TaqMan probe detection on the 7900HT ABI PRISM ® detection system (Applied Biosystems). A melting curve was included to verify single product amplification. In addition, the specificity of the amplicons was confirmed by sequencing. Transcript levels were normalized to 18S rRNA (*Taq*Man Ribosomal RNA Control Reagent, Applied Biosystems) and quantified to the mean value of homozygous wild types following the ΔC_t-method. Primers are summarized in Table 4.

Virtual Northern blots

For *Rho*, *Pde6b* and *Pdc* transcript detection, virtual Northern blots (BD SMART™ PCR cDNA Synthesis, BD Biosciences-Clontech, Basel, Switzerland) were prepared, representing whole eye-specific SMART PolyA$^+$ cDNA from two affected and two wild type mice. For this, total RNA extraction from eyes was performed in accordance to RNeasy Mini Kit (Qiagen). RNA concentration and quality were determined by Agilent System 2100 Bioanalyzer (Agilent Technologies). Through reverse transcription, 1 µg of total RNA were transcribed into cDNA, each, according to the BD Biosciences-Clontech protocol. Northern blots were hybridized 15 hours at 65°C, washed twice with 1xSSC/0.1%SDS for 5 min at 65°C and twice with 0.1xSSC/0.1%SDS for 30 min at 65°C. Finally, blots were exposed to BioMax (BioMax Eastman Kodak, Rochester, NY) films at -80°C over night. As loading control, mouse SAG probe hybridization was included. All applied robes are described elsewhere[22].

Statistics

Statistical analyses were performed using the statistical software SPSS for Windows (Release 13.0.1, 2004; SPSS, Chicago, USA), implemented on a PC running the Microsoft Windows XP operating system. The data of acoustic startle reactivity were analyzed using parametric analysis of variance (ANOVA) with the between-subject factor of genotype and the within-subject factor of pulse-level. Statistical significance was set at $p<0.05$.

Retinal whole-mount path-clamp (*on the basis of personal communication from Gian Carlo Demontis, University of Pisa, Italy)*

3.3.3. Results

Whole-mount retinal patch-clamp experiments (*preliminary data*)

Preliminary recordings of the inward barium currents in patch-clamp examinations of whole-mount retinas showed characteristics similar to those of retinal L-type calcium channels, involving the α1F pore-forming subunit (Fig. 2). Current activity ranged between ~-40 mV to ~+10 mV. No differences between wild type and heterozygous animals were observed. In homozygous *Cacna2d4*-mutant animals, barium currents in retinal whole-mounts were present but reduced. In addition, the activation curve of barium currents was shifted to more depolarized membrane potentials (*personal communication from G. Demontis, University of Pisa, Italy*).

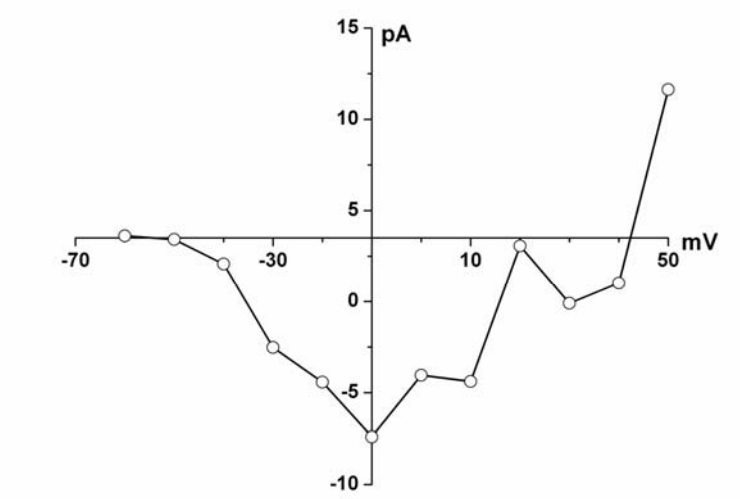

Figure 2. Whole-mount retinal currents of wild type mice. Barium inward current as a function of membrane voltage in a preliminary patch-clamp experiment. The current starts to activate at ~-40 mV and increases in amplitude up to ~-10 mV. Subsequently, current activities reduce and disappear at above ~+40 mV, showing a characteristic activation curve of α1F-associating L-type calcium channels (*personal communication from Gian Carlo Demontis, barium current curves of heterozygous and homozygous Cacna2d4-mutant mice are not yet available*).

Histology

Synaptic layers

Histological examinations of *Cacna2d4*-mutant retinas revealed severe thinning of the OPL, initiating by early postnatal days (Fig. 3). This morphological feature allowed discrimination between mutant and wild type animals by light microscopy at the early stage of P15. Quantitative analysis showed a reduction to ~60% of the OPL at P15 in mutant mice in comparison to wild type animals. However, no statistical significance could be demonstrated at this time point, presumably due to biological variation in progression of OPL shrinking (Fig. 4A).

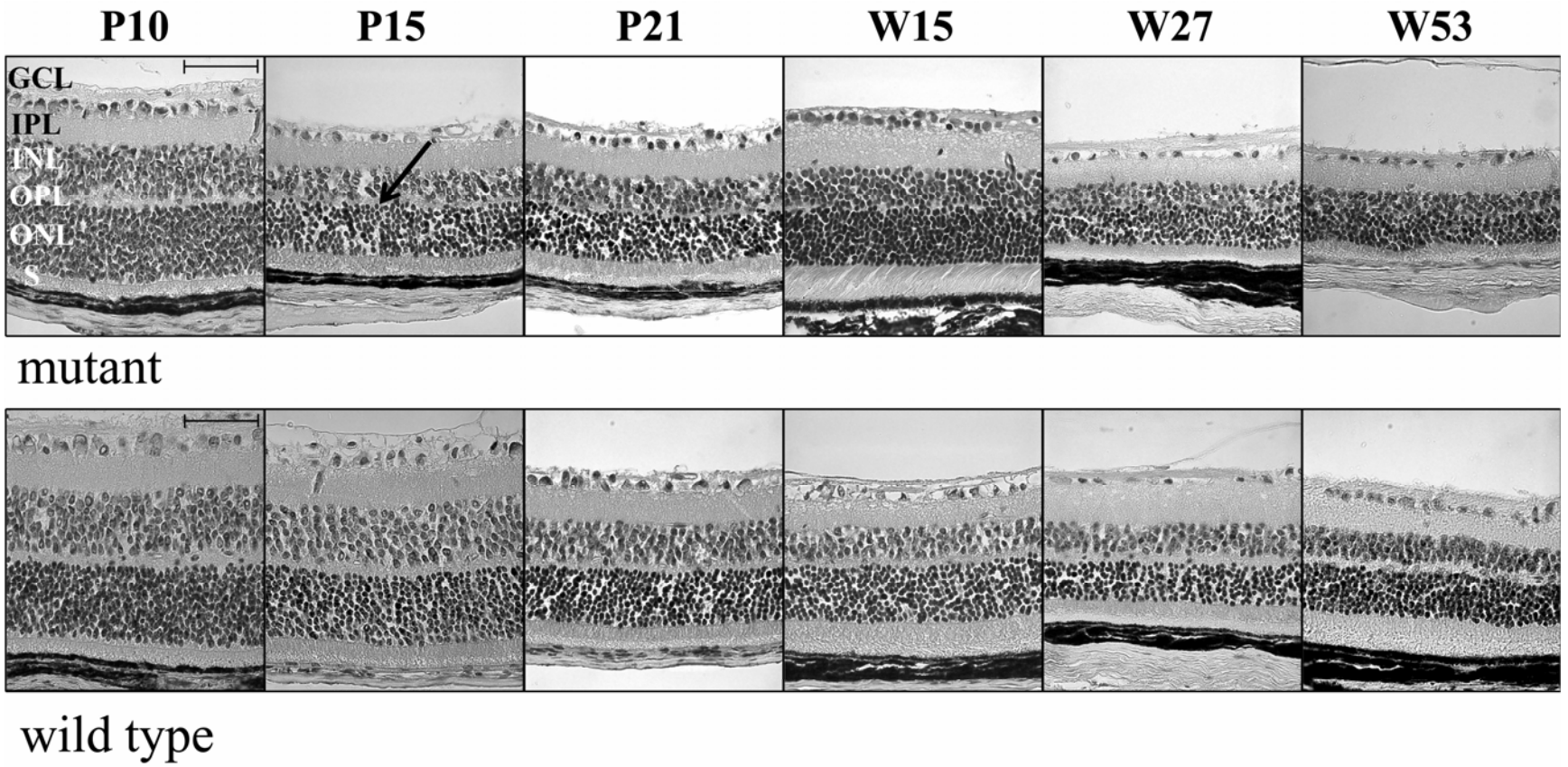

Figure 3. Thinning of the photoreceptor synaptic layer in *Cacna2d4*-mutant animals. Images of H&E stained paraffin sections were taken in the central retina at ~250 µm from the optic disc in mutant (*top*) and wild type (*bottom*) retinas. Magnification 63 x, bar equivalent to 50 µm in each image. Sections display time points of P10, P15, P21, W15, W27 and W53. Ganglion cell layer (GCL), inner plexiform layer (IPL), inner nuclear layer (INL), outer plexiform layer (OPL), outer nuclear layer (ONL), photoreceptor segments (S). The OPL emerges profoundly reduced in the *Cacna2d4*-mutant retina as soon as P15 (*arrow*).

At P21, a profound reduction to ~30% of the mutant OPL was detected in comparison to wild type mice. This decline in thickness of the synaptic outer plexiform layer was statistically significant. By W15 (~3 months), almost complete loss of the OPL was detected in mutant mice (Fig. 3, 4). Remaining synaptic tissue was measurable at a few diffusively occurring patches.
The inner synaptic layer (IPL) was preserved for six months (W27) (Fig. 4B). By W53 (~1 year), significant thinning to ~50% was observed in the peripheral retina relative to wild type mice, indicating an involvement of the IPL in synaptic retraction in the later disease course.

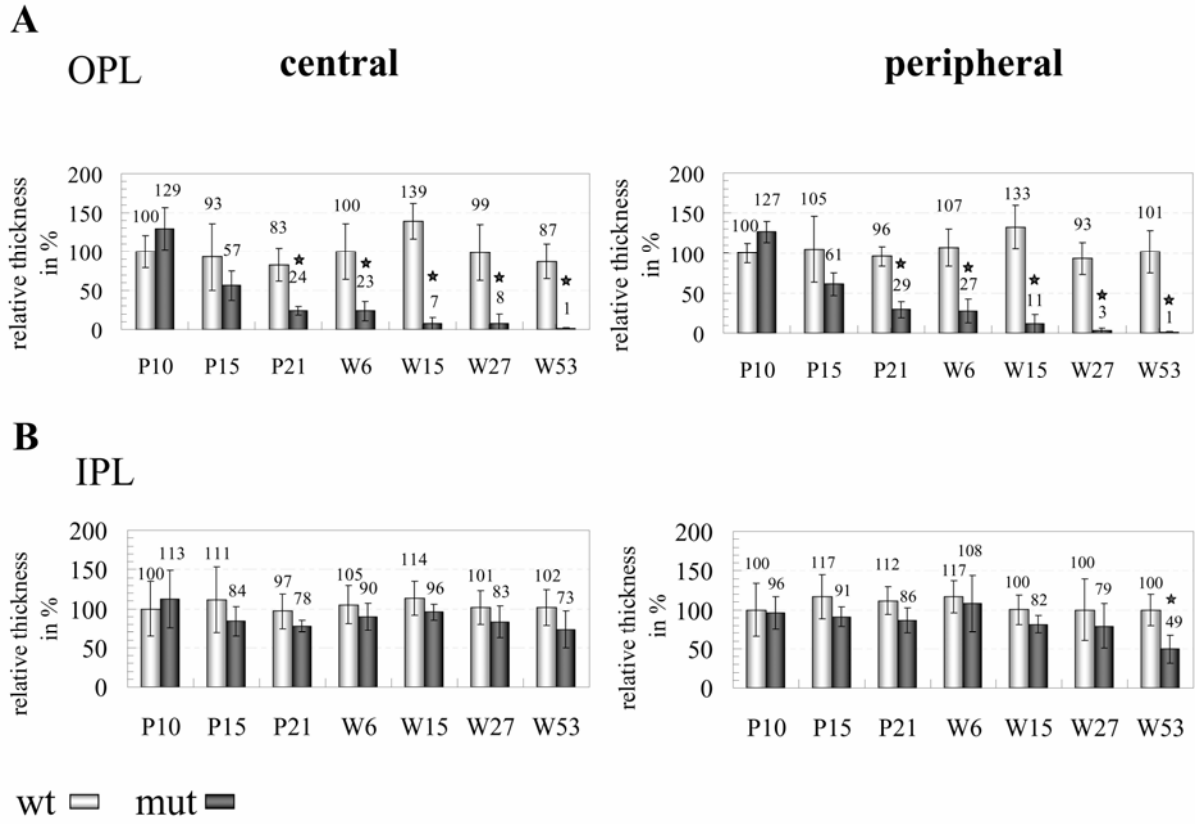

Figure 4. Synaptic layers in *Cacna2d4*-mutant animals. (**A**) Thickness of the outer plexiform layer (OPL) in the central (*left*) and in the peripheral retina (*right*). (**B**) Thickness of the inner plexiform layer (IPL) in the central (*left*) and peripheral (*right*) retina. X axis displays time stages. Y axis shows normalized thickness of the synaptic layers. At each time point, the synaptic breadth of each retina was normalized to the corresponding mean thickness of P10 wild type animals and expressed in percent. Error bars indicate confidence intervals of $P<0.05$. The measurements show significant OPL reduction from P21 in the central and the peripheral retina of *Cacna2d4*-mutant mice in comparison to wild type animals (★), which results in almost complete loss at W15. The central IPL displays no significant changes in thickness up to W53. However, the peripheral IPL becomes significantly reduced at W53 in comparison to wild type mice and may indicate progression of synapse layer shrinking also in the inner retina. Wild type mice (wt), mutant mice (mut).

Nuclear layers

Slow progression of an early onset photoreceptor degeneration was observed in *Cacna2d4*-mutant animals (Fig. 5A, 5B). The first degenerative process, noted between P10 and P21, resulted in a significant reduction of ~15% of photoreceptor nuclei in mutant retinas in comparison to wild type mice. Further slight loss of photoreceptors indicated rather an inhibited progression of the retinal degeneration. At one year of age, light microscopy examinations revealed loss of ~30% of photoreceptor nuclei in the central and ~45% in the peripheral retina when compared to wild type mice. This might indicate more pronounced degeneration in the peripheral retina (Fig. 5A, 5B).

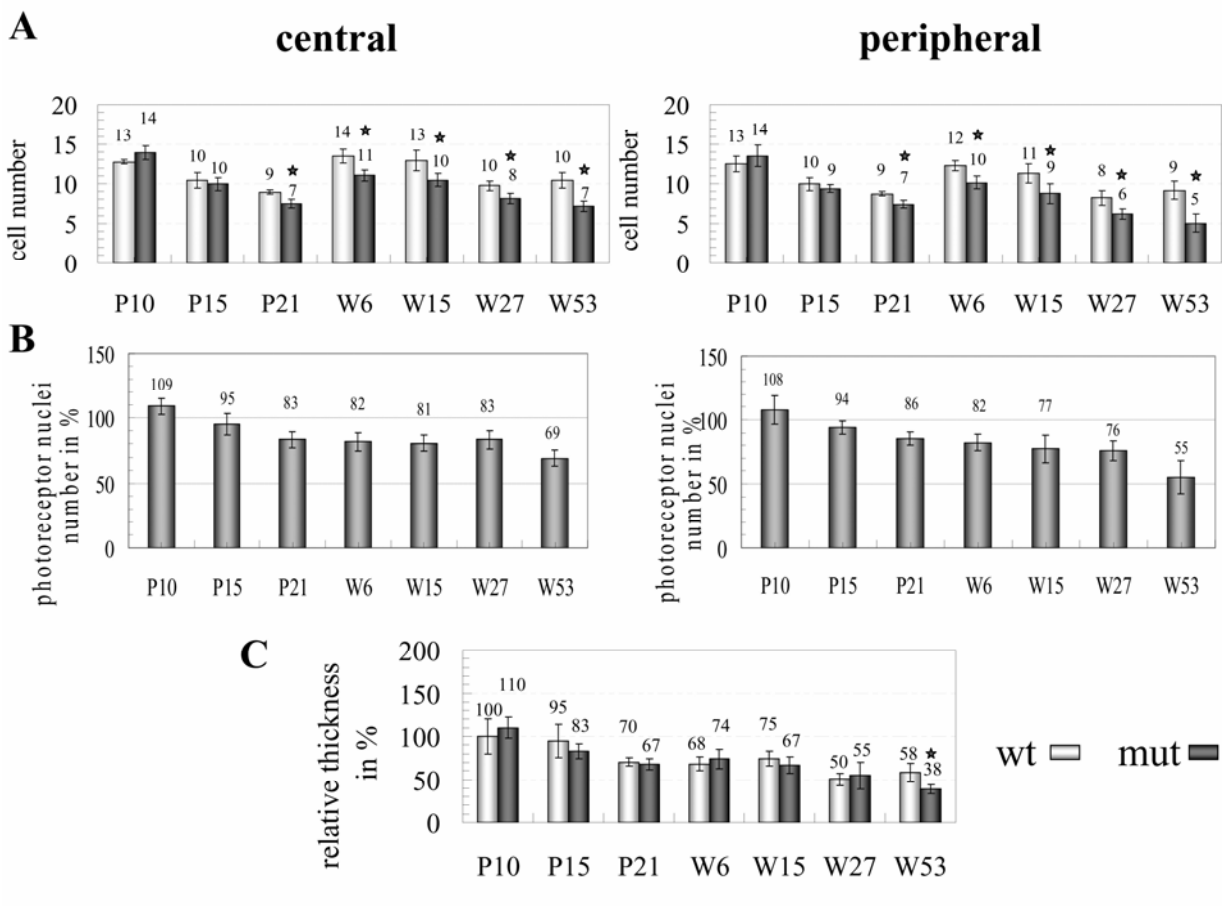

Figure 5. Photoreceptor degeneration in *Cacna2d4*-mutant mice. (**A**) Average number of photoreceptor nuclei counted per vertical row in the ONL. At P21, loss of photoreceptors in mutant retinas becomes significant (★). (**B**) Reduction of photoreceptor nuclei in mutant retinas relative to average nuclei numbers of wild type animals in each state (expressed in percent). (**C**) Relative thickness of the peripheral outer nuclear layer. The average thickness of each measured retina was normalized to the mean value of the ONL breadth of P10 wild type retinas and translated into percents. Whereas the central retina displayed no significant reduction, the peripheral retina revealed significant decrease in thickness at the age of one year, correspondingly to advanced photoreceptor loss. Error bars indicate confidence intervals of $P<0.05$. Wild type (wt), mutant mice (mut).

In the course of disease progression, the peripheral ONL became significantly thinned to ~60% at one year of age when compared with wild type mice (Fig. 5C). Accordingly, peripheral photoreceptor segments (S) diminished in length to ~57% (Fig. 6). The thickness of the ONL and the length of the S in the central retina did not reveal significant reduction in the time window of histological examinations (data not shown).

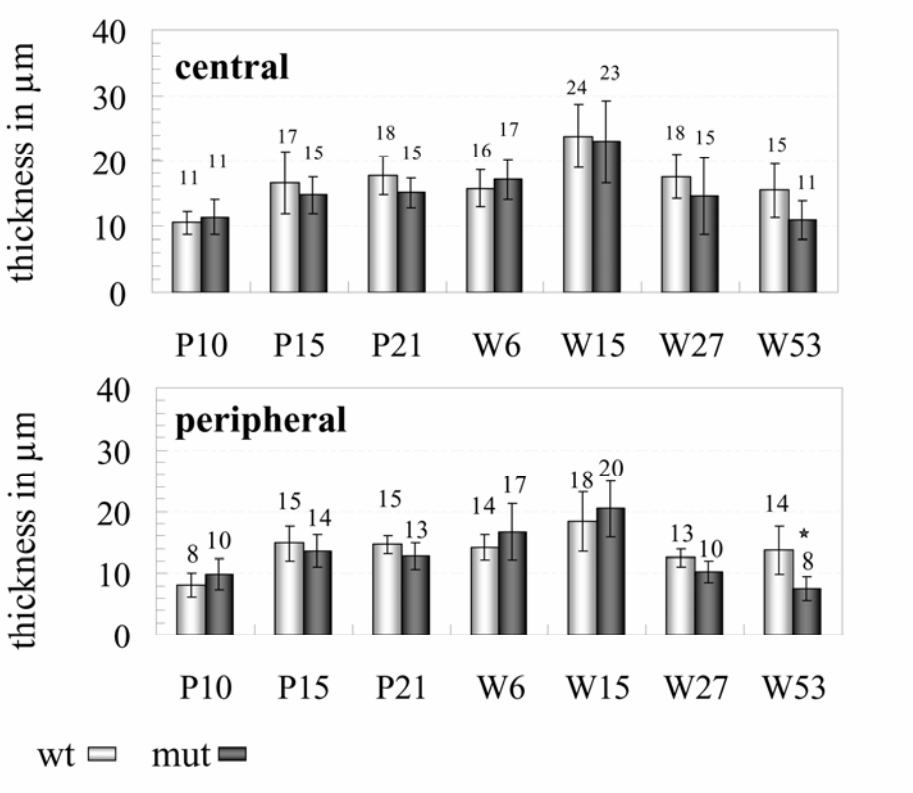

Figure 6. Length of photoreceptor segments in *Cacna2d4*-mutant mice. In one year-old mutant animals (W53), peripheral photoreceptors displayed a significant reduction (~57 %) of the segment length (★). In the central retina, a decrease (~73%) in the mean segment length of mutant retinas was observed, however with so far lacking statistical significance. Error bars indicate confidence intervals of $P<0.05$. Wild type (wt), mutant mice (mut).

The inner nuclear layer sustained normal in the time window of P10 to W27 (Fig. 7A). Similar to the outer retina, significant elimination of ~45% of cell nuclei occurred in the peripheral INL of mutant animals upon twelve months. This loss was accompanied by significant thinning of the peripheral INL to 65% in comparison to wild type (Fig. 7B).

The ganglion cell layer remained unaffected over the time of examinations (data not shown). However, by one year of age (W53), the mean diameter of the ganglion cell nuclei became significantly reduced (by ~22%) in mutant mice, most likely as a consequence of the overall progressing degeneration (Fig. 8).

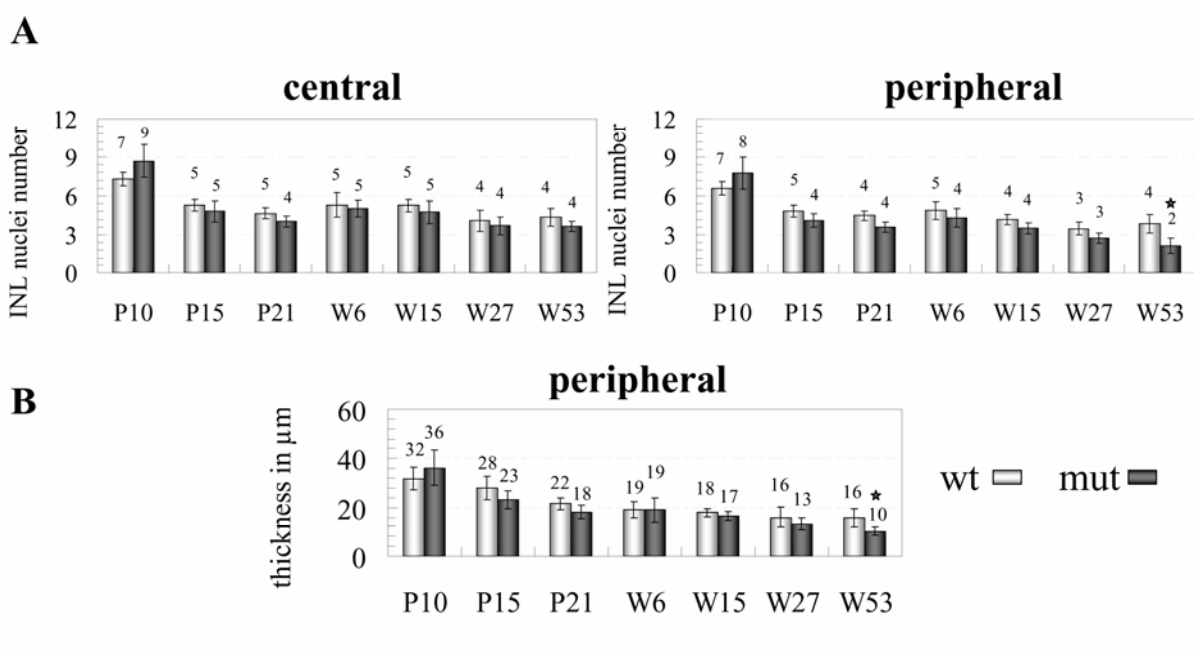

Figure 7. Histology of the inner nuclear layer. (**A**) Average nuclei number of the inner nuclear layer (INL) estimated per vertical row. Whereas no significant reduction was found in the central retina, loss of INL cells in mutant peripheral retinas became significant at one year of age (★). (**B**) Thickness of the peripheral INL. In the peripheral retina, significant decrease in breadth was detected at the age of one year, correspondingly to advanced INL nuclei loss. Error bars indicate confidence intervals of P<0.05. Wild type (wt), mutant mice (mut).

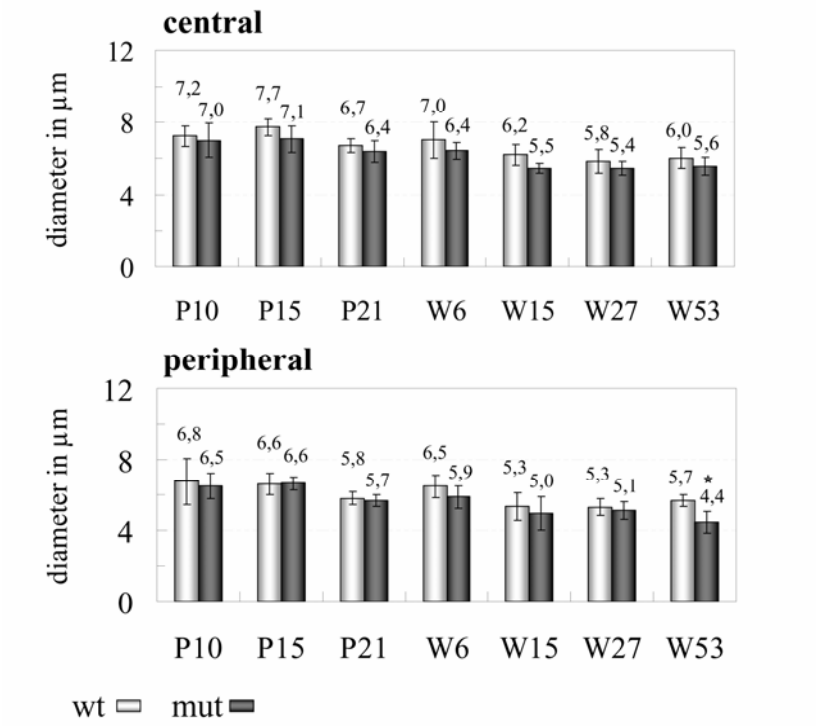

Figure 8. Ganglion cell nuclei diameter. In one year-old mutant animals (W53), peripheral ganglion cell nuclei displayed a significant reduction (~22 %) of their mean diameter (★). Error bars indicate confidence intervals of P<0.05. Wild type (wt), mutant mice (mut).

Hearing in *Cacna2d4*-mutant animals

Since *Cacna2d4* mutation affects retinal ribbon synapses, we asked whether it contributes to a perturbed function of these synapses in the cochlear system. The acoustic startle reflex examinations revealed severe loss of startle reactivity in both wild type and *Cacna2d4*-mutant mice (mostly no reaction even at 120 dB[A]) (Fig. 9A). For a rough comparison, male C57BL/6 wild type animals (age 2.5 months) exhibited twice the amount of mean startle response at 100 dB[A] compared to our B10A subjects, five times the amount at 110 dB[A], and eight times the amount at 120 dB[A]. A 2 × 10 (genotype × pulse level) ANOVA revealed no main effect of genotype ($F[1,24]=1.95$, $p=0.175$). A further analysis of the within-subject factor of pulse level yielded a main effect of pulse-level ($F[9,216]=10.82$, $p<0.001$), but no significant interaction of genotype × pulse levels ($F[9,216]=0.50$, $p=1.000$). Thus, no association between the *Cacna2d4* mutation and hearing impairment could be demonstrated. In addition, the profound startle decline in all mice suggested an impaired hearing in the entire B10A strain at the age of six months.

To exclude deafness due to homozygosity of the c.753G>A *Cadherin23* (*Cdh23*^{ahl753}) mutation arising in the AJ genetic background, we included genotyping of the examined B10A mice by direct sequencing. The *Cdh23*^{ahl753}-mediated splicing defect leads to the exclusion of exon 7 in the *Cadherin23* gene and thus to a protein deficiency resulting in age related hearing loss in several mouse strains.

Sequence analysis of the genomic DNA revealed homozygosity for the *Cdh23*^{ahl753} mutaion in all startle-examined B10A animals as well as in the heterozygous (C57BL/10 x AJ)F1 and homozygous C57BL/10 control mice (Fig. 9C). RT-PCR experiments confirmed skipping of exon 7 due to the *Cdh23*^{ahl753} defect in isogenic C57BL/10 mice (Fig. 9B). None such mutation has been reported for C57BL/10 mice previously.

At the morphological level, *Cdh23*^{ahl753}-mediated hearing loss in mice manifests upon disorganized stereocilia, loss of outer hair cells and spiral ganglion cells as well as ultimatively arising generalized degeneration of the organ of Corti[23]. In B10A animals of 10 days of age, no obvious cochlear abormalities were observed in *Cacna2d4*-mutant and wild type mice (Fig. 9D). This indicated that both, the *Cacna2d4* and *Cdh23*^{ahl753} mutations have no apparent effects on the cochlea during development.

For further elucidation of *Cacna2d4*-mutational effects on the hearing system in mice, we perfomed sensitive auditory-evoked brainstem response tests in 7 and 12 week-old animals. No statistically significant difference in the auditory brainstem thresholds were detectable between

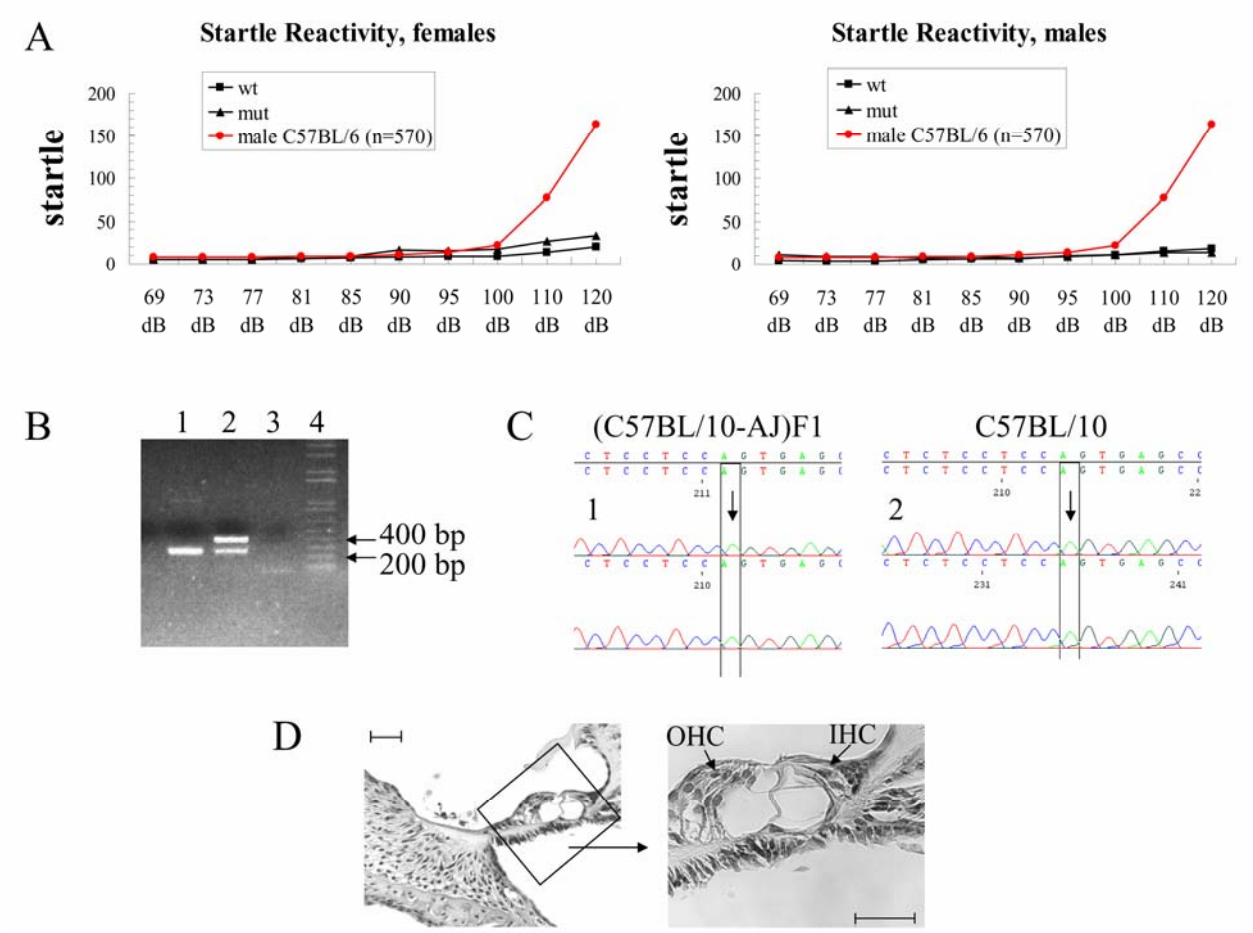

Figure 9. Characterization of the hearing capabilities in *Cacna2d4*-mutant animals. (**A**) Mean acoustic startle response in B10A mice evoked by a series of 69-120 dB[A] startle-eliciting stimuli (females left, males right). Both, *Cacna2d4*-mutant and wild type animals show loss of startle reactivity. Wild type (wt), mutant mice (mut). (**B**) *Cdh23*^{ahl753} mutation causes in-frame skipping of *Cdh23* exon 7. (**1**) 264-bp RT-PCR product in *Cdh23*^{ahl753} homozygous C57BL/10 mice. (**2**) 264- and 383-bp fragments of heterozygous (CBA/CaJ-C57BL/6J)F1 control mice. The 383-bp product corresponds to the wild type allele of CBA/CaJ unaffected mice. (**3**) Water control, (**4**) DNA ladder. (**C**) *left*, *Cdh23*-genotyping of two (C57BL/10-AJ)F1 hybrid mice, *right*, *Cdh23*-genotyping of two C57BL/10 mice. Homozygosity for the *Cdh23*^{ahl753} mutation can be observed in both strains (*arrows*). (**D**) Cross-section through the apical region of a 10 day-old B10A wild type cochlea. No qualitative abnormalities of the organ of Corti are detectable at this stage. Scale bar 50 µm. Inner (IHC) and outer hair (OHC) cells appear normal.

Cacna2d4-mutant and wild type animals at both examined ages. However, at 7 weeks of age, the mean ABR thresholds for the mutant mice appeared higher for the clicks and all tone burst stimuli (Fig. 10). This might suggest a small effect of the *Cacna2d4* mutation.

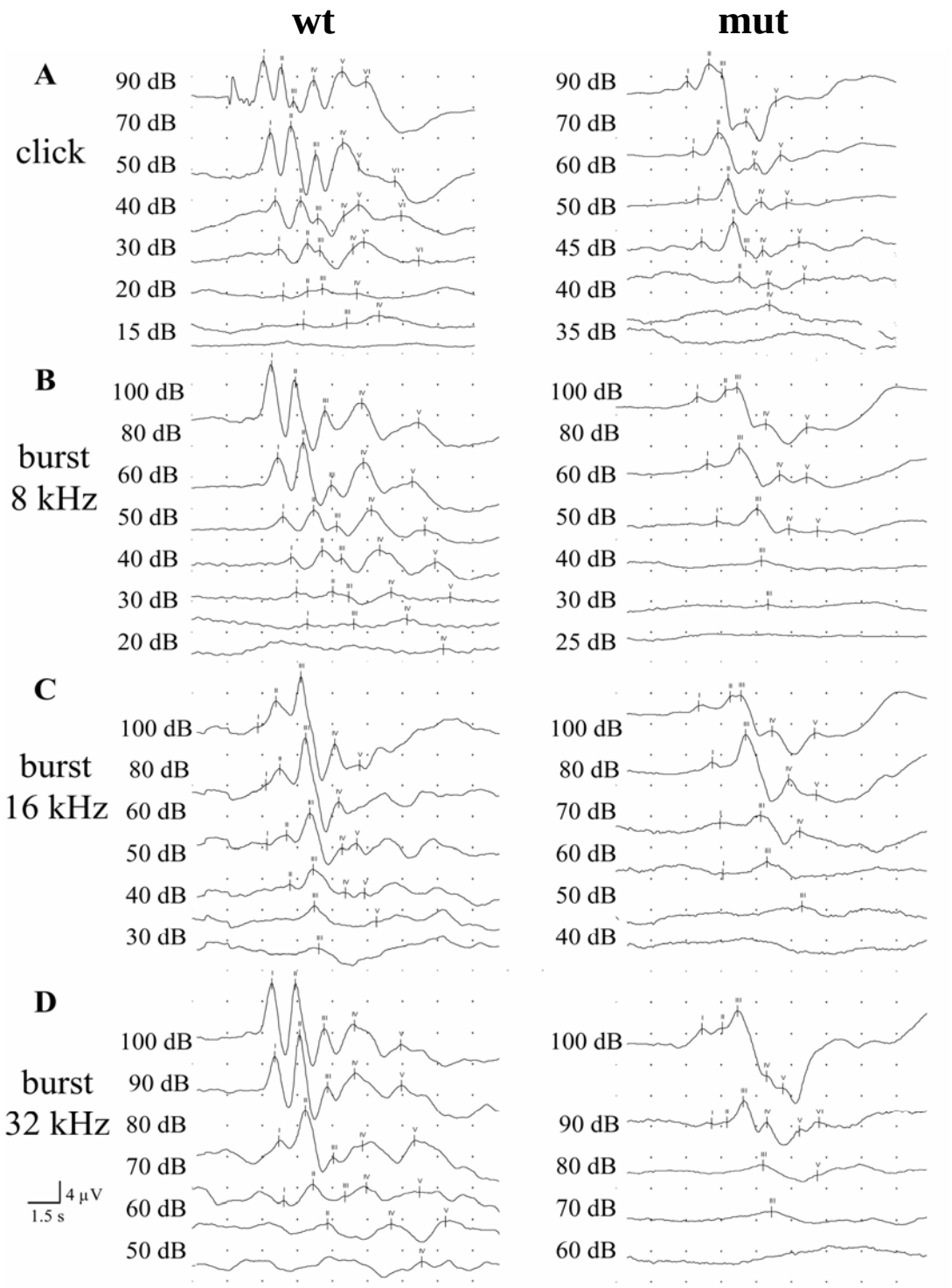

Figure 10. Auditory-evoked brainstem responses in *Cacna2d4*-mutant and wild type C57BL/10 mice (7 weeks). Typical auditory brainstem responses evoked with a click stimulus (**A**) and with different tone bursts of 8 kHz (**B**), 16 kHz (**C**) and 32 kHz (**D**), respectively. ABRs at different descending stimulus intensity levels of x dB[A] (*indicated in the graphs*). The X-axis of each courve reflects 1.5 ms/division with a total window of 15 ms (latency), the Y-axis response amplitude in µV. Left graphs show a typical example of a C57BL/10 wild type mouse (*wt*), right graphs show typical responses of a *Cacna2d4*-mutant mouse (*mut*). The latter shows lack of reproducible ABRs at lower stimulation intensities, corresponding to higher auditory thresholds.

Table 1 shows the mean ABR-threshold data of wild type and *Cacna2d4*-mutant mice at 7 weeks (upper part). Analysis of data showed no statistical significant differences between the two groups (t-tests, independent samples, 2-tailed, P>0.05). Eight mice were measured at the age of 12 weeks, however, ABR-threshold measurements revealed again no significant differences between wild type and mutant mice (lower part).

7 weeks (n=9)					
	n	click	8 kHz	16 kHz	32 kHz
Wild type	4	23 (8.1)	32 (8.2)	32 (14.1)	62 (8.2)
Mutant	5	26 (9.1)	45 (12.0)	50 (13.0)	75 (15.6)
12 weeks (n=8)					
	n	click	8 kHz	16 kHz	32 kHz
Wild type	4	29 (17.0)	39 (5.0)	52 (14.1)	87 (17.3)
Mutant	4	25 (14.5)	44 (3.5)	55 (9.6)	77 (12.9)

Table 1. Mean ABR-thresholds. Mean ABR-thresholds and standard deviations in dBSPL at the age of 7 and 12 weeks, obtained from C57BL/10 wild type *versus* mutant mice using clicks and tone burst stimuli.

Microarray analysis in *Cacna2d4*-mutant eyes

The microarray experiments were performed at six months of age, a time when the photoreceptor synaptic layer became almost completely retracted, but the photoreceptor degeneration showed an arrested or slow progression. Transcriptom analysis in *Cacna2d4*-mutant animals at this time point might thus elucidate photoreceptor-specific genes that experience differential expression in relation to synaptic degeneration. In the microarray experiments, ~2.950 gene equivalents revealed a positive signal on all 6 hybridized arrays. Upon statistical evaluation, we estimated a total number of ~302 genes, assumed to be differentially expressed in wild type and mutant animals, with ratios in the range of 0.26 to 3.59. Among these genes, 238 showed ratios of <1.0 and 64 >1.0. Most of these genes disclosed a reduction of ~25 to ~50% (ratios of 0.50 to 0.75) (Fig. 11). Using a cut-off of <0.5 for lower abundant and >1.5 for upregulated transcripts, 63 potential differentially expressed candidate genes remained, from which 12 were selected for further analysis. These genes were assumed to represent putative synaptic adhesion- and rod-specific genes that might play a role in the *Cacna2d4*-associated pathology (Table 2, 3, 4). Of note, filtering transcripts detected *´at least´* on all three arrays hybridised either with cRNA from wild type or with mutant eyes, statistical analyses and the cut-offs of <0.5 and >1.5 revealed no further differentially expressed genes.

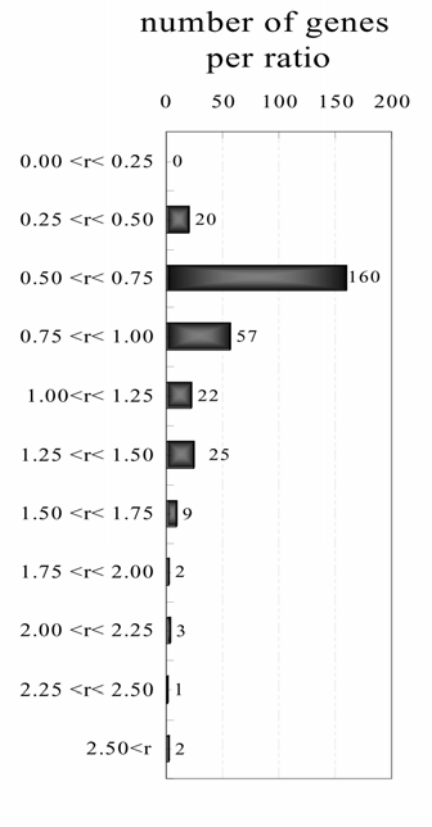

Figure 11. Ratios of differentially expressed transcripts in the microarray analysis. Most transcripts (n=303), detected to be differentially expressed in mutant eyes, showed lower abundance in the range of 25% to 50%.

Table 2. List of genes upregulated in *Cacna2d4* -mutant animals (cut-off >1.5)

Chip ID	gene symbol	gene name	ratio
93996_AT	*Cyp2e1*	cytochrome P450, family 2, subfamily e, polypeptide 1	3.6
102327_AT	***Aoc3***	**amine oxidase, copper containing 3**	**2.7**
93266_AT	***Tpm3***	**tropomyosin 3, gamma**	**2.5**
94904_I_AT	*Tmed7*	transmembrane emp24 protein transport domain containing	2.2
92407_AT	***Myom1***	**myomesin 1**	**2.1**
93497_AT	*C3*	complement component 3	2.0
101539_F_AT	*Ces3*	carboxylesterase 3	1.8
94324_F_AT	*Hmgcl*	3-hydroxy-3-methylglutaryl-coenzyme A lyase	1.8
95064_AT	*Acaa2*	acetyl-coenzyme A acyltransferase 2 (mitochondrial 3-oxoacyl-coenzyme A thiolase)	1.7
100886_F_AT	*Mrpl45*	mitochondrial ribosomal protein L45	1.6
94348_F_AT	*Pcmt1*	protein-L-isoaspartate (D-aspartate) O-methyltransferase 1	1.6
95478_AT	*Deb0*	differentially expressed in B16F10 1	1.6
94907_F_AT	1110001	RIKEN cDNA 1110001J03 gene	1.6
98018_AT	*Procr*	protein C receptor, endothelial	1.6
98984_F_AT	*Gpd2*	glycerol phosphate dehydrogenase 2, mitochondrial	1.5
103826_AT	*Zbtb7*	zinc finger and BTB domain containing 7	1.5
104663_AT	*Pip5k1b*	phosphatidylinositol-4-phosphate 5-kinase, type 1 beta	1.5

Genes in *bold* were selected for quantitative PCR analysis. (AT_transcript details at www.affymetrix.com)

Table 3. List of genes downregulated in *Cacna2d4* -mutant animals (cut-off <0.5)

Chip ID	gene symbol	gene name	ratio
96567_AT	***Rho***	**rhodopsin**	**0.26**
94139_AT	***Pdc***	**phosducin**	**0.37**
94238_AT	2310046G15Rik	RIKEN cDNA 2310046G15 gene	0.37
92642_AT	*Car2*	carbonic anhydrase 2	0.41
92992_I_AT	5730497N03Rik	RIKEN cDNA 5730497N03 gene	0.41
92988_I_AT	***Cadps***	**Ca^{2+} dependent activator protein for secretion**	**0.41**
95541_AT	D6Wsu176e	DNA segment, Chr 6, Wayne State University 176, expressed	0.42
101650_AT	*Pcdha*	protocadherin alpha	0.43
97834_G_AT	*Pfkp*	phosphofructokinase	0.43
92831_AT	*Sfxn1*	sideroflexin 1	0.43
94545_AT	***Rtn1***	**reticulon 1**	**0.43**
94232_AT	*Ccnd1*	cyclin D1	0.45
104419_AT	*Fndc3a*	fibronectin type III domain	0.47
99494_AT	*Serpini1*	serine (or cysteine) proteinase inhibitor	0.47
104477_AT	unknown	transcribed locus	0.47
101973_AT	*Cited2*	Cbp/p300-interacting transactivator	0.48
99947_AT	*Tial1*	Tial1 cytotoxic granule	0.48
100047_AT	***Snap25***	**synaptosomal-associated protein 25**	**0.49**
104501_AT	***Vapb***	**vesicle-associated membrane protein, associated protein B and C**	**0.49**
162167_F_AT	***Pde6b***	**phosphodiesterase 6b**	**0.50**
101965_AT	unknown	unknown	0.51
93011_AT	***Gabarapl1***	**gamma-aminobutyric acid (GABA(A)) receptor-associated protein-like1**	**0.51**
98946_AT	*Wsb1*	WD repeat and SOCS box-containing 1	0.51
94408_AT	*Nab1*	Ngfi-A binding protein 1	0.51
103061_AT	*Gad1*	glutamic acid decarboxylase 1	0.51
92228_AT	***Catna2***	**catenin alpha 2**	**0.52**
97124_AT	*unknown*	hypothetical ZNF-like protein	0.52
103440_AT	*Gabpa*	GA repeat binding protein, alpha	0.52
98133_AT	*Calb1*	calbindin-28K	0.52
98525_F_AT	*Erdr1*	erythroid differentiation regulator 1	0.53
103416_AT	*Mapk6*	mitogen-activated protein kinase 6	0.53
94325_AT	*Hmgcs1*	3-hydroxy-3-methylglutaryl-Coenzyme A synthase 1	0.53
92841_F_AT	*Chgb*	chromogranin B/ secretogranin 1	0.53
96084_AT	*Hnrpdl*	heterogeneous nuclear ribonucleoprotein D-like	0.53
98917_AT	5730414C17Rik	RIKEN cDNA 5730414C17 gene	0.53
94957_AT	D030028O16Rik	RIKEN cDNA D030028O16 gene	0.53
103734_AT	*Ahi1*	Abelson helper integration site	0.54
96623_AT	*Ugcg*	UDP-glucose ceramide glucosyltransferase	0.54
95417_AT	*Mgat2*	mannoside acetylglucosaminyltransferase 2	0.54
94903_AT	*Tmed7*	transmembrane emp24 protein transport domain containing 7	0.54
103222_AT	*Eps8*	epidermal growth factor receptor pathway substrate 8	0.55
104714_AT	*Dock9*	dedicator of cytokinesis 9	0.55
93043_AT	*Sdfr1*	stromal cell derived factor receptor 1	0.55
93390_G_AT	*Prom1*	prominin 1	0.55
103065_AT	*Slc20a1*	solute carrier family 20, member 1	0.55

Genes in *bold* were selected for verification by quantitative PCR. (AT_transcript details at www.affymetrix.com)

Table 4. Candidate genes selected for real time PCR verification.

Gene symbol	GI number	Real time primers	Function
Rtn1	56090140	5`-TCATGTGGCTCCTGACCTAC 5`-TCTACTCAGCGTGCCTCTTG	putative protein of the endoplasmic reticulum
Tmp3	40254524	5`-CAGAAGAGGCCGATAGGAAG 5`-GGTCATCAATGGTCTTCTCC	components of filaments, crucial for actin binding
Cadps	70906473	5`-ACGCCTACGTGACTTTCGTC 5´-AGCTGCAGGTCCATCCTGTC	calcium-binding protein, associated with plasma membranes and large dense core vesicles at
Aoc3	6753065	5`-CTTGGCTGTGACCCAGAGGA 5`-GGATATCTTCTGCATGAGGG	potential function in adhesion, adhesive properties are suggested
Myom1	6754787	5`-CCAAGACTTGATGACTGAAG 5`-TGGGCTCGTTGATCTGCAGC	potential function in adhesion
Catna2	6753295	5`-GGTTCAGAACCTAGGAGGAG 5`-TTGGAGCTCCCTCAGCACAG	cell adhesion proteins, crucial for synaptic and dendritic density
Snap25	24475932	5`-TGGAACGCATTGAGGAAGGG 5`-TCTGCTCCCGTTCATCCACC	involved in vesicular release and secretion of neurotransmitters, localized at the plasma
Gabarapl1	31340557	5`-GTTCCAGTATAAGGAGGACC 5`-GAATAAGGCGTCCTCAGGTC	potential interaction with GABA receptors in neurotransmitter release
Vapd	34328447	5`-TACGAGTGCATCCAAGACAG 5`-CTCGGCATCGCCTTCCTCAC	involved in vesicular release and intracellular membrane trafficking
Pde6b	113930734	TaqMan probe (Applied Biosystems)	involved in visual signal transmission cascade
Rho	21717804	TaqMan probe (Applied Biosystems)	involved in visual signal transmission cascade
Pdc	13277351	TaqMan probe (Applied Biosystems)	involved in visual signal transmission cascade

Verification of microarray expression analysis by quantitative PCR

Real time PCR analysis was used to verify the expression levels of 12 selected candidate genes (Fig. 12). The true-positives could not be confirmed for the putatively upregulated genes *Aoc*, *Myom1* and *Tmp3*. By quantitative PCR (qPCR), no significant differences in transcript expression were detected in those genes. Six of ten selected putative lower abundant transcripts were significantly downregulated by ~17 to ~40% when tested by qPCR (Fig. 12). However, in comparison to the ratios observed in the microarrays experiment, the changes in gene expression were lower when analysed by qPCR. *Rho* (*Rhodopsin*) emerged downregulated on the array to ~23% and by qRT-PCR to ~65%. Similarly, *Pdc* (*Phosducin*) showed a reduction to ~61% in contrast to ~37% (Fig. 12, Table 2).

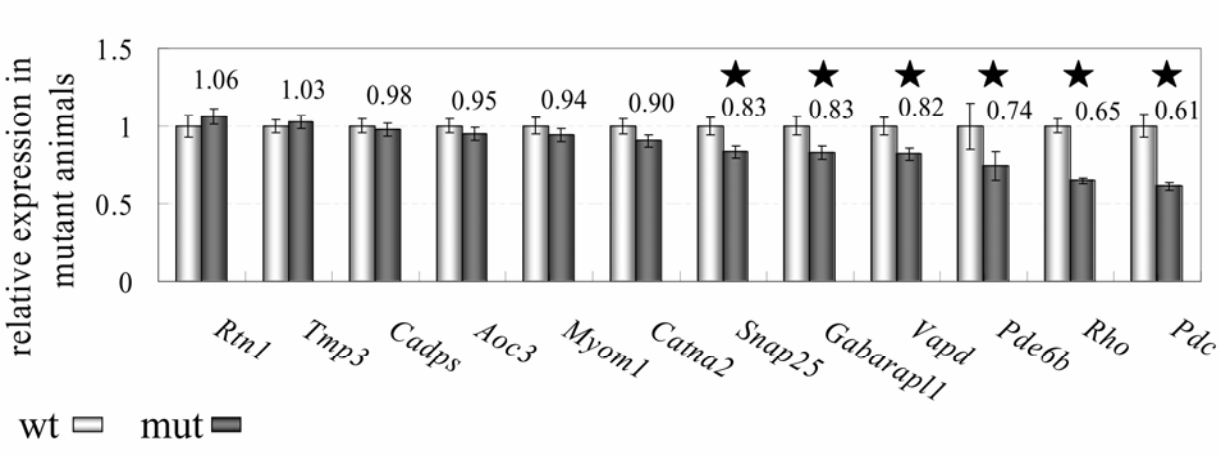

Figure 12. Quantitative PCR of selected candidate genes. The comparison of mRNA levels of selected candidate genes (X axis) shows significantly differential expression in six genes (★). Five mutant and five wild type animals were analysed for each transcript in total eye RNA. Error bars indicate confidence intervals of $P<0.05$ (n=5). Data is expressed in relative ratio to the mean value of wild type transcript levels normalized to 1.0 (Y axis). Wild type (wt), mutant mice (mut).

For three rod-specific transcripts, *Pde6b*, *Rho* and *Pdc,* that appeared most reduced in abundance in *Cacna2d4*-mutant eyes, we repeated qPCR analysis with the cDNA of all six animals used in microarray hybridisation (data not shown). Similar expression levels (ratios ~0.60-0.70) were observed as by quantitative PCR in Fig. 12. To fulfill the validation of microarray gene expression profiling, we performed virtual northern blot analysis for these three transcripts with total eye mRNA of two wild type and two mutant mice used in the microarray experiments. Slight signal reduction was observed in northern blot autoradiography for all three tested transcripts, detected in total eye RNA of mutant animals (Fig. 13).

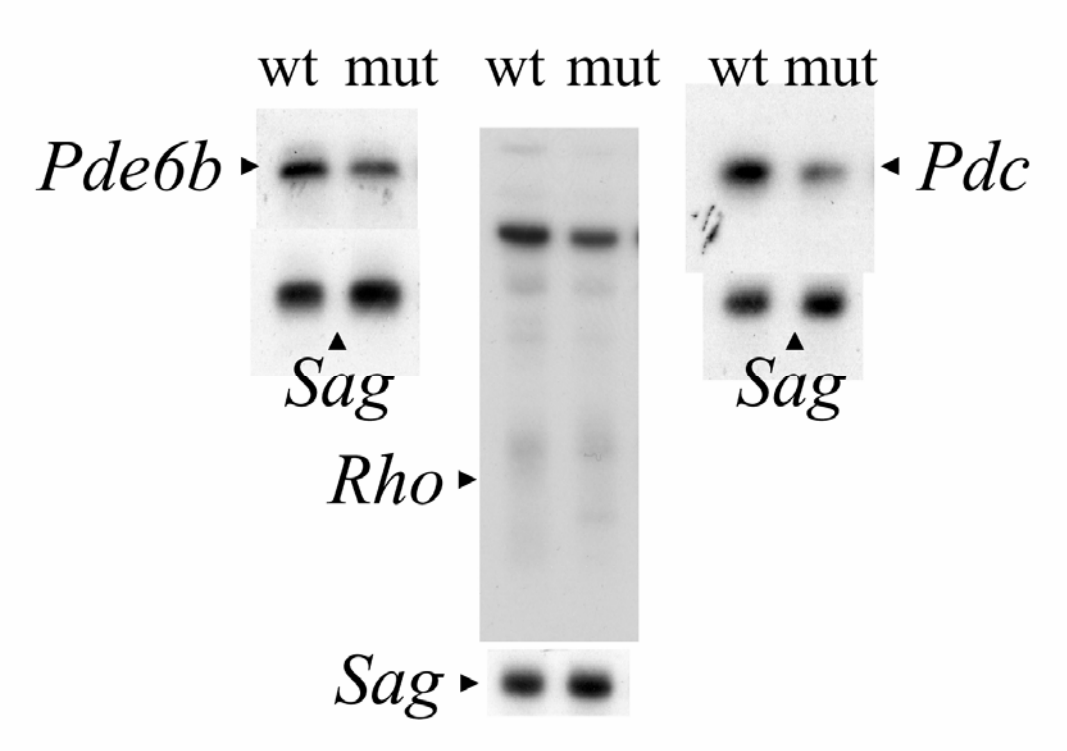

Figure 13. Virtual northern blots of three candidate genes, *Pde6b, Rho, Pdc*. *Sag* (*Arrestin*) was used as loading control. Lower band intensities can be observed for all three gene transcripts in mutant animals (*mut*) in comparison to wild type mice (*wt*).

3.3.4. Preliminary Conclusions

The c.2367insC mutation in the *Cacna2d4* gene of mutant mice manifesting a cone-rod-specific dysfunction induces a channelopathy of reduced calcium channel activities in retinal synapses. This channelopathy underlies an early onset retinal degeneration that primarily involves rapid retraction of the outer plexiform layer. Loss of ~15% of photoreceptor cells accompanies synaptic degeneration during the first three postnatal weeks, but stagnates and progresses slowly in the following 12 months.

Prior eye opening (P14), spontaneous pre-synaptic activity promotes the development and maturation of the retinal signal transmission pathways[24,25]. Thereby, spontaneous calcium signals are mediated by L-type calcium channels in precursor synaptic membranes of retinal neurons[26]. The synaptic population in the OPL is extraordinarily homogeneous and consists nearly exclusively of ribbon-type synapses that maturate by ~P10 to P15[27]. Thereby, junctions initially established by photoreceptors and horizontal cells are invaginated by bipolar cells in a final step, mostly at P12 to P15[28,29].

The integration of bipolar cell dendrites into photoreceptor presynaptic membranes requires critical interneuronal communication by calcium signaling[30,31]. As degenerative processes in the outer plexiform layer in *Cacna2d4*-mutant animals were detectable as soon as P15, this early spontaneous calcium signaling may be severely compromised and perturb synaptogenesis in the OPL of mutant animals. In consequence, retinal neurons can retract their axons and dendrites, a process that may result in thinning of the synaptic outer plexiform layer, as observed in mutant animals at P15. Of note, substantial *Cacna2d4* transcriptional activity in mouse eyes was observed at P5 and P10 (RT-PCR data not shown).

The early onset of degeneration may also be the consequence of synaptic complex collapse induced by light after eye opening. Light stimulation hyperpolarises the plasma membrane in developing photoreceptor outer segments. This drastically decreases calcium signaling and the initial synaptic release of glutamate[32]. The down-tuning of synaptic activities is required for neurotransmission of the visual input and also underlies the control of functional L-type calcium channels in the OPL[33]. As the activity of L-type calcium channel complexes in mutant animals is probably reduced, further diminution of calcium signaling by light may result in loss of synaptic firing. Non-operating synaptic processes may be eliminated subsequently in the process of synaptic remodeling during maturation[34,35].

The initial photoreceptor degeneration accompanying synaptic retraction in immature retina (before P21) probably involves rods, as cone photoreceptors were demonstrated to survive until the age of six weeks[15]. During normal retinal development, high frequency of photoreceptor apoptosis appears in the immature retina as a result of intense retinal remodelling prior to and upon light exposure[36]. Factors including the stage of synaptic maturity influence photoreceptor susceptibility to apoptosis[37]. In *Cacna2d4*-mutant animals, early synaptic dysfunction may render rod photoreceptors irresistant to retinal remodeling and induce initial cell death. In the mature retina (upon P21), degeneration of the OPL is likely accompanied by an arrested or slow progression of rod death, which might be the result of diminished remodeling processes. In some mouse models of retinal hereditary diseases, susceptibility of the retina to photoreceptor death was observed to be increased during the critical period of photoreceptor development and to stagnate after early adulthood[38].

In the inner retina, *Cacna2d4*-mutation contributes to loss of ribbon synapses in the bipolar cells, as it was previously shown in three month-old affected animals[16]. Yet, this synaptic loss does not include the overall degeneration of the inner plexiform layer at least in the time window of six months. The IPL possesses largely conventional synapses in contrast to the OPL. As these synapses are spared from structural disorganization in *Cacna2d4*-mutant mice, their maintenance might contribute to the preserved IPL integrity[39,40]. By one year of age however, retinal degeneration involves the entire retina, likely as a result of increased physiological stress.

The early onset retinal degeneration in *Cacna2d4*-mutant mice correlates with the results of previous electrophysiological examinations. At two weeks of age, loss of the scotopic b-wave and thus loss of photoreceptor synaptic transmission in the OPL is detectable upon scotopic electroretinography, reflecting nearly congenital loss in activities of the second-order neurons (*personal communication from K. Ruether*). Rod elimination prior to retinal maturity correlates with the reduction of the a-wave in dark-adapted electrophysiological responses recorded by two weeks of age. With increasing age, progressive loss of the OPL is reflected by further reduction of the scotopic b-wave[16]. The stationary or slow progression of photoreceptor loss appears as well in line with a non-significant decline of the scotopic a-wave[16]. Of note, *Cacna2d4*-mutant animals of the inbred strain C57BL/10 displayed the reduction of photoreceptor cell number of ~30% at three months of age, in contrast to ~17% in mutant animals of the B10A strain[16]. This difference may be the result of distinct genetic backgrounds or extrinsic factors during animal breeding. Significant differences in both morphological signs and the time course of retinal

degeneration caused by the same defective gene are observed between various mouse strains and demonstrate the influence of the genetic variability of an organism on the disease manifestation[41]. In both B10A and C57BL/10 strains, the *Cacna2d4*-mutation may, for instance, induce compensatory effects of different nature and effectiveness, depending on the genetic program. The genetic background may also have influence on the susceptibility to light-induced stress and damage. Variations in the resistance of the retina to light damage are found between mouse strains[42-44]. Extrinsic factors may include differences in intensities and times of light exposure during breeding which emerge in distinct animal facilities. It is possible that the B10A strain experienced less damaging light stimulation which has reflected in lower reduction of photoreceptor cell nuclei.

The histological analyses provided a 12 months window during which cellular mechanisms of damage in the photoreceptor synaptic layer and substantial survival of photoreceptors might underlie imperative transcriptome activities[45-48]. However, the expression profiling analyses revealed rather lack of profound changes in retinal transcript expression of *Cacna2d4*-mutant mice. The majority of genes showed ratios of approximately 1.0, indicating a normal expression in mutant mice. This may be the result of several effects. For many genes, regulation of expression may occur at the translational level. In addition, these genes that are differentially expressed in eyes of the *Cacna2d4*-mutant mice might be not represented on the microarrays. It is also possible that differentially expressed genes in mutant animals were not sensed by our analyses. Since ~2950 of 12.000 genes were detected on all hybridized arrays, loss of information might occur. Of note, ~13.000 non-redundant transcripts are assumed to be expressed in the retina[49-52].

Upon quantitative PCR, only six of twelve selected candidate genes were confirmed to display differential expression in mutant mice. This discrepancy may be the result of varying expression of various splicing isoforms encoded by each investigated gene. Microarray hybridisation may reflect cumulative effects in expression, whereas qPCR performed with gene-specific primers may generate expression data of a specific isoform(s) or *vice versa*.

Nonetheless, two genes involved in the rod phototransduction pathway, *Pde6b* and *Rho*, were shown to be present at considerably lower levels in *Cacna2d4*-mutant mice. The low abundance of these genes may be responsible for the diminished scotopic ERG responses[16]. *Pdc* has been shown to bind the beta and gamma subunits of the retinal G-protein transducin. Thus, this gene

participates in regulation of phototransduction. Its reduced transcript amounts in mutant animals may also contribute to lower responses in rods.

Regarding the cochlear system, normal hearing in *Cacna2d4*-mutant mice is suggested from ABR examinations until the age of 12 weeks. Electrophysiological data from the ABRs (Table 1, upper part) showed that mean values of the auditory thresholds of the wild type mice seem to be slightly better for high frequencies (8-32 kHz) compared to those of *Cacna2d4*-mutant mice at the age of 7 weeks. However, the 5% level of statistical significance was not reached. Interestingly, besides the absolute threshold levels, ABR morphologies in the mutant mice seemed to be slightly different compared to the control group. This may imply abnormal or less synchronous neuronal firing of the spiral ganglion cells, resulting in smaller peak amplitudes. This is in conformity with previous studies in hearing impaired mice, reporting that abnormalities in ABR morphology, in explicit different latencies and amplitudes, are not always associated with abnormal hearing thresholds[53,54]. Thus, *Cacna2d4*-mediated channelopathy in the organ of Corti cannot be excluded.

The identified *Cdh23*^{ahl753} mutation in the C57BL/10 genetic background likely exacerbates later elucidation of the *Cacna2d4*-induced channelopathy, when present. Functional and morphological defects of the cochear system specific for the *Cacna2d4*-deficiency may be indistinguishable from *Cdh23*^{ahl753} induced alterations. *Cadherin 23* is a component of the tip links in hair cell stereocilia and mice deficient in Cadherin23 develop structurally disorganized hair bundles rendering progressive cochlear degeneration. This loss of hair cells involves destruction of hair cell ribbon-type synapses[23]. ABR measurements at 12 weeks of age revealed a trend of higher auditory ABR thresholds for the control mice compared to the 7 week old mice, suggesting onset of hearing deterioration in the control group, especially for the high frequencies above 8 kHz. Genetic targeting on the Cast/Ei mice background, retaining normal hearing levels through almost entire life, could help to analyze effects of the *Cacna2d4*-associated channelopathy on the cochlear system. Of note, the *Cacna2d4* mutation may also act as a modifier of the *Cdh23*^{ahl753} defect in C57BL/10 or B10A mice and remain silent, if present alone. An allelic variant of the *Atp2b2* gene, encoding a calcium pump, was demonstrated to function as modifier for *Cdh23*^{ahl753}[55]. Haploinsufficiency at *Atp2b2* and homozygosity with respect to *Cdh23*^{ahl753} together, but neither alone, cause early onset hearing loss in mice[56].

3.3.5. References

1. Barnes S, Kelly MEM (2002) Calcium channels at the photoreceptor synapse. Photoreceptors and Calcium 514:465-476
2. Berntson A, Taylor WR, Morgans CW (2003) Molecular identity, synaptic localization, and physiology of calcium channels in retinal bipolar cells. Journal of Neuroscience Research 71:146-151
3. Heidelberger R, Thoreson WB, Witkovsky P (2005) Synaptic transmission at retinal ribbon synapses. Progress in Retinal and Eye Research 24:682-720
4. Arikkath J, Campbell KP (2003) Auxiliary subunits: essential components of the voltage-gated calcium channel complex. Current Opinion in Neurobiology 13:298-307
5. Birnbaumer L, Qin N, Olcese R, Tareilus E, Platano D, Costantin J, Stefani E (1998) Structures and functions of calcium channel beta subunits. Journal of Bioenergics and Biomembrane 30:357-375
6. Catterall WA (2000) Structure and regulation of voltage-gated Ca2+ channels. Annual Reviews in Cell and Develompmentl Biology 16:521-555
7. Chu PJ, Robertson HM, Best PM (2001) Calcium channel gamma subunits provide insights into the evolution of this gene family. Gene 280:37-48
8. Hanlon MR, Wallace BA (2002) Structure and function of voltage-dependent ion channel regulatory beta subunits. Biochemistry 41:2886-2894
9. Bech-Hansen NT, Naylor MJ, Maybaum TA, Pearce WG, Koop B, Fishman GA, Mets M, Musarella MA, Boycott KM (1998) Loss-of-function mutations in a calcium-channel alpha1-subunit gene in Xp11.23 cause incomplete X-linked congenital stationary night blindness. Nature Genetics 19:264-267
10. Boycott KM, Maybaum TA, Naylor MJ, Weleber RG, Robitaille J, Miyake Y, Bergen AA, Pierpont ME, Pearce WG, Bech-Hansen NT (2001) A summary of 20 CACNA1F mutations identified in 36 families with incomplete X-linked congenital stationary night blindness, and characterization of splice variants. Human Genetics 108:91-97
11. Jalkanen R, Mantyjarvi M, Tobias R, Isosomppi J, Sankila EM, Alitalo T, Bech-Hansen NT (2006) X-linked cone-rod dystrophy, CORDX3, is caused by a mutation in the CACNA1F gene. Journal of Medical Genetics 43:699-704
12. Mansergh F, Orton NC, Vessey JP, Lalonde MR, Stell WK, Tremblay F, Barnes S, Rancourt DE, Bech-Hansen NT (2005) Mutation of the calcium channel gene Cacna1f disrupts calcium signaling, synaptic transmission and cellular organization in mouse retina. Human Molecular Genetics 14:3035-3046
13. Ball SL, Powers PA, Shin HS, Morgans CW, Peachey NS, Gregg RG (2002) Role of the beta(2) subunit of voltage-dependent calcium channels in the retinal outer plexiform layer. Investigative Ophthalmology & Visual Science 43:1595-1603
14. Platzer J, Engel J, Schrott-Fischer A, Stephan K, Bova S, Chen H, Zheng H, Striessnig J (2000) Congenital deafness and sinoatrial node dysfunction in mice lacking class D L-type Ca2+ channels. Cell 102:89-97

15. Wycisk KA, Budde B, Feil S, Skosyrski S, Buzzi F, Neidhardt J, Glaus E, Nurnberg P, Ruether K, Berger W (2006) Structural and functional abnormalities of retinal ribbon synapses due to Cacna2d4 mutation. Investigative Ophthalmology & Visual Science 47:3523-3530
16. Ruether K, Grosse J, Matthiessen E, Hoffmann K, Hartmann C (2000) Abnormalities of the photoreceptor-bipolar cell synapse in a substrain of C57BL/10 mice. Investigative Ophthalmology & Visual Science 41:4039-4047
17. Wycisk KA, Zeitz C, Feil S, Wittmer M, Forster U, Neidhardt J, Wissinger B, Zrenner E, Wilke R, Kohl S, Berger W (2006) Mutation in the Auxiliary Calcium Channel Subunit CACNA2D4 Causes Autosomal Recessive Cone Dystrophy. American Journal of Human Genetics (in press)
18. Haeseleer F, Imanishi Y, Maeda T, Possin DE, Maeda A, Lee A, Rieke F, Palczewski K (2004) Essential role of Ca2+-binding protein 4, a Cav1.4 channel regulator, in photoreceptor synaptic function. Nature Neuroscience 7:1079-1087
19. Noben-Trauth K, Zheng QY, Johnson KR (2003) Association of cadherin 23 with polygenic inheritance and genetic modification of sensorineural hearing loss. Nature Genetics 35:21-23
20. Yee BK, Chang T, Pietropaolo S, Feldon J (2005) The expression of prepulse inhibition of the acoustic startle reflex as a function of three pulse stimulus intensities, three prepulse stimulus intensities, and three levels of startle responsiveness in C57BL6/J mice. Behavioural Brain Research 163:265-276
21. Jewett DL, WILLISTO.JS (1971) Auditory-Evoked Far Fields Averaged from Scalp of Humans. Brain 94:681-695
22. Lenzner S, Prietz S, Feil S, Schulz R, Ropers HH, Berger W (2000) Analysis of gene expression in a mouse model for Norrie disease by cDNA subtraction and microarrays. American Journal of Human Genetics 67:381
23. Di Palma F, Holme RH, Bryda EC, Belyantseva IA, Pellegrino R, Kachar B, Steel KP, Noben-Trauth K (2001) Mutations in Cdh23, encoding a new type of cadherin, cause stereocilia disorganization in waltzer, the mouse model for Usher syndrome type 1D. Nature Genetics 27:103-107
24. Bodnarenko SR, Jeyarasasingam G, Chalupa LM (1995) Development and regulation of dendritic stratification in retinal ganglion cells by glutamate-mediated afferent activity. Journal of Neuroscience 15:7037-7045
25. Bodnarenko SR, Chalupa LM (1993) Stratification of ON and OFF ganglion cell dendrites depends on glutamate-mediated afferent activity in the developing retina. Nature 364:144-146
26. Feller MB, Wellis DP, Stellwagen D, Werblin FS, Shatz CJ (1996) Requirement for cholinergic synaptic transmission in the propagation of spontaneous retinal waves. Science 272:1182-1187
27. Olney JW (1968) An electron microscopic study of synapse formation, receptor outer segment development, and other aspects of developing mouse retina. Investigative Ophthalmology 7:250-268
28. Olney JW (1968) Centripetal sequence of appearance of receptor-bipolar synaptic structures in developing mouse retina. Nature 218:281-282

29. Xu H, Tian N (2004) Pathway-specific maturation, visual deprivation, and development of retinal pathway. Neuroscientist 10:337-346
30. Redmond L, Ghosh A (2005) Regulation of dendritic development by calcium signaling. Cell Calcium 37:411-416
31. Redmond L, Kashani AH, Ghosh A (2002) Calcium regulation of dendritic growth via CaM kinase IV and CREB-mediated transcription. Neuron 34:999-1010
32. Bisti S, Gargini C, Chalupa LM (1998) Blockade of glutamate-mediated activity in the developing retina perturbs the functional segregation of ON and OFF pathways. Journal of Neuroscience 18:5019-5025
33. Yamashita M, Fukuda Y (1993) Calcium Channels and Gaba Receptors in the Early Embryonic Chick Retina. Journal of Neurobiology 24:1600-1614
34. Tian N, Copenhagen DR (2003) Visual stimulation is required for refinement of ON and OFF pathways in postnatal retina. Neuron 39:85-96
35. Tian N (2004) Visual experience and maturation of retinal synaptic pathways. Vision Research 44:3307-3316
36. Wang GY, Liets LC, Chalupa LM (2001) Unique functional properties of on and off pathways in the developing mammalian retina. Journal of Neuroscience 21:4310-4317
37. Jeyarasasingam G, Snider CJ, Ratto GM, Chalupa LM (1998) Activity-regulated cell death contributes to the formation of ON and OFF alpha ganglion cell mosaics. Journal of Comparative Neurology 394:335-343
38. Bravo-Nuevo A, Walsh N, Stone A (2004) Photoreceptor degeneration and loss of retinal function in the C57BL/6-C2J mouse. Investigative Ophthalmology & Visual Science 45:2005-2012
39. Mandell JW, Townes-Anderson E, Czernik AJ, Cameron R, Greengard P, De Camilli P (1990) Synapsins in the vertebrate retina: absence from ribbon synapses and heterogeneous distribution among conventional synapses. Neuron 5:19-33
40. Van Haesendonck E, Marc RE, Missotten L (1993) New aspects of dopaminergic interplexiform cell organization in the goldfish retina. Journal of Comparative Neurology 333:503-518
41. Linberg KA, Fariss RN, Heckenlively JR, Farber DB, Fisher SK (2005) Morphological characterization of the retinal degeneration in three strains of mice carrying the rd-3 mutation. Visual Neuroscience 22:721-734
42. Lavail MM, Gorrin GM (1987) Protection from Light Damage by Ocular Pigmentation - Analysis Using Experimental Chimeras and Translocation Mice. Experimental Eye Research 44:877-889
43. Lavail MM, Gorrin GM, Repaci MA, Thomas LA, Ginsberg HM (1987) Genetic-Regulation of Light Damage to Photoreceptors. Investigative Ophthalmology & Visual Science 28:1043-1048
44. Lavail MM, Gorrin GM, Repaci MA (1987) Strain Differences in Sensitivity to Light-Induced Photoreceptor Degeneration in Albino Mice. Current Eye Research 6:825-834
45. Constantine-Paton M, Cline HT (1998) LTP and activity-dependent synaptogenesis: the more alike they are, the more different they become. Current Opinion in Neurobiology 8:139-148

46. Gu XN, Spitzer NC (1995) Distinct Aspects of Neuronal Differentiation Encoded by Frequency of Spontaneous Ca2+ Transients. Nature 375:784-787
47. Spitzer NC, Olson E, Gu XN (1995) Spontaneous Calcium Transients Regulate Neuronal Plasticity in Developing Neurons. Journal of Neurobiology 26:316-324
48. Spitzer NC, Lautermilch NJ, Smith RD, Gomez TM (2000) Coding of neuronal differentiation by calcium transients. Bioessays 22:811-817
49. Schulz HL, Rahman FA, El Moula FMF, Stojic J, Gehrig A, Weber BHF (2004) Identifying differentially expressed genes in the mammalian retina and the retinal pigment epithelium by suppression subtractive hybridization. Cytogenetic and Genome Research 106:74-81
50. Schulz HL, Goetz T, Kaschkoetoe J, Weber BHF (2004) The retinome - Defining a reference transcriptome of the adult mammalian retina/retinal pigment epithelium. BMC Genomics 5:19-25
51. Schulz HL, Stohr H, Stojic J, Weber BHF (2003) Towards comprehensive characterization of the human retinal transcriptome. American Journal of Human Genetics 73:348
52. Zhang SS, Xu X, Li J, Liu MG, Zhao H, Soares MB, Barnstable CJ, Fu XY (2005) Comprehensive in silico functional specification of mouse retina transcripts. BMC Genomics 6:40-51
53. Evans EF (1986) Cochlear Frequency-Selectivity - Implications for Normal and Abnormal Hearing. Hearing Research 22:305-317
54. Fujiyoshi T, Hood L, Yoo TJ (1994) Restoration of Brain-Stem Auditory-Evoked Potentials by Gene-Transfer in Shiverer Mice. Annals of Otology Rhinology and Laryngology 103:449-456
55. Kozel PJ, Friedman RA, Erway LC, Yamoah EN, Liu LH, Riddle T, Duffy JJ, Doetschman T, Miller ML, Cardell EL, Shull GE (1998) Balance and hearing deficits in mice with a null mutation in the gene encoding plasma membrane Ca2+-ATPase isoform 2. Journal of Biological Chemistry 273:18693-18696
56. Yamoah EN, Lumpkin EA, Dumont RA, Smith PJS, Hudspeth AJ, Gillespie PG (1998) Plasma membrane Ca2+-ATPase extrudes Ca2+ from hair cell stereocilia. Journal of Neuroscience 18:610-624

Chapter 4.

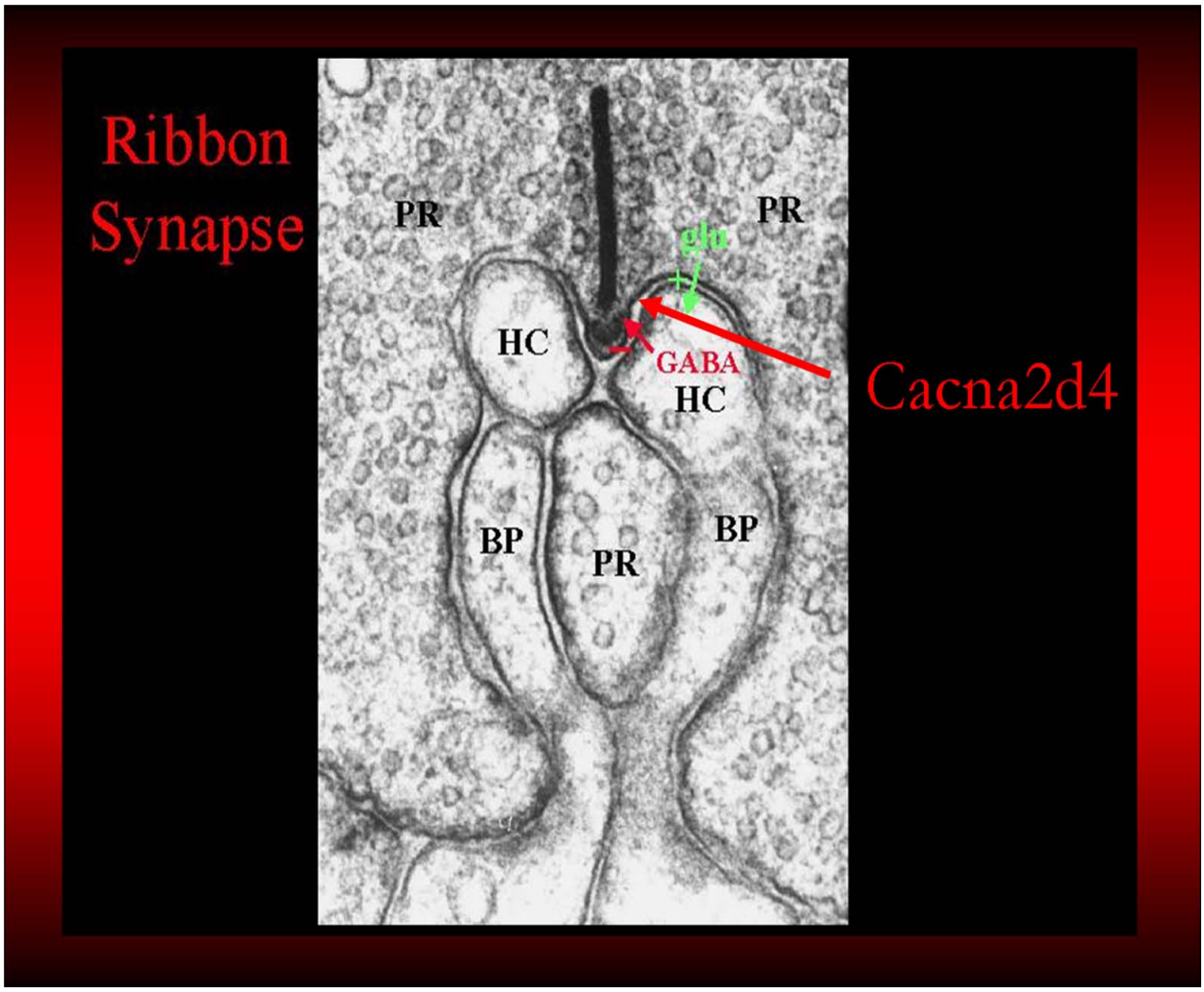

General Discussion

4. General Discussion

"The elementary issue of the present study was to identify a novel genetic defect underlying disturbed retinal signal transmission in a substrain of C57BL/10 mice. Upon genome-wide linkage analysis and positional candidate gene approach, a homozygous truncating mutation was detected in the Cacna2d4 gene, the fourth auxiliary α2δ subunit of voltage-dependent calcium channel complexes. The induced channelopathy affects the retinal synaptic apparatus at the functional and morphological level in mutant animals and involves an early onset retinal degeneration. Upon mutational analyses in the human orthologous CACNA2D4 gene, a deleterious homozygous transversion was identified in patients diagnosed with a mild form of cone dystrophy, a retinal disease associated with perturbed retinal signal transmission."

4.1. Hypothetical Origin of the Cacna2d4 Mutation in C57BL10 Mice

Without exterior physical and chemical factors, natural mutations underlie spontaneous events at random genomic locations and reflect mostly metabolic DNA base modifications or errors in the DNA replication process. They occur with a frequency of 10^{-7} to 10^{-9} per nucleotide and cell cycle and usually include point mutations, classified into substitutions, insertions and deletions[1]. Single base-pair substitutions constitute the most frequent genetic defects and estimate 73.8% of point mutations[2]. Some DNA motifs, however, may represent mutational hotspot for the remainder classes of genetic alterations. Repetitive DNA sequences, for instance, mutate at particularly high frequencies and are prone to insertion and deletion[3,4]. In mutational studies of yeast and bacteria, mononucleotide repeats were demonstrated to be the most unstable of repetitive sequences[5-7]. Thereby, poly-G mononucleotide segments emerged particularly mutable[5]. In *Escherichia coli*, a run of 8 Gs revealed mutation rates 12 to 36 times higher than a corresponding A_8 stretch[8]. Monorepeats were also reported to be most unstable in human and mouse cell lines[5]. Of note, a representative G_{17} sequence was 10 to 25 fold more variable that a corresponding A_{17} run[9,10].

The spontaneous mutation detected in the *Cacna2d4* gene of affected C57BL/10 mice evolved in a short stretch of six cytosine nucleotides, representing a repetitive sequence of the mononucleotide-type. This cytosine monorepeat (or guanine monorepeat on the reverse strand) might be subject to a mutational mechanism which introduced the respective genetic defect, an insertion of one cytosine molecule. Thus, although of a spontaneous origin, it is not astonishing that a sequence element of the poly-C nature mutated in the mouse *Cacna2d4*.

The major mechanism behind the high mutation rate of repeat containing sequences underlies polymerase slippage upon complementary strand mispairing[11] (Fig. 1). During replication of a repetitive region, the template and the newly synthesized DNA strand may temporally dissociate and incorrectly re-anneal either in a displaced loop on the template or the nascent strand. If this misalignment escapes proper repair, renewed replication of the repeat sequence, retained in a misaligned state, results in an insertion or deletion[12]. The loop-formed mutational intermediate is suggested to be more stable in G and C tracks than among poly-A and -T runs due to their stronger nucleotide-nucleotide interaction[8]. As the slippage occurs most frequently to an immediately adjacent repeat unit, the vast majority of mutations in repetitive sequences constitute additions or losses of one repeat unit[13-16].

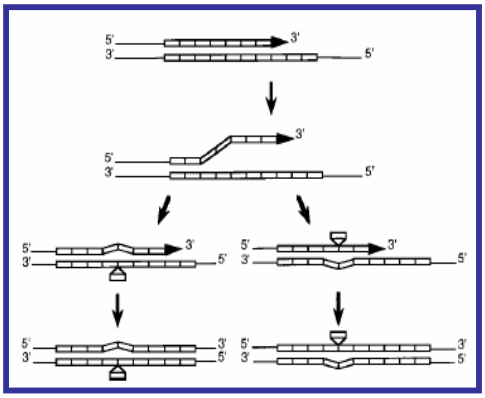

Figure 1. DNA polymerase slippage model. During the replication of a repetitive region, the template DNA strand and the newly synthesized strand may temporally dissociate and reassociate incorrectly either in a displaced loop on the template strand (**left**) or in a displaced loop on the nascent strand (**right**). If the resulting mismatch escapes proper repair, the sequence on the currently synthesized strand loses (**left**) or gains (**right**) one repeat unit upon a new replication cycle[15,16].

4.2. Mutational Hotspots in Human CACNA2D4

In light of these findings, DNA polymerase slippage mechanism may raise mutations in repetitive regions of the human *CACNA2D4* gene. Considering *CACNA2D4* exonic segments, numerous C_4 and G_4 monorepeats can be observed (Fig. 2). Exon 30 contains two G_5 runs and may represent a hotspot side for slippage-mediated genetic defects. This short repeat length (n>3) is relevant for the polymerase slippage mechanism, particularly for insertions, that may introduce critical frameshift errors in the protein coding sequences[14].

The prediction of *CACNA2D4* hotspot positions for single nucleotide substitutions emerges more difficult than for DNA length mutations, as the relevant mutable motifs are largely unknown. In addition, the mutability of a specified hotspot sequence also depends on high-level structural features of the genomic DNA and the surrounding chromatin. Nonetheless, CpG dinucleotides exemplify hotspot motifs well-known to transmute to TpG at frequencies that are ten times higher than these of mutations in other sequence contexts[17-21]. In *CACNA2D4*, numerous CpG dinucleotides can be observed (Fig. 2). The mechanism presumably underlies methylation-

mediated deamination of the 5`methylcytosine which occurs predominantly in CpG dinucleotides[17] (Fig. 3). Approximately, the half of generated TGA premature termination codons, frequently associated with severe genetic defects, appear due to the CpG to TpG transition[20]. Accordingly, the amino acid arginine encoded by the codon CGA constitutes a substantial hotspot site for a substitution to TGA. In the *CACNA2D4* open reading frame, eight arginine coding CGA triplets are present (Fig. 2).

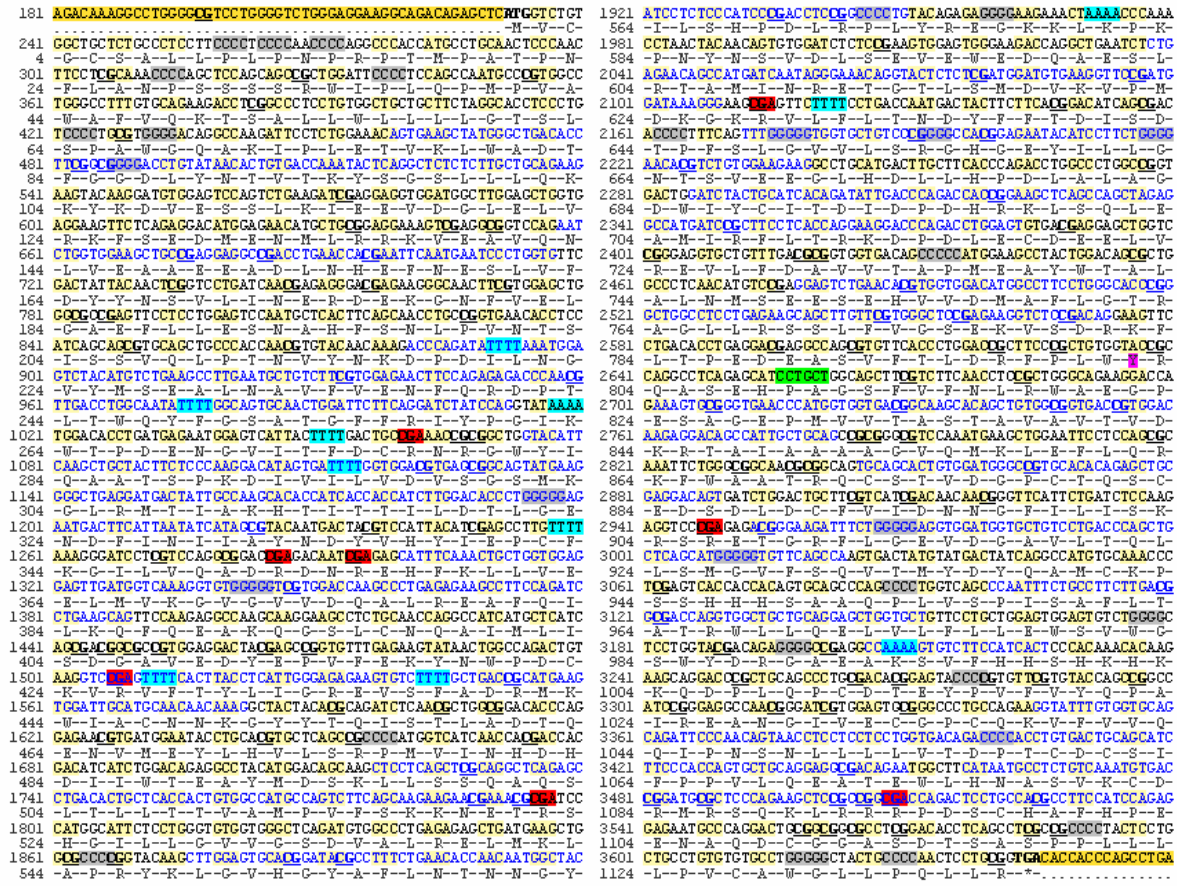

Figure 2. *CACNA2D4* open reading frame. The 3414-bp open reading frame (ORF, 232-3645 bp) of human *CACNA2D4* represents coding sequences of 38 exons (*black* and *blue* alternating characters). The start and termination triplets are marked in *bold*. The 5`- and 3`- UTRs are partially illustrated (*yellow*). Repetitive sequence structures (*n>3*) are emphasized in boxes (A_n and T_n runs in *light blue*, C_n and G_n tracks in *grey*). Stretches of G_5/C_5 occur in exons 8, 10, 20, 23, 30, and 38. Extended mononucleotides as well as repeat sequences of longer unit size (di-, trinucleotides units) are absent from *CACNA2D4* ORF. The repetitive motif defective in mouse *Cacna2d4* is also lacking (*CCTGCT versus CCCCCC*, exon 25, *green*). In contrast, numerous CpG dinucleotides are present in the *CACNA2D4* ORF and constitute potential targets of CpG to TpG transition (*bold, underlined*). Eight arginine residues encoded by the CGA triplet indicate putative mutational hotspot for the introduction of premature termination signals upon a CpG to TpG substitution (exons 8, 12, 14, 19, 31, 38, *red*). GpC dinucleotides corresponding to CpG mutational hotspot on the reverse strand are not marked. (Tyrosine amino acid residue mutated in the patients of mild cone dystrophy in *pink.*) (ENST00000280663, www.ensembl.org).

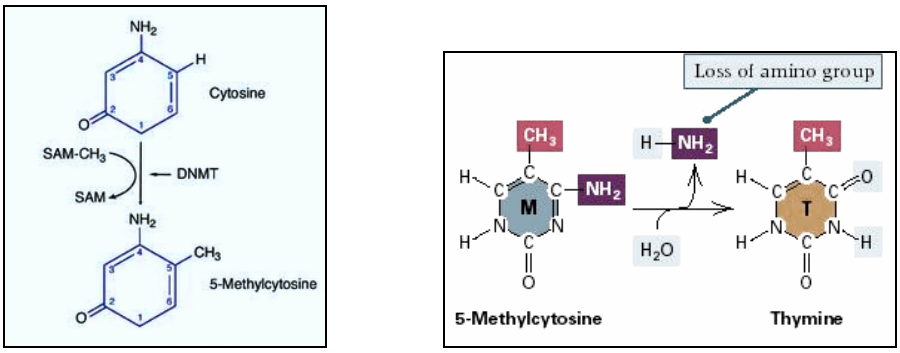

Figure 3. Mechanism of CpG mutability. The mechanism imparts methylation-mediated deamination of the 5`methylcytosine. The 5`methylcytosine intermediate (**left**) undergoes spontaneous non-enzymatic deamination to form a thymidine nucleotide (**right**). Of note, sperm DNA emerges heavily methylated. Most CpG to TpG mutations are therefore found in male germ line cells[21] (www.cbs.dtu.dk, www.medi-life.com).

In view of CpG dinucleotide mutability, it is tempting to speculate that the potentially deleterious substitution, p.R818C, detected in an iCSNB family, arose due to the mechanism (Chapter 7.1.). The respective arginine residue, encoded by a CGC codon, includes a potential CpG hotspot position that might be subject to methylation-mediated deamination, resulting in TGC cytosine coding triplet (Fig. 2).

4.3. Pathologies of CACNA2D4 Mutations

The CACNA2D4 auxiliary subunit of voltage-gated calcium channels constitutes a largely uncharacterized protein. Upon heterologous cell line expression, it was shown to stimulate chimeric α1C/β3 channel complexes and to augment the respective calcium currents[22]. Processes underlying the regulatory stimulation remain of unknown nature. Nonetheless, despite the absence of well-founded physiological characterization, scientific implications, attained from functional studies of homologous α2δ subunits, give rise to the potential mechanisms of CACNA2D4 action and aid in assessing pathological effects of distinct *CACNA2D4* allelic defects.

4.3.1. Pathological Effects on *CACNA2D4* Expression and Function

Principally, each mutation may remarkably tune *CACNA2D4* transcript expression and, in consequence, alter well-defined intracellular levels of CACNA2D4 proteins. Genetic defects underlying compromised transcription, processing, maturation and mRNA stability may affect CACNA2D4 protein amounts and predispose to disease[2]. Protein truncating mutations frequently activate transcript degradation upon nonsense mediated decay[23]. This process can remarkably contribute to CACNA2D4 loss (Fig. 4). Indeed, although the physiological role of NMD underlies a protective elimination of anomalous transcripts, in some instances, it may inhibit the

translation of partially or fully functional proteins. A truncating mutation in last exons of *CACNA2D4* (exons 37, 37L and 38) may play a minor role, as the aberrant transcripts can still encode functional proteins (Fig. 4). In contrast, activated NMD may induce intense transcript degradation and prevent CACNA2D4 synthesis[24]. Transcripts comprising a premature termination codon in the last exon were shown to undergo NMD[25]. Of note, NMD constitutes a natural regulatory mechanism that controls amounts and proportions of native splice variants, including premature termination signals[26,27]. Hence, an extensive degradation of a mutant *CACNA2D4* isoform may result in altered proportions of alternative CACNA2D4 proteins (Fig. 4).

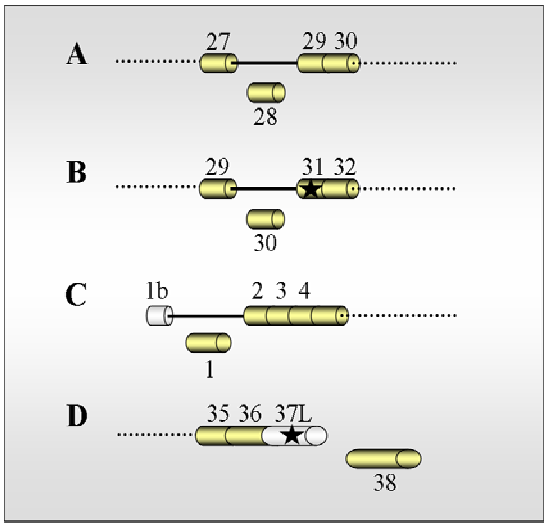

Figure 4. Splice variants of *CACNA2D4*. Four splice variants of human *CACNA2D4* were found by Qin et al. and further three are observed from EST databases[22]. (**A**) *CACNA2D4* transcript variant with an in frame exclusion of exon **28,** resulting in a deletion of 15 amino acid residues. (**B**) *CACNA2D4* transcript variant with a removal of exon **30**. The exclusion of exon 30 leads to a frameshift resulting in a premature termination codon in exon **31** (indicated by an *asterisk*). This alternative *CACNA2D4* variant encodes a shorter α2 subunit of 855 instead of 992 amino acid residues, which is presumably posttranslationally linked to a δ peptide from a longer *CACNA2D4* variant. In cell line experiments, α2 and δ peptides expressed from separate expression vectors were demonstrated to associate with each other and to form a functional α2δ subunit[28]. (**C**) Putative exon **1b** comprises an alternative in-frame start codon. (**D**) Exon **37L** continuously extends from the constitutive exon 37 introducing an alternative termination codon[28]. Noteworthy, the combination of the four alternative splicing events would account for >18 splice variants with potentially distinct function.

At the protein level, mutations in CACNA2D4 may promote enhanced degradation. The α2δ proteins undergo extensive glycosylation and structural remodeling upon disulfide bridge linking of cysteine residues. Approximately 15 conserved N-glycosylation sites and ~14 cysteine residues appear in all α2δ subunits. The respective modifications predominantly take place in the endoplasmatic reticulum (ER) and the Goldi system[29]. Mutation-mediated glycosylation

deficiency or folding abnormalities may affect CACNA2D4 maturation in the ER/Golgi and induce its removal[30]. Polypeptide chains of perturbed processing are directed to degradation upon prolonged retention in the ER or Goldi[31,32].

At the functional level, genetic defects in *CACNA2D4* can lead to "loss" or "gain" of function (Fig. 5). An upregulation of α2δ expression due to mutations in the promoter region or regulatory elements may underlie gain of function. The α2δ subunits facilitate trafficking of the α1 channel proteins to the cell membranes and increase calcium channel densities at the cell surfaces. This augmentation remarkably raises calcium currents in the range of 2 to 10 fold[33,34]. A well-defined number of intracellular α2δ proteins constitute thereby a regulatory mechanism, tuning the rate of α1 membrane integration[35]. An elevation of intracellular α2δ amounts due to abnormal rate of expression can enhance calcium currents, inducing intracellular calcium toxicity and excitability of neuronal cells. An upregulation of the CACNA2D1 (α2δ-1) subunit was found in the tactile allodynia. This neuronal disease manifests a persisting neuropathic pain in human patients, likely caused by augmented presynaptic activity[36].

Mutations inducing α2δ misrouting exemplify loss of function. The α2δ subunit constitutes an extracellular transmembrane protein with a C-terminal anchor that is responsible for the cell surface attachment[37]. A deleterious mutation in the *Cacna2d2* gene (α2δ-2) of the spontaneous mouse mutant "ducky" resulted in ~3-fold attenuated calcium currents of the Purkinje cells due to impeded α2δ-2 membrane anchoring. In addition, shifting in the voltage-dependent activation of calcium channel complexes to more negative potentials (Δ ~-5 mV) was abolished[37,38]. This defect was associated with severe epilepsy and episodic ataxia, accompanied by lethality of affected animals by the postnatal day 35[37].

Loss of function underlies also the pathology of site-directed mutagenesis of CACNA2D1 N-glycosylation sites[30]. Lack of glycosylation at the positions N136 and N184 in this α2δ subunit reduced calcium currents of heterologously expressed α1C/ß2 channel complexes by 79%. This effect was associated with inefficient α1C membrane trafficking due to a delayed exit of α2δ-1 mutant proteins from the ER and a perturbed cytosolic interaction with α1C[30,39,40]. Of note, in heterologous cell line expression systems, absence of CACNA2D4 was shown to reduce α1C/β3 calcium currents by ~67%[22].

The mechanisms of α2δ function in calcium channel assembly, membrane targeting and auxiliary modulation underlie conformational changes of the α1 proteins upon α2δ association[29]. Thereby, α2δ probably stabilize α1 proteins at distinct conformational conditions by either strengthening

the α1 pore at the closed or the release state[41-43]. Alterations of α1 conformation upon interaction with α2δ are observed in dihydropyridine* (DHP) binding studies. The α2δ subunits increase the number of DHP interaction sites at α1 surfaces, a phenomenon that must involve modifications of the α1 conformational state[41].

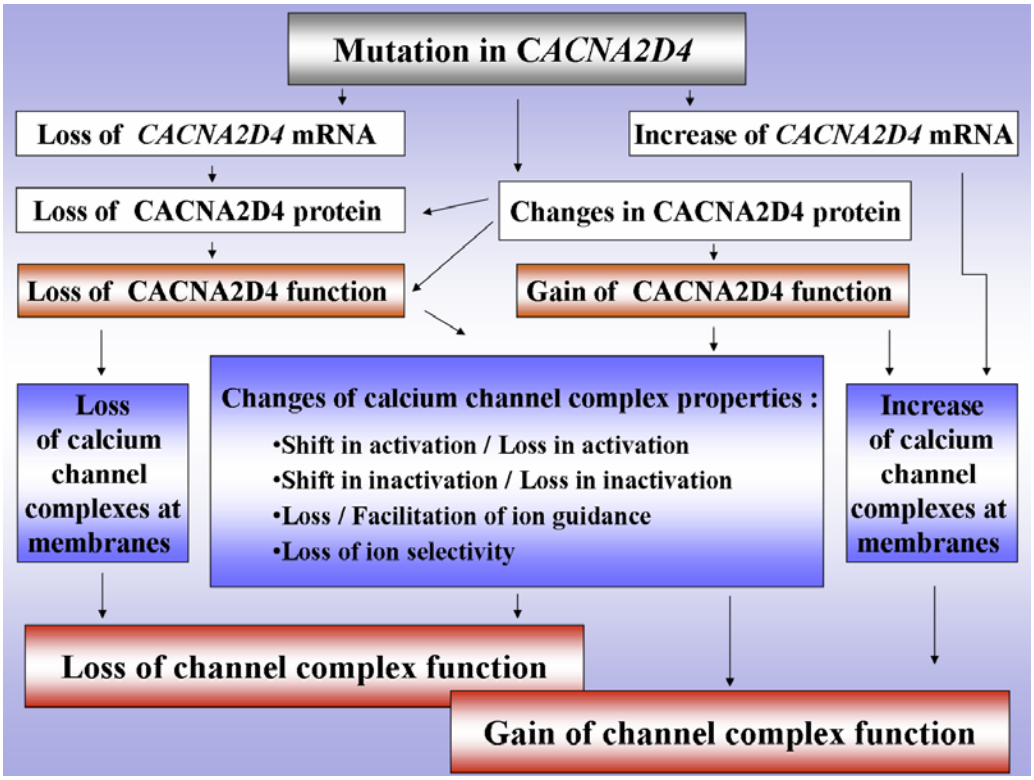

Figure 5. Pathogenic effects of mutations on *CACNA2D4* expression and function (summary). In this graph, the term "**loss**" is used to describe both a significant reduction and a complete loss of a considered target. Mutations in the *CACNA2D4* gene may activate pathological mechanisms that can act in a cascade or in parallel. Various genetic defects (*grey box*) may induce loss or gain of CACNA2D4 function (*brown box*). Decreased abundance of *CACNA2D4* mRNA may thereby be the primary mutational effect, remarkably reducing intracellular CACNA2D4 protein amounts. Of note, the number of proteins translated from an mRNA molecule is determined to ~1200[45]. Loss of CACNA2D4 function may decrease calcium channel densities at cell surfaces as well as reduce channel complex stimulation (*blue*). Voltage- and calcium-dependent activation/inactivation, ion selectivity, ion gating and activation/inactivation kinetics may be targets of α2δ stimulation. Alluding to the most observed functional features of homologous α2δ subunits, CACNA2D4 auxiliary stimulation presumably underlies a hyperpolarisation of the voltage dependence (Δ up to 10 mV), an acceleration of activation/inactivation kinetics (Δ in the range of 20 to 150 ms) and a facilitation of calcium gating in the α1 pores[35,41,46,47]. Gain of CACNA2D4 function may underlie an over-stimulated calcium channel activity or enhanced CACNA2D4 expression that can result in increased channel densities at membranes (*blue*). The overall impact of α2δ regulatory effects results in the modification of the calcium current amplitude. Thus, alterations in CACNA2D4 may trigger reduced (loss) or enhanced (gain) calcium currents mediated by calcium channel complexes at physiological conditions (*red*).

*DHP belongs to a family of chemical substances that constitutes specific pharmacological agents, affecting voltage-gated channel function[44].

Regarding alterations in the α1 configuration, lost or abnormal CACNA2D4 interaction may affect the release of binding motifs at the α1 surfaces and also perturb auxiliary stimulation by other α1 regulatory proteins[48-52]. **CaBPs** represent a family of calmodulin-like neuronal calcium-binding proteins that modulate voltage-dependent calcium channels[42]. CaPB2, CaPB4 and CaPB5 are retina-specific calcium binding proteins. The fourth member of this family, CaPB4, was shown to directly interact with the retina-specific α1F subunit. In cell line experiments, CaPB4 stimulation was demonstrated to shift maximal α1F channel activity to more hyperpolarised potentials (from -5 mV to -15 mV). Alluding to these results, the absence of CaPB4 at physiological conditions of photoreceptor synapses is assumed to result in decreased α1F calcium currents by roughly fivefold[42].

Calmodulin, a ubiquitously expressed calcium sensor, accelerates voltage-dependent activation/inactivation kinetics of calcium channel complexes[53]. Besides, it controls the calcium-dependent activation/inactivation properties[54-56]. Calcium-dependent inactivation (versus voltage-depended inactivation) reflects the process of channel closure during a maintained calcium flow, whereas calcium-dependent activation induced by basal calcium entrance leads to enhanced channel opening[57-59]. The dual function of calmodulin regulation is assumed to arise from different calmodulin-binding sites at the α1 subunit surface[60,61]. Notably, in the process of calcium-dependent facilitation, the interaction of calmodulin with calcium channel complexes was shown to elevate calcium current up to 200%[53,62].

G-coupled proteins suppress the activity of voltage-gated calcium channels and prolong the latency for the first opening[63]. Several binding sites for the interaction with G-coupled protein are supposed on the calcium channel α1 proteins[64,65]. Similarly, **syntaxin** interacts with α1 calcium channel subunits and depresses calcium currents by stabilization of the channel inactivation state[66-72].

Voltage-gated α1 channel subunits are additionally regulated by protein phosphorylation through second messenger-activated kinase pathways[72]. There is a dynamic balance between phosphorylation (activation) and dephosphorylation (inactivation) by a dual action of **kinases** and **phosphatases**. Thereby, both phosphorylation-dephosphorylation of the α_1 subunits can greatly increase/decrease the number of active calcium channels at membranes[73].

Worth mentioning, the α2δ subunits themselves are thought to participate in docking of distinct regulatory proteins. The α2δ-1 and -2 subunits bind with particularly high affinities the antineuropathic pain drug gabapentin[74]. This implies that α2δ subunits may comprise contact sites

for interaction with secondary regulatory proteins. In the *Cacna2d2*-mouse model for epilepsy and episodic ataxia, it was shown that the Purkinje cells discontinue maturation and synaptogenesis from the postnatal day 21 to 24 in the absence of functional $\alpha_2\delta$-2 subunit[37,38]. Blockade of the neurite extension was hypothesized to appear, in addition to altered calcium currents, due to the loss of $\alpha_2\delta$-2 interaction with adhesion proteins from the extracellular matrix and thus due to perturbed synaptic plasticity.

4.3.2. Pathological Impact of *CACNA2D4* Mutations on the Retinal Calcium Channel Complexes

The most apparent phenotypic features of *CACNA2D4* mutations in human patients and C57BL10 mice manifest upon perturbed electrophysiology of the retinal tissue and reflect defective synaptic signal transmission. This implies the critical role of CACNA2D4 in modulation of synaptic voltage-gated L-type calcium channels, involved in retinal neurotransmitters release.

Under darkness conditions, retinal synaptic L-type calcium channels mediate tonic release of the neurotransmitter glutamate from photoreceptor terminals to the secondary neurons[75,76]. The metabotropic glutamate receptors of postsynaptic membranes continuously bind glutamate and instigate permanent closure of adjacent postsynaptic channels, rendering the inner retinal neurons silent[77]. During the ongoing process of glutamate release, the photoreceptor synaptic membrane potentials rest at ~-36 to ~-40 mV[78] (Fig. 6). Light evokes graded hyperpolarisation to ~-70 mV, suppressing synaptic L–type calcium channel conductance[79,80]. Regarding the physiology of L-type calcium channels, they activate between ~-55 mV and ~+10 mV (Fig. 6). Their maximal activity emerges at ~-22 mV, clearly above -36 mV of the maximal physiological depolarization potentials. Since light absorption further hyperpolarize synaptic membranes to more negative voltages, the physiological operating range of photoreceptor synapses appears at the “foot” of the L–type channel activation[81-84] (Fig. 6). Correspondingly, the current mediated by L-type calcium channels at darkness amounts to ~4.6% at ~-40 mV of the maximal possible current and reduces to ~0.04% at ~-55 mV during illumination. Noteworthy, the decline during transition from darkness to light corresponds to a 100-fold current reduction (from ~4.6% to ~0.04%) and reflects a wide operating range of retinal L-type calcium channels under physiological conditions. In light of these insights, shifting the voltage-dependent activation/inactivation of photoreceptor L–type calcium channels to more positive potentials can reduce the voltage range at which calcium channel operate (Fig. 6). This reduction may result in earlier deactivation and thus

deficiency of neurotransmitter release at hyperpolarisation potentials with considerable effects on the daylight vision. At darkness, lower calcium current amplitudes may diminish rates of glutamate release. Subsequently, insufficient saturation of postsynaptic neurons may induce profound excitability of the inner retina[85]. In addition, an accumulation of unreleased glutamate can trigger metabolic toxicity in photoreceptors. A shift in the activation/inactivation curve to

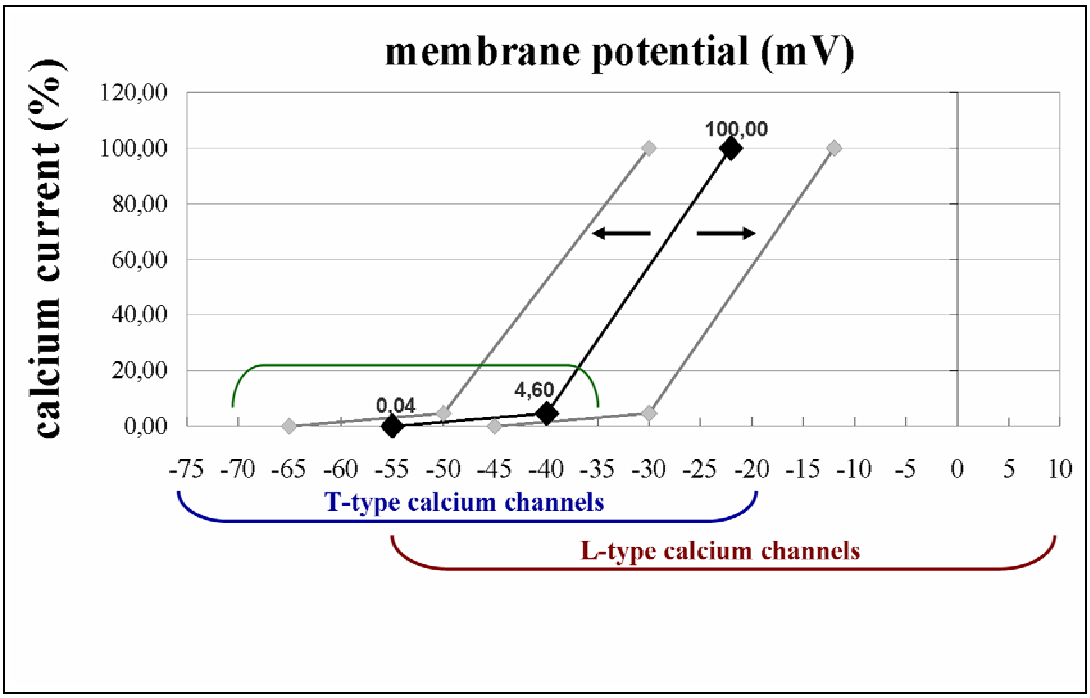

Figure 6. Pathological effects of *CACNA2D4* mutations on calcium channel function in retinal synapses. Photoreceptors operate between ~-36 mV of the resting potential at darkness and ~-70 mV of the hyperpolarisation potentials after light exposure (*green bracket*). The membrane potentials of adjacent bipolar cells are reported to range from ~-20 mV to ~-70 mV[87]. In this interval of physiological membrane potentials, L-type calcium channels are on the foot of their activation curve (*in part, black curve*). Their activity, indeed, ranges from ~-55 mV to ~+10 mV with the maximum calcium current (100%) at ~-22 mV (*brown bracket*). For comparison, the T-type calcium channels constitute more hyperpolarized kinetics and remain activated in the range of ~-75 to ~-20 mV (*blue bracket*). A shift (*arrow*) in activation curve by 10 mV in the depolarizing direction (*right grey curve*) illustrates the reduction of the L-type calcium channel operating range in the constitutive interval of retinal membrane potentials (from ~-45 mV to ~-35 mV instead of ~-55 mV to~-35 mV). Thus, light-induced hyperpolarizations of membrane potentials higher than ~-45 mV abolish calcium channel function (0% of calcium current), whereas at darkness potentials of ~-40 mV, lower activities of calcium channels probably results in attenuated calcium currents (~0.09% instead of ~4,6%). In contrast, a shift in the hyperpolarizing direction (*left grey curve*) probably induces increased activity of calcium channels and augments calcium currents at the entire operating range of retinal membrane potentials[85,88].

more negative potentials presumably leads to increased calcium influx at physiological membrane potentials, inducing photoreceptor synaptic excitability and impeding secondary responses during light exposure (Fig. 6). Native photoreceptor L-type calcium channels also show fast activation and low calcium- and voltage-dependent inactivation[86]. These physiological features emerge imperative in retinal signal transmission, as the channels should rapidly reactivate after light-induced channel closure and prevent deactivation during sustained depolarizations at darkness. CACNA2D4 may constitute the auxiliary subunit responsible for the acceleration of activation/inactivation kinetics of the retinal L-type calcium channels and defects affecting these biophysical properties of CACNA2D4 may underlie perturbed synaptic transmission.

The exact pathogenic effects of the identified *CACNA2D4* mutations remain to be elucidated. The truncating mutations in human and mice presumably result in reduced calcium currents at physiological potentials of photoreceptor synaptic membranes. Other mutations in the CACNA2D4 subunit may "mimic" alterations of the L-type calcium channel function in analogy to genetic defects, underlying α1F-associated channelopathies. Regarding models of perturbed L-type calcium channel function in the retinal synaptic apparatus, a substitution of a glycine amino acid to an asparagine acid residue in the α1F subunit was shown to remove calcium-dependent inactivation and to shift voltage-dependent activation to more negative potentials (Δ up to 11 mV)[85]. Estimation of the resultant dark current revealed an elevation from 4.6% to 83% of the maximal calcium influx. The facilitation of calcium gating was assumed to result from the introduction of a negative charge in the respective amino acid residue of the α1F pore forming domain*. This genetic defect was associated with the incomplete type of congenital stationary night blindness, characterized by disturbed retinal signal transmission[85] (Chapter 1). An isoleucine to threonine substitution in the α1F subunit was found to raise a remarkable leftward shift of ~-34 mV in the voltage dependent activation and to significantly slow channel inactivation kinetics[89]. These effects were, most likely, associated with profoundly increased calcium currents at physiological membrane potentials. The mutation was detected in patients with particularly severe symptoms of incomplete congenital stationary night blindness (iCSNB). Of note, heterozygous carriers of this α1F allelic variant manifested mild signs of iCSNB, albeit the inheritance of this disease usually underlies a recessive mode[89].

*(*versus positive charge of calcium ions, Ca^{2+}*)

4.3.3. Secondary Pathological Effects on the Retina due to *CACNA2D4* Mutations

Calcium toxicity

In the resting state, intracellular free calcium is maintained at low levels of 100 nM. Upon depolarization of a synaptic terminal, these levels increase to concentrations of 8.5-10 µM. In most neurons, including retinal bipolar cells, calcium must exceed 10 µM to evoke neurotransmitter release[90-92]. Elevated free calcium amounts undergo subsequent reduction through a complex interplay of calcium efflux, calcium buffering and internal calcium storage that prevent calcium overload after signal transmission[93]. In contrast, neurotransmitter release at the photoreceptor synapses is triggered by submicromolar calcium levels. Use of a high affinity release machinery minimizes the need for large calcium loads and reduces the potential of calcium-dependent toxicity[90,91]. Nonetheless, the function of buffering and extrusion mechanisms within photoreceptor terminals must be particularly powerful. The steady calcium influx at darkness, although low, would raise calcium concentrations to 500 µM in the absence of calcium buffering, transport and extrusion. In photoreceptors, the arciform density overlying calcium channels at the synaptic ridge presumably acts as a local buffer (Chapter 1). An important structural component of the photoreceptor terminals constitutes also the smooth endoplasmic reticulum (SER). SER forms numerous cisterns which serve as internal calcium stores. In addition, calmodulin molecules and mitochondria operate as intracellular calcium buffers[90,91]. Excessive synaptic activity, however, can overwhelm these regulatory systems and induce excitotoxic damage in retinal neurons. Excessive calcium load may involve changes in calcium-dependent gene transcription and disturb catalysis of calcium-sensitive enzymes[94-96]. Abnormal calcium levels are also known to enhance the activation of calcium-dependent lipases, phosphatases, and endonucleases that, under normal calcium concentration, remain dormant or operate at very low levels[94,97,98]. Thereby, excessive calcium concentrations particularly instigate a dysregulation of calcium-dependent metabolic activity of mitochondria[97]. Upon calcium overload, increased ATP production results in advanced activation of various ATP-dependent cellular processes. This raises metabolic toxicity and the formation of oxidative free radicals that affect mitochondrial membrane integrity and elicit damage of these organelles[98]. At higher calcium loads, mitochondria undergo devastating permeability transition that allows solutes pass

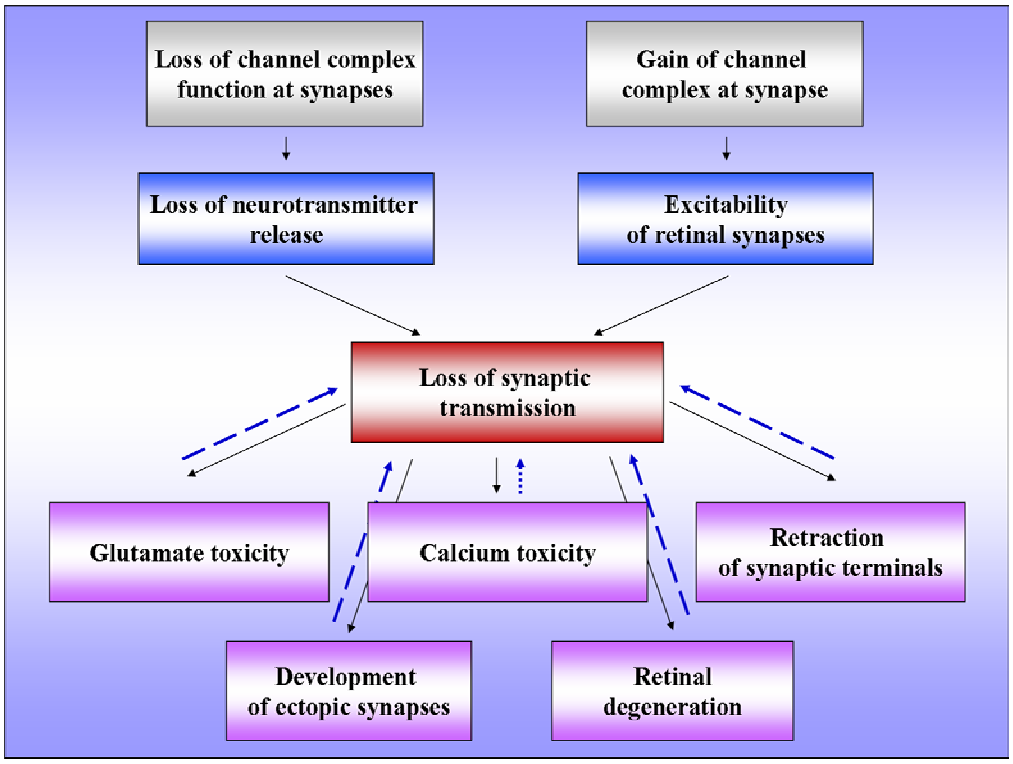

Figure 7. Effects of perturbed calcium channel function on the retinal system (summary). Mutations in *CACNA2D4* can result in loss or gain of synaptic L-type calcium channel function (*grey*). The term "loss" corresponds to a significant reduction and a complete loss of a considered target. Whereas loss of channel complex function may abolish neurotransmitter release, gain of function probably induces excitability of photoreceptor synapses (*blue*). Both mechanisms perturb normal synaptic transmission (*red*) and likely activate secondary pathological mechanisms. These can include calcium and glutamate toxicity as well as formation of ectopic synapses and retinal degeneration (synaptic and somatic) (*violet*). These processes, in turn, may retrogradely contribute to progression of the disease symptoms, like to the signal transduction deficiency (*blue arrows*).

though the usually impermeable mitochondrial membranes. This results in osmotic swelling and thus rupture of the organelles[99]. Of note, non-synaptic mitochondria are able to accumulate significantly more calcium than the synaptic mitochondria. The limited ability of the synaptic organelles to buffer calcium could result from their primary function in ATP production to support the energy demand of synaptic terminals[100-102]. In addition, their relative isolation in the synaptic space contributes to their increased damage[100-102]. Synaptic mitochondria, indeed, appear punctually and separated in comparison to mitochondrial clusters found in the soma. Finely, synaptic mitochondria are synthesized in cell bodies of neurons and transported afterwards to the axons or dendrites. They are thus older arriving at their destinations and exhibit already cumulative damage from oxidative stress in contrast to their non-synaptic counterparts[103].

Mitochondrial structural abnormalities and functional deficits are as well associated with the release of pro-apoptotic factors from these organelles that may be secondary precursors to neuronal cell death[97,104-106]. Deficiency in mitochondrial function was shown to be involved in various forms of retinal degeneration[105,106].

Calcium is also involved in the organization of neurofilaments, the main component of the neuronal cytoskeleton. The filaments are composed of filamentous actin proteins (F-actins) that participate in the regulation of axonal motility, synaptic plasticity, vesicle transport and synaptic function[107-110]. Elevation of intracellular calcium during synaptic activity initiates a cascade of reversible actin filament remodeling, suppressing vesicle transport and the translocation of proteins essential for a continuous renewal of synaptic membranes. This process probably serves as a feedback mechanism to attenuate synaptic activity and thus calcium accumulation, induced by prolonged membrane depolarisations[110]. Increased rate of actin rearrangement upon excessive calcium entry, however, may affect synaptic structure to an irreversible extend and contribute to synapse loss[109,110]. In a similar manner, excessive calcium may perturb structural complexity and integrity of the arciform density and the ribbon bodies of retinal ribbon-type synapses[111]. Resulting mislocalisation can hasten ribbon degradation at active zones.

Glutamate toxicity

A strong relationship exists between excessive calcium influx and glutamate-mediated neuronal excitotoxicity[112,113]. One of activated pathological mechanisms underlies changes in intracellular calcium and sodium concentrations of the post-photoreceptoral neurons. Indeed, enhanced activity of synaptic L-type calcium channels triggers excessive release of glutamate. Whereas cells of the retinal ON-signaling pathways remain permanently hyperpolarized, neurons belonging to the OFF-pathways experience over-stimulation by glutamate excess. Upon activation, their postsynaptic glutamate receptors permanently open associated ion channels and allow continuous influx of natrium, potassium and calcium through postsynaptic membranes. Long-lasting natrium influx induces irreversible swelling of cells[113]. Calcium neurotoxicity follows the activation of distinct signaling cascades downstream of the dendritic entry. Regarding the contribution of actin filaments to the synaptic function, the ultimate localization of glutamatergic receptors is partially governed by actin-binding proteins[114,115]. Glutamate receptors, anchored to the actin cytoskeleton, are released from the actin filaments upon calcium entry and leave the synaptic sites. Their extrasynaptic localization probably serves as regulatory mechanism

that abolishes synaptic function upon prolonged activation[116,117]. Postsynaptic excessive calcium, however, may induce severe disorganization of the F-actin network and a profound misdistribution of glutamate receptor clusters, leading to irreversible structural and functional changes of postsynaptic dendrites[118-123]. Of note, mislocated glutamate receptors remain their function and can trigger ion influx at ectopic cellular locations.

Glutamate excess in postsynaptic compartments may retrogradely affect photoreceptors and their synaptic terminals. An accumulation of glutamate in photoreceptors results in chronic changes in the photoreceptor outer and inner segments[124]. Toxic alterations in neurochemical architecture of amino acid metabolism have been demonstrated due to elevated glutamate concentrations[125-127]. Particularly, toxic increase in aspartate and glutamine levels, amino acids constituting either precursors or metabolites of glutamate, have been observed[128-130]. In addition, glutamate was reported to elicit currents generated by intracellular glutamate receptor-coupled chloride channels and to activate metabotropic receptors, dismodulating intracellular calcium concentrations[131]. Of note, loss of synaptic activity in photoreceptors may also underlie intra-photoreceptoral glutamate accumulation and trigger glutamate-coupled calcium toxicity in retinal ON signaling pathways.

Retinal degeneration

Dysfunction of retinal synapses during lifetime may lead to their retraction and involve retinal degeneration. In the CSPα-deficient mice, photoreceptor synapses undergo massive and rapid degeneration after light onset, including profound photoreceptor loss and blindness at two weeks of age[132]. The CSPα protein likely functions as a co-chaperone in folding of so far unknown substrates. Proteins of the synaptic vesicle fusion machinery like SNAP-25 are assumed to be the prime candidates to CSPα-mediated folding, as those proteins undergo degradation in CSPα-mutant animals before degeneration onset[132].

Human patients with mutations in the *RIM1* gene suffer from an autosomal dominant cone-rod dystrophy that initially manifests upon perturbed signal transmission at photoreceptor synapses[133] (Chapter 1.). Histopathological studies display most prominent morphological alterations in the cone synaptic terminals[133]. The primary disease pathology underlies perturbed synaptic vesicle docking and an altered interaction of the RIM1 protein with synaptic L-type calcium channels, resulting in disrupted glutamate release[134]. Similarly, the transgenic mouse model for the human *HRG4*-mediated cone-rod dystrophy shows delayed-onset retinal degeneration that initiates with photoreceptor synaptic retraction[135] (Chapter 1). Immunohistological examinations of affected

retinas reveal that the secondary pathogenic mechanisms involve the release of cytochrome *c* and an activation of caspase 3 from synaptic mitochondria. Once activated, caspase 3 probably stimulates other caspases in a protease cascade and, with time, triggers apoptotic death of photoreceptor cells, evident upon 20 months of age[135]. The cone-rod dysfunction of *Cacna2d4*-mutant mice, progressing with structural damage of the photoreceptor synaptic terminals, might underlie the release of pro-apoptotic factors from synaptic mitochondria, responsible for the degenerative processes in mutant mice and slow-course photoreceptor loss.

The *Cabp4*-mutant mouse constitutes an animal model for human iCSNB or a cone dystrophy-like disease and exhibits profound photoreceptor degeneration[136] (Chapter 1). In affected animals, 40% of the photoreceptor synapses retract initially at the age of two months[137]. In this early disease course, collapse of the photoreceptor synaptic layer parallels the ablation of photoreceptor outer segments. Upon electron microscopy, 15% reduction in outer segment length and lower disk density are observed in two-month-old mutant mice[42,137]. Synaptic dysfunction-associated stress presumably decreases the photoreceptor ability to produce outer segments and the rate of synthesis lags RPE phagocytosis.

Rods and cones with shortened outer segments are at risk[138,139]. A deconstruction of the outer segments includes redistribution of the opsin proteins to the inner segments. Their anomalous levels in inner segments affect post-goldi transport of other proteins and induce toxic accumulation in cytoplasmic compartments[139]. As consequence, photoreceptors may reduce opsin expression, enhancing illumination-induced stress or phototoxicity. A decrease in rhodopsin expression was observed in the *Cabp4*- and *Cacna2d4*-mutant mice[42]. In addition, other transcriptional, protein and metabolic key networks may experience dysregulation from the dynamic equilibrium and contribute to degeneration[140]. Finally, the summation of all these factors likely leads to photoreceptor loss. When rods die, they activate the recruitment of resident retinal microglia to the outer nuclear layer that apparently progress with generalized cell killing[141]. Of note, in *Cacna2d4*-deficient mice, photoreceptor outer segment shorting becomes evident upon one year of age and may be an antecedent of degeneration progression.

Ectopic synapses

Ectopic synaptogenesis occurs as a result of synaptic dysfunction or/and cell loss in various mouse models of retinal diseases[142-144]. Perturbed calcium and glutamatergic synaptic drive may stimulate dendritic growth to seek new synaptic partners. This synaptic remodeling begins upon removal of postsynaptic glutamate receptor proteins and dendrite retraction in secondary neurons. A fraction of rod, cone and bipolar cells can die at this stage[138].

Dendritic sprouting and ectopic synaptogenesis were reported to occur in mice deficient in the bassoon protein which is responsible for proper membrane anchoring of the ribbon organelles in photoreceptor synapses[137,145]. Disrupted targeting of synaptic bodies to the active zones during development has been suggested as a reason for ectopic synapse formation[145]. Thereby, secondary neurons expanded dendritic neurites towards the photoreceptor nuclear layer probably due to lacking synaptic activity in the lower localized photoreceptor synapses. In the *Cabp4*-knockout mice, dendritic expansion and formation of ectopic synapses between rods and rod bipolar or horizontal cells were observed[42]. *Cacna1f*-mutant mice showed abnormal dendritic sprouting of several second-order neurons in the photoreceptor nuclear layer[146]. In contrast, degenerating photoreceptors display anomalous sprouting of axons in the inner retina as a common response to advanced stress[138]. The mechanisms of ectopic axon extension probably underlie abnormal transcription of genes involved in developmental axonal growth, synaptic plasticity and cell size control. Photoreceptors, indeed, maintain their dimensions through balanced protein production and intracellular distribution[139]. Of note, axon sprouting retrogradely deprives photoreceptors of normal synaptic input/output.

As ectopic synapses are most likely functional, their activity is assumed to interfere with the retinal signal transmission and to contribute to retinal pathogenesis. ERG recordings from animal models with ectopic synapses show anomalous features, indicating alterations in retinal circuitries[142].

Concerning *Cacna2d4*-mutant mice, the absence of secondary neuron activities did not allow a detection of ectopic synapse-associated alterations in the ERG responses. Alluding to the *Cacna1f*- and *Cabp4*-mutant mouse phenotypes, however, ectopic synaptogenesis in *Cacna2d4*-mutant retinas emerges possible.

4.4. Vision in Patients of CACNA2D4-induced Cone Dystrophy

In the nervous system, calcium signaling may be of such essential importance that minor defects can lead to embryonic lethality or have devastating pathologies[147]. Otherwise, the large number of ion channels, pumps and transporters that are expressed in the nervous system reflects redundancy at the functional level and can compensate for genetic defects. Concerning the two deleterious mutations identified so far in the α2δ-4 calcium channel subunit of human and mice, limited tolerance of potential protein deficiency seems to arise exclusively in the ocular system. In all remaining α2δ-4 expressing tissues, deficits are presumably perceived and corrected by redundant proteins. Moreover, although affected, the human *CACNA2D4* patients also remain their visual function, implying compensatory effects for CACNA2D4 in the retina as well.

At least three α2δ homologous proteins may pair with synaptic α1 subunits and contribute to functional CACNA2D4 rescue. The expression of the α2δ-1 subunit was shown to emerge ubiquitously. The α2δ-2 and α2δ-3 subunits display broad expression patterns and are predominantly found in neuronal tissues[148]. In addition, possible low expression of these homologues in retinas of unaffected individuals can undergo upregulation in the absence of CACNA2D4. Alternatively, α1 subunits may sustain partial function despite of CACNA2D4 lack.

Whether voltage-gated calcium channels may correctly function in the absence of an α2δ subunit, was hitherto not demonstrated[43]. Nonetheless, heterologous expression of the T-type calcium channels emerges robust without co-expression of an accessory α2δ or β subunit. This implies that native T-type calcium channel complexes may operate in α2δ absence[43,149] (Fig. 6). T-type calcium channels, arranged by the main pore subunits α1G, α1H and α1I, were recently shown to be involved in the retinal synaptic signal transmission. In mammalian retina, they are co-localized with L-type calcium channels in a subclass of rod bipolar cells and contribute to glutamate release at synaptic contacts between bipolar and amacrine cells[150]. Interestingly, the membrane density of the T-type calcium channels in these cells is considerably higher compared to that of the L-type channels[151,152]. Besides, ~30 % of cone bipolar cell activities are evoked trough T-type calcium channels[151,153]. It is tempting to speculate that synaptic terminals of the photoreceptors also involve a fraction of T-type calcium channels.

In view of their physiology, T-type calcium channels impart more flexible calcium entrance at retinal membrane potentials. In comparison to L-type calcium channels, they activate at more negative potentials of ~-80 mV to ~-20 mV (*versus* ~-55 mV to ~+10 mV)[151,154]. Present T-type

calcium channels can thus compensate for calcium signaling in absence of sufficient L-type channel activity at physiological potentials. Alternatively, an upregulation in surface expression of T-type calcium channel may contribute to the maintenance of retinal synaptic transmission in affected individuals.

CACNA2D4-independent calcium signaling by ATPase-pumps may also stimulate retinal activity. The plasma membrane calcium ATPase isoform, PMCA2, is involved in the transmission of light responses at retinal synapses[155,156]. Cyclic nucleotide (cGMP)-gated calcium channels are tetrameric membrane proteins formed through complexes of α (CNGA) and β (CNGB) subunits. Whereas α subunits compose the channel pore, the β subunits modulate the properties of the channel complexes. cGMP-gated channels are predominantly expressed in the photoreceptor outer segments and play a key role in visual phototransduction (Chapter 1). In cones however, calcium influx through cGMP-gated calcium channels was also found to trigger synaptic glutamate release[157].

Ryanodine and inositol 1,4,5-trisphosphate (IP3) receptors play an active role in controlling presynaptic calcium dynamics and contribute to neurotransmission[158-160]. Ryanodine receptors act presynaptically at photoreceptor terminals[161]. In the mammalian retina, IP3 receptors localize to the synaptic terminals of photoreceptors and bipolar cells. Both receptor types were shown to mediate neurotransmitter release independent of voltage-gated calcium channels. Additionally, electrical gap junctions between rods and cones as well as direct coupling of rods to the cone OFF-bipolar cells constitute alternative signaling pathways for rod signals that do not depend on L-type calcium channel function[162-166]. An activation of calcium release from internal calcium stores also induces internal amplification of calcium concentrations required for the coordination of continuous vesicle release in retinal synapses[157,161]. This calcium signal strengthening may be upregulated in CACNA2D4-deficient retinas.

The absence of retinal signal transmission in *Cacna2d4*-mutant mice contradicts the human disease manifestation of sustained vision. Hence, photoreceptor synaptic activation in mice may underlie the unique control of Cacna2d4.

4.5. Further Clinical Risks in CACNA2D4-associated Diseases

As the *CACNA2D4*-associated cone dystrophy in our patients represents, although a mild, also a progressive disease, both affected individuals are at risk of symptoms worsening and might, with time, suffer from severe visual impairments or blindness.

Other mutations in *CACNA2D4* may show a broader spectrum of retinal pathologies ranging from incomplete congenital stationary night blindness to severe cone-rod dystrophy, in similarity to *CACNA1F*- or *CABP4*-mediated channelopathies[136,167,168]. The cone-rod disorder is characterized by a particular severity, as it frequently manifests at early childhood and leads to blindness.

Regarding further symptoms of these diseases, patients often show nystagmus (Table 1). The nystagmus response reflects a rapid involuntary rhythmic eye movement, arising due to a failure in synchronization of the sensory and motor components of the ocular system. Reduced contrast sensitivity or lack of visual acuity in a critical developmental period of the sensory organ and the corresponding cortical brain region may underlie the appearance of nystagmus[169]. Some examinations also indicate that abnormal spontaneous activity in the ganglion cells triggers its emergency[170,171]. Hence, structural alterations in the cortical structure or even changes in the brain may progress with abnormal visual experience and retinal dysfunction.

Furthermore, the photoreceptive pineal gland of the brain is able to perceive ambient illumination conditions and plays a key role in regulation of the circadian rhythm via melatonin production[175,176]. Abnormal visual perception or perturbed ganglion cell function may anomalously stimulate the pineal gland and influence patients' circadian activities. Many studies of the autistic disorder report sleep problems and altered circadian rhythms. Indeed, the nocturnal production of melatonin is reduced in autism[177]. Of note, in a iCSNB family with a mutation in the *CACNA1F* gene, three members were autistic[89].

Mutations in voltage-gated calcium channel subunits are also known to result in a wider array of neurological disorders, including episodic ataxia, epilepsy and migraine. In a family of *CACNA1F*-induced iCSNB, epilepsy was diagnosed in two of thirty six members[89]. In addition, eight individuals showed intellectual disability. The homozygous *Cacn2b*-mouse model for iCSNB is lethal without a transgenic rescue[172,173]. The Timothy syndrome, characterized by cardiac arrthymias, syndactyly, immune deficiency, cognitive abnormalities and autism, is caused by a mutation in the *CACNA1C* gene that is expressed in the retina[174]. These outcomes indicate that some defects in *CACNA2D4* might underlie similar severe neurological defects, particularly in the view the expression of *CACNA2D4* in the brain.

Table 1. Clinical features of channelopathy-associated retinal diseases.

	***CACNA2D4*-associated cone dystrophy human**	***Cacna2d4*-associated cone-rod dysfunction mouse**	***CACNA1F*-associated cone-rod dystrophy human**	***CACNA1F*-associated iCSNB human**
inheritance modus	recessive	recessive	recessive	recessive/dominant
progression	progressive	progressive	progressive	non-progressive
onset	2-3 decade of life	~ day 10	childhood	congenital
visual acuity	impaired	-	impaired	impaired
color vision	impaired	-	impaired	normal
photophobia	present		present	absent
visual field	normal	-	impaired	normal
fundus	normal	normal	affected	normal
nystagmus	absent	absent	present	absent/present
strabismus	absent	-	absent/present	absent/present
dark adaptation	normal	-	reduced	normal
rod ERG	reduced	negative	negative	reduced
cone ERG	absent	absent	reduced/absent	reduced
rod response	slightly reduced	reduced	normal/reduced	normal
cone response	slightly reduced	absent	reduced/absent	normal
oscillatory potentials rods	normal	absent	present	normal
oscillatory potentials cones	absent	absent	absent	reduced
30-Hz flicker	reduced	-	reduced	reduced

4.6. Future examinations

Studying *CACNA2D4* as a candidate gene in retinal disorders, the discrimination between neutral polymorphic variability and causative mutations is of imperative importance. Although the pathogenicity of identified genetic alterations can emerge apparent, *in silico* and/or *in vitro* remodeling may be required to provide evidence for the pathogenic relevance. Regarding the CACNA2D4 protein, its extracellular localization as well as the modulatory stimulation of calcium channels can aid in an experimental discrimination between pathogenic sequence alteration and neutral polymorphisms. The respective *CACNA2D4* allelic variants may be reproduced upon *in vitro* mutagenesis and expressed in heterologous cell line systems. Mutations, in contrast to neutral polymorphisms, might result in mislocalisation of the corresponding CACNA2D4 protein variant and thus demonstrate the pathogenic effects of an investigated sequence variation. The antigenic KVSDRKFLTPEDEASVC (737-752 amino acids) epitope of CACNA2D4-specific antibody generated by Qin et al., may be reproduced for immunohistochemistry-based localization studies. Of note, an accumulation in the cytoplasmic space or retention of CACNA2D4-mutant variants in the endoplasmatic reticulum might be simultaneously observed[22].

Functional examinations by means of standardized patch clamp experiments challenge a co-expression of calcium gating α1 subunit and an auxiliary subunit of the β-type. Endogenous expression of those calcium channel subunits in cell lines is usually low and patch-clamp recordings remain at the levels of noise. In addition, it does not allow the investigation of CACNA2D4 modulatory impact on a defined calcium channel complex. Alterations in calcium current amplitudes as well as kinetics between wild type and mutant channel complexes associating CACNA2D4 should imply the pathogenic consequences of a mutation.

Alternatively to the clamp-patch methodology, calcium currents of heterologously expressed calcium channel variants may be also estimated upon fluorescence-based approach. Thereby, the amounts of free calcium entering the cell after extrinsic depolarization are monitored by a fluorescence image analysis upon green fluorescent Flou3-AM staining[178]. Fluo3-AM dye binds specifically to the inflowing calcium and, by exposure to 488 nm light, increases its fluorescence emission at 630 nm. Hence, the fluorescence intensity depends on how much free calcium is bound and may be measured in relativity to controls[178].

Whether increased/decreased membrane density of CACNA2D4-associating calcium channel complexes contributes to an alteration in the calcium current amplitute, this pathology may be

proven, once more, by immunohistochemistry-based localization studies. The immunoreactivity of specific antibodies with heterologously expressed CACNA2D4/α1/β protein complex variants can demonsrate differences in immunohistological signal intensities and give rise to altered channel density at cellular membranes.

Specific antibodies against the CACNA2D4 protein as well as the α1 subunits may be further used in coimmunoprecipitation studies in order to elucidate those α1 subunits with which CACNA2D4 interacts *in vivo*. In addition, coimmunoprecipitation experiments could help in identification of proteins interacting with the α2δ-4 subunit in the extracellular matrix as well as in the intracellular space.

Advanced expression studies of α2δ-4 in human and mice on the transcript and protein levels would help to gain more insights into the pathologies induced by mutations in this gene. Clinical attention should be raised by an expression of *CACNA2D4* in the retinal epithelium (RPE). Slight mottling of the RPE in the foveal retina was observed in both affected patients of cone dystrophy and may be indicative of initiating atrophy[179]. RPE is known to predominantly express the L-type calcium channel α1C subunit and CACNA2D4 association with α1C was demonstrated. *CACNA2D4*-deficient RPE cells could suffer from increased metabolic accumulation, protein mottling or the expression of stress-responsive genes, including vascular endothelial growth factors. The latest, in some cases, might lead to a severe macula dysfunction and choroidal neovascularisation[180-182].

The elucidation of CACNA2D4 essentiality in the visual processing of human and mice revealed a novel mechanism of retinal pathophysiology in ocular disorders. Challenging concepts and scientific examinations may provide clarifying steps towards key processes in disease development and contribute to further characterization of the CACNA2D4 gene. This, in future research, will potentiate accurate diagnostics and aid in therapeutic interventions.

4.7. References of the General Discussion

1. Nachman MW, Crowell SL (2000) Estimate of the mutation rate per nucleotide in humans. Genetics 156:297-304
2. Antonarakis SE, Krawczak M, Cooper DN (2000) Disease-causing mutations in the human genome. European Journal of Pediatrics 159:S173-S178
3. Ripley LS (1999) Context-dependent genetic alteration: Cell and sequence context-dependent effects on genetic variation - Part III. Summary. Molecular Strategies in Biological Evolution 870:218-219
4. Ripley LS (1999) Predictability of mutant sequences - Relationships between mutational mechanisms and mutant specificity. Molecular Strategies in Biological Evolution 870:159-172
5. Boyer JC, Yamada NA, Roques CN, Hatch SB, Riess K, Farber RA (2002) Sequence dependent instability of mononucleotide microsatellites in cultured mismatch repair proficient and deficient mammalian cells. Human Molecular Genetics 11:707-713
6. Henderson ST, Petes TD (1992) Instability of Simple Sequence Dna in Saccharomyces-Cerevisiae. Molecular and Cellular Biology 12:2749-2757
7. Henderson ST, Petes TD (1993) Instability of A Plasmid-Borne Inverted Repeat in Saccharomyces-Cerevisiae. Genetics 134:57-62
8. Sagher D, Hsu A, Strauss B (1999) Stabilization of the intermediate in frameshift mutation. Mutation Research-Fundamental and Molecular Mechanisms of Mutagenesis 423:73-77
9. Schwartz S, Perucho M (2000) Somatic mutations in mitochondrial DNA do not associate with nuclear microsatellite instability in gastrointestinal cancer. Gastroenterology 119:1806-1807
10. Kim NG, Choi YR, Baek MJ, Kim YH, Kang H, Kim NK, Min JS, Kim H (2001) Frameshift mutations at coding mononucleotide repeats of the hRAD50 gene in gastrointestinal carcinomas with microsatellite instability. Cancer Research 61:36-38
11. STREISIN.G, Okada Y, Emrich J, Newton J, Tsugita A, Terzaghi E, Inouye M (1966) Frameshift Mutations and Genetic Code. Cold Spring Harbor Symposia on Quantitative Biology 31:77-89
12. Levinson G, Gutman GA (1987) Slipped-Strand Mispairing - A Major Mechanism for Dna-Sequence Evolution. Molecular Biology and Evolution 4:203-221
13. Schlotterer C, Tautz D (1992) Slippage Synthesis of Simple Sequence DNA. Nucleic Acids Research 20:211-215
14. Zhu Y, Queller DC, Strassmann JE (2000) A phylogenetic perspective on sequence evolution in microsatellite loci. Journal of Molecular Evolution 50:324-338
15. Sia EA, JinksRobertson S, Petes TD (1997) Genetic control of microsatellite stability. Mutation Research-DNA Repair 383:61-70
16. Sia EA, Kokoska RJ, Dominska M, Greenwell P, Petes TD (1997) Microsatellite instability in yeast: Dependence on repeat unit size and DNA mismatch repair genes. Molecular and Cellular Biology 17:2851-2858
17. Cooper DN (1983) Eukaryotic Dna Methylation. Human Genetics 64:315-333

18. Cooper DN, Taggart MH, Bird AP (1983) Unmethylated Domains in Vertebrate DNA. Nucleic Acids Research 11:647-658
19. Cooper DN, Gerberhuber S (1985) Dna Methylation and Cpg Suppression. Cell Differentiation 17:199-205
20. Cooper DN, Youssoufian H (1988) The Cpg Dinucleotide and Human Genetic-Disease. Human Genetics 78:151-155
21. Cooper DN, Krawczak M (1989) Cytosine Methylation and the Fate of Cpg Dinucleotides in Vertebrate Genomes. Human Genetics 83:181-188
22. Qin N, Yagel S, Momplaisir ML, Codd EE, D'Andrea MR (2002) Molecular cloning and characterization of the human voltage-gated calcium channel alpha(2)delta-4 subunit. Moleculare Pharmacology 62:485-496
23. Holbrook JA, Neu-Yilik G, Hentze MW, Kulozik AE (2004) Nonsense-mediated decay approaches the clinic. Nature Genetics 36:801-808
24. Schell T, Kocher T, Wilm M, Seraphin B, Kulozik AE, Hentze MW (2003) Complexes between the nonsense-mediated mRNA decay pathway factor human upf1 (up-frameshift protein 1) and essential nonsense-mediated mRNA decay factors in HeLa cells. Biochemical Journal 373:775-783
25. Chan D, Weng YM, Graham HK, Sillence DO, Bateman JF (1998) A nonsense mutation in the carboxyl-terminal domain of type X collagen causes haploinsufficiency in Schmid metaphyseal chondrodysplasia. Journal of Clinical Investigation 101:1490-1499
26. Maquat LE (2004) Nonsense-mediated mRNA decay: Splicing, translation and mRNP dynamics. Nature Reviews Molecular Cell Biology 5:89-99
27. Maquat LE (2004) Nonsense-mediated mRNA decay: A comparative analysis of different species. Current Genomics 5:175-190
28. Wang M, Offord J, Oxender DL, Su TZ (1999) Structural requirement of the calcium-channel subunit alpha2delta for gabapentin binding. Biochemical Journal 342:313-320
29. Ruddock LW and Molinari M (2006) N-glycan processing in ER quality control. Journal of Cellular Science 119:4373-4380
30. Sandoval A, Oviedo N, Andrade A, Felix R (2004) Glycosylation of asparagines 136 and 184 is necessary for the alpha2delta subunit-mediated regulation of voltage-gated Ca2+ channels. FEBS Letters 576:21-26
31. Kincaid MM and Cooper AA (2006) Misfolded proreins traffic from the ER due to ER export signals. Molecular Biology of the cell (*in press*)
32. Canti C, Nieto-Rostro M, Foucault I, Heblich F, Wratten J, Richards MW, Hendrich J, Douglas L, Page KM, Davies A, Dolphin AC (2005) The metal-ion-dependent adhesion site in the Von Willebrand factor-A domain of alpha2delta subunits is key to trafficking voltage-gated Ca2+ channels. Proceedings of the National Academy of Sciences of the United States of America 102:11230-11235

33. Gao B, Sekido Y, Maximov A, Saad M, Forgacs E, Latif F, Wei MH, Lerman M, Lee JH, Perez-Reyes E, Bezprozvanny I, Minna JD (2000) Functional properties of a new voltage-dependent calcium channel alpha(2)delta auxiliary subunit gene (CACNA2D2). Journal of Biological Chemistry 275:12237-12242
34. Bangalore R, Mehrke G, Gingrich K, Hofmann F, Kass RS (1996) Influence of L-type Ca channel alpha(2)/delta-subunit on ionic and gating current in transiently transfected HEK 293 cells. American Journal of Physiology-Heart and Circulatory Physiology 39:H1521-H1528
35. Shistik E, Ivanina T, Puri T, Hosey M, Dascal N (1995) Ca2+ current enhancement by alpha 2/delta and beta subunits in Xenopus oocytes: contribution of changes in channel gating and alpha 1 protein level. Journal of Physiology 489:55-62
36. Li CY, Song YH, Higuera ES, Luo ZD (2004) Spinal dorsal horn calcium channel alpha(2)delta-1 subunit upregulation contributes to peripheral nerve injury-induced tactile allodynia. Journal of Neuroscience 24:8494-8499
37. Brodbeck J, Davies A, Courtney JM, Meir A, Balaguero N, Canti C, Moss FJ, Page KM, Pratt WS, Hunt SP, Barclay J, Rees M, Dolphin AC (2002) The ducky mutation in Cacna2d2 results in altered Purkinje cell morphology and is associated with the expression of a truncated alpha 2 delta-2 protein with abnormal function. Journal of Biological Chemistry 277:7684-7693
38. Barclay J, Balaguero N, Mione M, Ackerman SL, Letts VA, Brodbeck J, Canti C, Meir A, Page KM, Kusumi K, Perez-Reyes E, Lander ES, Frankel WN, Gardiner RM, Dolphin AC, Rees M (2001) Ducky mouse phenotype of epilepsy and ataxia is associated with mutations in the Cacna2d2 gene and decreased calcium channel current in cerebellar Purkinje cells. Journal of Neuroscience 21:6095-6104
39. Gurnett CA, De Waard M, Campbell KP (1996) Dual function of the voltage-dependent Ca2+ channel alpha 2 delta subunit in current stimulation and subunit interaction. Neuron 16:431-440
40. van den Berg B, Ellis RJ, Dobson CM (1999) Effects of macromolecular crowding on protein folding and aggregation. Embo Journal 18:6927-6933
41. Felix R, Gurnett CA, De Waard M, Campbell KP (1997) Dissection of functional domains of the voltage-dependent Ca2+ channel alpha2delta subunit. Journal of Neuroscience 17:6884-6891
42. Haeseleer F, Imanishi Y, Maeda T, Possin DE, Maeda A, Lee A, Rieke F, Palczewski K (2004) Essential role of Ca2+-binding protein 4, a Cav1.4 channel regulator, in photoreceptor synaptic function. Nature Neuroscience 7:1079-1087
43. Canti C, Dolphin AC (2003) CaVbeta subunit-mediated up-regulation of CaV2.2 currents triggered by D2 dopamine receptor activation. Neuropharmacology 45:814-827
44. Hess P, Lansman JB, Tsien RW (1984) Modulation of Single Calcium Channels by the Calcium Agonist Bay K-8644. Biophysical Journal 45:A394
45. Bar-Even A, Paulsson J, Maheshri N, Carmi M, O'Shea E, Pilpel Y, Barkai N (2006) Noise in protein expression scales with natural protein abundance. Nature Genetics 38:636-643

46. Shirokov R, Ferreira G, Yi JX, Rios E (1998) Inactivation of gating currents of L-type calcium channels - Specific role of the alpha(2)delta subunit. Journal of General Physiology 111:807-823
47. Shirokov R, Ferreira G, Rios E (1998) Effects of the alpha(2)delta subunit on inactivation of gating currents interpreted with a continuum model of Ca2+ channel gating. Biophysical Journal 74:A100
48. Chen LW, Shen AY, Chen JS, Wu SN (2000) Differential regulation of Ca2+ influx by fMLP and PAF in human neutrophils: possible involvement of store-operated Ca2+ channel. Shock 13:175-182
49. Hibino H, Pironkova R, Onwumere O, Vologodskaia M, Hudspeth AJ, Lesage F (2002) RIM binding proteins (RBPs) couple Rab3-interacting molecules (RIMs) to voltage-gated Ca(2+) channels. Neuron 34:411-423
50. Zhong J, Hume JR, Keef KD (2001) beta-Adrenergic receptor stimulation of L-type Ca2+ channels in rabbit portal vein myocytes involves both alphas and betagamma G protein subunits. Journal of Physiology 531:105-115
51. Catterall WA (2000) Structure and regulation of voltage-gated Ca2+ channels. Annual Reviews in Cell Development and Biology 16:521-555
52. Zhou J, Olcese R, Qin N, Noceti F, Birnbaumer L, Stefani E (1997) Feedback inhibition of Ca2+ channels by Ca2+ depends on a short sequence of the C terminus that does not include the Ca2+ -binding function of a motif with similarity to Ca2+ -binding domains. Proceedings of the National Academy of Sciences of the United States of America 94:2301-2305
53. Lee A, Wong ST, Gallagher D, Li B, Storm DR, Scheuer T, Catterall WA (1999) Ca2+/calmodulin binds to and modulates P/Q-type calcium channels. Nature 399:155-159
54. Zuhlke RD, Pitt GS, Tsien RW, Reuter H (2000) Ca2+-sensitive inactivation and facilitation of L-type Ca2+ channels both depend on specific amino acid residues in a consensus calmodulin-binding motif in the(alpha)1C subunit. Journal of Biological Chemistry 275:21121-21129
55. Wingard JN, Chan J, Bosanac I, Haeseleer F, Palczewski K, Ikura M, Ames JB (2005) Structural Analysis of Mg2+ and Ca2+ Binding to CaBP1, a Neuron-specific Regulator of Calcium Channels. Journal of Biological Chemistry 280:37461-37470
56. Halling DB, Xiong LW, He R, Pedersen S, Hamilton S (2005) Calmodulin can bind to the IQ peptide of the Cav1.2 channel with its N-lobe calcium bound and its C-lobe calcium free. Biophysical Journal 88:276A
57. DeMaria CD, Soong TW, Alseikhan BA, Alvania RA, Yue DT (2001) Calmodulin bifurcates the local Ca2+ signal that modulates P/Q-type Ca channels. Biophysical Journal 80:197A
58. Zuhlke RD, Reuter H (1999) Identification of a single amino acid residue as molecular determinant of calcium-dependent inactivation or facilitation of L-type calcium channels. Biophysical Journal 76:A343
59. Zuhlke RD, Pitt GS, Deisseroth K, Tsien RW, Reuter H (1999) Calmodulin supports both inactivation and facilitation of L-type calcium channels. Nature 399:159-162
60. Mori MX, Erickson MG, Yue DT (2004) Functional stoichiometry and local enrichment of calmodulin interacting with L-type Ca channels. Biophysical Journal 86:186A

61. Mori MX, Yue DT (2005) Lobe-specific calmodulin (CaM) regulation of P/Q-type (CaV2.1) Ca2+channels probed by CaM/channel fusion constructs. Biophysical Journal 88:275A
62. Lee A, Scheuer T, Catterall WA (2000) Ca2+-calmodulin dependent inactivation and facilitation of P/Q-type Ca2+ channels. Biophysical Journal 78:265A
63. Dolphin AC (1995) Voltage-Dependent Calcium Channels and Their Modulation by Neurotransmitters and G-Proteins. Experimental Physiology 80:1-36
64. Zhang JF, Ellinor PT, Aldrich RW, Tsien RW (1996) Multiple structural elements in voltage-dependent Ca2+ channels support their inhibition by G proteins. Neuron 17:991-1003
65. Zhang JF, Ellinor PT, Aldrich RW, Tsien RW (1996) Molecular determinants involved in the modulation of N-type calcium channels by G-proteins. Biophysical Journal 70:423A
66. Beutner D, Voets T, Neher E, Moser T (2001) Calcium dependence of exocytosis and endocytosis at the cochlear inner hair cell afferent synapse. Neuron 29:681-690
67. Qin N, Olcese R, Zhou J, Cabello OA, Birnbaumer L, Stefani E (1996) Identification of a second region of the beta-subunit involved in regulation of calcium channel inactivation. American Journal of Physiology 271:C1539-C1545
68. Zhong HJ, Yokoyama CT, Scheuer T, Catterall WA (1999) Reciprocal regulation of P/Q-type Ca2+ channels by SNAP-25, syntaxin and synaptotagmin. Nature Neuroscience 2:939-941
69. Jarvis SE, Magga JM, Beedle AM, Braun JEA, Zamponi GW (2000) G protein modulation of N-type calcium channels is facilitated by physical interactions between syntaxin 1A and G beta gamma. Journal of Biological Chemistry 275:6388-6394
70. Jarvis SE, Zamponi GW (2005) Masters or slaves? Vesicle release machinery and the regulation of presynaptic calcium channels. Cell Calcium 37:483-488
71. Lu Q, AtKisson MS, Jarvis SE, Feng ZP, Zamponi GW, Dunlap K (2001) Syntaxin 1A supports voltage-dependent inhibition of alpha(1B) Ca2+ channels by G beta gamma in chick sensory neurons. Journal of Neuroscience 21:2949-2957
72. Zamponi GW (2003) Regulation of presynaptic calcium channels by synaptic proteins. Journal of Pharmacological Sciences 92:79-83
73. Nunoki K, Florio V, Catterall WA (1989) Activation of Purified Calcium Channels by Stoichiometric Protein-Phosphorylation. Proceedings of the National Academy of Sciences of the United States of America 86:6816-6820
74. Marais E, Klugbauer N, Hofmann F (2001) Calcium channel alpha(2)delta subunits - Structure and gabapentin binding. Molecular Pharmacology 59:1243-1248
75. Berntson A, Smith RG, Taylor WR (2004) Postsynaptic calcium feedback between rods and rod bipolar cells in the mouse retina. Visual Neuroscience 21:913-924
76. Berntson A, Smith RG, Taylor WR (2004) Transmission of single photon signals through a binary synapse in the mammalian retina. Visual Neuroscience 21:693-702
77. Vardi N, Duvoisin R, Wu G, Sterling P (2000) Localization of mGluR6 to dendrites of ON bipolar cells in primate retina. Journal of Comparative Neurology 423:402-412

78. Corey DP, Dubinsky JM, Schwartz EA (1984) The Calcium Current in Inner Segments of Rods from the Salamander (Ambystoma-Tigrinum) Retina. Journal of Physiology-London 354:557-575
79. Nawy S, Jahr CE (1991) Cgmp-Gated Conductance in Retinal Bipolar Cells Is Suppressed by the Photoreceptor Transmitter. Neuron 7:677-683
80. Nawy S, Jahr CE (1991) Effects of Cgmp on Light Responses of Depolarizing Bipolar Cells in Retinal Slices of the Tiger Salamander. Investigative Ophthalmology & Visual Science 32:1188-1196
81. Attwell D, Gray P (1984) Patch-Clamp Recording from Isolated Rods of the Salamander Retina. Journal of Physiology-London 351:9
82. Attwell D, Mobbs P, Tessierlavigne M, Wilson M (1985) Neurotransmitter-Induced Currents in Bipolar Cells Isolated from the Axolotl Retina, Recorded by Whole-Cell Patch-Clamping. Journal of Physiology-London 364:38
83. Attwell D, Tessierlavigne M, Wilson M, Mobbs P (1987) Bipolar Cell-Membrane Currents and Signal-Processing in the Axolotl Retina. Neuroscience Research 15:191-204
84. Witkovsky P, Schmitz Y, Akopian A, Krizaj D, Tranchina D (1997) Gain of rod to horizontal cell synaptic transfer: Relation to glutamate release and a dihydropyridine-sensitive calcium current. Journal of Neuroscience 17:7297-7306
85. Hoda JC, Zaghetto F, Koschak A, Striessnig J (2005) Congenital stationary night blindness type 2 mutations S229P, G369D, L1068P, and W1440X alter channel gating or functional expression of Ca(v)1.4 L-type Ca2+ channels. Journal of Neuroscience 25:252-259
86. Baumann L, Gerstner A, Zong X, Biel M, Wahl-Schott C (2004) Functional characterization of the L-type Ca2+ channel Cav1.4alpha1 from mouse retina. Investigative Ophthalmology & Visual Science 45:708-713
87. Saito T, Kaneko A (1983) Ionic Mechanisms Underlying the Responses of Off-Center Bipolar Cells in the Carp Retina .1. Studies on Responses Evoked by Light. Journal of General Physiology 81:589-601
88. Euler T, Masland RH (2000) Light-evoked responses of bipolar cells in a mammalian retina. Journal of Neurophysiology 83:1817-1829
89. Hemara-Wahanui A, Berjukow S, Hope CI, Dearden PK, Wu SB, Wilson-Wheeler J, Sharp DM, Lundon-Treweek P, Clover GM, Hoda JC, Striessnig J, Marksteiner R, Hering S, Maw MA (2005) A CACNA1F mutation identified in an X-linked retinal disorder shifts the voltage dependence of Cav1.4 channel activation. Proceedings of the National Academy of Sciences of the United States of America 102:7553-7558
90. Rieke F, Baylor DA (1996) Molecular origin of continuous dark noise in rod photoreceptors. Biophysical Journal 71:2553-2572
91. Rieke F, Schwartz EA (1996) Asynchronous transmitter release: Control of exocytosis and endocytosis at the salamander rod synapse. Journal of Physiology-London 493:1-8
92. Thoreson WB, Rabl K, Townes-Anderson E, Heidelberger R (2004) A highly Ca2+-sensitive pool of vesicles contributes to linearity at the rod photoreceptor ribbon synapse. Neuron 42:595-605

93. ElBasiouny SM, Bennett DJ, Mushahwar VK (2006) Simulation of Ca2+ persistent inward currents in spinal motoneurones: mode of activation and integration of synaptic inputs. Journal of Physiology-London 570:355-374
94. Bianchi K, Vandecasteele G, Carli C, Romagnoli A, Szabadkai G, Rizzuto R (2006) Regulation of Ca(2+) signalling and Ca(2+)-mediated cell death by the transcriptional coactivator PGC-1alpha. Cell Death and Differentiation 13:586-596
95. Bianchi K, Rimessi A, Prandini A, Szabadkai G, Rizzuto R (2004) Calcium and mitochondria: mechanisms and functions of a troubled relationship. Biochimica et Biophysica Acta-Bioenergetics 1742:119-131
96. Leo S, Bianchi K, Brini M, Rizzuto R (2005) Mitochondrial calcium signalling in cell death. FEBS Journal 272:4013-4022
97. Jouaville LS, Pinton P, Bastianutto C, Rutter GA, Rizzuto R (1999) Regulation of mitochondrial ATP synthesis by calcium: evidence for a long-term metabolic priming. Proceedings of the National Academy Science of the United States of America 96:13807-13812
98. Arundine M, Tymianski M (2003) Molecular mechanisms of calcium-dependent neurodegeneration in excitotoxicity. Cell Calcium 34:325-337
99. Zoratti M, Szabo D, De Marchi U (2005) Mitochondrial permeability transitions: how many doors to the house? Biochimica et Biophysica Acta-Bioenergetics 1706:40-52
100. Santos JH, Meyer JN, Van Houten B (2006) Mitochondrial localization of telomerase as a determinant for hydrogen peroxide-induced mitochondrial DNA damage and apoptosis. Human Molecular Genetics 15:1757-1768
101. Van Houten B, Woshner V, Santos JH (2006) Role of mitochondrial DNA in toxic responses to oxidative stress. DNA Repair 5:145-152
102. Collins TJ, Berridge MJ, Lipp P, Bootman MD (2002) Mitochondria are morphologically and functionally heterogeneous within cells. Embo Journal 21:1616-1627
103. Menzies RA, Gold PH (1971) Turnover of Mitochondria in A Variety of Tissues of Young Adult and Aged Rats. Journal of Biological Chemistry 246:2425-&
104. Campanella M, Pinton P, Rizzuto R (2004) Mitochondrial Ca2+ homeostasis in health and disease. Biological Research 37:653-660
105. Pinton P, Leo S, Wieckowski MR, Di Benedetto G, Rizzuto R (2004) Long-term modulation of mitochondrial Ca2+ signals by protein kinase C isozymes. Journal of Cell Biology 165:223-232
106. Rizzuto R, Pinton P, Ferrari D, Chami M, Szabadkai G, Magalhaes PJ, Di Virgilio F, Pozzan T (2003) Calcium and apoptosis: facts and hypotheses. Oncogene 22:8619-8627
107. Furukawa K, Mattson MP (1995) Cytochalasins Protect Hippocampal-Neurons Against Amyloid Beta-Peptide Toxicity - Evidence That Actin Depolymerization Suppresses Ca2+ Influx. Journal of Neurochemistry 65:1061-1068
108. Dillon C, Goda Y (2005) The actin cytoskeleton: Integrating form and function at the synapse. Annual Review of Neuroscience 28:25-55
109. Akopian A, Szikra T, Cristofanilli M, Krizaj D (2006) Glutamate-induced Ca2+ influx in third-order neurons of salamander retina is regulated by the actin cytoskeleton. Neuroscience 138:17-24

110. Cristofanilli M, Akopian A (2006) Calcium channel and glutamate receptor activities regulate actin organization in the salamander retinal neurons. Journal of Physiology 575: 543-554

111. Gerber SH, Garcia J, Rizo J, Sudhof TC (2001) An unusual C-2-domain in the active-zone protein piccolo: implications for Ca2+ regulation of neurotransmitter release. Embo Journal 20:1605-1619

112. Lucas DR, Newhouse JP (1957) The Effects of Nutritional and Endocrine Factors on An Inherited Retinal Degeneration in the Mouse. Archives of Ophthalmology 57:224-235

113. Lucas DR, Newhouse JP (1957) The Toxic Effect of Sodium L-Glutamate on the Inner Layers of the Retina. Archives of Ophthalmology 58:193-201

114. Sheng M, Wyszynski M (1997) Ion channel targeting in neurons. Bioessays 19:847-853

115. Wyszynski M, Lin J, Rao A, Nigh E, Beggs AH, Craig AM, Sheng M (1997) Competitive binding of alpha-actinin and calmodulin to the NMDA receptor. Nature 385:439-442

116. Sattler R, Tymianski M (2000) Molecular mechanisms of calcium-dependent excitotoxicity. Journal of Molecular Medicine 78:3-13

117. Sattler R, Xiong ZG, Lu WY, MacDonald JF, Tymianski M (2000) Distinct roles of synaptic and extrasynaptic NMDA receptors in excitotoxicity. Journal of Neuroscience 20:22-33

118. Jeon CJ, Kong JH, Strettoi E, Rockhill R, Stasheff SF, Masland RH (2002) Pattern of synaptic excitation and inhibition upon direction-selective retinal ganglion cells. Journal of Comparative Neurology 449:195-205

119. Strettoi E, Porciatti V, Falsini B, Pignatelli V, Rossi C (2002) Morphological and functional abnormalities in the inner retina of the rd/rd mouse. Journal of Neuroscience 22:5492-5504

120. Strettoi E, Volpini M (2002) Retinal organization in the bcl-2-overexpressing transgenic mouse. Journal of Comparative Neurology 446:1-10

121. Allison DW, Gelfand VI, Spector I, Craig AM (1998) Role of actin in anchoring postsynaptic receptors in cultured hippocampal neurons: Differential attachment of NMDA versus AMPA receptors. Journal of Neuroscience 18:2423-2436

122. Allison DW, Chervin AS, Gelfand VI, Craig AM (2000) Postsynaptic scaffolds of excitatory and inhibitory synapses in hippocampal neurons: Maintenance of core components independent of actin filaments and microtubules. Journal of Neuroscience 20:4545-4554

123. Craig AM, Stowell JN, Rao A, Allison DW, Crump FT, Cha EM, Chervin A, Gelfand VI (1999) Glutamate receptor targeting and assembly of excitatory synapses. Journal of Neurochemistry 73:S106

124. Sattayasai J, Zappia J, Ehrlich D (1989) Differential-Effects of Excitatory Amino-Acids on Photoreceptors of the Chick Retina - An Electron-Microscopical Study Using the Zinc-Iodide-Osmium Technique. Visual Neuroscience 2:237-245

125. Schmidt SY (1978) Biochemical Findings in Some Animals with Retinal Degenerations. Metabolic Ophthalmology 2:247-250

126. Ohno K, Okada M, Tsutsumi R, Sakamoto S, Yamaguchi T (1998) The AMPA-receptor antagonist YM90K reduces AMPA receptor-mediated excitotoxicity in rat hippocampal cultures. Japanese Journal of Pharmacology 76:105-108

127. Ohno K, Okada M, Tsutsumi R, Kohara A, Yamaguchi T (1997) Kainate excitotoxicity is mediated by AMPA- but not kainate-preferring receptors in embryonic rat hippocampal cultures. Neurochemistry International 31:715-722

128. Kalloniatis M, Tomisich G (1999) Amino acid neurochemistry of the vertebrate retina. Progress in Retinal and Eye Research 18:811-866

129. Ulshafer RJ, Sherry DM, Dawson R, Wallace DR (1990) Excitatory Amino-Acid Involvement in Retinal Degeneration. Brain Research 531:350-354

130. Ulshafer RJ, Allen CB, Rubin ML (1990) Distributions of Elements in the Human Retinal-Pigment Epithelium. Archives of Ophthalmology 108:113-117

131. Picaud SA, Larsson HP, Grant GB, Lecar H, Werblin FS (1995) Glutamate-Gated Chloride Channel with Glutamate-Transporter-Like Properties in Cone Photoreceptors of the Tiger Salamander. Journal of Neurophysiology 74:1760-1771

132. Schmitz F, Tabares L, Khimich D, Strenzke N, Villa-Polo P, Castellano-Munoz M, Bulankina A, Moser T, Fernandez-Chacon R, Sudhof TC (2006) CSP alpha-deficiency causes massive and rapid photoreceptor degeneration. Proceedings of the National Academy of Sciences of the United States of America 103:2926-2931

133. Michaelides M, Holder GE, Hunt DM, Fitzke FW, Bird AC, Moore AT (2005) A detailed study of the phenotype of an autosomal dominant cone-rod dystrophy (CORD7) associated with mutation in the gene for RIM1. British Journal of Ophthalmology 89:198-206

134. Johnson S, Halford S, Morris AG, Patel RJ, Wilkie SE, Hardcastle AJ, Moore AT, Zhang K, Hunt DM (2003) Genomic organisation and alternative splicing of human RIM1, a gene implicated in autosomal dominant cone-rod dystrophy (CORD7). Genomics 81:304-314

135. Mori N, Ishiba Y, Kubota S, Kobayashi A, Higashide T, McLaren MJ, Inana G (2006) Truncation mutation in HRG4 (UNC119) leads to mitochondrial ANT-1-mediated photoreceptor synaptic and retinal degeneration by apoptosis. Investigative Ophthalmology & Visual Science 47:1281-1292

136. Zeitz, C., Kloeckener-Gruissem B., Forster U., Kohl S., Magyar I., Bernd W., Mátyás G., Borruat F., Schorderet D.F., Zrenner E., Munier F.L., and Berger, W. (2006) Mutations in CABP4, encoding the Ca2+-binding protein 4, cause autosomal recessive night blindness. American Journal of Human Genetics. (*in press*)

137. Maeda T, Lem J, Palczewski K, Haeseleer F (2005) A critical role of CaBP4 in the cone synapse. Investigative Ophthalmology & Visual Science 46:4320-4327

138. Marc RE, Jones BW (2003) Retinal remodeling in inherited photoreceptor degenerations. Molecular Neurobiology 28:139-147

139. Marc RE, Jones BW, Watt CB, Strettoi E (2003) Neural remodeling in retinal degeneration. Progress in Retina and Eye Research 22:607-655

140. Mervin K, Valter K, Maslim J, Lewis G, Fisher S, Stone J (1999) Limiting photoreceptor death and deconstruction during experimental retinal detachment: The value of oxygen supplementation. American Journal of Ophthalmology 128:155-164

141. Gupta N, Brown KE, Milam AH (2003) Activated microglia in human retinitis pigmentosa, late-onset retinal degeneration, and age-related macular degeneration. Experimental Eye Research 76:463-471

142. Peng YW, Hao Y, Petters RM, Wong F (2000) Ectopic synaptogenesis in the mammalian retina caused by rod photoreceptor-specific mutations. Nature Neuroscience 3:1121-1127

143. Peng YW, Mahmoud TH, deOliveira LB, Tatebayashi M, Hao Y, Mccuen BW, Petters RM, Wong F (1999) Rhodopsin mutation induces ectopic cone-rod bipolar cell synaptic connections in transgenic swine. Molecular Biology of the Cell 10:76-82

144. Peng YW, Senda T, Hao Y, Matsuno K, Wong F (2001) Ectopic synaptogenesis is a common step in the progression of hereditary retinal degenerations. Investigative Ophthalmology & Visual Science 42:378-391

145. Dick O, Dieck ST, Altrock WD, Ammermuller J, Weiler R, Garner CC, Gundelfinger ED, Brandstatter JH (2003) The presynaptic active zone protein bassoon is essential for photoreceptor ribbon synapse formation in the retina. Neuron 37:775-786

146. Mansergh F, Orton NC, Vessey JP, Lalonde MR, Stell WK, Tremblay F, Barnes S, Rancourt DE, Bech-Hansen NT (2005) Mutation of the calcium channel gene Cacna1f disrupts calcium signaling, synaptic transmission and cellular organization in mouse retina. Human Molecular Genetics 14:3035-3046

147. Rizzuto R, Pozzan T (2003) When calcium goes wrong: genetic alterations of a ubiquitous signaling route. Nature Genetics 34:135-141

148. Klugbauer N, Lacinova L, Marais E, Hobom M, Hofmann F (1999) Molecular diversity of the calcium channel alpha2delta subunit. Journal of Neuroscience 19:684-691

149. Lacinova L, Klugbauer N (2004) Modulation of gating currents of the Ca(v)3.1 calcium channel by alpha 2 delta 2 and gamma 5 subunits. Archives of Biochemistry and Biophysics 425:207-213

150. Hartveit E (1999) Reciprocal synaptic interactions between rod bipolar cells and amacrine cells in the rat retina. Journal of Neurophysiology 81:2923-2936

151. Pan ZH, Hu HJ, Perring P, Andrade R (2001) T-type Ca2+ channels mediate neurotransmitter release in retinal bipolar cells. Neuron 32:89-98

152. Singer JH, Diamond JS (2003) Sustained Ca2+ entry elicits transient postsynaptic currents at a retinal ribbon synapse. Journal of Neuroscience 23:10923-10933

153. Pan ZH (2001) Voltage-activated Ca2+ channels and ionotropic GABA receptors localized at axon terminals of mammalian retinal bipolar cells. Visual Neuroscience 18:279-288

154. Altier C, Zamponi GW (2004) Targeting Ca2+ channels to treat pain: T-type versus N-type. Trends in Pharmacological Sciences 25:465-470

155. Duncan JL, Yang HD, Doan T, Silverstein RS, Murphy GJ, Nune G, Liu XR, Copenhagen D, Tempel BL, Rieke F, Krizaj D (2006) Scotopic visual signaling in the mouse retina is modulated by high-affinity plasma membrane calcium extrusion. Journal of Neuroscience 26:7201-7211

156. Copenhagen DA, Renteria RC, Strehler EE, Gillespie PG, Krizaj D (2003) Plasma membrane calcium ATPases 1b and 4b catalyze calcium extrusion from photoreceptor synaptic terminals. Investigative Ophthalmology & Visual Science 44:U455

157. Rieke F, Schwartz EA (1994) A Cgmp-Gated Current Can Control Exocytosis at Cone Synapses. Neuron 13:863-873

158. Krizaj D, Copenhagen DR (2003) Ryanodine receptors, PMCAs and mitochondria interact in inner segments of salamander rods and cones. Investigative Ophthalmology & Visual Science 44:U287

159. Krizaj D, Lai FA, Copenhagen DR (2003) Ryanodine stores and calcium regulation in the inner segments of salamander rods and cones. Journal of Physiology-London 547:761-774

160. Peng YW, Sharp AH, Snyder SH, Yau KW (1991) Localization of the Inositol 1,4,5-Trisphosphate Receptor in Synaptic Terminals in the Vertebrate Retina. Neuron 6:525-531

161. Suryanarayanan A, Slaughter MM (2006) Synaptic transmission mediated by internal calcium stores in rod photoreceptors. Journal of Neuroscience 26:1759-1766

162. Tsukamoto Y, Morigiwa K, Ueda M, Sterling P (2001) Microcircuits for night vision in mouse retina. Journal of Neuroscience 21:8616-8623

163. Soucy E, Wang YS, Nirenberg S, Nathans J, Meister M (1998) A novel signaling pathway from rod photoreceptors to ganglion cells in mammalian retina. Neuron 21:481-493

164. Khan NW, Kondo M, Hiriyanna KT, Jamison JA, Bush RA, Sieving PA (2005) Primate retinal signaling pathways: Suppressing ON-pathway activity in monkey with glutamate analogues mimics human CSNB1-NYX genetic night blindness. Journal of Neurophysiology 93:481-492

165. Nakajima Y, Iwakabe H, Akazawa C, Nawa H, Shigemoto R, Mizuno N, Nakanishi S (1993) Molecular characterization of a novel retinal metabotropic glutamate receptor mGluR6 with a high agonist selectivity for L-2-amino-4-phosphonobutyrate. Journal of Biological Chemistry 268:11868-11873

166. Nakanishi S, Nakajima Y, Nomura A, Masu M, Iwakabe H, Hayashi Y, Yokoi M (1996) Functions and roles of glutamate receptors in synaptic transmission and plasticity. Cold Spring Harbor Symposia on Quantitative Biology 61:67-75

167. Jalkanen R, Mantyjarvi M, Tobias R, Isosomppi J, Sankila EM, Alitalo T, Bech-Hansen NT (2006) X-linked cone-rod dystrophy, CORDX3, is caused by a mutation in the CACNA1F gene. Journal of Medecal Genetics 43:699-704

168. Nakamura M, Ito S, Piao CH, Terasaki H, Miyake Y (2003) Retinal and optic disc atrophy associated with a CACNA1F mutation in a Japanese family. Archives of Ophthalmology 121:1028-1033

169. Harris CM, Berry DL (2006) A distal model of congenital nystagmus as nonlinear adaptive oscillations. Nonlinear Dynamics 44:367-380

170. Demas E (1971) New Method of A New Science - Study of Vico,G. Journal of the History of Ideas 32:85-94

171. Baseler HA, Brewer AA, Sharpe LT, Morland AB, Jagle H, Wandell BA (2002) Reorganization of human cortical maps caused by inherited photoreceptor abnormalities. Nature Neuroscience 5:364-370

172. Ball SL, Powers PA, Shin HS, Morgans CW, Peachey NS, Gregg RG (2002) Role of the beta(2) subunit of voltage-dependent calcium channels in the retinal outer plexiform layer. Investigative Ophthalmology & Visual Science 43:1595-1603

173. Ball SL, Gregg RG (2002) Using mutant mice to study the role of voltage-gated calcium channels in the retina. Photoreceptors and Calcium 514:439-450

174. Splawski I, Timothy KW, Sharpe LM, Decher N, Kumar P, Bloise R, Napolitano C, Schwartz PJ, Joseph RM, Condouris K, Tager-Flusberg H, Priori SG, Sanguinetti MC, Keating MT (2004) Ca(v)1.2 calcium channel dysfunction causes a multisystem disorder including arrhythmia and autism. Cell 119:19-31

175. Chik CL, Li B, Negishi T, Karpinski E, Ho AK (1999) Ceramide inhibits L-type calcium channel currents in rat pinealocytes. Endocrinology 140:5682-5690

176. Chik CL, Li B, Karpinski E, Ho AK (1999) Regulation of the L-type Ca2+ channel current in rat pinealocytes: Role of basal phosphorylation. Journal of Neurochemistry 72:73-80

177. Tordjman S, Anderson GM, Pichard N, Charbuy H, Touitou Y (2005) Nocturnal excretion of 6-sulphatoxymelatonin in children and adolescents with autistic disorder. Biological Psychiatry 57:134-138

178. Kao JPY, Harootunian AT, Tsien RY (1989) Photochemically Generated Cytosolic Calcium Pulses and Their Detection by Fluo-3. Journal of Biological Chemistry 264:8179-8184

179. Friel D (2004) Interplay between ER Ca2+ uptake and release fluxes in neurons and its impact on [Ca2+] dynamics. Biological Research 37:665-674

180. Travers K, Pollard M, Weissman JS (1997) DUD7: A novel and ubiquitous resident ER protein that plays an essential role in oxidative folding in the endoplasmic reticulum. Molecular Biology of the Cell 8:565

181. Roybal CN, Marmorstein LY, Jagt DLV, Abcouwer SF (2005) Aberrant accumulation of fibulin-3 in the endoplasmic reticulum leads to activation of the unfolded protein response and VEGF expression. Investigative Ophthalmology & Visual Science 46:3973-3979

182. Roybal CN, Marmorstein LY, Vander Jagt DL, Abcouwer SF (2005) Aberrant accumulation of EFEMP1 leads to activation of the unfolded protein response and VEGF expression. Investigative Ophthalmology & Visual Science 46: 449-469

5. Summary (*in German, advanced*)

Die Blindheit stellt das Extrem einer als Kontinuum aufzufassenden Dimension der Sehstörung dar. Ihr zugrunde liegen oft genetische Defekte des Netzhautsystems, deren Identifizierung und pathophysiologische Charakterisierung die Grundlage zur therapeutischen Intervention schaffen. Die Anlehnung an Modellorganismen erleichtert eine raschere und ethisch vertretbare Erforschung der komplexen Vielfalt von humanen Netzhauterkrankungen. Dabei trägt das retinale Mausmodellsystem zum Fortschritt bei, denn es ähnelt in biologischer und genetischer Hinsicht dem menschlichen Sinnesorgan und gestattet nahezu synonyme Aufklärung pathologischer Prozesse.

Eine Fehlfunktion der intraretinalen Signaltransmission wurde in einer Mauspopulation des isogenen C57BL/10 Stamms diagnostiziert. Dabei fiel der Verlust der postrezeptoralen Aktivierung besonders auf. Sowohl unter skotopischen wie photopischen Bedingungen wurden keine Antworten der den Photorezeptoren nachgeschalteten Neuronen registriert. Zudem wies die Stäbchenantwort eine erhebliche Reduktion ihrer Amplitude auf, während eine Zapfenaktivität nicht erfasst wurde. Die derart geprägte Manifestation der ermittelten Retinopathie ließ einen Defekt im synaptischen Transduktionsprozess vermuten, der wahrscheinlich von dem Zapfen- wie dem Stäbchensystem herrührte. Morphologische Studien bestätigten, dass der Aktivitätsverlust in postrezeptoralen Erregungskreisläufen auf eine schwerwiegende Missbildung der für die Photorezeptoren charakteristischen Ribbonsynapsen zurückzuführen war. Die Anzahl der Photorezeptorzellen in den betroffenen Tieren war zugleich um ein Drittel verringert. Klassische Kreuzungsexperimente deuteten auf eine monogene, dem autosomal-rezessiven Vererbungsmodus folgende Erkrankung hin. Der genetische Defekt und die verantwortliche Erbanlage blieben jedoch unentdeckt.

Der Fokus dieser Studie lag in der Identifizierung der kausalen Mutation, die das Verständnis um das betroffene Gen und die induzierten Pathogenesemechanismen herbeiführen sollte. Im Rahmen einer genomweiten Kopplungsanalyse wurde die genetische Veränderung in einem 15Mb-grossen Intervall auf dem Mauschromosom 6 lokalisiert. Mit Hilfe einer auf Literatursuche-basierenden Funktionsanalyse wurden 27 Kandidatengene in diesem genetischen Intervall ermittelt und einer anschließend folgenden Sequenzanalyse unterzogen. Veränderungen in der Sequenzstruktur dieser Gene wurden jedoch nicht aufgedeckt. Eine systematisch fortgeführte Feinkartierung ließ eine Eingrenzung des identifizierten Lokus auf 275kbp zu. Innerhalb dieser chromosomalen Region verblieben sechs potentielle Kandidatengene.

Sequenzanalysen in vorhergesagten protein-kodierenden Abschnitten dieser Erbanlagen ergaben wiederum keine genetischen Defekte und ließen Rückschlüsse auf einen möglichen Erbfehler in einer weiteren Spleißvariante bzw. einem neuen Gen zu. Demnach wurde das Mutationsscreening auf das gesamte Kopplungsintervall von 275kbp ausgedehnt. In einer zuvor als genfrei annotierten Region wurde eine homozygote Insertion in einer repetitiven Cysteinsequenz bei erkrankten Mäusen detektiert. Diese genetische Veränderung (c.2367insC) verursacht eine Verschiebung des Leserasters in einer neuen, verlängerten Spleißvariante des *Cacna2d4*-Gens. Die molekulargenetische Aufklärung der Exon-Intron-Struktur in dieser *Cacna2d4*-Variante ergab 38 Exone, statt der anfänglich annotierten 22. Das komplette Transkript kodiert die für einen offenen Leserahmen von 3350bp, der 1116 Aminosäureresten entspricht. Die Insertion resultiert in einer Substitution von 14 nachfolgenden Aminosäuren und einem vorzeitigen Stopp-Kodon in der korrespondierenden Proteinsequenz. Wahrscheinlich werden 327 Aminosäuren vom C-terminalen Ende trunkiert, welches konservierte und funktionsrelevante Strukturmotive, unter anderem eine Membranverankerung, aufweist. Den Expressionsexperimenten nach findet die *Cacna2d4*-Transkription ohne zeitliche Begrenzung in allen Geweben statt. Die trunkierende Mutation zeigt demgegenüber eine erhebliche Auswirkung auf die Verfügbarkeit des *Cacna2d4*-Transkriptes im retinalen Gewebe, denn sie führt in betroffenen Tieren zur nahezu 70%-igen Reduktion der *Cacna2d4*-mRNA. Die Transkript-Defizienz kann zum beträchtlichen Verlust des Cacna2d4-Proteins führen und demnach den Ausgangspunkt der Pathogenese bilden. Auf der Proteinebene agieren wahrscheinlich weitere pathogene Mechanismen, die auf eine Funktionsstörung des trunkierten Cacna2d4-Proteins zurückzuführen sind. *Cacna2d4* kodiert für eine regulatorische Untereinheit des Typs $\alpha_2\delta$ von spannungsabhängigen Kalzium-Kanälen. Die $\alpha_2\delta$-Untereinheiten sind für die Modulation der biophysikalischen Eigenschaften und die Erhöhung der Dichte der Kalzium-Kanal-Komplexe in neuronalen Membranen verantwortlich. Spannungsabhängige Kalzium-Kanäle vom Typ L binden $\alpha_2\delta$-Untereinheiten in ihre Membran-komplexe ein und werden bevorzugt in die Signalübertragungswege der Ribbonsynapsen involviert. Die Mutation in *Cacna2d4* kann das Schaltverhalten, die Ionenleitfähigkeit und die Lebensdauer dieser Kalzium-Kanäle beeinflussen, wodurch die Erregbarkeit des betroffenen Netzhautgewebes beeinträchtigt und die Impulsfortleitung aufgehoben werden. Auf der histologischen Ebene führt die wahrscheinlich eintretende Kanalopathie zur schweren Atrophie des photorezeptor-spezifischen synaptischen Gewebes und einem progressiven Verlust der Sinneszellen in betroffenen Tieren. Dabei setzt die erste degenerative Phase schon während der

postnatalen retinalen Reifung ein und resultiert im nahezu vollständigen Schwund der synaptischen Schicht in den folgenden drei Lebensmonaten. In adulten Stadien stagniert der degenerative Prozess, um nach einem Lebensjahr in einer zweiten verstärkten neuronalen Degeneration seinen Fortgang zu nehmen. Während die reifende Retina ausschliesslich Stäbchen in den Zelltod involviert, umfasst dieser in späteren Stadien wahrscheinlich alle Neuronen. Zur Manifestation der zweiten degenerativen Phase kommt eine fortschreitende Rückbildung aller nuklearen und synaptischen Netzhautschichten hinzu. Die retinale Degeneration schliesst geringgradige Veränderungen im Transkriptom betroffener Tiere ein. Stäbchen-spezifische Gene wie *Rhodopsin, Phosducin* oder *die cGMP Phosphodiesterase6B* gehören zu den Transkripten mit einer am stärksten reduzierten Verfügbarkeit von bis zu ~60% und spiegeln wahrscheinlich den dominierenden Stäbchen-Verlust wider. Ein weiteres neurosensorisches Gewebe, die Cochlea, zeigt keine Fehlfunktion der mit der Netzhaut verwandten cochlearen Ribbonsynapsen in jungen betroffenen Tieren. Eine spätere Untersuchung der *Cacna2d4*-spezifischen Cochlea-Dysfunktion ist aufgrund einer altersabhängigen progressiven Taubheit des C57BL/10 Stamms, die einer *Cadherin23*-Mutation zugrunde liegt, nicht möglich.

Im Zusammenhang mit dem vorliegenden Phänotyp mag das humane *CACNA2D4*-Ortholog das Spektrum menschlicher hereditärer Netzhauterkrankungen um ein weiteres Gen ergänzen. Mutationsanalysen in 78 Patienten deckten interessante Sequenzpolymorphismen in *CACNA2D4* auf. Drei der identifizierten Polymorphismen entsprechen einem heterozygoten Aminosäurenaustausch an konservierten Stellen des CACNA2D4-Proteins. Zwei Patienten einer nicht Familie mit beschriebener Zapfen-Dystrophy weisen eine homozygote Nonsense-Mutation auf. Diese Mutation erweist sich als pathologisch relevant. Zukünftige Studien werden zeigen, inwiefern weitere Mutationen und der *CACNA2D4*-Kanalopathie zugrunde liegende pathophysiologische Mechanismen eine retinale Erkrankung herbeiführen.

6. Summary (*in English*)

Severe visual impairments frequently emerge in consequence of genetic defects that affect signal processing of the retinal system. Their identification helps to understand the essential processes in the retinal neurotransmission and the nature of activated pathogenic mechanisms. An astonishing phenotype of perturbed retinal signal transduction arose in a subpopulation of C57BL/10 mice. Characteristic abnormalities, detected upon electrophysiological examinations, indicated a preferential loss of the post-photoreceptoral activation. Whereas rod responses, although reduced, were remained, absent activities of the secondary neurons implied defective neurotransmission from photoreceptor synapses to the inner-retinal signaling pathways. Cone photoreceptor-specific responses were not detectable. In analogy to negative retinal electrophysiology, mutant mice displayed severely affected morphology of the ribbon-type synapses, formed by rods, cones and ON-bipolar cells. In addition, apparent photoreceptor elimination of 30% occurred in affected retinas. Studies of classical genetics suggested an autosomal recessive genetic origin of the photoreceptor processing failure in C57BL/10 mutant mice. Upon genome-wide linkage analysis, the genetic defect was localized on mouse chromosome 6 in an interval of 275 kb. Following sequence examinations of the entire genomic locus, a single nucleotide insertion (c.2367insC) was identified in exon 25 of the *Cacna2d4* gene, encoding the fourth auxiliary L-type calcium channel subunit of the $\alpha_2\delta$-type. Importantly, retinal signal transmission depends on the activity of high voltage-gated L-type calcium channels in photoreceptor ribbon synapses. The α2δ subunits modulate biophysical properties of the multimeric L–type calcium channel complexes. They are also involved in the regulation of surface expression and proper assembly of the pore-forming α1 subunits of the calcium channel complex. The homozygous frame shifting mutation results in a substitution of 14 amino acid residues and a premature termination codon that truncates 327 amino acids from the C-terminus of Cacna2d4. A severe reduction of 70% in *Cacna2d4* transcript levels observed in mutant retinas probably leads to deficiency of the Cacna2d4 protein in the retinal tissue. In consequence, loss of Cacna2d4 function apparently promotes a channelopathy, underlying a cone-rod-specific dysfunction and an early-onset rod degeneration in mice. Alluding to the retinal phenotype of *Cacna2d4*-mutant animals, mutational analyses of the human orthologue, *CACNA2D4*, disclosed a homozygous truncating mutation (c.2406C>A) in two siblings, sharing symptoms of slowly progressing cone dystrophy. These results define a novel autosomal recessive form of a cone dystrophy and may, in future, potentiate accurate diagnostics and strategic paths for therapeutic interventions.

7. Appendix

7.1. Allelic Variations Identified in the CACNA2D4 Gene

Four heterozygous sequence variations in four unrelated individuals with clinical diagnosis of incomplete night blindness were additionally detected in the *CACNA2D4* sequence (Table 1). Two of them represented exonic missense changes and two occurred in intronic sequences closely adjacent to exonic splice sites. These variations, not observed in 100 control chromosomes, remain of uncertain pathogenic potential. Worth mentioning, one heterozygous nucleotide substitution, c.2452C>T, found in the index patient 13760 was predicted to be deleterious (mutation prediction programs at http://blocks.fhcrc.org/sift/SIFT.html and http://coot.embl.de/PolyPhen, Table 2). This c.2452C>T transition, indeed, exchanges a highly conserved arginine residue into a cytosine residue at position 818 of CACNA2D4. The arginine residue of a wild type CACNA2D4 protein features hydrophilic properties, in contrast to the introduced cysteine residue with a rather hydrophobic character. Cysteine residues also show high reactivity in disulfide bridge formation and may alter conformational states of proteins. The substitution might thus affect the conformation and function of CACNA2D4. Whether a second mutation is present in an alternative exon or non-coding regions, or whether it might be reflected by a heterozygous deletion in one of the parental *CACNA2D4* alleles must be clarified in the future. Of note, a second mutation in another gene may result in the iCSNB phenotype of this family. So far, no mutation was detected in the *CACNA1F* gene of the index patient.

The substitution c.419C>G in the index patient G1 diagnosed with cone-rod dystrophy, represents a homozygous exchange of alanine to glycine at position 140 (p.A140G). This substitution might be of minor importance as both amino acid residues exhibit similar characteristics. The nucleotide substitution, however, is predicted to produce an exonic splicing enhancer sequence recognized by the *SC35* protein of the splicing apparatus (score 2.890 with 2.383 *SC35* threshold, prediction software http://rulai.cshl.edu/tools/ESE; X1). Exonic splicing enhancers are important *cis* elements required for exon inclusion. The introduced splicing enhancer sequence for the *SC35* protein may lead to the recognition of a cryptic splice site in *CACNA2D4* and generate an aberrant or frame-shifting mRNA from both alleles of this patient.

Table 1. Sequence variants identified in the *CACNA2D4* gene.

	patient ID	disease	exon/ intron number	transmission status	transcript position	amino acid residue	frequency (persons)	SIFT	PolyPhen	ESE prediction
1	G1	CORD	exon 3	heterozygous	c.364C>G	p.L122V	1 in 78	0.02	benign	no
2	G1	CORD	exon 3	homozygous	c.419C>G	p.A140G	1 in 78	0.03	benign	SC35 (site creation, 2.89)
3	13760	CSNB	exon 25	heterozygous	c.2452C>T	p.R818C	1 in 128	0.00	deleterious	SRp40 (site creation, 3.832) SF2/ASF (site loss)
4	A10	COD	exon 29	heterozygous	c.2714C>T	p.S905F	1 in 178	tolerated	benign	SF2/ASF (site loss)
5	G3	COD	exon 34	heterozygous	c.2987T>C	p.F996S	1 in 178	tolerated	benign	SRp40 (site creation, 3.062)
6	B3	COD	exon 37	heterozygous	c.3241A>G	p.K1081R	1 in 78	tolerated	benign	SF2/ASF (site creation, 3.466) SRp40 (site loss)
7	6273	CSNB	exon 38	heterozygous	c.3356C>A	p.P1119Q	1 in 78	0.25	benign	SF2/ASF (site loss) SRp55 (site creation, 3.883)
8	10766	CSNB	intron 16	heterozygous	IVS16+4G>A	"-"	1 in 78	"-"	"-"	"-"
9	5873	CSNB	intron 22	heterozygous	IVS21+37G>T	"-"	1 in 78	"-"	"-"	"-"
10	F7	COD	intron 28	heterozygous	IVS28+50C>T	"-"	1 in 78	"-"	"-"	"-"

The identified nonsense mutation is indicated in bold. SIFT program predicts an amino acid exchange as tolerated by a threshold of >0.5. The thresholds for the ESE (exonic splicing enhancer) are 1.956 for SF2/ASF, 2.383 for SC35, 2.67 for SRp40 and 2.676 for SRp55. Higher values indicate putative ESE sites. Cone-rod dystrophy (CORD), cone dystrophy (COD), congenital stationary night blindness (CSNB).

7.2. Contributions of the co-authors

External cooperations :

Max Delbrueck Centre Berlin, Germany : cooperation in genome-wide linkage analysis

Budde B., Nuernberg P.

Charite-Virchow Eye Clinic, Berlin, Germany : electroretinographic phenotyping of mice

Ruether K., Skosyrski S.

University Eye Hospital, Eberhard-Karls University Tuebingen, Germany : patient recruitment, clinical report of symptoms

Kohl S., Wilke R., Wissinger B., Zrenner E.

Department of Otorhinolaryngology, **Radboud University Medical Center Nijmegen, The Netherlands :** examinations of acoustic brain stem responses

Beynon A. J, Kremers H., Peters T.

Department of Psychiatry and Neurobiology, University of Pisa, Italy : electrophysiological patch-clamp experiments*

Demontis G. C.

*The final results of the patch-clamp experiments will not be part of the presented manuscript (Chapter 3.3). They will be published in an independent publication by an independent author.

Group-internal cooperations at the Institute of Medical Genetics, University of Zurich, Schwerzenbach, Switzerland :

group and laboratory head, supervisor

Berger W.

sequence analysis of 12 candidate genes, help in microarray experiments

Buzzi F. (diploma student)

broad experimental assistance in several units of the project

Feil S.

experimental assistance in human *CACNA2D4* sequence analysis

Forster U.

scientific exchange, evaluation of potential splicing defects in the human *CACNA2D4* gene, cone immunohistochemistry in mice

Neidhardt J.

technical assistance in human *CACNA2D4* sequence analysis

Wittmer M.

technical assistance in human *CACNA2D4* sequence analysis

Zeitz C.

7.3. Curriculum vitae

WYCISK

Katharina Agnes

Day of birth : 25.11.1973

Place of birth : Peiskretscham / Gleiwitz

Address: Eichliackerstrasse 65, CH-8406 Winterthur

Nationality : German

School Education

1988 – 1994	Hermann-Ehlers-Gymnasium, University Entrance Diploma, Berlin, Germany

Study

10.1994 – 05.2001	**Biotechnology** Study, Engineer Degree, Technical University of Berlin, Germany
11.1996 – 03.1997	**Pre-Diploma Thesis,** Institute of Environmental Biotechnology, University of Natural Resources and Applied Life Science, Austria
05.2000 – 05.2001	**Diploma Thesis**, Max Planck Institute of Molecular Plant Physiology, Germany

Dissertation

11.2001 - 04.2006	Max Planck Institute of Molecular Genetics, Berlin, Germany and Division of Medical Molecular Genetics and Gene Diagnostics, Institute of Medical Genetics, University of Zurich, Switzerland

Further Research

06.2001 – 10.2001	**Scientific Associate,** Max Planck Institute of Molecular Plant Physiology, Germany
12.1998 – 02.2000	**Scientific Associate,** Institute of Microbiology und Genetics, Technical University of Berlin, Germany

Winterthur, 15.11.2006 Katharina A. Wycisk

7.4. Publications and Conferences

published:

- **K. A. Wycisk**, B. Budde, S. Feil, S. Skosyrski, F. Buzzi, J. Neidhardt, E. Glaus, P. Nürnberg, K. Ruether, W. Berger (2006) **Structural and functional abnormalities of retinal ribbon synapses due to *Cacna2d4* mutation.** *Invest. Ophthalmol.Vis.Sci.,* 47: 3523-3530
- J. Neidhardt, **K. A. Wycisk**, B. Klöckener-Gruissem (2005) **Virale und nichtvirale Gentherapieansätze zur Behandlung von Netzhauterkrankungen.** *Ophthalmologe*. 102:764-71. Review.
- C. Zeitz, M. van Genderen, J. Neidhardt, U. F. O. Luhmann, F. Hoeben, U. Forster, **K. A. Wycisk,** G. Matyas, C. B. Hoyng, F. Riemslag, F. Meire, F. P. M. Cremers, and W. Berger (2005) **Mutations in GRM6 cause autosomal recessive congenital stationary night blindness with a distinctive scotopic 15-Hz flicker electroretinogram**. *Invest. Ophthalmol. Vis. Sci.*, 46: 4328-4335.
- **K. A. Wycisk**, E. J. Kim, J. I. Schroeder, U. Krämer (2004) **Enhancing the first enzymatic step in the histidine biosynthesis pathway increases the free histidine pool and nickel tolerance in *A. thaliana.*** *FEBS Letters.* 578: 128-134.

epub ahead of print:

- **K. A. Wycisk,** C. Zeitz, S. Feil, M. Wittmer, U. Forster, J. Neidhardt, Bernd Wissinger, E. Zrenner, R. Wilke, S. Kohl, W. Berger (2006) **Mutation in the auxiliary calcium channel subunit CACNA2D4 causes autosomal recessive cone dystrophy.** *Am. J. Hum. Genet.*

in preparation:

- **K. A. Wycisk,** F. Buzzi, S. Feil, S. Skosyrski, H. Kremers, A. J. Beynon, T. Peters, K. Ruether, N. Hagenbuch, G. Demontis, W. Berger (2006) **Histological and molecular characterization of *Cacna2d4*-mutant mice.**

conferences:

- **K. A. Wycisk,** B. Meyer, S. Feil, S. Skosyrski, F. Buzzi, J. Neidhardt, E. Glaus, P. Nürnberg, K. Ruether, W. Berger (2006) Structural and Functional Abnormalities of Retinal Ribbon Synapses due to *Cacna2d4* Mutation. *Pro Retina Meeting*, Potsdam, Germany, April 7.-8., presentation

- C. Zeitz, U. Forster, J. Neidhardt, M. van Genderen, U. F. O. Luhmann, F. Hoeben, **K. A. Wycisk,** S. Feil, G. Mátyás, C. B. Hoyng, F. Meire, F. Riemslag, F. P. M. Cremers, P. Flor, W. Berger (2006) Night blindness-associated mutations in the metabotropic glutamate receptor 6 show a distinctive scotopic 15-Hz flicker ERG and abolish protein trafficking. *Pro Retina Meeting*, Potsdam, Germany, April 7.-8., presentation C. Zeitz

- **K. A. Wycisk,** S. Feil, F. Buzzi, S. Skosyrski, K. Rüther, W. Berger (2005) Ocular gene expression profiling in a mouse mutant with a retinal ribbon synapse defect and mutation analyses of candidate genes. *Association for Research in Vision and Ophthalmology (ARVO) Annual Meeting*, Fort Lauderdale/Florida, USA, Mai 1.-5., poster presentation

- C. Zeitz, M. van Genderen, J. Neidhardt, U. F. O. Luhmann, F. Hoeben, U. Forster, **K. A. Wycisk,** G. Mátyás, C. B. Hoyng, F. Riemslag, F. Meire, F. P. M. Cremers, W. Berger (2005) Mutations in *GRM6* cause autosomal recessive congenital stationary night blindness with a distinctive scotopic 15 Hz flicker electroretinogram (ERG). *55th Annual Meeting of the American Society of Human Genetics*, Salt Lake City, Utah, USA, October 25.-29., presentation C. Zeitz

- C. Zeitz, M. van Genderen, J. Neidhardt, U. F. O. Luhmann, F. Hoeben, U. Forster, **K. A. Wycisk,** G. Mátyás, C. B. Hoyng, F. Riemslag, F. Meire, F. P. M. Cremers, W. Berger. (2005) Mutations in *GRM6* cause autosomal recessive congenital stationary night blindness (CSNB) with a distinctive scotopic 15 Hz flicker electroretinogram (ERG). ZNZ Symposium, Zurich, Switzerland, October 21., poster presentation

- **K. A. Wycisk** (2004) Ribbon synapses. *Nijmegen-Berlin Minisymposium on Blindness***,** Nijmegen, The Netherlands, October 14.-16., presentation

- **K. A. Wycisk** (2004) Linkage analysis of a monogenic defect in a spontaneous mouse mutant with abnormal ribbon synapses. *Swiss-Retina-Meeting*, Villars, Switzerland, January 27., presentation

- U. Kraemer, A. G. Desbrosses-Fonrouge, M. Becher, D. Draeger, L. Kerkeb, **K. A. Wycisk** (2002) The role of membrane transporters and low-molecular-weight chelators in metal homeostasis in hyperaccumulators and closely related model plants. *9th New Phytologist Symposium*, Heavy metals and plants, University of Pennsylvania, Philadelphia, USA, September 29.-0ctober 1., presentation U. Krämer

- **K. A. Wycisk** (2001) Identification of the gene defect in a spontaneous mouse mutant with abnormal ribbon synapses. *Nijmegen-Berlin Minisymposium on Blindness*, Berlin, Germany, November 23., presentation